Oxidation of Substrates Tethered to N-donor Ligands
for Modeling Non-Heme Diiron Enzyme Active Sites

by

Emily Carrig Carson

B.Sc., Chemistry

University of Virginia, 2000

SUBMITTED TO THE DEPARTMENT OF CHEMISTRY IN PARTIAL FULFILLMENT OF
THE REQUIREMENTS FOR THE DEGREE OF

DOCTOR OF PHILOSOPHY IN INORGANIC CHEMISTRY
AT THE
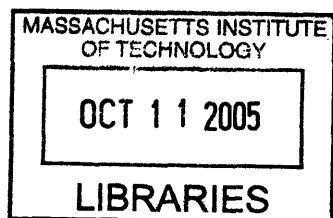MASSACHUSETTS INSTITUTE OF TECHNOLOGY

September 2005

Signature of Author: _____

Department of Chemistry

July 16, 2005

Certified by: _____

Stephen J. Lippard

Arthur Amos Noyes Professor of Chemistry

Thesis Supervisor

Accepted by: _____

Robert W. Field

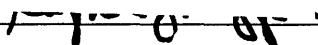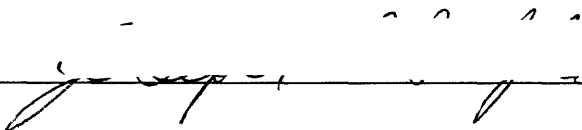Chairman, Departmental Committee on Graduate Studies

2

This doctoral thesis has been examined by a committee of the Department of Chemistry as follows:

_____

Christopher C. Cummins
Professor of Chemistry
Committee Chairman

_____

Stephen J. Lippard
Arthur Amos Noyes Professor of Chemistry
Thesis Supervisor

_____

Joseph P. Sadighi
Assistant Professor of Chemistry

Oxidation of Substrates Tethered to N-donor Ligands
for Modeling Non-Heme Diiron Enzyme Active Sites

by
Emily Carrig Carson

Submitted to the Department of Chemistry on July 16, 2005, in partial
fulfillment of the requirements for the degree of Doctor of Philosophy.

Abstract

Chapter 1.   Modeling Carboxylate-Rich Diiron Sites of Dioxygen-Dependent Non-Heme Enzymes

Carboxylate-bridged diiron centers are employed in a variety of biological systems to activate dioxygen for substrate oxidation, and small molecule models have been synthesized to mimic this chemistry outside of the natural systems. In this introductory chapter a brief overview of terphenyl-based carboxylate systems is given and progress toward achieving structural, spectroscopic, and functional models of the protein active sites is reviewed.

Chapter 2.   Synthesis and Reactivity of Carboxylate-Bridged Diiron(II) Complexes with Primary Alkyl Amine Ligands

The synthesis and crystallographic characterization of a series of diiron(II) complexes with sterically hindered terphenyl carboxylate ligands and alkyl amine donors are presented. The compounds $[Fe_2(\mu\text{-}O_2CAr^{Tol})_4(L)_2]$ (L = $NH_2(CH_2)_2SBn$ (**1**); $NH_2(CH_2)_3SMe$ (**2**); $NH_2(CH_2)_3CCH$ (**3**)), where $^-O_2CAr^{Tol}$ is 2,6-di(p-tolyl)benzoate, and $[Fe_2(\mu\text{-}O_2CAr^{Xyl})_2\text{-}$

$(O_2CAr^{Xyl})(L)_2]$ $(L = NH_2(CH_2)_3SMe$ (**4**); $NH_2(CH_2)_3CCH$ (**5**)), where $^-O_2CAr^{Xyl}$ is 2,6-di(3,5-dimethylphenyl)benzoate, were prepared as small molecule mimics of the catalytic sites of carboxylate-bridged non-heme diiron enzymes. The compounds with the $^-O_2CAr^{Tol}$ carboxylate form tetrabridged structures, but those containing the more sterically demanding $^-O_2CAr^{Xyl}$ ligand have only two bridging ligands. The ancillary nitrogen ligands in these carboxylate-rich complexes incorporate potential substrates for the reactive metal centers. Their oxygenation chemistry was studied by product analysis of the organic fragments following decomposition. Compound **1** reacts with dioxygen to afford PhCHO in ~30% yield, attributed to oxidative dealkylation of the pendant benzyl group. Compound **3** decomposes by established bimolecular pathways upon exposure to dioxygen at low temperatures. When the $^-O_2CAr^{Tol}$ carboxylate is replaced by the $^-O_2CAr^{Xyl}$ ligand, as in **5**, this behavior no longer occurs. Instead the six-coordinate iron(III) complex with one bidentate and two monodentate carboxylate ligands, $[Fe(O_2CAr^{Xyl})_3(NH_2(CH_2)_3CCH)_2]$ (**6**), was isolated from the reaction mixture following the oxidation of **5**.

Chapter 3. C–H Activation with Benzyl- and Ethyl- Substituted Pyridine Ligands in Carboxylate-Bridged Diiron(II) Complexes with Dioxygen

In this study benzyl and ethyl groups were appended to pyridine and aniline ancillary ligands in diiron(II) complexes of the type $[Fe_2(\mu-O_2CAr^R)_2(O_2CAr^R)_2(L)_2]$, where $^-O_2CAr^R$ is the sterically hindered 2,6-di(*p*-tolyl)- or 2,6-di(*p*-fluorophenyl)benzoate (R = Tol or 4-FPh, respectively). These crystallographically characterized compounds were prepared as models for the diiron(II) center in the hydroxylase component of soluble methane monooxygenase (MMOH). Use of 2-

benzylpyridine (2-Bnpy) afforded doubly-bridged [Fe$_2$(μ-O$_2$CAr^{Tol})$_2$(O$_2$CAr^{Tol})$_2$(2-Bnpy)$_2$] (**1**)

and [Fe$_2$(μ-O$_2$CAr$^{4\text{-}FPh}$)$_2$(O$_2$CAr$^{4\text{-}FPh}$)$_2$(2-Bnpy)$_2$] (**4**), whereas tetra-bridged [Fe$_2$(μ-O$_2$CAr^{Tol})$_4$-(4-Bnpy)] (**3**) resulted when 4-benzylpyridine (4-Bnpy) was employed. Similarly, 2-(4-chloro-benzyl)pyridine (2-(4-ClBn)py) and 2-benzylaniline (2-Bnan) were employed as N-donor ligands to prepare [Fe$_2$(μ-O$_2$CAr^{Tol})$_2$(O$_2$CAr^{Tol})$_2$(2-(4-ClBn)py)$_2$] (**2**) and [Fe$_2$(μ-O$_2$CAr^{Tol})$_2$(O$_2$CAr^{Tol})$_2$-(2-Bnan)$_2$] (**5**). Placement of the substituent on the pyridine ring had no effect on the geometry of the diiron(II) compounds isolated when 2-, 3-, or 4-ethylpyridine (2-, 3-, or 4-Etpy) was introduced as the ancillary nitrogen ligand. The isolated [Fe$_2$(μ-O$_2$CAr^{Tol})$_2$(O$_2$CAr^{Tol})$_2$(2-Etpy)] (**6**), [Fe$_2$(μ-O$_2$CAr^{Tol})$_2$(O$_2$CAr^{Tol})$_2$(3-Etpy)] (**7**), [Fe$_2$(μ-O$_2$CAr^{Tol})$_2$(O$_2$CAr^{Tol})$_2$(4-Etpy)] (**8**), and [Fe$_2$(μ-O$_2$CAr$^{4\text{-}FPh}$)$_2$(O$_2$CAr$^{4\text{-}FPh}$)$_2$(2-Etpy)$_2$] (**9**) complexes all contain doubly-bridged metal centers. The oxygenation of compounds **1 – 9** was studied by product analysis of the organic fragments following decomposition. Hydrocarbon fragment oxidation occurred for compounds in which the substrate moiety is in close proximity to the diiron center. The extent of oxidation depended on the exact makeup of the ligand set.

Chapter 4. A Thermally Sensitive Intermediate Generated in the Reaction of [Fe$_2$(μ-O$_2$CAr^{Tol})$_2$(O$_2$CAr^{Tol})$_2$(2-Etpy)$_2$] with Dioxygen

In this chapter the reaction of [Fe$_2$(μ-O$_2$CAr^{Tol})$_2$(O$_2$CAr^{Tol})$_2$(2-Etpy)$_2$] (**1a**) with dioxygen at low temperature to form the O$_2$-sensitive intermediate (**1b**) was investigated. Various spectroscopic methods including UV-visible, resonance Raman (rR), electron paramagnetic resonance (EPR), and Mössbauer were applied to study the mechanism and the intermediates involved.

Chapter 5.   Synthesis and Reactivity Studies of Carboxylate-Bridged Diiron(II) Compounds with Dangling Sulfur-Containing Substrates

Functional models of the carboxylate-bridged diiron active site in soluble methane monooxygenase are described in which potential substrates are introduced as substituents on bound pyridine ligands. Thiol, sulfide, and sulfoxide moieties tethered to pyridine were allowed to react with the prefabricated diiron(II) complex [$Fe_2(\mu$-$O_2CAr^{Tol})_2(O_2CAr^{Tol})_2(THF)_2$], where $^-O_2CAr^R$ is a sterically hindered 2,6-di(p-tolyl)benzoate. The resulting diiron(II) complexes were characterized crystallographically. Triply- and doubly-bridged compounds [$Fe_2(\mu$-$O_2CAr^{Tol})_3$-(O_2CAr^{Tol})(2-PhSpy)] (**1**), [$Fe_2(\mu$-$O_2CAr^{Tol})_3(O_2CAr^{Tol}$)(2-MeSpy)] (**2**), and [$Fe_2(\mu$-$O_2CAr^{Tol})_2$-($O_2CAr^{Tol})_2$(2-MeS(O)py)$_2$] (**3**) resulted when 2-phenylthiopyridine (2-PhSpy), 2-methylthio-pyridine (2-MeSpy) and 2-pyridylmethylsulfoxide (2-MeS(O)py), respectively, were employed. Use of 2-mercaptopyridine (2-HSpy) afforded the mononuclear complex [$Fe(O_2CAr^{Tol})_2$-(2-HSpy)$_2$] (**4a**). The dioxygen reactivity of these iron(II) complexes was investigated. A dioxygen-dependent intermediate (**4b**) formed upon exposure of **4a** to O_2, the electronic structure of which was probed by various spectroscopic methods. Exposure of **1 – 3** to dioxygen revealed both sulfide and sulfoxide oxidation.

Chapter 6.   Effect of Substrate Position in Diphenylphosphinopyridine Ligands on Geometry and Reactivity of Diiron(II) Carboxylate-Bridged Compounds

In this chapter the exploration of carboxylate-bridged diiron(II) compounds containing phosphino-derivatized pyridine ligands to mimic aspects of chemistry at the active site of soluble

methane monooxygenase (sMMO) is presented. 2-, 3-, or 4-Diphenylphosphino moieties incorporated into a pyridine ligand (2-, 3-, or 4-Ph$_2$Ppy) were allowed to react with the preassembled diiron(II) complex [Fe$_2$(μ-O$_2$CAr^R)$_2$(O$_2$CAr^R)$_2$(THF)$_2$], where $^-$O$_2$CAr^R is a sterically hindered 2,6-di(*p*-tolyl)- or 2,6-di(*p*-fluorophenyl)benzoate (R = Tol or 4-FPh). Triply-, doubly-, and tetrabridged compounds [Fe$_2$(μ-O$_2$CAr^{Tol})$_3$(O$_2$CAr^{Tol})(2-Ph$_2$Ppy)] (**1**), [Fe$_2$(μ-O$_2$C-Ar^{Tol})$_2$(O$_2$CAr^{Tol})$_2$(3-Ph$_2$Ppy)$_2$] (**2**), [Fe$_2$(μ-O$_2$CAr^{Tol})$_4$(4-Ph$_2$Ppy)$_2$] (**3**), [Fe$_2$(μ-O$_2$CAr^{4-FPh})$_3$(O$_2$CAr^{4-FPh})(2-Ph$_2$Ppy)] (**4**) resulted and were characterized crystallographically. Exposure of **1** – **4** to dioxygen revealed both stoichiometric and catalytic phosphine oxidation. Oxidation of **4** in CH$_2$Cl$_2$ affords [Fe$_2$(μ-OH)$_2$(μ-O$_2$CAr^{4-FPh})(O$_2$CAr^{4-FPh})$_3$(OH$_2$)(2-Ph$_2$P(O)py)] (**6**), which contains the biologically relevant {Fe$_2$(μ-OH)$_2$(μ-O$_2$CR)}$^{3+}$ core. This reaction is sensitive to the choice of carboxylate ligands, however, since the *p*-tolyl analog **1** yielded a hexanuclear species, **5**, upon oxidation.

Thesis Supervisor: Stephen J. Lippard
Title: Arthur Amos Noyes Professor of Chemistry

Dedicated To My Husband, Brec Carson

Acknowledgements

There are so many people to whom I am indebted upon the completion of my dissertation. I am grateful for the opportunity to express my gratitude and acknowledge their efforts.

First, I thank my advisor, Stephen J. Lippard, for giving me the opportunity to work in his lab. Steve has challenged me from the start, and I hope that he has enjoyed our interactions as much as I have. He has assembled a diverse and well-equipped lab, and it has been a pleasure to take part of it all. I also thank Professor Kit Cummins for serving as my thesis chair and helpful discussions throughout the years, Professor Joseph Sadighi for serving on my committee and all three professors for letting Katie and I realize our dream of defending on the same day.

The diiron modeling subgroup has been my home in the Lippard group, and I could not have been more pleased with the people with whom I've had the privilege of working. Josh Farrell and Jane Kuzelka welcomed me into the modeling subgroup and proved to be excellent mentors. Jane was the original "inner poise goddess" and a calming presence both in person and in emails during orals and thesis writing. Rayane Moreira was a unique addition to our subgroup whose joy of living is unlike anyone's I've ever known. Jeremy Kodanko brought both knowledge and humor to the subgroup, and I thoroughly enjoyed working beside him for the past three years. Simone Friedle, the most recent addition, I have enjoyed getting to know during our coffee breaks, and I'm sure will do great things in the diiron modeling subgroup and be an expert on inorganic physical methods upon completion of her degree. Finally my fellow classmate, Sungho Yoon: for four years I had a desk beside "this guy". He is both an amazing scientist and great person. There have not been many that worked harder than he. I appreciate the help with EPR, Mössbauer, SQUID, stopped-flow, and general scientific advice as well as friendship over the years.

At the beginning of my tenure in the Lippard lab, Dan Kopp was very helpful, allowing me to share his space in the bio bay and patiently answering all of my synthetic questions. Scott Hilderbrand, an honorary member of the modeling subgroup, is one of the most handy people I know, and without him, I'd still be assembling my Schlenk line. Leslie Murray, I'm sure, has come to dread when I show up at his desk, but he has been invaluable solving my computer problems and most importantly reconstructing the GC-MS computer. I'd still be doing measurements if it weren't for him. I am grateful for Liz Nolan's unwavering patience and competence in obtaining resonance Raman measurements, and also for Mi Hee Lim's aid with the $^{18}O_2$ experiments and use of her own high vacuum line . In the process of science happening, friendships were also forged, along with our Italian pal Vivianna Izzo, and I know I shall miss them and the many others, including Yongwon Jung, Evan Guggenheim, Matt Clark, Christiana Zhang, and Chris Chang, when I leave the Lippard lab.

On hand in the Lippard lab we have had several X-ray postdocs whose advice has been invaluable. A special thanks to Weiming Bu for teaching me X-ray crystallography beginning at square one - everything from mounting an air-sensitive crystal to solving the data set. Also I appreciate Dr. Peter Müller's help with some "last minute" disorder problems that I could not have tackled on my own.

To Mark and Dave in the Spec lab: thanks for the donuts, the patience, always lending an ear, the help when my research was at a stand-still, and the instrumental advice with NMR and EPR.

To Mr. Alberti, in whose class I was first introduced to those seductive mole-mole calculations, thanks for the induction into chemistry. Dr. Benjamin Brooks and Professor Dean Harman, my mentors at UVA, thank you: Ben, for leading me into the world of synthetic inorganic chemistry and being such a wonderful teacher and Dean for taking a chance on me, welcoming me into his lab, and encouraging me to apply and attend graduate school at MIT.

A special thanks to all of my family and close friends outside of MIT and the world of chemistry. I could not have persevered without you. Alex, our Saturday morning ritual became just that and will be sorely missed, along with your company, when I depart Boston. Mom, Dad, Jack, and Lucy, thanks for always being there and answering the phone, especially in the last six months. I couldn't have done without your support and love.

Finally to my friend Katie and my husband Brec: As I've said before, you guys took opposite fronts, and without Katie at work and Brec at home, I never would have made it through…

Katie, there is so much to thank you for and so many wonderful memories to look back on during our time here together . I know that our friendship is one for life. We've experienced so much together, and my life is better having befriended you.

"Best of Emily and Katie."
Alias recaps. Artemisia Gentileschi. BBQ Fritos. *Barber of Seville*. BCNH's. Bee-Boppin' & Scattin'. BFB. Big KATs. Bio Café Mockingbird. Birding. BLT's. Bobs. Breakfast Sandwich. Bridget Jones. British Bramble. Carrigs, Zimmeramans, Murdochs, & Robinsons. Chewy Sprees. Chick-a-dee-dee-dee. *Cold Mountain*. Cryosurgery. Cup O' Soup. Danglars. Donuts. DMD. Don Giovanni. Dr. Dre. Dr. Olds. DSW. Eh… Eh, Alta! Ernesto's. Farmer Oak. F-that. Felipe's. Flex-points. *Girl with a Pearl Earring. Gone with the Wind*. Matted Chips. Hannibal. Hawk Walk. Henry and Clare. Hines Ward. Hi-Low. Hot Beethoven. Inner Poise. Jack Bristow. Killian Court Statues. Koreana. Mary Magdalene. Michelangelo. Moleskin. Mr. Big. Mr. Darcy. Nerds Ropes. Nutty Bars. Nicky & Coby. Oding. Patriots *vs* Steelers. Paul McCartney. Peanut Butter Cookies. Pittsburgh. Platy & Ferroque. Poop Rockets. Pumpkin Spice Anything. Rebecca's Café. *Red Tent*. Rembrandt van Rijn. Rhett Bulter. Richmond. *Rigoletto*. Sam Adams Summer Ale. Samantha Jones. Saugus. Scarlett O'Hara. Scone Buffet. Second Year Orals. *Secret Life of Bees*. Skizzin' and Strizzin'. SJP. Snoop Dogg. So-jou. Star Wars Calendar. Steven Tyler. Tedi Bruschi. The Coop. The Duke. Joint Thesis Defense! *Time Traveler's Wife*. Third Year Orals. Train Wreck. Old Yeller to the Vineyard. W.A. Mozart. Will Ladislaw. WTF. Z-Center Nemesis. Zen Garden.
Brec, I never would have gotten to this point without you by my side. I'll treasure the memories we've made together in Boston always and look forward to spending the rest of my life with you.

Table of Contents

Chapter 3.   C–H Activation of Benzyl- and Ethyl- Substituted Pyridine Ligands in the

16

17

List of Tables

List of Charts

Chapter 6

List of Schemes

Chapter 1

Chapter 3

Chapter 4

Chapter 5

Chapter 6

23

List of Figures

Chapter 2

Chapter 3

Chapter 4

Chapter 5

Chapter 1

Modeling Carboxylate-Rich Diiron Sites of Dioxygen-Dependent Non-Heme Enzymes

Diiron Cores in Natural Systems

Iron is an essential element for life on planet Earth.[1] As a result and with its large

bioavailability, iron is incorporated into many proteins and enzymes that perform critical

biochemical functions.[2] Carboxylate-rich non-heme diiron centers are a common motif found in

biological systems involved in the activation of dioxygen. Several examples of dioxygen-

dependent metalloproteins are the R2 subunit of ribonucleotide reductase (RNR-R2),[3] soluble

methane monooxygenase (sMMO),[4,5] Δ^9-desaturase (Δ^9D),[6] toluene/o-xylene monooxygenase

(ToMO),[7,8] alkene monooxygenase,[9] and phenol hydroxylase (PH).[10] These enzymes share

similar coordination environments that consist of four carboxylate ligands in both bridging and

terminal binding modes as well as two coordinated histidine residues arranged in a syn

disposition with respect to the Fe–Fe vector. Despite similar coordination environments at the

active sites of these enzymes, a wide range of functions are carried out. Included are the

generation and storage of a tyrosyl radical in RNR-R2, catalytic oxidation of methane to

methanol under ambient conditions in sMMO, insertion of a *cis* double bond into the alkyl chain

of an acyl carrier protein-linked fatty acid in Δ^9-desaturase, hydroxylation of toluene to *o*- and *p*-

cresol in ToMO, epoxidation of alkenes in alkene monooxygenase, and oxidation of phenol to

catechol in PH.[11-14]

Binding Dioxygen to Metal Ions

The need for metal co-factors in biological systems using dioxygen as an oxidant arises

from the inherent properties of the O_2 molecule.[15] Dioxygen is a paramagnetic species with a

$(1s\sigma)^2(1s\sigma*)^2(2s\sigma)^2(2s\sigma*)^2(2p\pi)^4(2p\pi*)^2$ electronic configuration. The reaction of organic

molecules that usually have paired electrons and singlet ground state, with dioxygen is spin

forbidden because of the triplet ground state of O_2. Formation of a metal-O_2 adduct allows for

the interaction of unpaired O_2 electrons with the d electrons of the metal ion, affording a spin-allowed, low-energy pathway for oxidation reactions.[16]

Why Study Monooxygenases?

sMMO and ToMO are members of a larger family of enzymes known as bacterial multicomponent monooxygenases (BMMs). These BMMs catalyze the selective conversion of hydrocarbons to alcohols and can oxidize other substrates including methane derivatives, olefins, amines, and sulfides.[17,18] The carboxylate-bridged non-heme diiron active site housed in the hydroxylase components (MMOH; ToMOH) of MMO and ToMO is responsible for the binding and reductive activation of dioxygen.[8,12,13,19,20] The signature transformation of MMOH, the oxidation of methane to methanol under ambient conditions, is remarkable from a chemical standpoint. A selective catalyst for this reaction would be both of fundamental and practical importance with implications in chemical manufacturing, pollution cleanup, and alternative energy applications, specifically the more efficient exploitation of natural gas.[21-23] The catalytic cycle, pictured in Scheme 1.1, shows the process beginning when electrons are shuttled from the reductase protein to reduce the di(μ-hydroxo)diferric center to the diiron(II) fully reduced active site (MMOH_{red}), which can bind dioxygen. The first spectroscopically characterized intermediate is the diiron(III) peroxo (H_{peroxo}). H_{peroxo} collapses to yield a di(μ-oxo)diiron(IV) high valent intermediate Q which carries out the hydroxylation chemistry, finally returning the dimetallic center to the resting state (MMOH_{ox}).[24]

Probing the Reactivity of Diiron Cores with Model Complexes

The preparation and study of structural, spectroscopic, and functional models for the active sites in metalloproteins can enhance and extend our understanding of the natural systems. In the case of the MMO hydroxylase, the ultimate goal is to obtain carboxylate-bridged diiron

units with the stoichiometry and geometry of the enzyme that can react with dioxygen, generate intermediates analogous to H_{peroxo} and Q, and hydroxylate C–H bonds. The kinetic lability of high-spin ferrous and ferric complexes and their propensity to decompose to unreactive, thermodynamically stable species, makes this chemistry challenging. The important chemical transformations that occur at carboxylate-bridged diiron centers in nature have prompted the synthesis of small molecule model compounds in order to achieve this chemistry in the absence of a protein scaffold.

Sterically Hindering *m*-Terphenyl Carboxylate Ligands

Many diiron complexes using nitrogen and phenolic oxygen ligands have been reported as mimics for the diiron sites in natural systems having carboxylate-rich metal coordination environments.[25-29] However, to understand the factors that relate structure and function of these metalloenzymes, small molecule models containing the (μ-carboxylato)diiron(II) structural motif are desired. The synthesis of such compounds, however, often relies upon self-assembly, which can afford unpredictable and undesired product formation. To isolate discrete dinuclear iron centers, a balance must be achieved in the ligand framework. Too much steric bulk around the metal center yields only mononuclear species, while not enough leads to polymers.[30-36]

A successful route to the synthesis of such biomimetic diiron(II) complexes is afforded by terphenyl-based carboxylate ligands.[37-39] (Chart 1.1) These ligands facilitate the assembly of a dinuclear core, mimic the protective pocket present at the protein active sites, and are flexible enough to accommodate a range of Fe···Fe distances (~2.7 – 4.6 Å). Examination of the model compounds provides insight to guide future strategies for preparing diiron complexes that will fulfill the role as structural, spectroscopic, and function models of the active sites of the metalloenzymes.

Carboxylate-Rich Structural, Spectroscopic, and Functional Models

Structural Models of MMOH$_{red}$

The active site housed in the hydroxylase subunit (MMOH) is a non-heme diiron center surrounded by four carboxylate and two histidine residues.[5,40] In the reduced diiron(II) form of the enzyme (MMOH$_{red}$), the metal centers are bridged by two carboxylates, and two are monodentate, one of which is involved in hydrogen bonding with a coordinated water molecule. In the oxidized resting state of the enzyme, (MMOH$_{ox}$), the diiron(III) center is bridged by only one carboxylate and two hydroxide ions. The other three carboxylates are monodentate, one hydrogen bonded to a coordinated water molecule. Representations of MMOH$_{red}$ and MMOH$_{ox}$ are proffered in Chart 1.2.

Combining the sodium salt of the *m*-terphenyl carboxylate with Fe(OTf)$_2$·2MeCN[41] in THF produces [Fe$_2$(μ-O$_2$CAr^R)$_2$(O$_2$CAr^R)$_2$(THF)$_2$]^{37,42} ((**1**), R = Tol, (**2**) R = 4-FPh) (Chart 1.3) in high yield, which can be used as diiron(II) starting materials in subsequent reactions with N-donor ligands. Depending on the R-substituents of the carboxylates and the ancillary ligands, primarily three structures are isolated, a quadruply bridged "paddlewheel" species with two N-donors, a triply-bridged diiron center with only one N-donor, or a doubly-bridged "windmill" structure with two N-donor ligands.[43] A representation of each commonly occurring geometry is depicted in Chart 1.4.

The interconversion of the paddlewheel and windmill geometries in solution via carboxylate shifts, pictured in Scheme 1.2, was confirmed by ^{19}F NMR studies employing a diiron(II) complex with *p*-fluorophenyl substituted terphenyl carboxylate ligands.[37] Flexibility inherent in a carboxylate shift process opens a coordination site for dioxygen binding, as is proposed during catalysis in the native enzyme.[12,44]

Analogously, the corresponding diiron(II) complex is synthesized with the $^-O_2CAr^{Mes}$ carboxylate ligand in MeCN to yield $[Fe_2(\mu\text{-}O_2CAr^{Mes})_2(O_2CAr^{Mes})_2(MeCN)_2]$ (3), Chart 1.5.[31] However unlike the $^-O_2CAr^{Tol}$ and $^-O_2CAr^{4\text{-}FPh}$ carboxylates, addition of a variety of N-donors to 3 affords only mononuclear ferrous compounds. To ease the steric crowding around the metal centers, an additional methylene unit was introduced between the aryl ring and the benzoate unit ($^-O_2CDXL$, Chart 1.6), and dinuclear paddlewheel compounds were isolated with various ancillary ligands, $[Fe_2(\mu\text{-}O_2CDXL)_4(L)_2]$ where L = THF, py, or MeIm.[45]

Another synthetic challenge has been to position the N-donor ligands syn to the Fe–Fe vector, as occurs in the native systems. Theoretical predictions suggest that the relative orientation of nitrogen donors may influence the reactivity of Q.[13] Development of a 1,2-diethynylbenzene-based dinucleating ligand with quinoline moieties as the N-donors yielded Et_2BCQEB^{Et}, 1,2-bis(3-ethynyl-8-carboxylatequinoline)benzene ethyl ester. When this ligand was combined with 1, $[Fe_2(Et_2BCQEB^{Et})(\mu\text{-}O_2CAr^{Tol})_3]^+$ (4), was produced. A representation of the structure (Chart 1.7) reveals the desired syn coordination of the N-donor atoms.[46]

One aspect of the diiron coordination environment that until recently has only been appreciated through direct studies of the metalloproteins themselves is the effect of water molecules. The importance of water on the oxygenation cycle has primarily been a focus of computational studies and recently the coordinated H_2O molecule, used as a hydrogen-bond donor was considered to be a significant component in forming reactive intermediate(s) upon oxygenation of the diiron(II) site.[13] A recent modeling study has allowed the effects of water-dependent equilibria and the effects of water on the rate of oxygenation of the diiron(II) carboxylate complexes to be addressed.[47] This investigation was facilitated by the introduction of 4-cyanopyridine (4-CNpy) as a ligand which shifts the metal-to-ligand charge-transfer bands of

the starting diiron(II) compounds, $[Fe_2(\mu-O_2CAr^R)_4(4\text{-CNpy})_2]$ and $[Fe_2(\mu-O_2CAr^R)_2$-$(O_2CAr^R)_2(OH_2)_2]$, where R is either Tol or 4-FPh, into the visible region of the spectrum.

Structural Models of MMOH$_{ox}$

The synthesis of complexes with $\{Fe_2(\mu\text{-}OH_2)(\mu\text{-}O_2CR)\}^{3+}$ or $\{Fe_2(\mu\text{-}O)(\mu\text{-}O_2CR)\}^{3+}$

cores, geometries structurally similar to those of diiron(III) sites in oxidized MMOH and RNR-R2, respectively, is a goal of small molecule modeling chemistry. Self assembly of these structures from ferric salts in a carboxylate rich environment is difficult due to the propensity of iron(III) salts to form oligo- or polynuclear iron(III) complexes. Another approach is direct oxygenation of carboxylate-bridged diiron(II) compounds. This tactic mimics the oxidation of the dinuclear ferrous center that occurs at the enzyme active sites to yield the $\{Fe_2(\mu\text{-}OH_2)$-$(\mu\text{-}O_2CR)\}^{3+}$ or $\{Fe_2(\mu\text{-}O)(\mu\text{-}O_2CR)\}^{3+}$ units. The first synthetic analogue of the $\{Fe_2(\mu\text{-}OH)_2$-$(\mu\text{-}O_2CR)\}^{3+}$ core of MMOH$_{ox}$ was synthesized by direct oxygenation of the diiron(II) complex $[Fe_2(\mu-O_2CAr^{Tol})_2(O_2CAr^{Tol})_2(N,N\text{-Bn}_2en)_2]$ **(5)**, where N,N-Bn$_2$en is N,N-dibenzylethylene-diamine, to give **6**, Scheme 1.3.[48,49] Oxygenation of mononuclear $[Fe(O_2CAr^R)_2(Hdmpz)_2]$ **(7)**, where R is either Tol or 4-FPh and Hdmpz is dimethylpyrazole, led to the formation of both the $\{Fe_2(\mu\text{-}OH)_2(\mu\text{-}O_2CR)\}^{3+}$ and $\{Fe_2(\mu\text{-}O)(\mu\text{-}O_2CR)\}^{3+}$ cores, shown in Scheme 1.4, as **8** and **9**, respectively.[50] In the $[Fe_2(\mu-O_2CAr^R)_3(O_2CAr^R)(2\text{-Ph}_2Ppy)]$ system upon reaction with dioxygen, when the carboxylate ligand was the $^-O_2CAr^{Tol}$, a hexanuclear ferric material was isolated, but the $^-O_2CAr^{4\text{-FPh}}$ substituted ferrous complex yielded the $\{Fe_2(\mu\text{-}OH_2)(\mu\text{-}O_2CR)\}^{3+}$ core in $[Fe_2(\mu\text{-}OH)_2(\mu\text{-}O_2CAr^{4FPh})(O_2CAr^{4\text{-FPh}})_3(2\text{-Ph}_2P(O)py)(OH_2)]$ **(10)**, pictured in Scheme 1.5, resembling the oxidized form of MMOH.[51]

Spectroscopic Models of H$_{peroxo}$ and X

The first well-characterized intermediate of the catalytic cycles of MMOH and RNR-R2 following the addition of O$_2$ to the fully reduced diiron site is a peroxo diiron(III) species. The diiron center of the RNR-R2 subunit is oxidized further to form a (μ-oxo)diiron(III, IV) mixed valent species, X,[52-56] whereas the H$_{peroxo}$ is oxidized to a di(μ-oxo)diiron(IV) moiety.[57-59] It is of great interest to mimic this dioxygen reactivity in synthetic complexes to understand the natural system better and allow for the possibility to replicate the reaction chemistry. The H$_{peroxo}$ is identified by its absorption in the UV-visible region at 725 nm (ε = ~1800 M^{-1} cm^{-1}).[60,61] The species is EPR silent,[12] but has a characteristic Mössbauer spectrum of a single quadrupole doublet with an isomer shift of 0.66 mm s^{-1} and a quadrupole splitting of 1.51 mm s^{-1}.[58]

There are several examples of diiron(II) complexes that form diiron(III) peroxo species upon reaction with O$_2$, and a few have even been isolated at low temperature and structurally characterized.[62-68] The coordination environments of these compounds are nitrogen-rich, composed of polyamine/imine donor ligands, quite different from that of the carboxylate rich active sites of MMOH.

There have also been reported several examples of high-valent dioxygen intermediates with diiron complexes containing the *m*-terphenyl carboxylates,$^-$O$_2$CAr^{Mes} and $^-$O$_2$CAr^{Tol}, whose configuration more closely mimic the structure of the active site in the native enzyme. The reaction of **3** with dioxygen at –50 °C forms a (μ-peroxo)diiron(III) species, observed by UV-vis spectroscopy.[31] When the pyridine analogue of the related compound with the $^-$O$_2$CDXL carboxylate is used, an unsymmetrical peroxo species is formed.[45,69]

Exposure of the pyridine or 4-*tert*-butylpyridine analogues of **1** with the $^-$O$_2$CAr^{Tol} carboxylate to dioxygen at –78 °C results in the formation of a broad visible absorption at 660

nm (ε = 1600 M^{-1} cm^{-1}) or 670 nm (ε = 1700 M^{-1} cm^{-1}), respectively. EPR and Mössbauer

spectroscopic studies revealed the presence of equimolar amounts of valence-delocalized Fe^{II}Fe^{III}

and valence-trapped Fe^{III}Fe^{IV} species as the major components of these dark green

intermediates.[70] The electronic absorption bands are assigned to intervalence charge transfer

transitions of diiron(II,III) cations.[71] The spectroscopic and reactivity properties of the Fe^{III}Fe^{IV}

species are similar to those of the intermediate X in the RNR-R2 catalytic cycle. Similar low

temperature dioxygen reactivity was also observed with the *p*-methoxybenzylamine, 1-amino-5-

pentyne, 4-benzylpyridine, and 4-pyridyldiphenylphosphine analogues of **1**.[72-74] When 2-

ethylpyridine was employed as the N-donor in another analogue of **1**, an intermediate bearing

much resemblance to the H$_{peroxo}$ was observed. The UV-visible absorption band of this species at

−78 °C, was centered at 725 nm, ε = 1400 M^{-1} cm^{-1}. Investigation by EPR, Mössbauer, and

resonance Raman spectroscopy, however, failed to confirm the existence of a peroxo diiron(III)

species; the data were consistent with a mixed valent Fe^{II}Fe^{III} species.[75]

Functional Models of MMOH

The ultimate goal in modeling the BMM systems is to mimic the chemistry of the native

enzyme. There are several examples[39] of substrate oxidation by dioxygen activated diiron(II)

complexes, but rarely with the coordination environment found in the active site of the

monooxygenase. In the carboxylate-rich systems with diaryl substituted benzoate ligands, a few

examples of substrate oxidation have been reported. Oxidative N-dealkylation of a tethered

benzyl substituent occurs when 5 reacts with dioxygen, Scheme 1.3.[48,49] Confirmation that >90%

of the oxygen in the benzaldehyde product originates from dioxygen was obtained by ^{18}O-

labeling studies. The proposed mechanism for this process, based on Hammett and KIE$_{intra}$

analyses, involves a single-electron transfer from a non-bonding electron pair in the dangling

amine substrate to the generated intermediate, followed by proton transfer and rearrangement.[49,76]

Benzaldehyde is also evolved from intramolecular benzylic oxidation of one of the amine ligands for both $[Fe_2(\mu\text{-}O_2CAr^{Tol})_4(BA)_2]$ and $[Fe_2(\mu\text{-}O_2CAr^{Tol})_4(BA^{p\text{-}OMe})_2]$, where BA is benzylamine and $BA^{p\text{-}OMe}$ is p-methoxybenzylamine, upon reaction with dioxygen.[72] Due to the absence of a lone pair of electrons in the benzylamine ligands, the mechanism adopted by **5** is eliminated as a possibility. Stepwise oxygen recoil/rebound and a concerted mechanism are still viable options.

This strategy to use tethered substrates as ligands has been extended to include phosphino-, sulfido-, benzyl-, or ethyl-derivatized pyridines. The substrates are brought into close proximity to the carboxylate-bridged diiron(II) center through coordination of the N-donor ligand. The position of substitution affects both the geometry of the starting diiron(II) complex and the subsequent chemistry following exposure to dioxygen. The nature of the substrate also affects the extent of oxidation.[43]

The overall goals of modeling the active sites of non-heme diiron enzymes are to develop structural, functional, and spectroscopic archetypes to understand the chemistry occurring in the natural system. The terphenyl-based carboxylate ligands have provided the scaffold for assembling dimetallic cores capable of carrying on the bio-inspired transformations. Progress towards these ultimate goals using the approaches outlined above are presented in this dissertation which was undertaken to create synthetic models of the carboxylate-bridged diiron centers in MMOH that reproduce the coordination sphere, physical properties, and function of the natural system. The first half of this current work focuses on C–H activation while the second part concentrates on oxygen-atom transfer. Chapter 2 explores the synthesis and

dioxygen reactivity of carboxylate-rich diiron(II) complexes with alkyl amine ligands. In chapter 3 benzyl- and ethylpyridine derivatives serve as ancillary ligands for dioxygen-sensitive diiron(II) compounds to probe intramolecular oxidation of the N-donor species. A low temperature O_2-dependent intermediate is studied by various spectroscopic techniques in chapter 4 with the hope of determining the nature of the species formed. The exploration of the intramolecular oxidation of dangling sulfido and phosphino substrates tethered to N-donor ligands in carboxylate-rich diiron(II) complexes is the subject of chapters 5 and 6.

References

(1)   Greenwood, N. N.; Earnshaw, A. *Chemistry of the Elements*; 2nd ed.; Oxford University Press: New York, 2002.

(2)   Holm, R. H.; Kennepohl, P.; Soloman, E. I. *Chem. Rev.* **1996**, *96*, 2239-2314.

(3)   Logan, D. T.; Su, X.-D.; Åberg, A.; Regnström, K.; Hajdu, J.; Eklund, H.; Nordlund, P. *Structure* **1996**, *4*, 1053-1064.

(4)   Elango, N.; Radhakrishnan, R.; Froland, W. A.; Wallar, B. J.; Earhart, C. A.; Lipscomb, J. D.; Ohlendorf, D. H. *Protein Sci.* **1997**, *6*, 556-568.

(5)   Whittington, D. A.; Lippard, S. J. *J. Am. Chem. Soc.* **2001**, *123*, 827-838.

(6)   Lindqvist, Y.; Huang, W.; Schneider, G.; Shanklin, J. *EMBO J.* **1996**, *15*, 4081-4092.

(7)   Pikus, J. D.; Studts, J. M.; Achim, C.; Kauffmann, K. E.; Münck, E.; Steffan, R. J.; McClay, K.; Fox, B. G. *Biochemistry* **1996**, *35*, 9106-9119.

(8)   Sazinsky, M. H.; Bard, J.; Donato, A. D.; Lippard, S. J. *J. Biol. Chem.* **2004**, *279*, 30600-30610.

(9)   Small, F. J.; Ensign, S. A. *J. Biol. Chem.* **1997**, *272*, 24913-24920.

(10)   Cadieux, E.; Vrajmasu, V.; Achim, C.; Powlowski, J.; Munck, E. *Biochemistry* **2002**, *41*.

(11)   Stubbe, J. *Curr. Opin. Chem. Biol.* **2003**, *7*, 183-188.

(12)   Merkx, M.; Kopp, D. A.; Sazinsky, M. H.; Blazyk, J. L.; Müller, J.; Lippard, S. J. *Angew. Chem., Int. Ed. Engl.* **2001**, *40*, 2782-2807.

(13)   Baik, M.-H.; Newcomb, M.; Friesner, R. A.; Lippard, S. J. *Chem. Rev.* **2003**, *103*, 2385-2419.

(14)   Yang, Y.-S.; Broadwater, J. A.; Pulver, S. C.; Fox, B. G.; Soloman, E. I. *J. Am. Chem. Soc.* **1999**, *121*, 2770-2783.

(15)   Jones, R. D.; Summerville, D. A.; Basolo, F. *Chem. Rev.* **1979**, *79*, 139-179.

(16)   Punniyamurthy, T.; Velusamy, S.; Iqbal , J. *Chem. Rev.* **2005**, *105*, 2329 -2364.

(17)   Colby, J.; Stirling, D. I.; Dalton, H. *Biochem. J.* **1977**, *165*, 395-402.

(18)   Fuse, H.; Ohta, M.; Takimura, O.; Murakami, K.; Inoue, H.; Yamaoka, Y.; Oclarit, J. M.; Omori, T. *Biosci. Biotechnol. Biochem.* **1998**, *62*, 1925-1931.

(19)   Feig, A. L.; Lippard, S. J. *Chem. Rev.* **1994**, *94*, 759-805.

(20)   Wallar, B. J.; Lipscomb, J. D. *Chem. Rev.* **1996**, *96*, 2625-2657.

(21)   Vardar, G.; Wood, T. K. *Appl. Environ. Microbiol* **2004**, *70*, 3253-3161.

(22)   Erwin, D. P.; Erickson, I. K.; Delwiche, M. E.; Colwell, F. S.; Strap, J. L.; Crawford, R. L. *Appl. Environ. Microbiol* **2005**, *71*, 2016-2024.

(23)   Periana, R. A.; Taube, D. J.; Evitt, E. R.; Loffler, D. G.; Wentrcek, P. R.; Voss, G.; Masuda, T. *Science* **1993**, *259*, 340-343.

(24)   Kopp, D. A.; Lippard, S. J. *Curr. Opin. Chem. Biol.* **2002**, *6*, 568-576.

(25)   Hartman, J. R.; Rardin, R. L.; Chaudhuri, P.; Pohl, K.; Wieghardt, K.; Nuber, B.; Weiss, J.; Papaefthymiou, G. C.; Frankel, R. B.; Lippard, S. J. *J. Am. Chem. Soc.* **1987**, *109*, 7387–7396.

(26)   Holz, R. C.; Elgren, T. E.; Pearce, L. L.; Zhang, J. H.; O'Connor, C. J.; Que, L., Jr. *Inorg. Chem.* **1993**, *32*, 5844-5850.

(27)   Dong, Y.; Ménage, S.; Brennan, B. A.; Elgren, T. E.; Jang, H. G.; Pearce, L. L.; Que, L., Jr. *J. Am. Chem. Soc.* **1993**, *115*, 1851-1859.

(28)   Que, L., Jr.; Dong, Y. *Acc. Chem. Res.* **1996**, *29*, 190-196.

(29)   Que, L., Jr. *J. Chem. Soc., Dalton Trans.* **1997**, 3933-3940.

(30)   Lee, D.; Lippard, S. J. *Inorg. Chim. Acta* **2002**, *341*, 1-11.

(31) Hagadorn, J. R.; Que, L., Jr.; Tolman, W. B. *J. Am. Chem. Soc.* **1998**, *120*, 13531-13532.

(32) Lee, D.; Sorace, L.; Caneschi, A.; Lippard, S. J. *Inorg. Chem.* **2001**, *40*, 6774-6781.

(33) Mandal, S. K.; Young, V. G., Jr.; Que, L., Jr. *Inorg. Chem.* **2000**, *39*, 1831-1833.

(34) Herold, S.; Lippard, S. J. *J. Am. Chem. Soc.* **1997**, *119*, 145-156.

(35) Goldberg, D. P.; Telser, J.; Bastos, C. M.; Lippard, S. J. *Inorg. Chem.* **1995**, *34*, 3011-3024.

(36) Rardin, R. L.; Poganiuch, P.; Bino, A.; Goldberg, D. P.; Tolman, W. B.; Liu, S.; Lippard, S. J. *J. Am. Chem. Soc.* **1992**, *114*, 5240-5249.

(37) Lee, D.; Lippard, S. J. *Inorg. Chem.* **2002**, *41*, 2704-2719.

(38) Tolman, W. B.; Que, L., Jr. *J. Chem. Soc., Dalton Trans.* **2002**, 653-660.

(39) Tshuva, E. Y.; Lippard, S. J. *Chem. Rev.* **2004**, *104*, 987-1012.

(40) Rosenzweig, A. C.; Frederick, C. A.; Lippard, S. J.; Nordlund, P. *Nature* **1993**, *366*, 537-543.

(41) Hagen, K. S. *Inorg. Chem* **2000**, *39*, 5867-5869.

(42) Lee, D.; Lippard, S. J. *J. Am. Chem. Soc.* **1998**, *120*, 12153-12154.

(43) Carson, E. C.; Lippard, S. J. *J. Am. Chem. Soc.* **2004**, *126*, 3412-3413.

(44) Rardin, R. L.; Tolman, W. B.; Lippard, S. J. *New J. Chem.* **1991**, *15*, 417-430.

(45) Chavez, F. A.; Ho, R. Y. N.; Pink, M.; Young, V. G., Jr.; Kryatov, S. V.; Rybak-Akimova, E. V.; Andres, H.; Münck, E.; Que, L., Jr.; Tolman, W. B. *Angew. Chem. Int. Ed. Engl.* **2002**, *41*, 149-152.

(46) Kuzelka, J.; Farrell, J. R.; Lippard, S. J. *Inorg. Chem.* **2003**, *42*, 8652-8662.

(47) Yoon, S.; Lippard, S. J. *J. Am. Chem. Soc.* **2005**, *127*, 8386-8397.

(48) Lee, D.; Lippard, S. J. *J. Am. Chem. Soc.* **2001**, *123*, 4611-4612.

(49)   Lee, D.; Lippard, S. J. *Inorg. Chem.* **2002**, *41*, 827-837.

(50)   Yoon, S.; Lippard, S. J. *J. Am. Chem. Soc.* **2004**, *126*, 2666-2667.

(51)   Carson, E. C. In *Doctoral Dissertation in Inorganic Chemistry*; Massachusetts Institute of
         Technology: Cambridge, MA, 2005; Chapter 6.

(52)   Ravi, N.; Bollinger, J. M., Jr.; Huynh, B. H.; Edmondson, D. E.; Stubbe, J. *J. Am. Chem.
         Soc.* **1994**, *116*, 8007-8014.

(53)   Bollinger, J. M., Jr.; Tong, W. H.; Ravi, N.; Huynh, B. H.; Edmondson, D. E.; Stubbe, J.
         J. Am. Chem. Soc. **1994**, *116*, 8015–8023.

(54)   Sturgeon, B. E.; Burdi, D.; Chen, S.; Huynh, B. H.; Edmondson, D. E.; Stubbe, J.;
         Hoffman, B. M. *J. Am. Chem. Soc.* **1996**, *118*, 7551-7557.

(55)   Burdi, D.; Sturgeon, B. E.; Tong, W. H.; Stubbe, J.; Hoffman, B. M. *J. Am. Chem. Soc.*
         1996, *118*, 281-282.

(56)   Willems, J.-P.; Lee, H.-I.; Burdi, D.; Doan, P. E.; Stubbe, J.; Hoffman, B. M. *J. Am.
         Chem. Soc.* **1997**, *119*, 9816-9824.

(57)   Lee, S.-K.; Fox, B. G.; Froland, W. A.; Lipscomb, J. D.; Münck, E. *J. Am. Chem. Soc.*
         1993, *115*, 6450-6451.

(58)   Liu, K. E.; Valentine, A. M.; Wang, D.; Huynh, B. H.; Edmonson, D. E.; Salifoglou, A.;
         Lippard, S. J. *J. Am. Chem. Soc.* **1995**, *117*, 10174-10185.

(59)   Shu, L.; Nesheim, J. C.; Kauffmann, K.; Münck, E.; Lipscomb, J. D.; Que, L., Jr. *Science*
         1997, *275*, 515-518.

(60)   Valentine, A. M.; Stahl, S. S.; Lippard, S. J. *J. Am. Chem. Soc.* **1999**, *121*, 3876-3887.

(61)   Beauvais, L. G.; Lippard, S. J. *J. Am. Chem. Soc.* **2005**, *127*, 7370-7378.

(62)   Kim, K.; Lippard, S. J. *J. Am. Chem. Soc.* **1996**, *118*, 4914-4915.

(63) Ookubo, T.; Sugimoto, H.; Nagayama, T.; Masuda, H.; Sato, T.; Tanaka, K.; Maeda, Y.; Okawa, H.; Hayashi, Y.; Uehara, A.; Suzuki, M. *J. Am. Chem. Soc.* **1996**, *118*, 701-702.

(64) Dong, Y.; Yan, S.; Young, V. G., Jr.; Que, L., Jr. *Angew. Chem., Int. Ed. Engl.* **1996**, *35*, 618-620.

(65) Zheng, H.; Zang, Y.; Dong, Y.; Young, V. G. J.; Que, L. J. *J. Am. Chem. Soc.* **1999**, *1999*, 2226-2235.

(66) Kodera, M.; Taniike, Y.; Itoh, M.; Tanahashi, Y.; Shimakoshi, H.; Kano, K.; Hirota, S.; Iijima, S.; Ohba, M.; Okawa, H. *Inorg. Chem* **2001**, *40*, 4821-4822.

(67) Costas, M.; Cady, C. W.; Kryatov, S. V.; Ray, M.; Ryan, M. J.; Rybak-Akimova, E. V.; Que, L., Jr. *Inorg. Chem.* **2003**, *42*, 7519-7530.

(68) Kryatov, S. V.; Rybak-Akimova, E. V. *Chem. Rev.* **2005**, *105*, 2175-2226.

(69) Kryatov, S. V.; Chavez, F. A.; Reynolds, A. M.; Rybak-Akimova, E. V.; Que, L., Jr.; Tolman, W. B. *Inorg. Chem.* **2004**, *43*, 2141-2150.

(70) Lee, D.; Pierce, B.; Krebs, C.; Hendrich, M. P.; Huynh, B. H.; Lippard, S. J. *J. Am. Chem. Soc.* **2002**, *124*, 3993-4007.

(71) Lee, D.; Du Bois, J.; Petasis, D.; Hendrich, M. P.; Krebs, C.; Huynh, B. H.; Lippard, S. J. *J. Am. Chem. Soc.* **1999**, *121*, 9893–9894.

(72) Yoon, S.; Lippard, S. J. *Inorg. Chem.* **2003**, *42*, 8606-8608.

(73) Carson, E. C. In *Doctoral Dissertation in Inorganic Chemistry*; Massachusetts Institute of Technology: Cambridge, MA, 2005; Chapter 2.

(74) Carson, E. C.; Lippard, S. J. Unpublished results.

(75) Carson, E. C. *Doctoral Dissertation in Inorganic Chemistry*; Massachusetts Institute of Technology: Cambridge, MA, 2005; Chapter 4.

(76)   Yoon, S.; Lippard, S. J. **2004**, Submitted for publication.

Chart 1.1.

$Ar^{Mes}CO_2H$ $Ar^{Xyl}CO_2H$ $Ar^{Tol}CO_2H$ $Ar^{4\text{-}FPh}CO_2H$

Chart 1.2.

$MMOH_{red}$ $MMOH_{ox}$

Chart 1.3.

R = Tol, **1**
R = 4-FPh, **2**

Chart 1.4.

Paddlewheel   Triply-bridged   Windmill

Chart 1.5.

3

Chart 1.6.

DXLCO$_2$H

Chart 1.7.

4
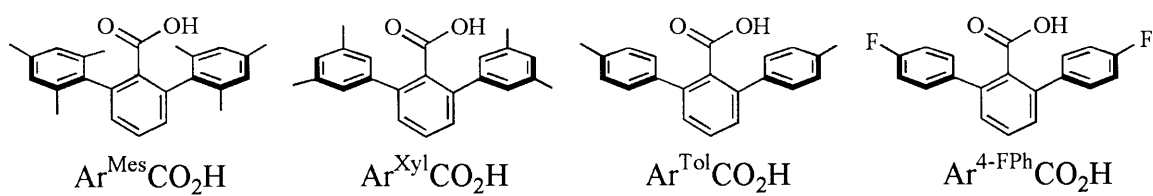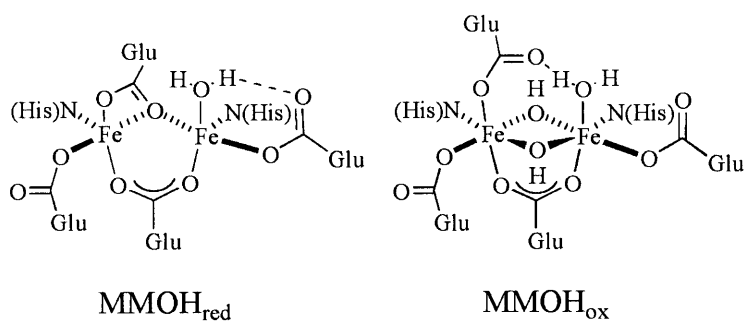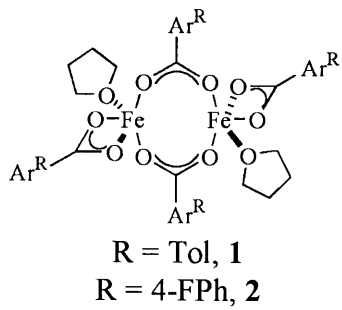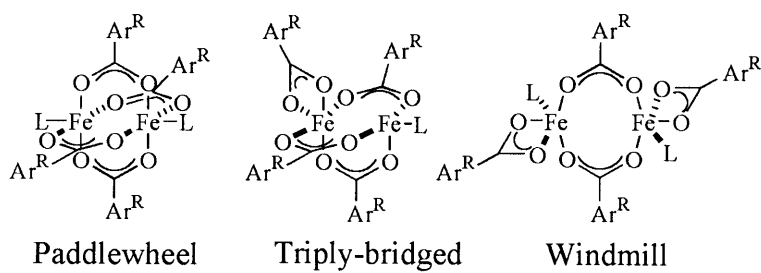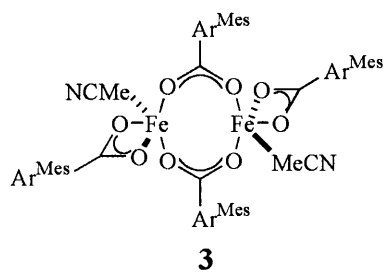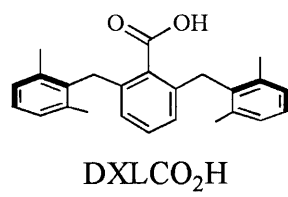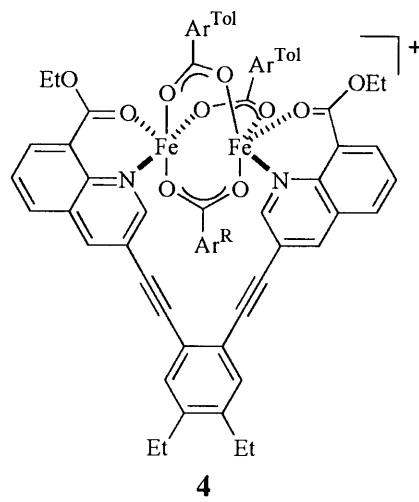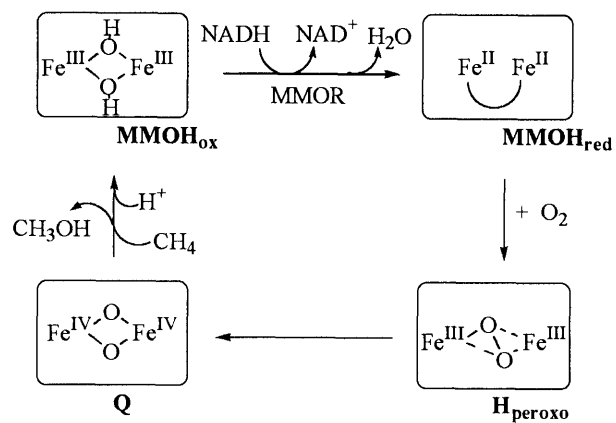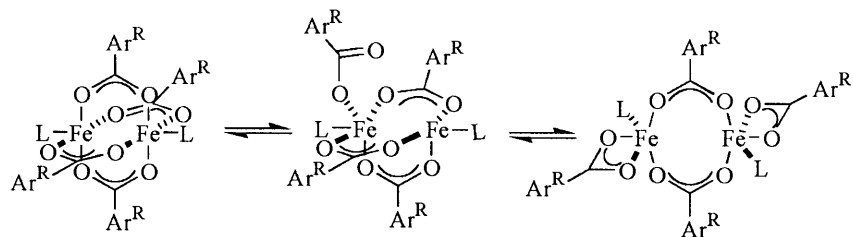
Scheme 1.1.

Scheme 1.2.

Scheme 1.3.
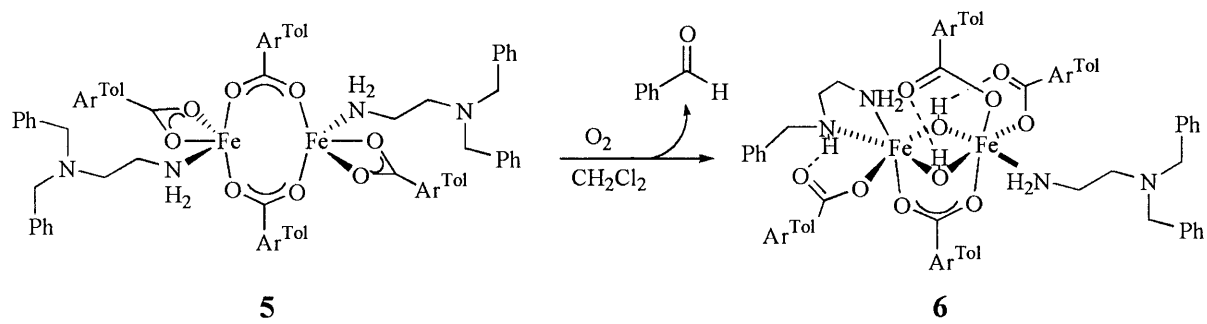
Scheme 1.4.

Scheme 1.5.

10
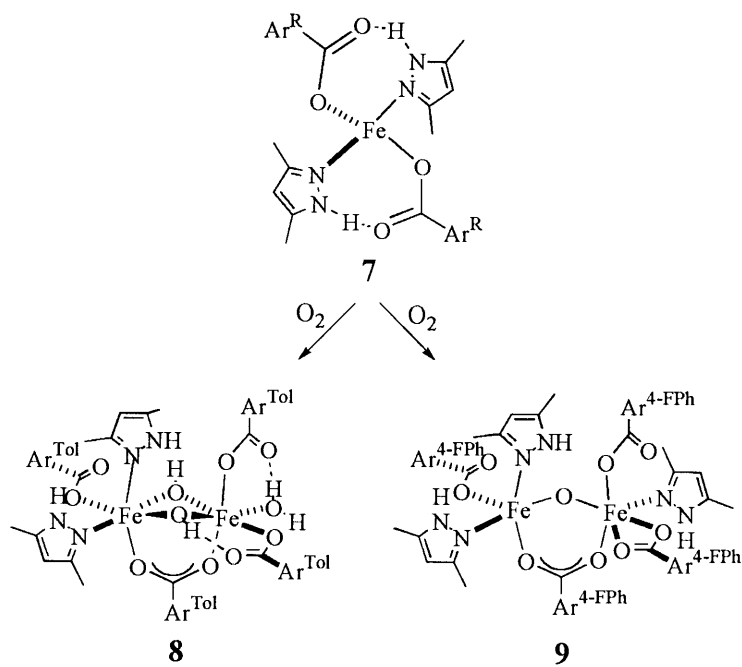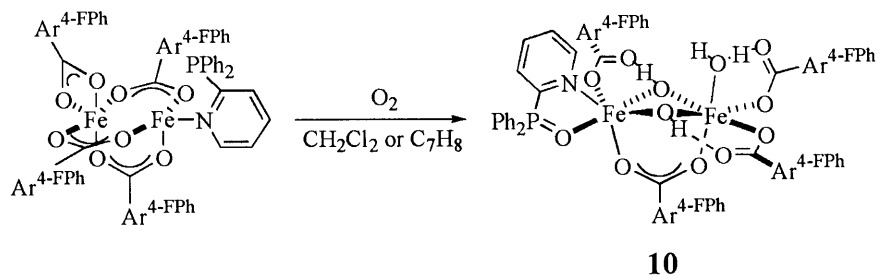
Chapter 2

Synthesis and Oxidation of Carboxylate-Bridged Diiron(II) Complexes

with Substrates Tethered to Primary Alkyl Amine Ligands

Introduction

Non-heme diiron monooxygenases comprise an important family of dioxygen-activating enzymes that can perform the selective oxidation of hydrocarbons under ambient conditions. The diiron core contained in the hydroxylase component (MMOH) of soluble methane monooxygenase, for example can bind and activate dioxygen to convert methane selectively to methanol.[1-4] Four carboxylate and two histidine ligand coordinate two iron atoms and allow for the formation of high-valent intermediates necessary to achieve this chemistry. MMOH can oxidize other substrates including methane derivatives, olefins, alkynes, amines, and sulfides.[5-9]

Inspired by the chemistry performed at the active site of MMOH, we and others have synthesized small molecule mimics of these enzyme cores to elucidate possible functional intricacies of the oxidation mechanism occurring at the diiron site. Application of terphenyl-based carboxylates as ligands for iron(II) provides access to the desired dinuclear core and a surrounding protective sheath such as that in the protein.[10-13]

Previous research focused on the design and synthesis of model complexes that activate dioxygen for the oxidation of external substrates.[1,14] In the diiron(II) complexes [Fe$_2$(μ-O$_2$CAr^{Tol})$_2$(O$_2$CAr^{Tol})$_2$(N,N-Bn$_2$en)$_2$][15,16] and [Fe$_2$(μ-O$_2$CAr^{Tol})$_4$(BA$^{p\text{-}OMe}$)$_2$],[17] where Ar^{Tol}CO$_2^-$ is 2,6-di(p-tolyl)benzoate, N,N-Bn$_2$en is N,N-dibenzylethylenediamine, and BA$^{p\text{-}OMe}$ is p-methoxy-benzylamine, the potential substrate was incorporated as part of a terminal N-donor ligand. Upon reaction with dioxygen, intramolecular benzylic oxidation occurred, followed by N-dealkylation to afford benzylaldehyde.

Presented here are a series of related diiron(II) compounds in which the substrate tethered to the N-donor ligands and the m-terphenyl group substituents are varied. These variations significantly alter the reactivity of the complexes toward dioxygen. The syntheses and structural

characterization of the compounds $[Fe_2(\mu\text{-}O_2CAr^{Tol})_4(NH_2(CH_2)_2SBn)_2]$ (**1**), $[Fe_2(\mu\text{-}O_2CAr^{Tol})_4\text{-}$

$(NH_2(CH_2)_3SCH_3)_2]$ (**2**), $[Fe_2(\mu\text{-}O_2CAr^{Tol})_4(NH_2(CH_2)_3CCH_3)_2]$ (**3**), $[Fe_2(\mu\text{-}O_2CAr^{Xyl})_2\text{-}$

$(O_2CAr^{Xyl})_2(NH_2(CH_2)_3SCH_3)_2]$ (**4**), and $[Fe(\mu\text{-}O_2CAr^{Xyl})_2(O_2CAr^{Xyl})_2\text{-}(NH_2(CH_2)_3CCH)_2]$ (**5**)

are reported. The diiron(II) center of **2** was further investigated by Mössbauer and EPR

spectroscopy. The influence of the differing carboxylate and N-donor ligands on the dioxygen

reactivity was examined by EPR and UV-visible spectroscopic studies as well as by X-ray

crystallographic analysis of a final iron(III) reaction product. A comparison is made of the

reactivity of the reported compounds with that of related systems containing alkyl amine ligands.

Experimental Section

General Considerations. All reagents were obtained from commercial suppliers and

used as received, unless otherwise noted. Dichloromethane, acetonitrile, diethyl ether (Et_2O), and

pentane were saturated with nitrogen and purified by passage through activated Al_2O_3 columns

under argon.[18] Dioxygen (99.994%, BOC Gases) was dried by passing the gas stream through a

column of Drierite. The compounds 1-amino-5-pentyne $(NH_2(CH_2)_3CCH)$,[19,20]

$Fe(OTf)_2\cdot2MeCN$,[21] and $[Fe_2(\mu\text{-}O_2CAr^{Tol})_2(O_2CAr^{Tol})_2(THF)_2]$,[22] were prepared as described in

the literature. 2,6-Di(3,5-dimethylphenyl)benzoic acid $(Ar^{Xyl}CO_2H)$ was synthesized by a

procedure analogous to that used to make 2,6-di(p-tolyl)benzoic acid,[23-25] and the purity was

checked by ^1H NMR spectroscopy. The sodium salt of this compound, NaO_2CAr^{Xyl}, was

prepared by treating a MeOH solution of $Ar^{Xyl}CO_2H$ with 1.1 equiv of NaOH and removing the

volatile fractions under reduced pressure. Full conversion of the acid to the sodium salt was

confirmed by FT-IR spectroscopy. 2-Benzylsulfanyl-ethylamine $(NH_2(CH_2)_2SBn)$ was obtained

by neutralizing its HCl salt with $NaOCH_3$ followed by vacuum distillation. Air-sensitive

manipulations were carried out under nitrogen in an Mbraun drybox. All samples were crushed

and thoroughly dried to remove solvent prior to determining their elemental composition. Acceptable analytical data were never obtained for **5** and **6** despite the crystallinity of the samples.

[Fe$_2$(μ-O$_2$CAr^{Tol})$_4$(NH$_2$(CH$_2$)$_2$SBn)$_2$] **(1)**. A CH$_2$Cl$_2$ solution (5 mL) of [Fe$_2$(μ-O$_2$CAr^{Tol})$_2$(O$_2$CAr^{Tol})$_2$(THF)$_2$] (60.6 mg, 0.0415 mmol) was combined with NH$_2$(CH$_2$)$_2$SBn (20.2 mg, 0.121 mmol) with stirring for 20 min. The solvent was removed in vacuo, and the residue was extracted into dichloroethane (DCE) (4 mL). Pentane vapor diffusion into the DCE solution yielded X-ray quality green crystals of **1** (78.5 mg, 70%). FT-IR (KBr, cm^{-1}): 3318 (m), 3267 (m), 3079 (w), 3044 (w), 3021 (w), 2915 (w), 2859 (w), 1947 (w), 1882 (w), 1608 (s), 1583 (m), 1549 (m), 1513 (s), 1493 (w), 1439 (s), 1403 (s), 1383 (s), 1303 (w), 1237 (w), 1183 (w), 1148 (w), 1108 (w), 1071 (w), 1043 (m), 1020 (w), 989 (w), 913 (w), 841 (s), 812 (s), 787 (s), 761 (m), 705 (s), 584 (m), 557 (w), 525 (s), 463 (w). Anal. Calcd. for C$_{102}$H$_{94}$N$_2$Fe$_2$O$_8$S$_2$: C, 74.17; H, 5.74; N, 1.70. Found: C, 73.90; H, 5.64; N, 1.68.

[Fe$_2$(μ-O$_2$CAr^{Tol})$_4$(NH$_2$(CH$_2$)$_3$SCH$_3$)$_2$] **(2)**. Dropwise addition of 3-methylsulfanyl-propylamine (NH$_2$(CH$_2$)$_3$SCH$_3$) (30.2 mg, 0.287 mmol) to a stirred CH$_2$Cl$_2$ (4 mL) solution of [Fe$_2$(μ-O$_2$CAr^{Tol})$_2$(O$_2$CAr^{Tol})$_2$(THF)$_2$] (108.6 mg, 0.0745 mmol) produced a pale green solution that was stirred for 15 min. Diethyl ether vapor diffusion into the reaction mixture yielded green crystals (78.9 mg, 69%) of **2** suitable for X-ray diffraction study. FT-IR (KBr, cm^{-1}): 3318 (w), 3270 (w), 3048 (w), 3022 (w), 2916 (w), 2860 (w), 1608 (s), 1585 (m), 1551 (m), 1514 (s), 1441 (s), 1404 (s), 1384 (s), 1304 (w), 1187 (w), 1146 (w), 1109 (w), 1020, 842 (w), 814, 791 (m), 764 (w), 706 (m), 584 (w), 525 (m), 463 (m). Anal. Calcd. for C$_{92}$H$_{90}$N$_2$Fe$_2$O$_8$S$_2$: C, 72.34; H, 5.94; N, 1.83. Found: C, 72.26; H, 6.05; N, 1.81.

[Fe$_2$(μ-O$_2$CAr^{Tol})$_4$(NH$_2$(CH$_2$)$_3$CCH)$_2$] (3). Displacement of THF from [Fe$_2$(μ-O$_2$C-Ar^{Tol})$_2$(O$_2$CAr^{Tol})$_2$(THF)$_2$] (89.8, 0.0614 mmol) by NH$_2$(CH$_2$)$_3$CCH (20.8 mg, 0.0250 mmol) yielded a bright green solution. Vapor diffusion of diethyl ether into the reaction mixture produced green crystals (86.8 g, 95%) of **3**, identified by a low resolution X-ray crystal structure FT-IR (KBr, cm^{-1}): 3319 (m), 3285 (m), 3269 (m), 3048 (w), 3021 (w), 2115 (w), 2019 (m), 2861 (w), 2117 (w), 1608 (s), 1585 (m), 1551 (m), 1514 (s), 1451 (m), 1404 (s), 1384 (s), 1304 (w), 1181 (w), 1109 (w), 1020 (w), 842 (w), 814 (m), 790 (m), 764 (w), 705 (m), 641 (w), 584 (w), 525 (m), 463 (w). Anal. Calcd. for C$_{94}$H$_{86}$N$_2$Fe$_2$O$_8$: C, 76.11; H, 5.84; N, 1.89. Found: C, 76.38; H, 5.66; N, 2.02.

[Fe$_2$(μ-O$_2$CAr^{Xyl})$_2$(O$_2$CAr^{Xyl})$_2$(NH$_2$(CH$_2$)$_3$SCH$_3$)$_2$] (4). To a stirred CH$_2$Cl$_2$ (12 mL) solution of Fe(OTf)$_2$·2MeCN (116 mg, 0.266 mmol), NH$_2$(CH$_2$)$_3$SCH$_3$ (33.8 mg, 0.321 mmol) in CH$_2$Cl$_2$ (1 mL) was added dropwise, followed by the NaO$_2$CAr^{Xyl} (195 mg, 0.554 mmol) to form a yellow-orange slurry that was allowed to react overnight. A white precipitate was removed by filtration, and diffusion of diethyl ether vapor into the filtrate yielded pale yellow crystals of **4** (83.3 mg, 38%) that were suitable for X-ray diffraction. FT-IR (KBr, cm^{-1}): 3316, (m), 3266 (m), 3004, (w), 2941 (w), 2915 (m), 2871 (w), 1581 (s), 1564 (s), 1530 (s), 1455 (s), 1424 (s), 1390 (s), 1307 (w), 1037 (w), 1021 (w), 902 (w), 858 (s), 824 (w), 806 (m), 786 (m), 764 (m), 753 (w), 704 (s), 690 (m), 682 (m), 588 (w), 471 (w), 448 (w). Anal. Calcd. for C$_{100}$H$_{106}$N$_2$Fe$_2$O$_8$S$_2$: C, 73.25; H, 6.52; N, 1.71. Found: C, 72.91; H, 6.51; N, 1.89.

[Fe(μ-O$_2$CAr^{Xyl})$_2$(O$_2$CAr^{Xyl})$_2$(NH$_2$(CH$_2$)$_3$CCH)$_2$] (5). A yellow-orange slurry was formed when NH$_2$(CH$_2$)$_3$CCH (54.1 mg, 0.651 mmol) in MeCN (1 mL), followed by NaO$_2$CAr^{Xyl} (326 mg, 0.926 mmol), were added to a stirred MeCN (15 mL) solution of Fe(OTf)$_2$·2MeCN (201 mg, 0.461 mmol). The resultant mixture was stirred overnight, after

which the solvent was removed under vacuum, and the residue was extracted into CH_2Cl_2 and stirred for 10 min. A white precipitate was removed by filtration, and vapor diffusion of diethyl ether into the filtrate yielded pale yellow crystals (199 mg, 54%) that were suitable for X-ray diffraction. FT-IR (KBr, cm^{-1}): 3334 (w), 3308 (w), 3243 (m), 3023 (w), 2914 (m), 2860 (w), 2115 (w), 1581(s), 1455 (m), 1415 (m), 1372 (s), 1331 (m), 1148 (m), 1103 (m), 1040 (m), 989 (m), 852 (s), 813 (m), 787 (m), 746 (w), 702 (s), 681 (m), 660 (w), 646 (w), 623 (w), 549 (w), 499 (w), 446 (w).

[Fe(O$_2$CAr^{Xyl})$_3$(NH$_2$(CH$_2$)$_3$CCH)$_2$] (6). Dry dioxygen (1 atm) was bubbled through a CH_2Cl_2 solution of **5** (70.3 mg, 0.0441 mmol) for 10 min, and the solution was allowed to stir for 20 additional min. The solvent was removed under reduced pressure, the residue was extracted into 2 mL of chlorobenzene, and pentane vapor was diffused into the solution. Yellow needles (13.0 mg, 25%) were isolated and identified to be [Fe(O$_2$CAr^{Xyl})$_3$(NH$_2$(CH$_2$)$_3$CCH)$_2$] (**6**) by X-ray crystallography. FT-IR (KBr, cm^{-1}): 3310 (w), 3298 (m), 3239 (w), 3010 (w), 2915 (m), 2858 (w), 2719 (w), 2119 (w), 1637 (s), 1601 (s), 1577 (m), 1548 (m), 1483 (m), 1456 (m), 1377 (w), 1300 (s), 1135 (s), 1066 (m), 1035 (m), 1011 (m), 902 (w), 870 (w), 852 (s), 825 (w), 808 (s), 781 (w), 757 (m), 705 (s), 634 (m), 611 (w), 474 (s).

X-ray Crystallographic Studies. Intensity data were collected on a Bruker (formerly Siemens) SMART (**2, 3**) or APEX (**1, 4 – 6**) CCD diffractometer with graphite-monochromated Mo Kα radiation (λ = 0.71073 Å), controlled by a Pentium-based PC running the SMART software package.[26,27] Single crystals were mounted on the tips of glass fibers and coated with paratone-N oil. The temperature under a stream of N$_2$ was cooled to −70 °C for data collection of **2 – 3**, cooled to −85 °C for the data collection of **4 – 5**, and maintained by a Bruker LT-2A nitrogen cryostat. For the data collection of **1** and **6**, the temperature under a stream of N$_2$ was

cooled to –100 °C and maintained by a KRYO-FLEX low-temperature apparatus. Data collection and reduction protocols are described elsewhere.[28] The structures were solved by direct or Patterson methods and refined on F^2 by using the SHELXTL-97 software[29] incorporated in the SHELXTL software package.[30] Empirical absorption corrections were applied by using the SADABS program,[31] and the structures were checked for higher symmetry by using the PLATON software.[32] All non-hydrogen atoms were located and their positions refined with anisotropic thermal parameters by least-squares cycles and Fourier syntheses. Hydrogen atoms were assigned to idealized positions and given thermal parameters equivalent to either 1.5 (methyl hydrogen atoms) or 1.2 (all other hydrogen atoms) times the thermal parameter of the carbon atom to which they were attached. The structure of **1** has a half occupied $C_2H_4Cl_2$ molecule in the unit cell, half of which is disordered over two positions, each refined at 50% occupancy. The 2-benzylsulfanyl-ethylamine ligands in **1** and the 3-methylsulfanylpropyl amine ligands in **2** and **4** are disordered over two positions, each refined at 50% occupancy. The diethyl ether molecule in the structure of **5** is located on a special position of twofold symmetry. Data collection and experimental details for the complexes are summarized in Table 2.1 and relevant interatomic bond lengths and angles for **1, 2**, and **4 – 6** are listed in Tables 2.2 and 2.3.

Physical Measurements. FT-IR spectra were recorded on a Bio-Rad FTS 135 instrument for **2** and **3** or a Thermo Nicolet Avatar 360 spectrometer for **1, 4 – 6**. ^{1}H NMR spectra were recorded on a Varian 300 spectrometer housed in the Massachusetts Institute of Technology Department of Chemistry Instrument Facility (MIT DCIF). Chemical shifts were referenced to residual solvent peaks. All spectra were recorded at ambient probe temperature, 293 K.

EPR Spectroscopy. X-band EPR spectra were recorded on a Bruker EMX EPR spectrometer (9.37 GHz) running WinEPR software. The temperature (5 K) was maintained with

an Oxford Instruments EPR 900 cryostat and an ITC503 controller. Samples were prepared under a dinitrogen atmosphere. To obtain spectra of the ferrous compounds, ~300 μL aliquots of 5.3 and 4.6 mM CH_2Cl_2 solutions of **2** and **3** were transferred to EPR tubes in the drybox. The tubes were septum-sealed, the samples were removed from the chamber, and the solutions were frozen at 77 K. To study spectroscopic behavior upon exposure to dioxygen, a separate sealed sample of **3** was cooled to 195 K, exposed to O_2 for 15 s, allowed to react for an additional 30 s, and frozen at 77 K.

^{57}Fe Mössbauer Spectroscopy. Mössbauer spectra were recorded on an MSI spectrometer (WEB Research Co.) with a ^{57}Co source in a Rh matrix maintained at room temperature in the MIT DCIF. A solid sample of **2** was prepared by suspending 0.033 mmol of the pale green powdered material in Apeizon N grease and coating the mixture on the lid of a nylon sample holder. Data were collected at 4.2 K, and the isomer shift (δ) values are reported with respect to natural iron foil that was used for velocity calibration at room temperature. The spectra were fit to Lorentzian lines by using the WMOSS plot and fit program.[33]

UV-visible Spectroscopy. UV-vis spectra were recorded on a Hewlett-Packard 8453 diode array spectrophotometer. Low temperature UV-vis experiments were performed using a custom made quartz cuvette, 1 cm path length, fused into a vacuum jacketed dewar. A solution of **3**, 0.8 mM in CH_2Cl_2 (6 mL) under N_2 in the low T UV-vis cell, was cooled to $-78\ ^{o}C$. Dried O_2 was purged through the solution for 60 s, and the UV-vis spectra were recorded at various time intervals.

Oxidation Product Analyses. Oxidation reactions were performed by exposing a CH_2Cl_2 solution of **1 – 5** to dioxygen overnight. All samples were prepared in an anaerobic glove box prior to dried dioxygen bubbling. For analysis of the products from the oxygenation

reactions, it was necessary to remove iron from the solutions. Silica gel and NH_4OH were employed for this purpose. The oxygenated solution of **1** was passed through a plug of silica gel, eluting the organic species with CH_2Cl_2. Addition of NH_4OH to the reaction solutions of **2 – 5** resulted in two layers; the ligands were extracted into the organic layer with CH_2Cl_2 and the basic layer was washed twice more with CH_2Cl_2. In both methods the solvent was then removed in vacuo and products were identified by NMR spectroscopy and/or GC-MS by comparing their properties with those of authentic samples. The amount of oxidized ligand obtained was quantified by GC-MS using 2-bromonaphthalene as an internal standard for **1**. Control experiments established that, in the absence of the diiron(II) complexes, neither dioxygen saturated CH_2Cl_2 nor the workup procedure induced significant ligand oxidation.

GC-MS Analyses. Analyses were carried out on a Hewlett-Packard HP-5890 gas chromatograph connected to a HP-5971 mass analyzer. A J&W Scientific HP-5MS capillary column of dimensions (30 m x 0.25 mm x 0.25 μm) was employed for GC-MS studies. The following method was used to effect all separations: initial temperature = 90 °C; initial time = 7 min; temperature ramp = 90 – 210 °C at 20 deg/min, and a final time = 2 min. Quantitations were made by comparison of the total ion count of benzaldehyde with the internal standard, 2-bromonaphthalene. Calibration plots for the detector response were prepared for authentic samples of benzaldehyde and 2-bromonaphthalene by using stock solutions of known concentrations.

Results

2,6-Di(*p*-tolyl)benzoate Carboxylate-Bridged Diiron(II) Complexes of Substituted Alkyl Amine Ligands. 2-Benzylsulfanyl-ethylamine displaces the THF ligand from $[Fe_2(\mu\text{-}O_2CAr^{Tol})_2(O_2CAr^{Tol})(THF)_2]$ to afford $[Fe_2(\mu\text{-}O_2CAr^{Tol})_4(NH_2(CH_2)_2SBn)_2]$ (**1**), in which a

diiron(II) unit is bridged by four carboxylates (Chart 2.2). Figures 2.1 shows the structure of **1**, and pertinent bond lengths and angles are listed in Table 2.2. Each iron atom is coordinated by the four bridging carboxylates that form the base of a square pyramid with an aliphatic amine ligand capping the metal center. A short 2.7832(7) Å Fe⋯Fe distance, typical of the paddlewheel geometry,[34] is observed.

Analogous syntheses using 3-methylsulfanyl-propylamine and 1-amino-5-pentyne as the N-donor ligands yielded $[Fe_2(\mu\text{-}O_2CAr^{Tol})_4(NH_2(CH_2)_3SCH_3)_2]$ (**2**) and $[Fe_2(\mu\text{-}O_2CAr^{Tol})_4\text{-}(NH_2(CH_2)_3CCH)_2]$ (**3**), respectively (Chart 2.2). Compound **2** adopts a paddlewheel structure in the solid state with the N-donors capping the diiron center and completing the square-pyramidal geometry at each metal. The structure of **2** is shown in Figure 2.2 and selected bond lengths and angles are provided in Table 2.2. The Fe⋯Fe distance of 2.7707(6) Å is nearly identical to that in **1**. The quality of the data obtained for **3** was insufficient to extract accurate bond lengths and angles, but the structure could be ascertained. Like **1** and **2**, **3** adopts a tetracarboxylate-bridged diiron(II) core.

2,6-Di(3,5-dimethylphenyl)benzoate Carboxylate-Bridged Diiron(II) Complexes of Substituted Alkyl Amine Ligands. To prepare analogs of **2** and **3** with the $^-O_2CAr^{Xyl}$ carboxylate, $Fe(OTf)_2\cdot2MeCN$, NaO_2CAr^{Xyl}, and the N-donor ligand were used to assemble $[Fe_2(\mu\text{-}O_2CAr^{Xyl})_2(O_2CAr^{Xyl})_2(NH_2(CH_2)_3SCH_3)_2]$ (**4**) and $[Fe_2(\mu\text{-}O_2CAr^{Xyl})_2(O_2CAr^{Xyl})_2\text{-}(NH_2(CH_2)_3CCH)_2]$ (**5**) (Chart 2.2). Figures 2.3 and 2.4 present their structures, and Table 2.2 lists selected bond lengths and angles. Both **4** and **5** form windmill structures with two bidentate carboxylate and two alkyl amine ligands coordinated to each iron atom in *anti* positions across the Fe–Fe vector.

Physical Properties of 2. The zero-field Mössbauer spectrum, measured at 4.2 K, of a powdered sample of **2** is displayed in Figure 2.5. The single sharp ($\Gamma = 0.23 - 0.30$ mm s^{-1}) slightly asymmetric quadrupole doublet reflects the equivalent iron centers related by a virtual C_2 axis. The quadrupole splitting ($\Delta E_Q = 2.22(2)$ mm s^{-1}) and isomer shift (δ shift = 1.08(2) mm s^{-1}) values are consistent with those of other high spin diiron(II) complexes having oxygen-rich coordination environments, indicating that **2** has a high spin S = 2 ground state.[13,35,36] The frozen solution EPR spectrum of **2**, in Figure 2.6, shows a single absorbance at g = 16 characteristic of ferromagnetically coupled diiron(II) centers reflecting an $S_{tot} = 4$ spin system.[37]

Dioxygen Reactivity of 1 – 5. Analysis of the N-donor ligands of **2 – 5** following exposure of their respective diiron(II) compounds to dioxygen revealed no evidence for oxidation. In all four cases the original alkyl amines were quantitatively recovered. The reaction of **1** with O_2, however, afforded benzaldehyde. The overall extent of ligand oxidation was 31% based on **1**.

A g = 16 signal is present in the frozen solution EPR spectrum of **3** at 4.2 K (Figure 2.7). Exposure of **3** to dioxygen at 195 K led to the formation of an emerald green intermediate. The UV-visible spectrum of this species, shown in Figure 2.8, exhibits a broad visible absorption band at 645 nm ($\varepsilon = 1500$ M^{-1} cm^{-1}) consistent with formation of a mixed-valent Fe^{II}Fe^{III} species, the color originating from an intervalence charge transfer band.[38,39] The EPR spectrum of this green species confirms the presence of the mixed-valent Fe^{II}Fe^{III} complex (g = 10) and further reveals the Fe^{III}Fe^{IV} unit (g = 2.0); no evidence of the g = 16 peak of the starting material remained (Figure 2.7). These observations are identical to those reported for the dioxygen reaction products of tetracarboxylate-bridged diiron(II) complexes [Fe$_2$(μ-O$_2$CAr^{Tol})$_4$(4-^{t}Bupy)$_2$] and [Fe$_2$(μ-O$_2$CAr^{Tol})$_4$(BA$^{p\text{-OMe}}$)$_2$], where 4-^{t}Bupy is 4-*tert*-butylpyridine.[17,39]

64

No colored intermediates were observed in the reaction of **5** with dioxygen. A mononuclear ferric species [Fe(O$_2$CAr^{Xyl})$_3$(NH$_2$(CH$_2$)$_3$CCH)$_2$] (**6**) (Chart 2.2) was isolated from the reaction at room temperature. The structure of **6** is shown in Figure 2.9 and selected bond lengths and angles are provided in Table 2.3. Three $^-$O$_2$CAr^{Xyl} carboxylate, two monodentate and one bidentate, ligands make up the equatorial plane of the pseudo-octahedral metal center. The O-atoms that form the smallest O–Fe–O angle of 61.90° have the longest Fe–O distances, 2.1085(17) and 2.1151(17) Å. These Fe–O bonds of the bidentate carboxylate ligand are >0.15 Å longer than those of the monodentate carboxylate ligands, 1.9241(17) and 1.9539(17) Å. The other three equatorial angles are 102.53(7)°, 96.73(7)°, and 99.11(7)°. The Fe–N bond lengths in **6**, both 2.137(2) Å, are only 0.01 Å shorter than those in **5**. The average N–Fe–O bond angle is 89.55(8)° for N1 and 89.70(8)° for N2. The dangling oxygen atoms of the monodentate carboxylates are involved in hydrogen-bonding interactions with the amine protons, N1···O6, 2.816(3) Å and N2···O4, 2.802(3) Å.

Discussion

The ligands 2-benzylsulfanyl-ethylamine, 3-methylsulfanyl-propylamine, and 1-amino-5-pentyne were chosen as N-donors in the preparation of carboxylate-bridged diiron(II) complexes for several reasons. Previous systems in which a coordinated amine ligand containing a tethered benzylamine include *N,N*-dibenzylethylenediamine, benzylamine, and *p*-methoxybenzyl-amine.[15-17] Upon exposure to O$_2$, all three yield benzaldehyde. One possible mechanism proposed for oxidation of the *N,N*-dibenzylethylenediamine ligand involves removal of one-electron from the dangling N-atom to form a radical cation that rearranges with liberation of benzaldehyde.[16] The NH$_2$(CH$_2$)$_2$SBn ligand substrate was selected for study because the benzyl moiety is located in the same position in *N,N*-Bn$_2$en, adjacent to the heteroatom, which is now

sulfur instead of nitrogen. The thioether unit in $NH_2(CH_2)_3SCH_3$ was chosen to mimic dimethylsulfide, which MMOH oxidizes to dimethylsulfoxide.[9] Finally, since acetylene is an inhibitor of sMMO[6] and reacts with the high-valent intermediate Q in the reaction cycle,[40] we investigated the $NH_2(CH_2)_3CCH$ complex. The lengths of the alkyl chains were selected to be the same as that in *N,N*-Bn$_2$en.

The paddlewheel structures of the diiron(II) amine compounds **1** – **3** with $^-O_2CAr^{Tol}$ carboxylates are similar to one another. Each iron atom is ligated by one N-atom from the aliphatic amine and four O-atoms from the bridging carboxylate ligands. There are two longer and two shorter Fe–O bonds on each metal center, ~2.10 and ~2.06 Å. The Fe–N bond distances are the same to within 0.01 Å.

Several physical properties of these small molecule model complexes are comparable to those of the diiron(II) core in MMOH$_{red}$. The g = 16 signal present in the EPR spectra of **2** and **3**, a property shared with the active site of the reduced protein,[41-43] is indicative of ferromagnetic coupling between diiron(II) centers in **2** and **3**. The isomer shift and quadrupole splitting in the Mössbauer spectrum of **2**, 1.08(2) and 2.22(2) mm s^{-1}, respectively, are smaller than those of MMOH$_{red}$, 1.3 and 3.01 mm s^{-1}.[44] The isomer shift of **2** is close to those of other diiron(II) complexes having square pyramidal NO$_4$ coordination geometry, but the quadrupole splitting of ~0.80 mm s^{-1} is less than values typically observed.[45]

The windmill geometry, enforced for diiron(II) compounds **4** and **5** accommodates the more sterically demanding 3,5-dimethyl-substituted carboxylate $^-O_2CAr^{Xyl}$. Each metal center is five coordinate, bound by one N-atom from an alkyl amine ligand and four O-atoms from two bridging and one bidentate carboxylate ligands. One of the Fe–O bonds of the terminal carboxylate is significantly longer than the average of the other three Fe–O distances, 2.3114(15)

vs 2.0338(14) Å for **4** and 2.271(4) vs 2.019(4) Å for **5**. The metal-metal separations of 3.2475(8) and 3.4629(17) Å reported for **4** and **5**, respectively, are ~0.4-0.6 Å shorter than in any previously reported structures with the $\{Fe_2(\mu\text{-}O_2CAr^{Tol})_2(O_2CAr^{Tol})_2\}$ core and in the range of those reported for triply-bridged diiron(II) complexes.[22,34] Diiron(II) complexes containing the O_2CAr^{Xyl} carboxylate show a preference for the windmill isomer, but with aliphatic amine donor ligands are able to accommodate shorter metal-metal distances.

Despite the fact that **1** has a paddlewheel geometry in the solid state, exposure of its solutions to dioxygen affords benzaldehyde, owing to oxidation of the 2-benzylsulfanyl-ethylamine ligand. The yield is about half that observed for the N,N-Bn$_2$en system[15] but similar to that of the $BA^{p\text{-}OMe}$ complex, which also has a tetra-bridged structure in the solid state.[17] The mechanism proposed for this process in the N,N-Bn$_2$en system, based on Hammett and intramolecular KIE analyses, involves single-electron transfer from a non-bonding electron pair on the dangling amine substrate to the generated intermediate, followed by proton transfer and rearrangement.[16,46] Oxidative dealkylation of **1** may proceed through the same pathway, and the decreased yield may be a direct result of replacing the nitrogen atom adjacent to the benzyl group by a sulfur atom. The ionization potential of benzylmethylamine is 0.56 eV lower than that of benzylmethylsulfide (7.85 vs 8.41 eV).[47,48] Extrapolating, the lower reactivity of **1** compared to $[Fe_2(\mu\text{-}O_2CAr^{Tol})_2\text{-}(O_2CAr^{Tol})_2(N,N\text{-}Bn_2en)_2]$ may be a result of a higher ionization potential for the sulfur atom in $NH_2(CH_2)_2SBn$ compared to the nitrogen atom in N,N-Bn$_2$en, making it more difficult to generate the heteroatom-based cation necessary for N-dealkylation of the ancillary ligand. No sulfide oxidation was observed in **1**, whereas oxidation of a methylthio moiety tethered to pyridine in $[Fe_2(\mu\text{-}O_2CAr^{Tol})_3(O_2CAr^{Tol})(2\text{-}MeSpy)]$ leads only to the formation of the sulfoxide. No C–H bond activation of the methyl substituent was observed.[49]

The failure to oxidize the ligands in **2** and **3** was initially attributed to their adopting a paddlewheel geometry, which appears to be less reactive toward dioxygen than the windmill structure because of its more sterically hindered diiron center.[45] This conclusion is supported by the present low temperature spectroscopic study of **3**, which revealed reactivity consistent with established bimolecular chemistry, affording $Fe_2^{II,III}/Fe_2^{III,IV}$ mixed-valent complexes.[39] Compounds **4** and **5** were therefore synthesized for investigation. The more sterically demanding 3,5-dimethyl-substituted benzoate carboxylate ligands in these compounds produce windmill, rather than paddlewheel, structures formed by complexes having *p*-tolyl-substituted benzoate ligands. Despite the change in geometry, ligand oxidation still did not occur.

The use of the bulkier carboxylates did prevent formation of the mixed-valent intermediates observed in the $[Fe_2(\mu\text{-}O_2CAr^{Tol})_4(NH_2(CH_2)_3CCH)_2]$ system, but upon exposure of **5** to dioxygen, the product isolated was a mononuclear ferric species, in which the 1-amino-5-pentyne remains intact. The resulting octahedral metal center is coordinated by two N-atoms from the aminopentyne ligand and four O-atoms from one bidentate and two monodentate $^{-}O_2CAr^{Xyl}$ carboxylate ligands. The reaction is not quantitative, suggesting that species formed initially in solution are rearranging to form **6**. Other products required to obtain a mass balance were not isolated. To date, the only model systems that react with dioxygen to form the $\{Fe_2(\mu\text{-}OH)_2(\mu\text{-}O_2CR)_2\}^{3+}$ core are resting state $MMOH_{ox}$ have $^{-}O_2CAr^{Tol}$ carboxylates.[15,50,51]

Conclusion

The oxidation of a benzyl group following dioxygen activation of a diiron center has now been observed in a system in which the heteroatom adjacent to the site of oxidation is sulfur rather than nitrogen. Other diiron(II) systems explored with alkyl amine donors to the diiron centers react with dioxygen but do not oxidize tethered substrates incorporated into the ligand

framework. A more sterically demanding carboxylate ligand that converted these latter derivatives to the windmill isomer still did not lead to oxidation of the dangling substrate, but instead afforded a mononuclear species as the final isolated product.

References

(1)   Feig, A. L.; Lippard, S. J. *Chem. Rev.* **1994**, *94*, 759-805.

(2)   Wallar, B. J.; Lipscomb, J. D. *Chem. Rev.* **1996**, *96*, 2625-2657.

(3)   Merkx, M.; Kopp, D. A.; Sazinsky, M. H.; Blazyk, J. L.; Müller, J.; Lippard, S. J. *Angew. Chem., Int. Ed. Engl.* **2001**, *40*, 2782-2807.

(4)   Baik, M.-H.; Newcomb, M.; Friesner, R. A.; Lippard, S. J. *Chem. Rev.* **2003**, *103*, 2385-2419.

(5)   Colby, J.; Stirling, D. I.; Dalton, H. *Biochem. J.* **1977**, *165*, 395-402.

(6)   Prior, S. D.; Dalton, H. *FEMS Microbiol. Lett.* **1985**, *29*, 105-109.

(7)   Green, J.; Dalton, H. *J. Biol. Chem.* **1989**, *264*, 17698-17703.

(8)   Fox, B. G.; Borneman, J. G.; Wackett, L. P.; Lipscomb, J. D. *Biochemistry* **1990**, *29*, 6419-6427.

(9)   Fuse, H.; Ohta, M.; Takimura, O.; Murakami, K.; Inoue, H.; Yamaoka, Y.; Oclarit, J. M.; Omori, T. *Biosci. Biotechnol. Biochem.* **1998**, *62*, 1925-1931.

(10)   Lee, D.; Lippard, S. J. *J. Am. Chem. Soc.* **1998**, *120*, 12153-12154.

(11)   Hagadorn, J. R.; Que, L., Jr.; Tolman, W. B. *J. Am. Chem. Soc.* **1998**, *120*, 13531-13532.

(12)   Tolman, W. B.; Que, L., Jr. *J. Chem. Soc., Dalton Trans.* **2002**, 653-660.

(13)   Tshuva, E. Y.; Lippard, S. J. *Chem. Rev.* **2004**, *104*, 987-1012.

(14)   Du Bois, J.; Mizoguchi, T. J.; Lippard, S. J. *Coord. Chem. Rev.* **2000**, *200–202*, 443–485.

(15)   Lee, D.; Lippard, S. J. *J. Am. Chem. Soc.* **2001**, *123*, 4611-4612.

(16)   Lee, D.; Lippard, S. J. *Inorg. Chem.* **2002**, *41*, 827-837.

(17)   Yoon, S.; Lippard, S. J. *Inorg. Chem.* **2003**, *42*, 8606-8608.

(18)   Pangborn, A. B.; Giardello, M. A.; Grubbs, R. H.; Rosen, R. K.; Timmers, F. J. *Organometallics* **1996**, *15*, 1518-1520.

(19)   Barentsen, H. M.; van Dijk, M.; Kimkes, P.; Zuilhof, H.; Sudholter, E. J. R. *Macromolecules* **1999**, *32*, 1753-1762.

(20)   L'abbe, G.; Leurs, S.; Sannen, I.; Dehaen, W. *Tetrahedron* **1993**, *49*, 4439-4446.

(21)   Hagen, K. S. *Inorg. Chem* **2000**, *39*, 5867-5869.

(22)   Lee, D.; Lippard, S. J. *Inorg. Chem.* **2002**, *41*, 2704-2719.

(23)   Du, C.-J. F.; Hart, H.; D., N. K.-K. *J. Org. Chem.* **1986**, *51*, 3162-3165.

(24)   Saednya, A.; Hart, H. *Synthesis* **1996**, 1455-1458.

(25)   Chen, C.-T.; Siegel, J. S. *J. Am. Chem. Soc.* **1994**, *116*, 5959-5960.

(26)   *SMART v5.05: Software for the CCD Detector System*; Bruker AXS: Madison, WI, 1998.

(27)   *SMART v5.626: Software for the CCD Detector System*; Bruker AXS: Madison, WI, 2000.

(28)   Kuzelka, J.; Mukhopadhyay, S.; Spingler, B.; Lippard, S. J. *Inorg. Chem.* **2003**, *42*, 6447-6457.

(29)   Sheldrick, G. M. *SHELXTL97-2: Program for Refinement of Crystal Structures*: University of Göttingen, Germany, 1997.

(30)   *SHELXTL v5.10: Program Library for Structure Solution and Molecular Graphics*; Bruker AXS: Madison, WI, 1998.

(31)   Sheldrick, G. M. *SADABS: Area-Detector Absorption Correction*; University of Göttingen, Germany, 1996.

(32)   Spek, A. L. *PLATON, A Multipurpose Crystallographic Tool*; Utrecht University: Utrecht, The Netherlands, 1998.

(33)   Kent, T. A. *WMOSS v2.5: Mössbauer Spectral Analysis Software*; WEB Research Co.:

Minneapolis, 1998.

(34)   Carson, E. C.; Lippard, S. J. *J. Am. Chem. Soc.* **2004**, *126*, 3412-3413.

(35)   Kurtz, D. M., Jr. *Chem. Rev.* **1990**, *90*, 585-606.

(36)   Münck, E. In *Physical Methods in Bioinorganic Chemistry: Spectroscopy and*

Magnetism; Que, L., Jr., Ed.; University Science Books: Sausalito, CA, 2000; pp 287-319.

(37)   Solomon, E. I.; Brunold, T. C.; Davis, M. I.; Kemsley, J. N.; Lee, S.-K.; Lehnert, N.;

Neese, F.; Skulan, A. J.; Yang, Y.-S.; Zhou, J. *Chem. Rev.* **2000**, *100*, 235-349.

(38)   Lee, D.; DuBois, J. L.; Pierce, B.; Hedman, B.; Hodgson, K. O.; Hendrich, M. P.;

Lippard, S. J. *Inorg. Chem.* **2002**, *41*, 3172-3182.

(39)   Lee, D.; Pierce, B.; Krebs, C.; Hendrich, M. P.; Huynh, B. H.; Lippard, S. J. *J. Am.*

Chem. Soc. **2002**, *124*, 3993-4007.

(40)   Valentine, A. M.; Stahl, S. S.; Lippard, S. J. *J. Am. Chem. Soc.* **1999**, *121*, 3876-3887.

(41)   Fox, B. G.; Surerus, K. K.; Münck, E.; Lipscomb, J. D. *J. Biol. Chem.* **1988**, *263*, 10553-

10556.

(42)   Fox, B. G.; Froland, W. A.; Dege, J. E.; Lipscomb, J. D. *J. Biol. Chem.* **1989**, *264*,

10023-10033.

(43)   Hendrich, M. P.; Münck, E.; Fox, B. G.; Lipscomb, J. D. *J. Am. Chem. Soc.* **1990**, *112*,

5861-5865.

(44)   DeWitt, J. G.; Bentsen, J. G.; Rosenzweig, A. C.; Hedman, B.; Green, J.; Pilkington, S.

J.; Papaefthymiou, G. C.; Dalton, H.; Hodgson, K. O.; Lippard, S. J. *J. Am. Chem. Soc.*

1991, *113*, 9219-9235.

(45)   Yoon, S.; Lippard, S. J. *J. Am. Chem. Soc.* **2005**, *127*, 8386-8397.

(46)   Yoon, S.; Lippard, S. J. **2004**, Manuscript in preparation.

(47)   Bodor, N.; Dewar, M. J. S.; Jennings, W. B.; Worley, S. D. *Tetrahedron* **1970**, *26*, 4109-

       4113.

(48)   Glass, R. S.; Broeker, J. L.; Jatcko, M. E. *Tetrahedron* **1989**, *45*, 1263-1272.

(49)   Carson, E. C. In *Doctoral Dissertation in Inorganic Chemistry*; Massachusetts Institute of

       Technology: Cambridge, MA, 2005; Chapter 5.

(50)   Yoon, S.; Lippard, S. J. *J. Am. Chem. Soc.* **2004**, *126*, 2666-2667.

(51)   Carson, E. C. In *Doctoral Dissertation in Inorganic Chemistry*; Massachusetts Institute of

       Technology: Cambridge, MA, 2005; Chapter 6.

Table 2.1. Summary of X-ray Crystallographic Data

	$1 \cdot 0.5 C_2 H_4 Cl_2$	**2**
Empirical Formula	$Fe_2 C_{103} H_{96} N_2 O_8 S_2 Cl$	$Fe_2 C_{92} H_{90} N_2 O_8 S_2$
Formula Weight	1701.09	1527.48
Space Group	$P\bar{1}$	$P2_1/n$
a, Å	16.334(2)	14.6718(19)
b, Å	16.542(2)	19.618(3)
c, Å	16.867(2)	27.676(3)
α, deg	87.348(2)	
β, deg	88.610(2)	93.157(2)
γ, deg	71.978(2)	
V, Å^3	4329.1(10)	7953.9(17)
Z	2	4
ρ_{calc}, g/cm^3	1.305	1.276
T, °C	-100	-85
μ(Mo Kα), mm^{-1}	0.474	0.476
θ limits, deg	1.74 – 26.37	1.61 – 26.37
total no. of data	35431	65502
no. of unique data	17415	16221
no. of params	1258	1073
Goodness-of-fit on F^2	1.376	1.018
R1[a]	0.0674	0.0475
wR2[b]	0.1933	0.1045
max, min peaks, e/Å^3	1.553, -0.959	0.320, -0.366

[a]$R1 = \Sigma ||F_o|-|F_c||/\Sigma|F_o|$. [b]$wR^2 = \{\Sigma[w(F_o^2-F_c^2)^2]/\Sigma[w(F_o^2)^2]\}^{1/2}$.

Table 2.1. Continued

	4	5·0.5C$_4$H$_{10}$O	6
Empirical Formula	Fe$_2$C$_{100}$H$_{106}$N$_2$O$_8$S$_2$	Fe$_2$C$_{104}$H$_{107}$N$_2$O$_{8.5}$	FeC$_{79}$H$_{81}$N$_2$O$_6$
Formula Weight	1639.69	1632.62	1210.31
Space Group	C2/c	C2/c	P2$_1$/c
a, Å	25.027(4)	24.549(3)	24.6380(18)
b, Å	16.539(4)	16.992(2)	13.3991(9)
c, Å	21.634(4)	21.994(2)	22.4464(16)
α, deg			
β, deg	91.126(4)	92.789(3)	114.2280(10)
γ, deg			
V, Å^3	8953(3)	9163.6(18)	6757.5(8)
Z	4	4	4
ρ$_{calc}$, g/cm^3	1.216	1.183	1.190
T, °C	-85	-100	-80
μ(Mo Kα), mm^{-1}	0.427	0.374	0.277
θ limits, deg	1.48 – 26.38	1.66 – 26.73	1.77 – 26.37
total no. of data	25690	26803	54800
no. of unique data	9148	9638	13804
no. of params	568	545	805
Goodness-of-fit on F^2	1.004	0.963	1.017
R1^a	0.0447	0.0917	0.0600
wR^{2b}	0.1294	0.2371	0.1543
max, min peaks, e/Å^3	0.425, -0.423	1.227, -0.942	0.662, -0.524

^{a}R1 = $\Sigma||F_o|-F_c||/\Sigma|F_o|$. ^{b}wR^2 = $\{\Sigma[w(F_o{}^2-F_c{}^2)^2]/\Sigma[w(F_o{}^2)^2]\}^{1/2}$.

Table 2.2. Selected Interatomic Distances (Å) and Angles (deg) for **1**, **2**, **4**, and **5**[a]

	1	**2**	**4**	**5**
Fe1···Fe2	2.7832(7)	2.7707(6)	3.2475(8)	3.4629(17)
Fe1–N1	2.090(8)	2.068(7)	2.145(2)	2.147(7)
Fe1–O1	2.112(2)	2.1031(16)	2.0179(14)	1.994(4)
Fe1–O2	2.058(2)	2.0817(16)	2.0050(14)	2.003(4)
Fe1–O3	2.078(2)	2.0531(17)	2.0786(15)	2.060(4)
Fe1–O4	2.112(2)	2.0933(16)	2.3114(15)	2.271(4)
Fe2–N2	2.126(5)	2.100(6)		
Fe2–O5	2.054(2)	2.0638(16)		
Fe2–O6	2.103(2)	2.0579(16)		
Fe2–O7	2.080(2)	2.1507(17)		
Fe2–O8	2.051(2)	2.0456(16)		
O1–Fe1–N1	86.66(17)	85.3(3)	90.59(7)	87.7(2)
O2–Fe1–N1	98.73(17)	86.7(3)	89.77(7)	91.4(3)
O3–Fe1–N1	110.40(18)	111.3(3)	114.41(7)	113.0(2)
O4–Fe1–N1	96.91(17)	109.3(3)	174.21(7)	173.3(2)
O1–Fe1–O2	89.08(9)	87.85(6)	150.43(6)	143.64(18)
O1–Fe1–O3	162.82(9)	163.26(7)	101.63(6)	109.32(18)
O1–Fe1–O4	88.00(8)	87.10(6)	91.33(6)	93.97(16)
O2–Fe1–O3	90.19(9)	86.11(5)	105.09(6)	104.45(17)
O2–Fe1–O4	163.89(9)	162.72(7)	91.25(6)	91.12(16)
O3–Fe1–O4	87.96(8)	89.62(7)	59.85(6)	60.34(16)

[a]Numbers in parentheses are estimated standard deviations of the last significant figure. Atoms are labeled as indicated Figures 2.1, 2.2, 2.4, and 2.5.

Table 2.3. Selected Interbond Lengths and Angles for $[Fe(O_2CAr^{Xyl})_3(NH_2(CH_2)_3CCH)_2]$ **(6)**[a]

	Bond Length (Å)		Bond Angle (deg)
Fe1–N1	2.137(2)	N2–Fe1–N1	172.71(9)
Fe1–N2	2.137(2)	O1–Fe1–N1	82.38(8)
Fe1–O1	2.1085(17)	O2–Fe1–N1	89.32(7)
Fe1–O2	2.1151(17)	O3–Fe1–N1	92.66(8)
Fe1–O3	1.9241(17)	O5–Fe1–N1	93.85(8)
Fe1–O5	1.9539(16)	O1–Fe1–N2	91.81(8)
		O2–Fe1–N2	84.04(8)
N1⋯O6	2.816(3)	O3–Fe1–N2	92.39(8)
N2⋯O4	2.802(3)	O5–Fe1–N2	90.54(8)
		O1–Fe1–O2	61.90(7)
		O1–Fe1–O3	96.73(7)
		O1–Fe1–O5	163.87(7)
		O2–Fe1–O3	158.08(7)
		O2–Fe1–O5	102.53(7)
		O3–Fe1–O5	99.11(7)

[a]Numbers in parentheses are estimated standard deviations of the last significant figure. Atoms are labeled as indicated Figure 2.9.

Chart 2.1.

Ar^{Xyl}CO$_2$H   Ar^{Tol}CO$_2$H
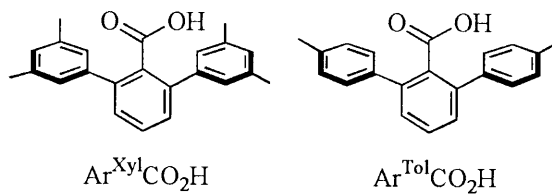
Chart 2.2.
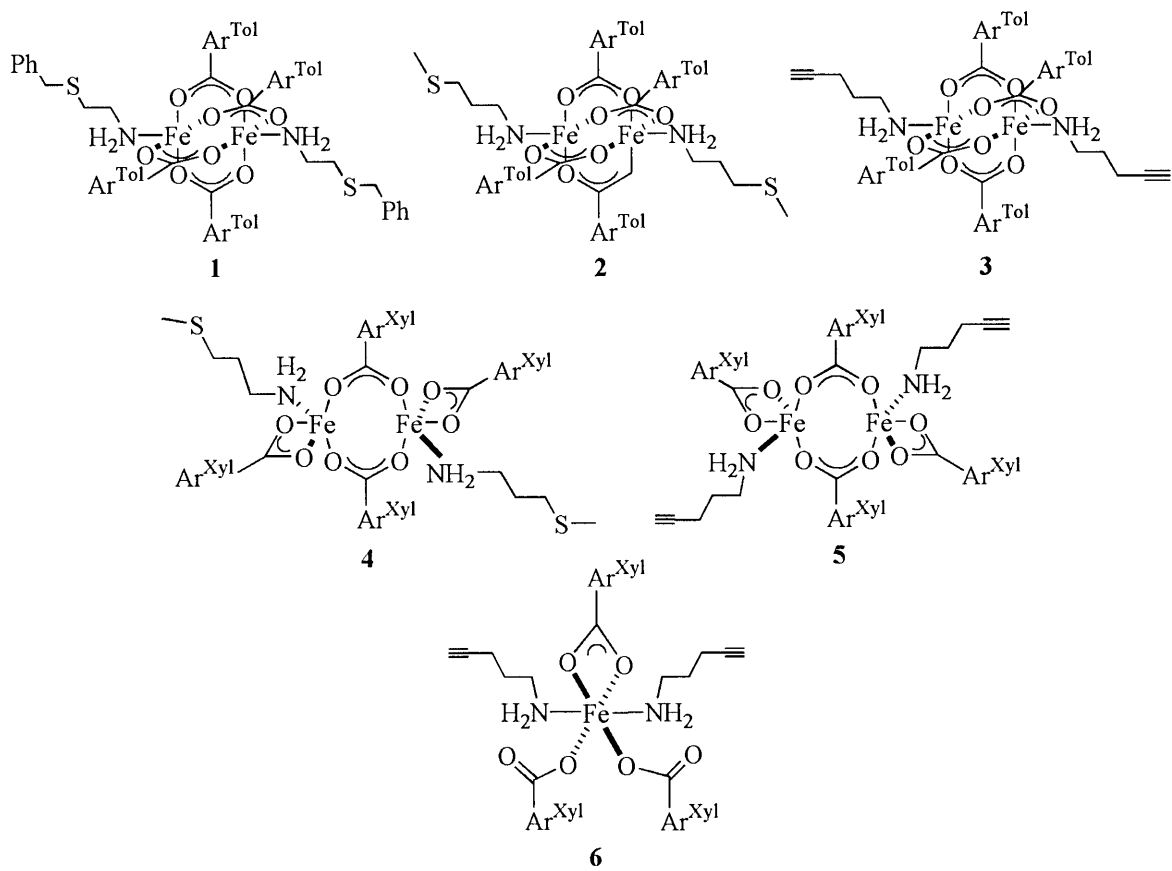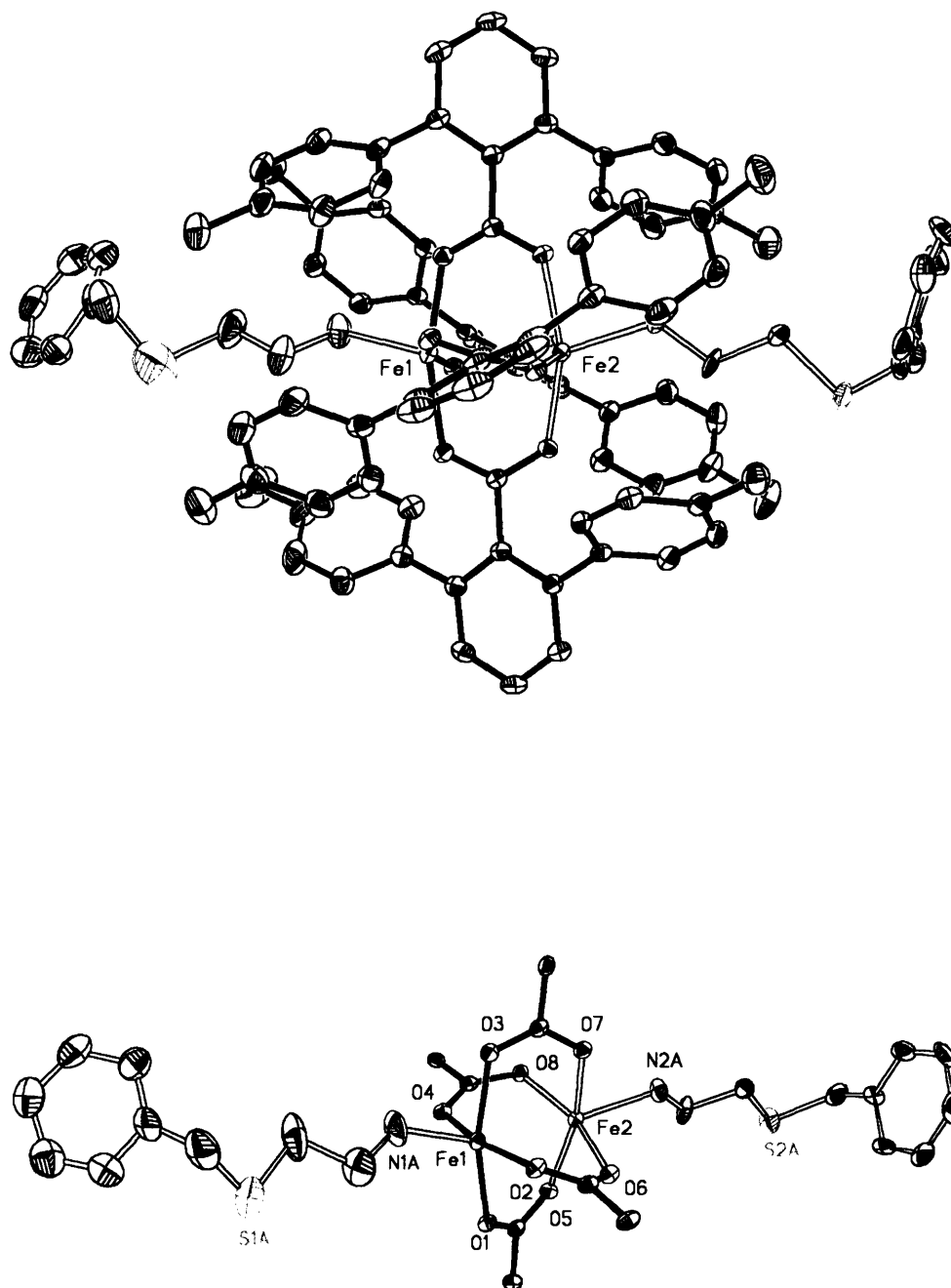
Figure 2.1. Top: ORTEP diagram of [Fe$_2$(μ-O$_2$CAr^{Tol})$_4$(NH$_2$(CH$_2$)$_2$SBn)$_2$] (**1**) illustrating 30% probability thermal ellipsoids for all non-hydrogen atoms. Bottom: Drawing in which the aromatic rings of the $^-$O$_2$CAr^{Tol} ligands are omitted for clarity.
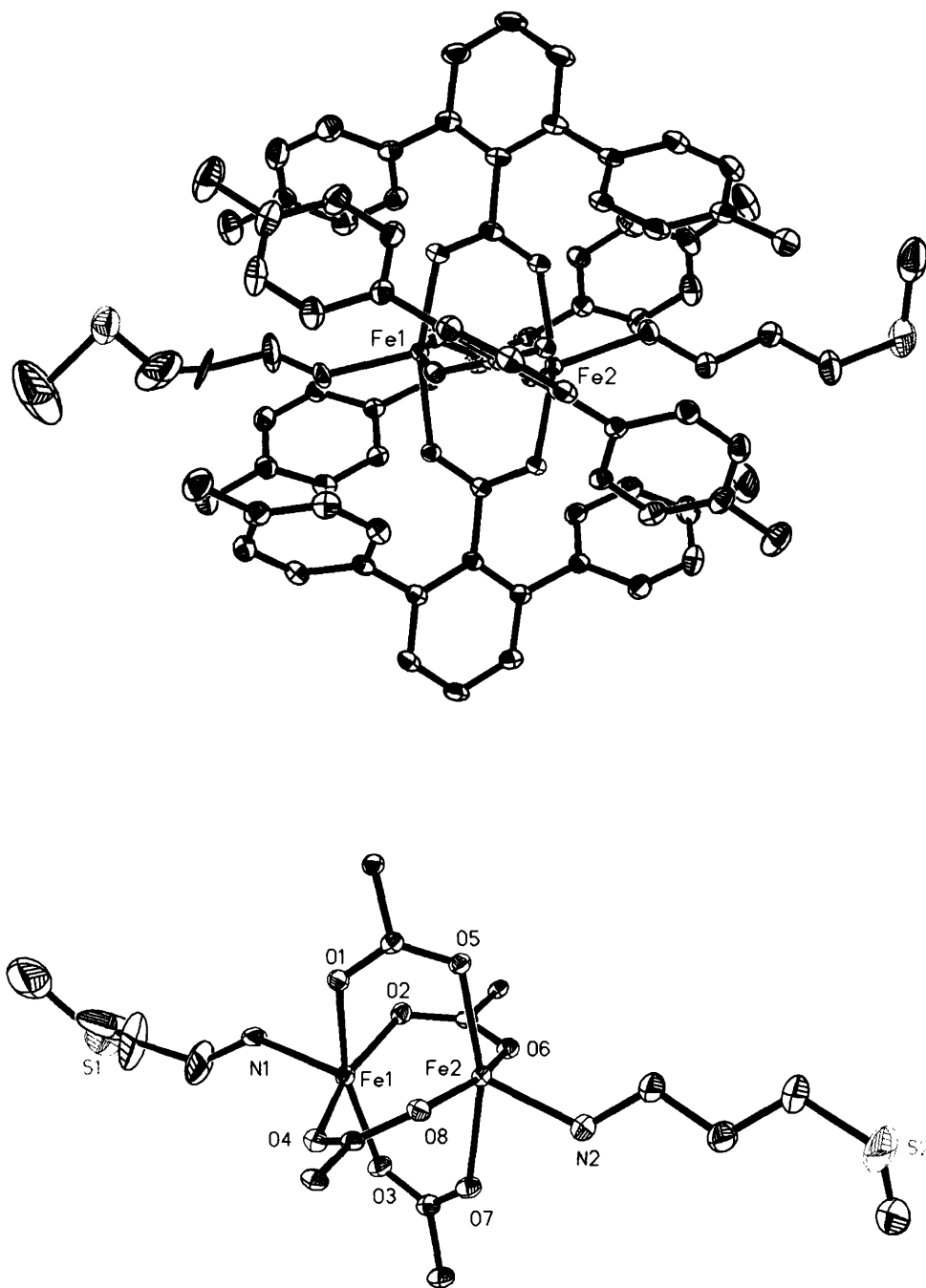
Figure 2.2. Top: ORTEP diagram of [Fe$_2$(μ-O$_2$CAr^{Tol})$_4$(NH$_2$(CH$_2$)$_3$SMe)$_2$] (**2**) illustrating 30% probability thermal ellipsoids for all non-hydrogen atoms. Bottom: Drawing in which the aromatic rings of the $^-$O$_2$CAr^{Tol} ligands are omitted for clarity.
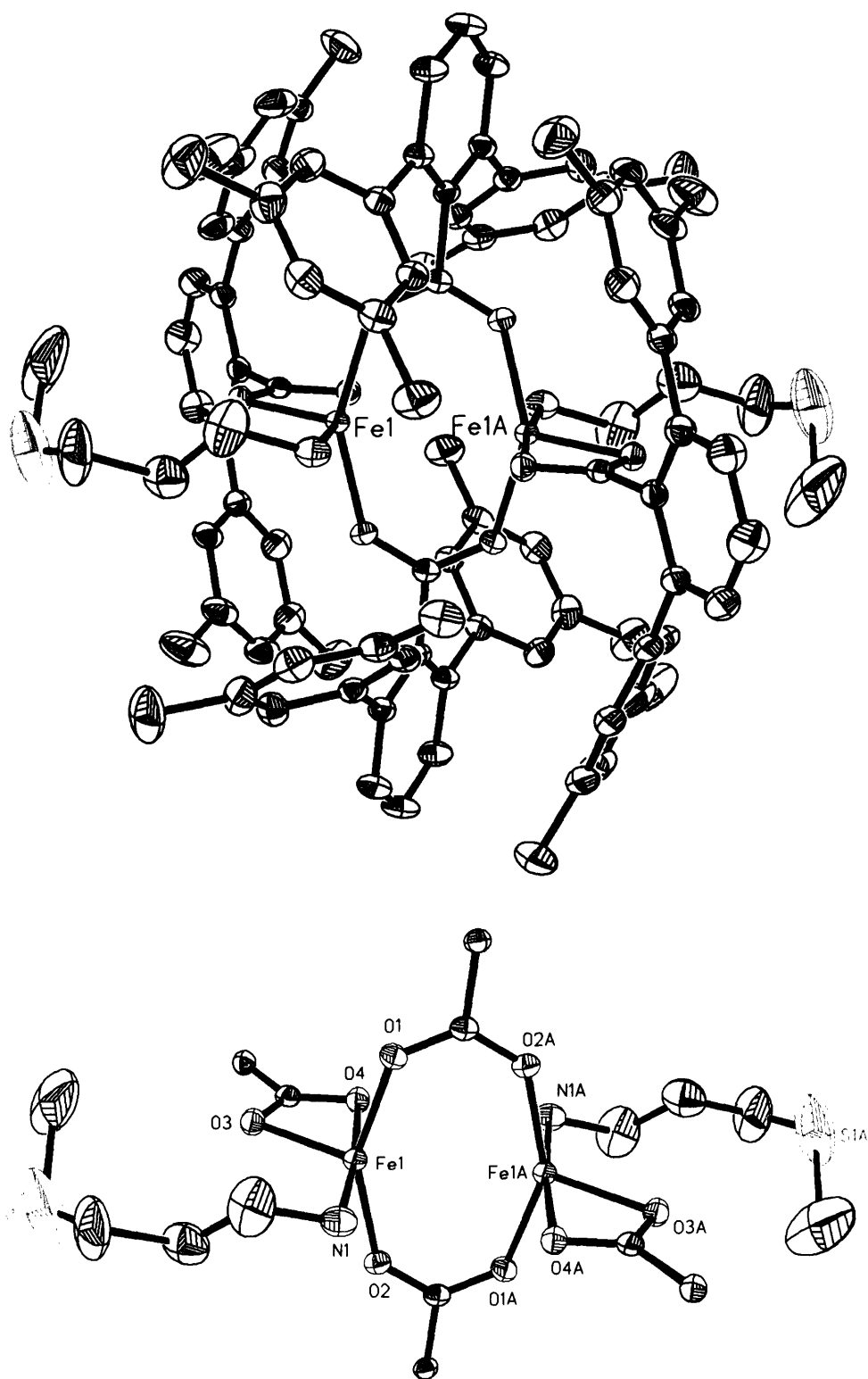
Figure 2.3. Top: ORTEP diagram of [Fe$_2$(μ-O$_2$CAr^{Xyl})$_2$(O$_2$CAr^{Xyl})$_2$(NH$_2$(CH$_2$)$_3$SMe)$_2$] (**4**) illustrating 30% probability thermal ellipsoids for all non-hydrogen atoms. Bottom: Drawing in which he aromatic rings of the $^-$O$_2$CAr^{Xyl} ligands are omitted for clarity.
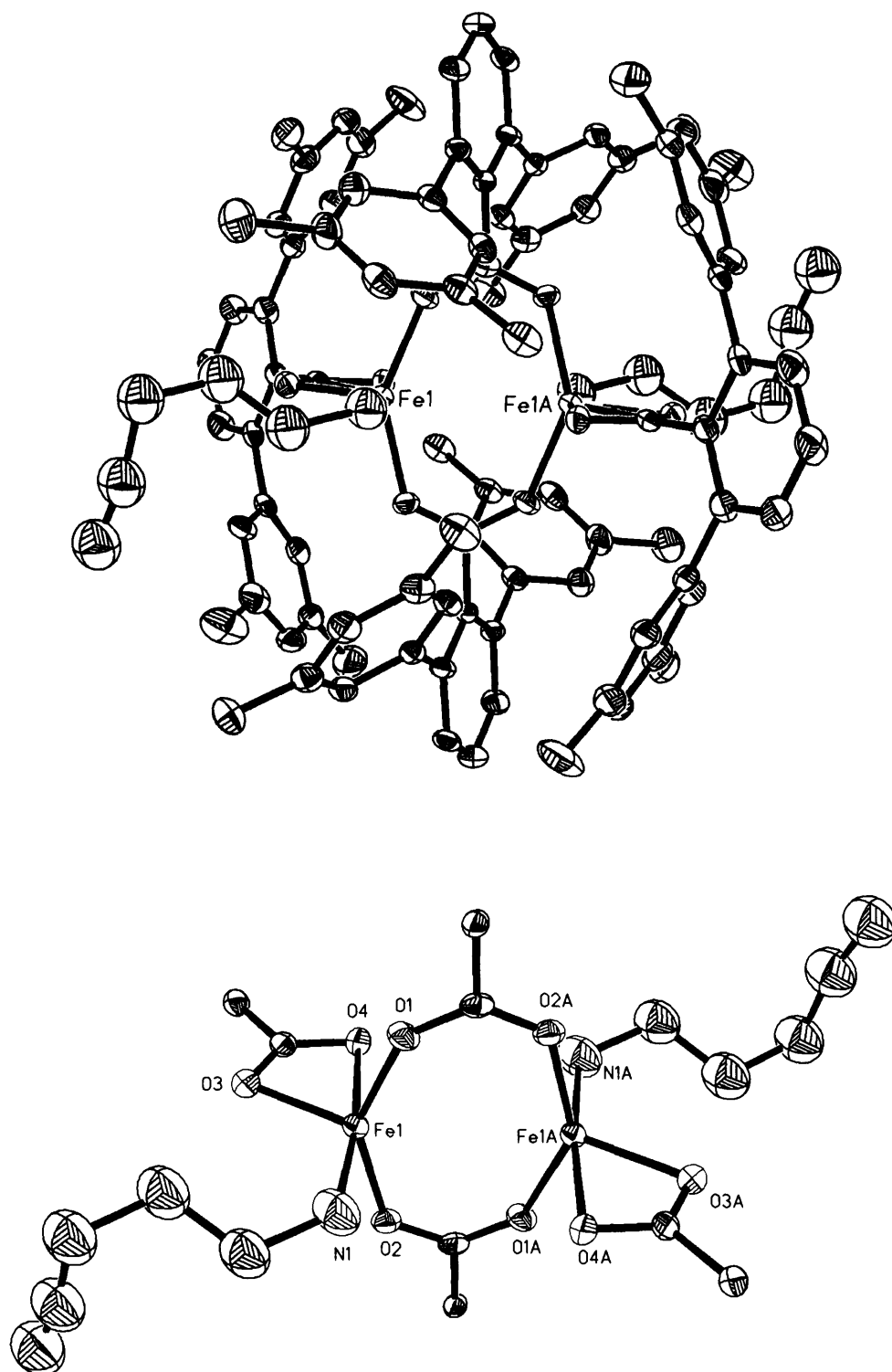
Figure 2.4. Top: ORTEP drawing of [Fe$_2$(μ-O$_2$CAr^{Xyl})$_2$(O$_2$CAr^{Xyl})$_2$(NH$_2$(CH$_2$)$_3$CCH)$_2$] (**5**) illustrating 30% probability thermal ellipsoids for all non-hydrogen atoms. Bottom: Drawing in which the aromatic rings of the $^-$O$_2$CAr^{Xyl} ligands are omitted for clarity.
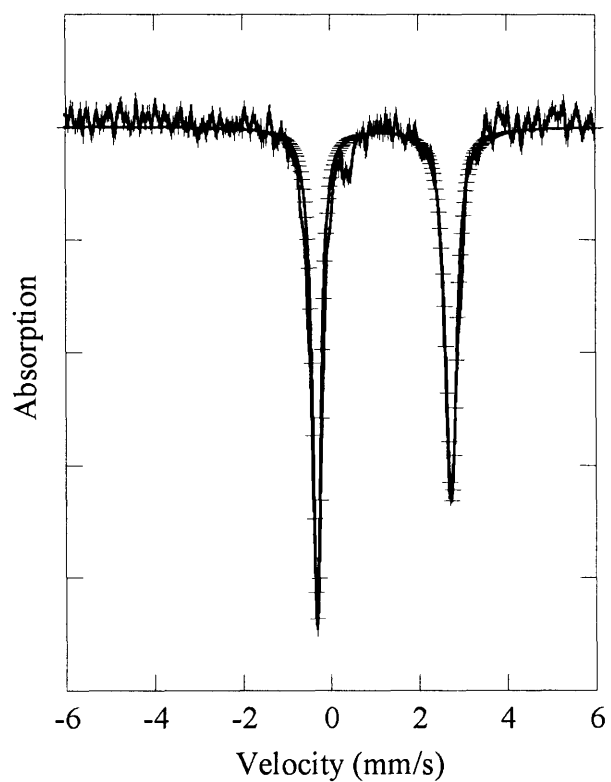
Figure 2.5. Mössbauer spectrum (experimental data (|), calculated (–)) recorded at 4.2 K for a solid sample of $[Fe_2(\mu\text{-}O_2CAr^{Tol})_4(NH_2(CH_2)_3SMe)_2]$ (**2**).

g = 16

H (Gauss)
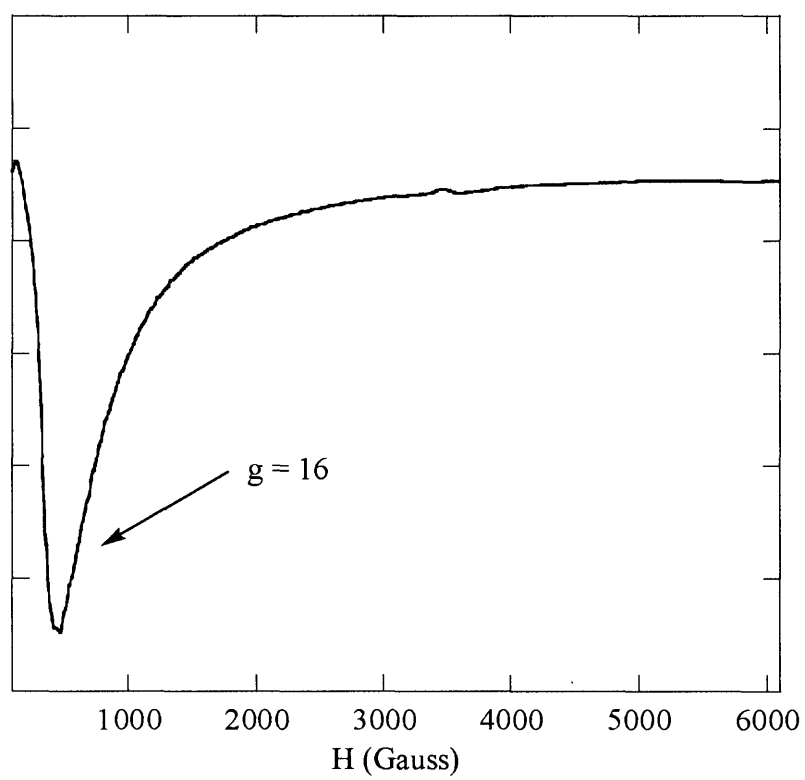
Figure 2.6. X-band EPR spectrum collected at 5 K of a CH_2Cl_2 solution of **2**.
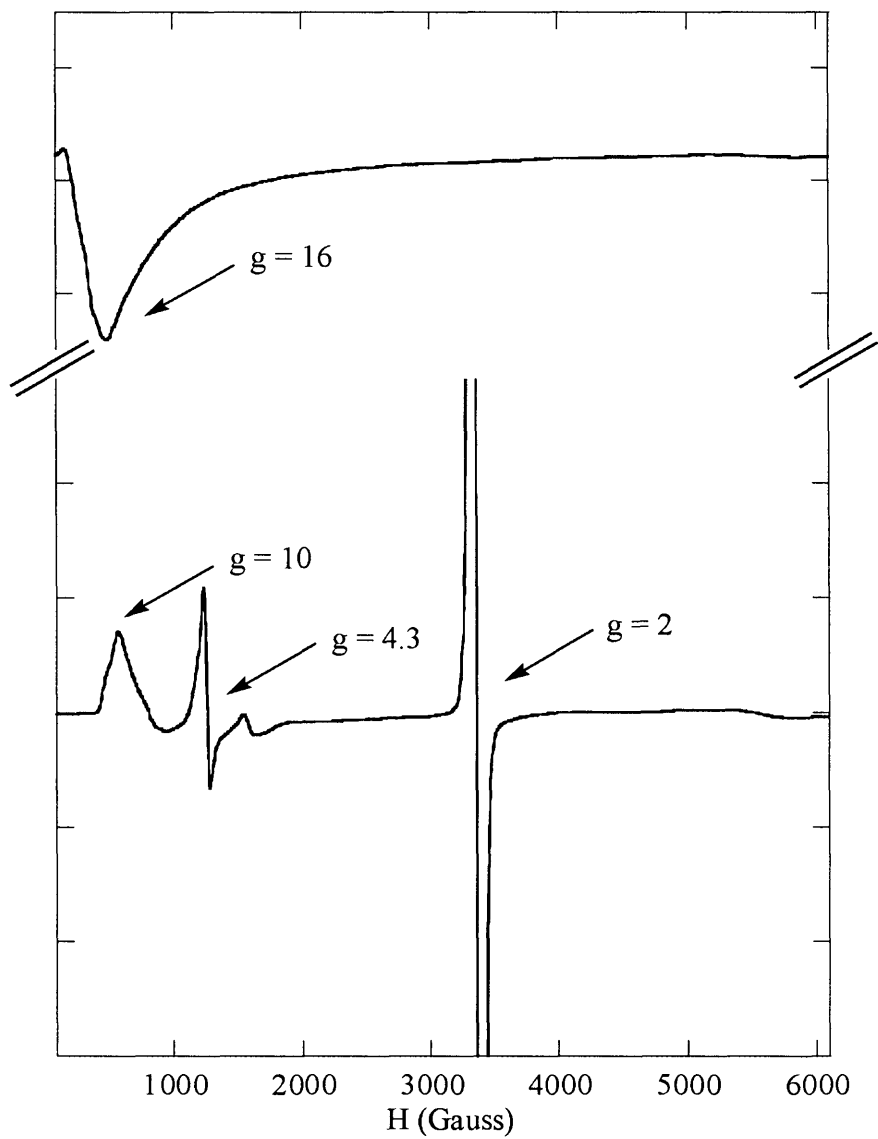
Figure 2.7. X-band EPR spectra collected at 5 K showing a CH₂Cl₂ solution of **3** (top) and a CH₂Cl₂ solution of **3** after exposure to O₂ at −78 °C (bottom).
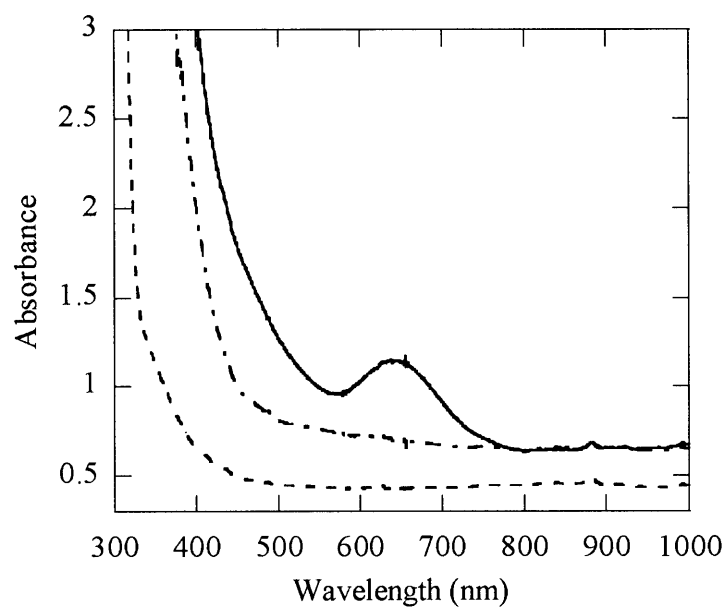
Figure 2.8. UV-vis spectra of $[Fe_2(\mu-O_2CAr^{Tol})_4(NH_2(CH_2)_3CCH)_2]$ (**3**) (---), the intermediate (—) generated upon addition of O_2, and after 2h (- —) in CH_2Cl_2 at $-78\ ^oC$.
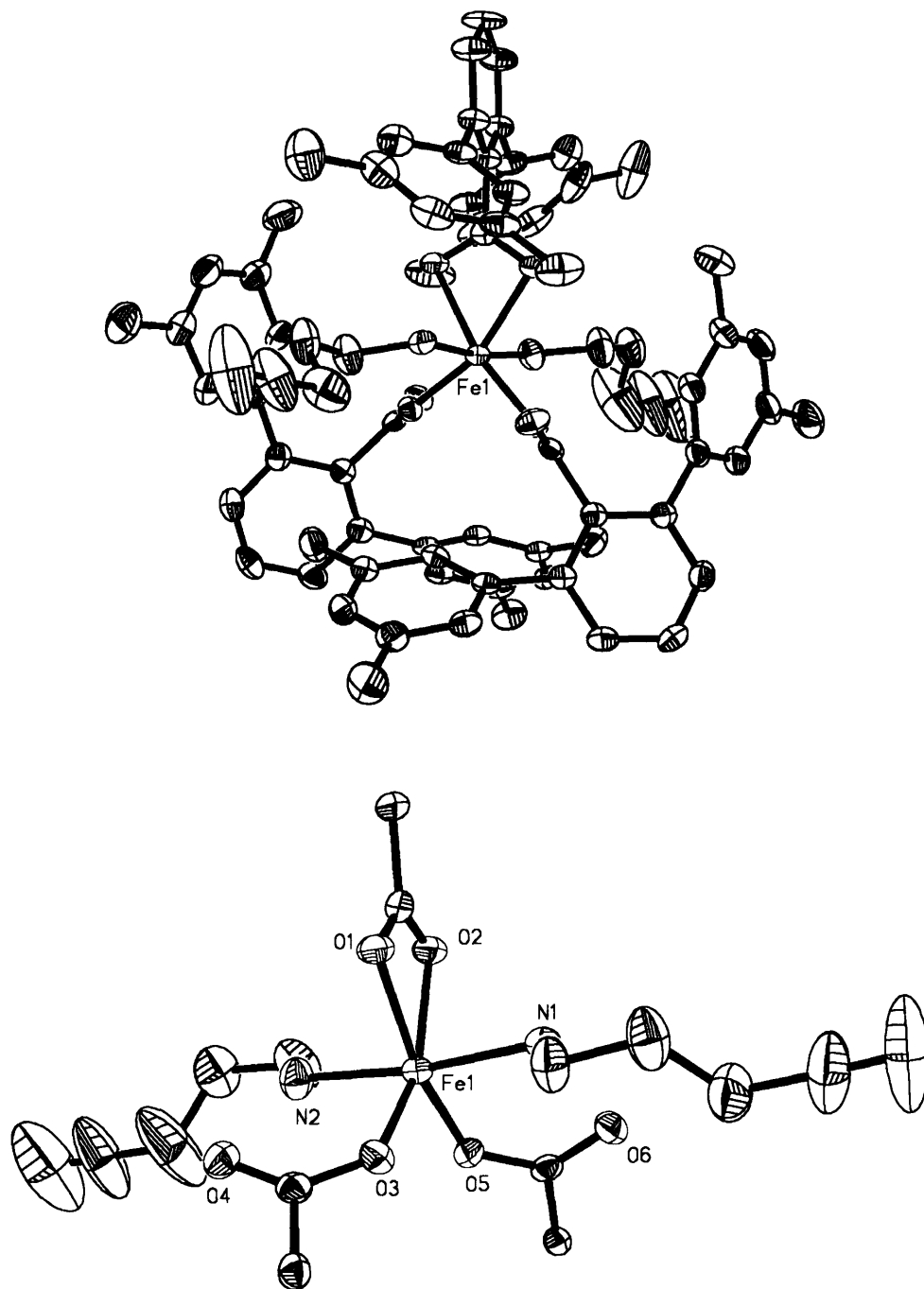
Figure 2.9. Top: ORTEP diagram of [Fe(O$_2$CAr^{Xyl})$_3$(NH$_2$(CH$_2$)$_3$CCH)$_2$] (**6**) illustrating 50% probability thermal ellipsoids for all non-hydrogen atoms. Bottom: Drawing in which the aromatic rings of the $^-$O$_2$CAr^{Xyl} ligands are omitted for clarity.

Chapter 3

C–H Activation of Benzyl- and Ethyl- Substituted Pyridine Ligands in the Reactions of

Carboxylate-Bridged Diiron(II) Complexes with Dioxygen

Introduction

The selective oxidation of hydrocarbons under ambient conditions is important for both industrial and ecological reasons.[1,2] Dioxygen can be harnessed by certain iron-containing bacterial enzymes to effect the controlled two-electron oxidation of organic substrates. Bacterial multicomponent monooxygenases that catalyze the selective conversion of hydrocarbons to alcohols are of particular interest because of their wide range of substrates.[3] The hydroxylase component of soluble methane monooxygenase (MMOH) performs this function by first activating dioxygen to afford reactive intermediates which can in turn insert one oxygen atom selectively into the C–H bond.[4-7] The benefits to understanding this process on a molecular level are two-fold. Such knowledge would provide insight into the mechanics of metalloproteins which, in turn, would facilitate the design of catalysts for dioxygen activation and selective hydrocarbon oxidation.

To discern the intricacies of these systems, investigators have turned to small molecule models compounds to sharpen the connection between structure and function in the enzymes. The active site of MMOH houses a diiron center, surrounded by four carboxylate and two histidine residues, which performs the selective hydroxylation.[8,9] To represent the core structure of the native enzyme accurately in a synthetic compound requires a carboxylate-rich ligand environment. Isolation of discrete dinuclear iron centers demands ligand framework that provides sufficient steric bulk around the metal center to avoid oligomer formation,[10-14] without forming only mononuclear species.[15,16]

The introduction of *m*-terphenyl-based carboxylates, depicted in Chart 3.1, has facilitated the assembly of the desired dinuclear cores.[16-20] The protective pocket of aromatic rings prevents bimolecular decomposition reactions but can also block access of substrate to the O_2-activated

diiron center. To address this problem, substrates have been incorporated into the ancillary N-donor ligands coordinated to the iron atoms. The formation of benzaldehyde from a benzyl moiety occurs upon exposure to O_2 of the diiron(II) complexes [Fe$_2$(μ-O$_2$CAr^{Tol})$_2$(O$_2$CAr^{Tol})$_2$-(N,N-Bn$_2$en)$_2$],[21,22] [Fe$_2$(μ-O$_2$CAr^{Tol})$_4$(BA$^{p\text{-}OMe}$)$_2$],[23] and [Fe$_2$(μ-O$_2$CAr^{Tol})$_4$(NH$_2$(CH$_2$)$_2$SBn)$_2$],[24] where Ar^{Tol}CO$_2$$^-$ is 2,6-di(p-tolyl)benzoate, N,N-Bn$_2$en is N,N-dibenzylethylenediamine, and BA$^{p\text{-}OMe}$ is p-methoxybenzylamine.

In the present study we have expanded the family of substrate-tethered carboxylate-bridged diiron(II) compounds in which benzyl- or ethyl- derivatized pyridine or aniline donor ligands have been incorporated into the compound. The oxygenation reaction chemistry of these complexes were studied by analysis of the organic fragments produced following introduction of O_2 into their methylene chloride solutions. A portion of this work has been previously communicated.[25]

Experimental Section

General Considerations. All reagents were obtained from commercial suppliers and used as received, unless otherwise noted. Methylene chloride, diethyl ether (Et$_2$O), and pentane were saturated with nitrogen and purified by passing through activated Al$_2$O$_3$ columns under argon.[26] Dioxygen (99.994%, BOC Gases) was dried by passing the gas stream through a column of Drierite. The synthesis and characterization of [Fe$_2$(μ-O$_2$CAr^{Tol})$_2$(O$_2$CAr^{Tol})$_2$(THF)$_2$] and [Fe$_2$(μ-O$_2$CAr$^{4\text{-}FPh}$)$_2$(O$_2$CAr$^{4\text{-}FPh}$)$_2$(THF)$_2$] were reported previously.[27] Purification of 2-benzyl-pyridine (2-Bnpy), 4-benzylpyridine (4-Bnpy), 2-(4-chlorobenzyl)pyridine (2-(4-ClBn)py), 2-ethylpyridine (2-Etpy), 3-ethylpyridine (3-Etpy), and 4-ethylpyridine (4-Etpy) was accomplished by vacuum distillation prior to use. Authentic samples of α-phenyl-2-pyridyl-methanol (2-PhCHOHpy) and α-methyl-2-pyridinemethanol (2-MeCHOHpy) were synthesized

in a manner analogous to pyridyl alcohols reported in the literature.[28] Air-sensitive manipulations were carried out under nitrogen in an Mbraun drybox. All samples were pulverized and thoroughly dried to remove solvent prior to determining their elemental composition. Solvent molecules included in the elemental composition of **1, 2, 3,** and **6** were found in the crystal lattice or detected in the ^{1}H NMR spectra of these compounds. Acceptable analytical data were never obtained for **5** despite the crystallinity of the sample.

[Fe$_2$(μ-O$_2$CAr^{Tol})$_2$(O$_2$CAr^{Tol})$_2$(2-Bnpy)$_2$] (1). To a stirred CH$_2$Cl$_2$ (3.2 mL) solution of [Fe$_2$(μ-O$_2$CAr^{Tol})$_2$(O$_2$CAr^{Tol})$_2$(THF)$_2$] (232 mg, 0.159 mmol), 2-Bnpy (55.2 mg, 0.326 mmol) in CH$_2$Cl$_2$ (1 mL) was added dropwise and allowed to react for 20 min. Vapor diffusion of diethyl ether into the resulting green solution yielded pale blue-green crystals (229 mg, 87%) of **1** suitable for X-ray crystallography. FT-IR (KBr, cm^{-1}): 3055 (w), 3026 (w), 2917 (w), 2859 (w), 1606 (s), 1570 (s), 1514 (s), 1482 (m), 1453 (s), 1410 (s), 1379 (s), 1242 (w), 1187 (w), 1142 (w), 1109 (w), 1074 (w), 1020 (m), 850 (m), 816 (m), 798 (s), 780 (m), 765 (m), 744 (m), 700 (m), 644 (w), 619 (w), 581 (w), 542 (m), 518 (m), 469 (w). Anal. Calcd. for C$_{108}$H$_{90}$N$_2$Fe$_2$O$_8$·CH$_2$Cl$_2$: C, 75.22; H, 5.33; N, 1.61. Found: C, 75.25; H, 5.63; N, 1.55.

[Fe$_2$(μ-O$_2$CAr^{Tol})$_2$(O$_2$CAr^{Tol})$_2$(2-(4-ClBn)py)$_2$] (2). Freshly distilled 2-(4-ClBn)py (40.6 mg, 0.199 mmol) in CH$_2$Cl$_2$ (1 mL) was added dropwise to a CH$_2$Cl$_2$ (3 mL) solution of [Fe$_2$(μ-O$_2$CAr^{Tol})$_2$(O$_2$CAr^{Tol})$_2$(THF)$_2$] (102 mg, 0.0699 mmol) with stirring for 20 min. Vapor diffusion of diethyl ether into the olive green solution yielded mint green crystals (96.1 mg, 80%) of **2** suitable for X-ray crystallography. FT-IR (KBr, cm^{-1}): 3057 (w), 2971 (w), 2918 (w), 2850 (w), 1607 (s), 1570 (s), 1543 (s), 1514 (s), 1488 (s), 1452 (s), 1406 (s), 1380 (s), 1187 (w), 1100 (w), 1079 (w), 1016 (m), 950 (w), 856 (m), 819 (s), 800 (s), 780 (m), 767 (s), 760 (s), 735

(m), 711 (m), 696 (w), 641 (w), 601 (w), 581 (w), 542 (s), 517 (s). Anal. Calcd. for

$C_{108}H_{88}N_2Fe_2O_8Cl_2 \cdot 0.25CH_2Cl_2$: C, 74.48; H, 5.11; N, 1.60. Found: C, 74.22; H, 5.49; N, 1.96.

$[Fe_2(\mu\text{-}O_2CAr^{Tol})_4(4\text{-}Bnpy)_2]$ (3). Bright green X-ray quality crystals (172 mg) of **3** were

isolated in 88% yield by 4-benzylpyridine (46.0 mg, 0.272 mmol) displacement of THF in

$[Fe_2(\mu\text{-}O_2CAr^{Tol})_2(O_2CAr^{Tol})_2(THF)_2]$ (173 mg, 0.119 mmol) in a CH_2Cl_2 (4 mL) solution. FT-IR

(KBr, cm^{-1}): 3024 (w), 2972 (w), 2916 (w), 2857 (w), 1614 (s), 1584 (m), 1548 (m), 1512 (m),

1429 (s), 1382 (s), 1302 (w), 1183 (w), 1151 (w), 1109 (w), 1069 (w), 1029 (w), 841 (m), 810

(s), 788 (s), 762 (w), 726 (w), 705 (s), 616 (w), 583 (m), 564, 524 (s), 483 (w), 460 (w). Anal.

Calcd. for $C_{108}H_{90}N_2O_8Fe_2 \cdot 0.25CH_2Cl_2$: C, 77.54; H, 5.44, N, 1.67. Found: C, 77.55; H, 5.54; N,

1.57.

$[Fe_2(\mu\text{-}O_2CAr^{4\text{-}FPh})_2(O_2CAr^{4\text{-}FPh})_2(2\text{-}Bnpy)_2]$ (4). 2-Benzylpyridine (34.1 mg, 0.202

mmol) was added to $[Fe_2(\mu\text{-}O_2CAr^{4\text{-}FPh})_2(O_2CAr^{4\text{-}FPh})_2(THF)_2]$ (91.2 mg, 0.0611 mmol), and

immediately the light sea-green solution was subjected to pentane vapor diffusion. Light-green

blocks of **4** (97.7 mg, 95%) suitable for X-ray diffraction studies were recovered. FT-IR (KBr,

cm^{-1}): 3061 (w), 2959 (w), 2923 (w), 2863 (w), 1604 (s), 1569 (s), 1510 (s), 1454 (s), 1409 (m),

1379 (m), 1224, 1299 (w), 1186 (w), 1159 (s), 1095 (w), 1073 (w), 1013 (w), 855 (m), 837 (s),

806 (s), 793 (m), 702 (m), 622 (w), 581 (w), 559 (m), 526 (m), 469 (w). Anal. Calcd. for

$C_{100}H_{66}N_2Fe_2O_8F_8$: C, 71.18; H, 3.94; N, 1.66. Found: C, 70.97; H, 3.91; N, 1.93.

$[Fe_2(\mu\text{-}O_2CAr^{Tol})_2(O_2CAr^{Tol})_2(2\text{-}Bnan)_2]$ (5). A pale yellow solution of

$[Fe_2(\mu\text{-}O_2CAr^{Tol})_2(O_2CAr^{Tol})_2(THF)_2]$ (87.0 mg, 0.0595 mmol) in 4 mL of CH_2Cl_2 was allowed

to react with 2-benzylaniline (2-Bnan) (24.7 mg, 0.135 mmol). After 30 min the solution was

reduced almost to dryness under vacuum, at which time 2 mL of ClPh were added. Diffusion of

pentane vapor into the solution yielded pale yellow blocks (50.1 mg, 50%) of **5** suitable for X-

ray crystallography. FT-IR (KBr, cm^{-1}): 3334, 3281, 3026, 2918, 1598 (s), 1549 (s), 1514 (s), 1494 (m), 1453 (m), 1413 (m), 1377 (s), 1306 (w), 1272 (s), 1233 (w), 1186 (w), 1144 (w), 1109 (w), 1078 (w), 1021 (m), 855 (m), 818 (s), 801 (s), 784 (s), 714 (s), 699 (s), 687 (w), 616 (w), 583 (w), 544 (s), 520 (s), 458 (w), 414 (w).

[Fe$_2$(μ-O$_2$CAr^{Tol})$_2$(O$_2$CAr^{Tol})$_2$(2-Etpy)$_2$] (6). A stirred solution of [Fe$_2$(μ-O$_2$CAr^{Tol})$_2$-(O$_2$CAr^{Tol})$_2$(THF)$_2$] (336 mg, 0.230 mmol) in CH$_2$Cl$_2$ (8 mL) was combined with 2-ethylpyridine (54.5 mg, 0.509 mmol) and allowed to react for 20 min. Vapor diffusion of Et$_2$O into the yellow-green solution resulted in the formation of white needles of **6** (330 mg, 95%). FT-IR (KBr, cm^{-1}): 3053 (w), 2970 (w), 2919 (w), 1604 (s), 1567 (s), 1514 (s), 1481 (m), 1452 (s), 1408 (s), 1367 (s), 1306 (w), 1264 (m), 1213 (w), 1144 (w), 1109 (m), 1062 (w), 1018 (m), 849(s), 799 (s), 780 (s), 767 (s), 736 (s), 709 (s), 644 (w), 609 (w), 558 (w), 542 (m), 522 (m), 444 (w), 416 (w). Anal. Calcd. for C$_{98}$H$_{86}$N$_2$O$_8$Fe$_2$·0.5CH$_2$Cl$_2$: C, 75.17; H, 5.57; N, 1.78. Found: C, 75.52; H, 5.57; N, 1.65.

[Fe$_2$(μ-O$_2$CAr^{Tol})$_2$(O$_2$CAr^{Tol})$_2$(3-Etpy)$_2$] (7). 3-Ethylpyridine (11.3 mg, 0.105 mmol) was added to a CH$_2$Cl$_2$ (4 mL) solution of [Fe$_2$(μ-O$_2$CAr^{Tol})$_2$(O$_2$CAr^{Tol})$_2$(THF)$_2$] (73.1 mg, 0.0500 mmol), and the mixture was stirred for 20 min. Diethyl ether vapor diffusion into the resulting pale yellow-green solution led to the formation of colorless block crystals of **7** (63.6 mg, 83%) suitable for X-ray crystallography. FT-IR (KBr, cm^{-1}): 3054 (w), 2962 (w), 2922 (w), 2864 (w), 1604 (s), 1514 (s), 1454 (s), 1413 (m), 1353 (s), 1262 (w), 1188 (w), 1146 (w), 1109 (m), 1018 (m), 845 (m), 819 (s), 799 (s), 781 (s), 765 (s), 735 (m), 700 (m), 653 (w), 601 (w), 582 (w), 543 (m), 517 (s), 492 (w), 451 (w), 413 (w). Anal. Calcd. for C$_{98}$H$_{86}$N$_2$O$_8$Fe$_2$: C, 76.86; H, 5.66; N, 1.83. Found: C, 76.63; H, 5.78; N, 2.04.

[Fe$_2$(μ-O$_2$CAr^{Tol})$_2$(O$_2$CAr^{Tol})$_2$(4-Etpy)$_2$] (8). Colorless block crystals (66.0 mg, 68%) of

8 were obtained by vapor diffusion of Et$_2$O into a CH$_2$Cl$_2$ (4 mL) reaction mixture of

[Fe$_2$(μ-O$_2$CAr^{Tol})$_2$(O$_2$CAr^{Tol})$_2$(THF)$_2$] (92.6 mg, 0.0634 mmol) with 4-ethylpyridine (21.6 mg,

0.202 mmol). FT-IR (KBr, cm^{-1}): 3054 (w), 3023 (w), 2966 (w), 2915 (w), 1609 (s),1543 (s),

1514 (s), 1453 (s), 1406 (m), 1380 (s), 1312 (w), 1224 (w), 1186 (w), 1109 (w), 1069 (w), 1025

(w), 968 (w), 910 (w), 856 (m), 816 (s), 799 (s), 785 (s), 732 (s), 712 (s), 609 (w), 584 (m), 545

(m), 519, 489 (w), 448 (w). Anal. Calcd. for C$_{98}$H$_{86}$N$_2$O$_8$Fe$_2$: C, 76.86; H, 5.66; N, 1.83. Found:

C, 77.04; H, 5.85; N, 1.72.

[Fe$_2$(μ-O$_2$CAr^{4-FPh})$_2$(O$_2$CAr^{4-FPh})$_2$(2-Etpy)$_2$] (9). To a stirred CH$_2$Cl$_2$ (4 mL) solution of

[Fe$_2$(μ-O$_2$CAr^{4-FPh})$_2$(O$_2$CAr^{4-FPh})$_2$(THF)$_2$] (112 mg, 0.0751 mmol), was added 2-ethylpyridine

(34.8 mg, 0.325 mmol), forming a light yellow-green solution that was stirred for 20 min before

pentane vapor was diffused into the reaction mixture. Colorless block crystals (107 mg) were

isolated in 92% yield. FT-IR (KBr, cm^{-1}): 3062 (w), 2971 (w), 2880 (w), 1606 (s), 1571 (m),

1546 (m), 1510 (s), 1483 (w), 1455 (s), 1413 (m), 1380 (s), 1300 (w), 1222 (s), 1160 (s), 1096

(m), 1021 (w), 856 (s), 846 (s), 836 (s), 806 (s), 787 (m), 775 (m), 737 (w), 713 (m), 644 (w),

582 (w), 555 (s), 528 (m), 472 (w), 455 (w). Anal. Calcd. for C$_{90}$H$_{62}$N$_2$Fe$_2$O$_8$F$_8$: C, 69.15; H,

4.00; N, 1.79. Found: C, 69.44; H, 3.98; N, 2.09.

Physical Measurements. FT-IR spectra were recorded on a Thermo Nicolet Avatar 360

spectrometer with OMNIC software. ^{1}H NMR spectra were measured with a Varian 300

spectrometer housed in the Massachusetts Institute of Technology Department of Chemistry

Instrument Facility (MIT DCIF). Chemical shifts were referenced to the residual solvent peaks.

All spectra were recorded at ambient probe temperature, 293 K.

X-ray Crystallographic Studies. Intensity data were collected on a Bruker (formerly Siemens) APEX CCD diffractometer with graphite-monochromated Mo Kα radiation (λ = 0.71073 Å), controlled by a Pentium-based PC running the SMART software package.[29] Single crystals were mounted on the tips of glass fibers, coated with paratone-N oil, and cooled to −100 °C under a stream of N_2 maintained by a KRYO-FLEX low-temperature apparatus. Data collection and reduction protocols are described elsewhere.[30] The structures were solved by direct methods and refined on F^2 by using the SHELXTL-97 software[31] incorporated in the SHELXTL software package.[32] Empirical absorption corrections were applied by using the SADABS program,[33] and the structures were checked for higher symmetry by using the PLATON software.[34] All non-hydrogen atoms were located and their positions refined with anisotropic thermal parameters by least-squares cycles and Fourier syntheses. Hydrogen atoms were assigned to idealized positions and given thermal parameters equivalent to either 1.5 (methyl hydrogen atoms) or 1.2 (all other hydrogen atoms) times the thermal parameter of the carbon atom to which they were attached. Compound **1** contains one CH_2Cl_2 molecule disordered over two positions; the atoms were distributed equally. One Et_2O molecule is present in the lattice of compound **3**. In the asymmetric unit of **6** are contained CH_2Cl_2 molecules, one of which is half occupied and lies on a center of symmetry and the other is disordered and was refined with the atoms distributed equally over two positions. Data collection and experimental details are summarized in Table 3.1. The structures of **1** − **3**, and **5** − **9** are shown in Figures 3.1 − 3.8. Selected bond lengths and angles for **1** − **3**, and **5** − **9** are provided in Tables 3.2 and 3.3.

Mössbauer Spectroscopy. Mössbauer spectra were recorded on an MSI spectrometer (WEB Research Co.) with a [57]Co source in a Rh matrix maintained at room temperature in the MIT DCIF. Solid samples of **1** and **6** were prepared by suspending ~0.028 mmol of pulverized

crystalline material in Apeizon N grease and coating the mixture on the lid of a nylon sample holder. Data were collected at 4.2 K, and the isomer shift (δ) values are reported with respect to natural iron foil that was used for velocity calibration at room temperature. The spectra were fit to Lorentzian lines by using the WMOSS plot and fit program.[35]

Oxidation Product Analyses. Oxidation reactions were performed by exposing a CH_2Cl_2 solution of the diiron(II) complex to dioxygen over a period of time. All samples were prepared in an anaerobic glove box prior to bubbling dried dioxygen through them. To work up the oxygenation reactions, Chelex was added to the solutions to remove the iron. The resulting slurry was stirred for 2 h, after which the Chelex was removed by filtration. The resin was washed with CH_2Cl_2 twice more, and the filtrates were combined. The solvent was removed in vacuo to afford the N-donor ligands for analysis. The products were identified by NMR spectroscopy and/or GC-MS by comparing their NMR spectra and/or their retention times and mass spectral patterns to those of authentic samples. The amount of oxidized ligand obtained for **1**, **2**, and **4** was quantified by ^{1}H NMR spectroscopy using 1,4-bis(trimethylsilyl)benzene as an internal standard. For compounds **6** and **9** the amount of ligand oxidized was quantitated by GC-MS using 2-bromonaphthalene as an internal standard. Control experiments established that, in the absence of the diiron(II) complexes, neither dioxygen-saturated CH_2Cl_2 nor the workup process induces significant ligand oxidation.

GC-MS Analyses. Analyses were carried out on a Hewlett-Packard HP-5890 gas chromatograph connected to a HP-5971 mass analyzer. A J&W Scientific HP-5MS capillary column of dimensions (30 m x 0.25 mm x 0.25 μm) was employed for GC-MS studies. The following program was used to effect all separations: initial temperature = 90 °C; initial time = 7 min; temperature ramp = 90 – 210 °C at 20 deg/min; and a final time = 1.5 min. Quantitations

were made by comparison of the total ion count of 2-Etpy, 2-MeCHOHpy, and 2-acetylpyridine with that of 2-bromonaphthalene, the internal standard. Calibration plots for the detector response were prepared for authentic samples of 2-Etpy, 2-MeCHOHpy, 2-acetylpyridine, and 2-bromonaphthalene by using stock solutions of known concentrations.

Results

Synthesis and Characterization of Diiron(II) Complexes Containing Benzylpyridine and Benzylaniline Ligands. Displacement of THF from $[Fe_2(\mu\text{-}O_2CAr^{Tol})_2(O_2CAr^{Tol})_2(THF)_2]$ by two equiv of 2-Bnpy led to the formation of the diiron(II) complex $[Fe_2(\mu\text{-}O_2CAr^{Tol})_2$-$(O_2CAr^{Tol})_2(2\text{-}Bnpy)_2]$ (**1**), Scheme 3.1. The structure of **1** is displayed in Figure 3.1 and selected bond lengths and angles are listed Table 3.2. Two inequivalent, centrosymmetric diiron(II) complexes are located in the unit cell of **1** with Fe⋯Fe distances of 4.2385(9) Å and 4.6050(9) Å. In one dimer the geometry of the iron center is distorted trigonal bipyramidal with two oxygen atoms from bridging carboxylates, two from a bidentate carboxylate, and the N-atom of benzylpyridine ligand forming the coordination sphere. The iron atoms are four-coordinate in the other dimer because the terminal carboxylate is monodentate with a long Fe⋯O interaction of 2.463(2) Å. Both dimers have windmill structures (Chart 3.2). The methylene carbon atoms of the benzyl groups are 3.247(3) Å and 3.219(3) Å, respectively, away from the closest iron atom.

The 2-(4-ClBn)py analog, $[Fe_2(\mu\text{-}O_2CAr^{Tol})_2(O_2CAr^{Tol})_2(2\text{-}(4\text{-}ClBn)py)_2]$ (**2**) was also prepared (Scheme 3.1), the structure of which is presented in Figure 3.2. Selected bond lengths and angles are listed in Table 3.2. Scrutiny of these structural parameters reveals close similarities to **1**. One metal center comprises the asymmetric unit and is related to the other in the complex by a crystallographically imposed center of symmetry. The separation of the two metal

centers in **2** is 4.3907(11) Å and the distance between Fe1 and the benzyl carbon atom is 3.254(3) Å.

Bright green crystals of **3** were isolated from the reaction of $[Fe_2(\mu-O_2CAr^{Tol})_2-(O_2CAr^{Tol})_2(THF)_2]$ with 4-Bnpy (Scheme 3.1). The X-ray structure confirms the formation of the diiron(II) complex, (Figure 3.3). Table 3.2 lists selected bond lengths and angles. The diiron core is bridged by four carboxylate ligands, the O-atoms of which form the base of a square pyramid that is capped by 4-Bnpy ligands. The distance between the two metal centers in this paddlewheel structure (Chart 3.2) is 2.7715(6) Å, almost 2 Å less than the 4.6050(9) Å separation in **1**; the iron-to-benzyl carbon distance in **3** is 6.392(2) Å, ~3 Å longer than that observed in **1**.

Treatment of the $[Fe_2(\mu-O_2CAr^{4-FPh})_2(O_2CAr^{4-FPh})_2(THF)_2]$ complex with 2-Bnpy results in the formation of **4**, Scheme 3.2. The structure of **4** could not be completely solved due to severe solvent disorder, however the connectivity of the metal fragment could be ascertained. The windmill geometry is adopted, and the bond lengths and angles are comparable to those in **1**. Distorted trigonal bipyramidal iron centers, related by an inversion center, are coordinated by two bridging carboxylates, one bidentate carboxylate, and one benzylpyridine

A doubly carboxylate-bridged diiron(II) complex $[Fe_2(\mu-O_2CAr^{Tol})_2(O_2CAr^{Tol})_2-(2-Bnan)_2]$ (**5**) is isolated from the reaction of 2-Bnan with $[Fe_2(\mu-O_2CAr^{Tol})_2(O_2CAr^{Tol})_2(THF)_2]$ (Scheme 3.1). A structural determination revealed two iron centers related by an inversion center. Figure 3.4 shows the structure of **5** and pertinent bond lengths and angles are listed in Table 3.2. These atoms are bridged by two carboxylates which coordinate in an unsymmetrical *syn,syn*-bidentate mode between the two metal centers, which are separated by 4.0644(10) Å.[36] The Fe···Fe separation is 4.0644(10) Å. In addition each metal center is ligated to one bidentate

carboxylate ligand and a benzylaniline moiety. The methylene carbon atom of the benzyl group is 4.522(3) Å away from the closest iron atom.

Synthesis and Characterization of Diiron(II) Complexes Containing Ethylpyridine Ligands. Compounds **6**, **7**, and **8** were prepared by displacement of the THF molecules in $[Fe_2(\mu-O_2CAr^{Tol})_2(O_2CAr^{Tol})_2(THF)_2]$ with 2 equiv of 2-, 3-, or 4-ethylpyridine, respectively (Scheme 3.3). Their X-ray structures are depicted in Figures 3.5 – 3.7, and selected bond lengths and angles are available in Table 3.3. Each compound adopts windmill geometry in which the iron centers, related by crystallographically imposed centers of symmetry, are coordinated by two bridging carboxylate O-atoms, one from a terminal carboxylate, and one N-atom from ethylpyridine. A fourth O-atom from the terminal carboxylate binding in a bidentate fashion completes the coordination sphere of **8**. Among the three compounds, the Fe···Fe distance in **7** is shortest at 4.0872(10) Å, followed by **8** with a distance of 4.1546(13) Å. A significantly larger separation between metal centers of 4.3361(12) Å occurs in **6**, probably because its pyridine ortho substituent offers the most steric bulk near the diiron core. The nearest iron-to-substrate (Fe1···C6) distance is 3.237(4) Å in the 2-Etpy compound, **6**, being 5.446(3) Å in **7** and 6.439(4) Å in **8**.

Treatment of $[Fe_2(\mu-O_2CAr^{4\text{-FPh}})_2(O_2CAr^{4\text{-FPh}})_2(THF)_2]$ with 2-Etpy results in the formation of **9** (Scheme 3.2). Figure 3.8 display the structure, and Table 3.3 lists selected bond lengths and angles. The structure of **9** has two centrosymmetric molecules in the unit cell that exhibit the windmill geometry with Fe···Fe separations of 4.4826(9) Å for Fe1···Fe1A and 4.4433(9) Å for Fe2···Fe2A. Distorted trigonal bipyramidal iron centers are coordinated by two bridging carboxylate O-atoms, two from a bidentate carboxylate, and one N-atom from

ethylpyridine. The iron-to-methylene carbon distances are 3.197(3) Å for Fe1···C6 and 3.214(3) Å for Fe2···C51.

Mössbauer Spectroscopy. The zero-field Mössbauer spectra, measured at 4.2 K, of powder samples of **1** and **6** are portrayed in Figure 9. The following parameters refer to **1** and **6**, respectively. Both spectra exhibit a single sharp (Γ = 0.23 – 0.30 and 0.25 – 0.27 mm s^{-1}), slightly asymmetric quadrupole doublet. The quadrupole splitting (ΔE_Q = 3.05(2) and 2.96(2) mm s^{-1}) and isomer shift (δ = 1.22(2) and 1.20(2) mm s^{-1}) values are consistent with those of high spin diiron(II) complexes having oxygen-rich coordination environments, indicating that **1** and **6** have high spin S = 2 ground states.[20,37,38]

Dioxygen Reactivity of Diiron(II) Complexes Containing Benzyl Substrates. Table 3.4 summarizes of the conditions and amount of oxidation product isolated for the reactions of compounds **1** – **5** with dioxygen in CH_2Cl_2. The product formed upon exposure of a CH_2Cl_2 solution of **1** to dioxygen at ambient temperature, identified by GC-MS and quantitated by ^{1}H NMR spectroscopy, is α-phenyl-2-pyridylmethanol, in an 82% yield based on **1**. The remaining recovered material is unmodified benzylpyridine. Similarly, upon exposure of **2** to dioxygen, the 2-(4-ClBn)py was oxidized at the benzyl position. The alcohol is produced in an average yield of 40% based on **2**, established by ^{1}H NMR spectroscopy. Reaction of **4** with dioxygen resulted in the formation of α-phenyl-2-pyridylmethanol, with a yield of 66%. Product analysis following the oxygenation of **3** or **5** revealed only unmodified 4-benzylpyridine or 2-benzylaniline. No evidence of the alcohol was obtained.

Dioxygen Reactivity of Diiron(II) Complexes Containing Ethyl Substrates. A summary of the conditions and amount of oxidation product isolated for the reaction of compounds **6** – **9** with dioxygen in CH_2Cl_2 is included in Table 3.5. The reactivity of the

diiron(II) complexes **6 – 9** was probed by decomposing the oxygenated CH_2Cl_2 solution and analyzing the contents by GC-MS. Despite the different carboxylate ligands, analysis of the reaction solutions of **6** and **9** with dioxygen by GC-MS displayed three peaks with $M^+ = 107$, 123, and 121. By comparing their retention times with those of authentic samples, we identified them as 2-ethylpyridine, 2-pyridylmethanol, and 2-acetylpyridine, respectively. ^1H NMR spectroscopy confirmed that α-methyl-2-pyridinemethanol is indeed the product and not 2-pyridylethanol, the other possible isomer with a molecular weight of 123. Slightly more oxidized ligand is isolated for **6** than **9**, 46% vs 35% based on starting dimer, but in both systems four times more 2-acetylpyridine was recovered than the pyridylalcohol product. Analysis of the analogous dioxygen reactions of **7** and **8** revealed a species with $M^+ = 107$, corresponding to unmodified 3- or 4-ethylpyridine.

Discussion

Intramolecular oxidation of benzylic C–H bonds of coordinated aliphatic amine ligands in carboxylate-rich diiron(II) complexes upon exposure to dioxygen has been achieved.[21-24] There are many examples of mononuclear and dinuclear iron complexes with pyridine or pyridine-modified ligands in both nitrogen- and oxygen-rich ligand environments.[20,39] Aniline is not commonly employed as a ligand in iron complexes, but aniline derivatives, including bidentate ligands such as 1,2-phenylenediamine and o-aminothiophenol,[40-42] a macrocycle bearing pendant anilino donors on the 1,4,7-triazacyclononane scaffold,[43] and other aliphatic amines have successfully coordinated ferrous metal centers.[15,21-23] In preparing carboxylate-bridged diiron(II) complexes described herein, pyridine and aniline were chosen as alternative ancillary nitrogen donors. The choice of benzylpyridines and benzylaniline was made to preserve the same dangling substrate moiety.

To provide access to the oxidizing intermediates formed upon reaction of the diiron(II) center with O_2, substrates were placed in the ortho position of the ancillary ligands. In all cases resulting steric demands of the ligands afforded windmill structures, which were isolated and crystallographically characterized for **1**, **2**, **4**, **5**, **6**, and **9**. The position of the substrate on the pyridine ring can affect both the stereochemistry and dioxygen reactivity of the resultant diiron(II) complex.[25] To investigate further this relationship for C–H activation, two series of ligands were employed, namely, 2-, 3-, or 4-benzylpyridine and 2-, 3-, or 4-ethylpyridine. Using 3-Bnpy as the N-donor for carboxylate-bridged diiron(II) complexes resulted only in the formation of insoluble powders,[44] but isolation of the 4-Bnpy complex, **3**, revealed a tetrabridged-carboxylate diiron(II) complex. Movement of the ethyl-substituent from the ortho to meta and para positions with 3- and 4-Etpy respectively did not alter the geometry of the resultant diiron(II) centers. Both **7** and **8** contain doubly carboxylate-bridged dimetallic units.

The use of terphenyl carboxylate ligands has enabled the synthesis of coordinatively unsaturated carboxylate-bridged diiron(II) complexes that are geometrically analogous to those of reduced RNR-R2,[45] MMOH,[8,46] and Δ9D[47] enzyme active sites. The windmill structures of diiron(II) benzylpyridine compounds **1**, **2**, and **4** are very similar. Each metal atom is coordinated by one N-atom from benzylpyridine and three O-atoms from one terminal and two bridging carboxylate ligands. The iron atoms are four- or five-coordinate depending on the length of the fourth Fe–O interaction from the terminal carboxylate. The exchange of $^-O_2CAr^{Tol}$ for $^-O_2CAr^{4\text{-FPh}}$, or 2-benzyl- for 2-(4-chloro)benzylpyridine, causes little difference in the resultant diiron(II) complexes **4** and **2** compared to **1**. There are two inequivalent centrosymmetric molecules in the crystal lattice of **1**. A four coordinate iron (Fe1) has three short Fe–O bonds, the average of which, denoted as Fe–O_{av}, being 1.999(2) Å, and one long bond (Fe–O_L), 2.463(3) Å.

A second molecule of **1**, which includes Fe2, has Fe–O_{av} = 2.033(2) Å and an Fe–O_L of 2.281(2) Å, thus rendering the Fe2 center five-coordinate. As a result, the Fe⋯Fe separation is larger for five-coordinate Fe2 compared to four-coordinate Fe1, the respective distances being 4.6052(9) Å and 4.2380(9) Å. The five-coordinate iron center in **2** has Fe –O_{av} of 2.013(2) with Fe–O_L bond equal to 2.308(2). Its metal-metal separation is 4.3908(11) Å. The smaller the difference between Fe–O_L and Fe–O_{av}, the larger the separation between the two metal centers. Typically when the Fe–O_{av} and Fe–O_L distances are disparate, the coordination number of the iron center reduces from 5 to 4 and the metal-metal distance is shortened. A presentation of this information is contained in Table 3.6.

The windmill structure of the diiron(II) benzylaniline derivative **5** is closely related to those of the benzylpyridine compounds, the differences being a slightly longer Fe–N distance (~0.05 Å) and shorter Fe–O bonds. The Fe–O_{av} is 2.016(3) Å, with the Fe–O_L being 2.214(2) Å. Despite the five-coordinate metal centers, the Fe⋯Fe separation of 4.0656(10) Å is the shortest yet observed. This result reflects the decreased steric crowding at the metal center for benzylaniline compared to benzylpyridine, because the aromatic ring of the N-donor is an additional atom removed from the metal center.

When the benzyl group is shifted from the ortho to the para position of the pyridine ring, the structure converts to the paddlewheel isomer. The tetracarboxylate-bridged diiron center of **3** differs greatly from the other benzylpyridine complexes. Each metal atom has two long and two short Fe–O bonds, with the average distances for each of 2.1338(14) Å and 2.0246(13) Å. The Fe–N bond is ~0.05 Å shorter than those of the windmill isomers, and the metal-metal distance is 2.7715(6) Å, 1.3 Å shorter than the smallest separation observed in a windmill structure.

The structural parameters of diiron(II) ethylpyridine complexes **6** – **9** are comparable, irrespective of the geometry of the ethylpyridine moiety or the substituents on the terphenyl carboxylate ligands. The Fe–N bond lengths of **6** and **9** are within 0.01 Å of one another. The four-coordinate metal center has Fe–O_{av} = 1.998(3) Å and Fe–O_L = 2.517(3) Å. There are two five-coordinate centrosymmetric molecules in **9**. The Fe–O_{av} is 2.025(2) Å for Fe1 and 2.002(2) Å for Fe2, and the Fe–O_L bond lengths are 2.225(2) Å and 2.330(2) Å for Fe1 and Fe2, respectively, ~0.2-0.3 Å shorter than in **6**. As a result the respective Fe⋯Fe separations are longer for **9** than for **6**, 4.4830(10) and 4.4434(10) Å vs 4.3361(12) Å. Both **7** and **8** have much smaller Fe⋯Fe distances, 4.0861(10) Å and 4.1542(14) Å, respectively. The removal of the ethyl substituent from the ortho position of the pyridine ring relieves steric strain. In addition four-coordinate iron atoms occur in **7** resulting in the shortest Fe–O_{av} of 1.9714(17) Å and longest Fe–O_L interaction of 2.715(2) Å. The metal-metal distance of **8**, short for five-coordinate iron, is balanced by a longer Fe–O_{av} of 2.068(3) Å. This information is included in Table 3.6.

The single sharp quadrupole doublet exhibited in the Mössbauer spectra of **1** and **6** reflects the fact that, for both compounds, the iron centers are in equivalent coordination environments that are related by a virtual C_2 axis. The quadrupole splitting (ΔE_Q = 3.05(2) and 2.96(2) mm s^{-1}) and isomer shift (δ = 1.22(2) and 1.20(2) mm s^{-1}) values of **1** and **6**, respectively, are consistent with those of high spin diiron(II) complexes in nitrogen and oxygen coordination environments.[20,37] Even though both **1** and **6** have iron(II) sites with coordination number 4, their isomer shifts are slightly higher than those usually observed (1.0 – 1.1 mm s^{-1}) for this geometry.[38] The quadrupole splitting and isomer shift parameters obtained for **1** and **6** are analogous to those of MMOH$_{red}$, which are 3.01 and 1.3 mm s^{-1}, respectively.[48] This similarity reflects their oxygen-rich ligand environment mimicking that of the enzyme active site.

The reactivity of the benzylpyridine complexes is greater than that of the ethylpyridine analogs, as expected from the slightly weaker ~2 kcal/mol[49-51] C–H bond energy of the benzyl moiety. In both systems C–H activation only occurs when the substrate is located at the ortho position of the coordinated pyridine ligand. No oxidation occurs when pyridine is replaced by aniline as coordinating ligand to which the substrate is appended. Although **1** and **5** have similar solid state geometries, the benzyl moiety is 1.5 Å farther away from the closest iron atom in the unreactive 2-benzylaniline, compared to the 2-benzylpyridine, complex.

When the benzyl group is moved from the ortho to the para position of the pyridine ring, the substrate is more distant from the diiron core than in **5**, and the resultant diiron(II) complex is affected. Upon addition of dioxygen to a CH_2Cl_2 solution of **3**, no ancillary ligand oxidation occurs. The benzyl carbon of the 4-Bnpy is more than 3 Å farther away from the closest iron atom than it is in **1** and is directed outward by the geometry of the ligand. Only by ligand dissociation or intermolecular reactions would it be possible to access any oxidizing species formed at the diiron core.

The core structures of the four ethylpyridine complexes **6** – **9** are virtually identical. Despite differences in the carboxylate ligands between **6** and **9** and in the pyridine ring substitution position for **6**, **7**, and **8**, the compounds all adopt windmill structures with two ethyl-substituted pyridines as the N-donor ligands. Only where the ethyl group is in the ortho position, however, is the 2-pyridylmethanol formed upon addition of dioxygen. For **7** and **8**, ethylpyridine is quantitatively recovered. This result is very strong evidence that an O_2-activated diiron species is responsible for intramolecular hydroxylation of the ethyl group, as occurs in MMOH.

The carboxylate ligands with *p*-tolyl substituents form more reactive diiron oxidants than their *p*-fluorophenyl substituent analogs for both the benzyl- and ethylpyridine systems. Since

steric requirements of these two terphenyl carboxylate groups are similar, we attribute the decreased yield of alcohol product between the $^-O_2CAr^{Tol}$ and $^-O_2CAr^{4-FPh}$ systems to electronic factors. The pK_a values of HO_2CAr^{4-FPh} and HO_2CAr^{Tol} are 6.14 and 6.50, respectively,[52] but there are four such ligands, which may be sufficient to alter the reactivity of O_2-generated species required to oxidize the C–H bonds and alter the yield.

Electronic factors are similarly likely to influence the relative reactivities of **1** and **2**. The chloro substituent of the benzylpyridine in 2-(4-ClBn)py is far enough removed from the diiron center so as not to affect steric properties at the dimetallic center, but will withdraw electron density from the benzylic position. The pK_a values of pyridinium and 4-chloropyridinium are 5.25 and 3.84, respectively.[53] This difference in donating ability of H vs Cl may be responsible for diminished amount of substrate that is oxidized in **2** compared to **1**.

Conclusions

A series of diiron(II) complexes were prepared with benzyl- and ethylpyridine ligands to serve as substrates for C–H activation following introduction of dioxygen. Intramolecular oxidation of organic moieties tethered in this manner to the diiron core was accomplished without the adjacent heteroatom employed in previous work.[21-24] The current range of substrates was also extended from benzyl C–H to include less reactive ethyl C–H bonds. Substrate oxidation occurs only when the group is in close proximity to the diiron core by positioning it ortho to the coordinated N-atom of pyridine ring. No oxidation was observed for substituents placed in the meta or para positions of the pyridine. When steric factors remain constant, more electron-donating carboxylate and pyridine ligands increase the amount of oxidized product compared to their electron more deficient counterparts, suggesting the need to stabilize an electrophilic intermediate to carry out these transformations.

References

(1)   Erwin, D. P.; Erickson, I. K.; Delwiche, M. E.; Colwell, F. S.; Strap, J. L.; Crawford, R. L. *Appl. Environ. Microbiol* **2005**, *71*, 2016-2024.

(2)   Vardar, G.; Wood, T. K. *Appl. Environ. Microbiol* **2004**, *70*, 3253-3161.

(3)   Colby, J.; Stirling, D. I.; Dalton, H. *Biochem. J.* **1977**, *165*, 395-402.

(4)   Feig, A. L.; Lippard, S. J. *Chem. Rev.* **1994**, *94*, 759-805.

(5)   Wallar, B. J.; Lipscomb, J. D. *Chem. Rev.* **1996**, *96*, 2625-2657.

(6)   Merkx, M.; Kopp, D. A.; Sazinsky, M. H.; Blazyk, J. L.; Müller, J.; Lippard, S. J. *Angew. Chem., Int. Ed. Engl.* **2001**, *40*, 2782-2807.

(7)   Baik, M.-H.; Newcomb, M.; Friesner, R. A.; Lippard, S. J. *Chem. Rev.* **2003**, *103*, 2385-2419.

(8)   Whittington, D. A.; Lippard, S. J. *J. Am. Chem. Soc.* **2001**, *123*, 827-838.

(9)   Rosenzweig, A. C.; Frederick, C. A.; Lippard, S. J.; Nordlund, P. *Nature* **1993**, *366*, 537-543.

(10)   Lee, D.; Sorace, L.; Caneschi, A.; Lippard, S. J. *Inorg. Chem.* **2001**, *40*, 6774-6781.

(11)   Mandal, S. K.; Young, V. G., Jr.; Que, L., Jr. *Inorg. Chem.* **2000**, *39*, 1831-1833.

(12)   Herold, S.; Lippard, S. J. *J. Am. Chem. Soc.* **1997**, *119*, 145-156.

(13)   Goldberg, D. P.; Telser, J.; Bastos, C. M.; Lippard, S. J. *Inorg. Chem.* **1995**, *34*, 3011-3024.

(14)   Rardin, R. L.; Poganiuch, P.; Bino, A.; Goldberg, D. P.; Tolman, W. B.; Liu, S.; Lippard, S. J. *J. Am. Chem. Soc.* **1992**, *114*, 5240-5249.

(15)   Lee, D.; Lippard, S. J. *Inorg. Chim. Acta* **2002**, *341*, 1-11.

(16)   Hagadorn, J. R.; Que, L., Jr.; Tolman, W. B. *J. Am. Chem. Soc.* **1998**, *120*, 13531-13532.

(17)   Lee, D.; Lippard, S. J. *J. Am. Chem. Soc.* **1998**, *120*, 12153-12154.

(18)   Tolman, W. B.; Que, L., Jr. *J. Chem. Soc., Dalton Trans.* **2002**, 653-660.

(19)   Lee, D.; Lippard, S. J. In *Comprehensive Coordination Chemistry II Bio-Coordination Chemistry*; Que, L., Jr., Tolman, W. B., Eds.; Elsevier Inc.: San Diego, CA, 2004; Vol. 8, pp 309-342.

(20)   Tshuva, E. Y.; Lippard, S. J. *Chem. Rev.* **2004**, *104*, 987-1012.

(21)   Lee, D.; Lippard, S. J. *J. Am. Chem. Soc.* **2001**, *123*, 4611-4612.

(22)   Lee, D.; Lippard, S. J. *Inorg. Chem.* **2002**, *41*, 827-837.

(23)   Yoon, S.; Lippard, S. J. *Inorg. Chem.* **2003**, *42*, 8606-8608.

(24)   Carson, E. C. In *Doctoral Dissertation in Inorganic Chemistry*; Massachusetts Institute of Technology: Cambridge, MA, 2005; Chapter 2.

(25)   Carson, E. C.; Lippard, S. J. *J. Am. Chem. Soc.* **2004**, *126*, 3412-3413.

(26)   Pangborn, A. B.; Giardello, M. A.; Grubbs, R. H.; Rosen, R. K.; Timmers, F. J. *Organometallics* **1996**, *15*, 1518-1520.

(27)   Lee, D.; Lippard, S. J. *Inorg. Chem* **2002**, *41*, 2704-2719.

(28)   Bellezza, F.; Cipiciani, A.; Cruciani, G.; Fringuelli, F. *J. Chem. Soc., Perkin Trans. 1* **2000**, *24*, 4439-4444.

(29)   *SMART v5.626: Software for the CCD Detector System*; Bruker AXS: Madison, WI, 2000.

(30)   Kuzelka, J.; Mukhopadhyay, S.; Spingler, B.; Lippard, S. J. *Inorg. Chem* **2003**, *42*, 6447-6457.

(31)   Sheldrick, G. M. *SHELXTL97-2: Program for Refinement of Crystal Structures;* University of Göttingen, Germany, 1997.

110

(32) *SHELXTL v5.10: Program Library for Structure Solution and Molecular Graphics;* Bruker AXS: Madison, WI, 1998.

(33) Sheldrick, G. M. *SADABS: Area-Detector Absorption Correction;* University of Göttingen, Germany, 1996.

(34) Spek, A. L. *PLATON, A Multipurpose Crystallographic Tool;* Utrecht University: Utrecht, The Netherlands, 1998.

(35) Kent, T. A. *WMOSS v2.5: Mössbauer Spectral Analysis Software;* WEB Research Co.: Minneapolis, 1998.

(36) Rardin, R. L.; Tolman, W. B.; Lippard, S. J. *New J. Chem.* **1991**, *15*, 417-430.

(37) Münck, E. In *Physical Methods in Bioinorganic Chemistry: Spectroscopy and Magnetism;* Que, L., Jr., Ed.; University Science Books: Sausalito, CA, 2000; pp 287-319.

(38) Yoon, S.; Lippard, S. J. *J. Am. Chem. Soc.* **2005**, *127*, 8386-8397.

(39) Costas, M.; Mehn, M. P.; Jensen, M. P.; Que, L., Jr. *Chem. Rev.* **2004**, *104*, 939-986.

(40) Takács, J.; Soós, E.; Nagy-Magos, Z.; Markó, L; Gervasio, G.; Hoffmann, T. *Inorg. Chim. Acta* **1989**, *166*, 39-46.

(41) Dickman, M. H. *Acta Cryst.* **2000**, *C56*, 58-60.

(42) Ghosh, P.; Begum, A.; Bill, E.; Weyhermüller, T.; Wieghardt, K. *Inorg. Chem* **2003**, *42*, 3208-3215.

(43) Fallis, I. A.; Farley, R. D.; Malik, K. M. A.; Murphy, D. M.; Smith, H. J. *J. Chem. Soc., Dalton Trans.* **2000**, 3632-3639.

(44) Carson, E. C.; Lippard, S. J. Unpublished results.

(45)   Logan, D. T.; Su, X.-D.; Åberg, A.; Regnström, K.; Hajdu, J.; Eklund, H.; Nordlund, P.
        Structure **1996**, *4*, 1053-1064.

(46)   Rosenzweig, A. C.; Nordlund, P.; Takahara, P. M.; Frederick, C. A.; Lippard, S. J. *Chem.*
        Biol. **1995**, *2*, 409-418.

(47)   Lindqvist, Y.; Huang, W.; Schneider, G.; Shanklin, J. *EMBO J.* **1996**, *15*, 4081-4092.

(48)   DeWitt, J. G.; Bentsen, J. G.; Rosenzweig, A. C.; Hedman, B.; Green, J.; Pilkington, S.
        J.; Papaefthymiou, G. C.; Dalton, H.; Hodgson, K. O.; Lippard, S. J. *J. Am. Chem. Soc.*
        1991, *113*, 9219-9235.

(49)   McMillen, D. F.; Golden, D. M. *Ann. Rev. Phys. Chem.* **1982**, *33*, 493-532.

(50)   Barton, B. D.; Stein, S. E. *J. Chem. Soc., Faraday Trans. 1* **1981**, *77*, 1755-1762.

(51)   Rossi, M. J.; McMillen, D. F.; Golden, D. M. *J. Phys. Chem.* **1984**, *88*, 5031-5039.

(52)   Chen, C.-T.; Siegel, J. S. *J. Am. Chem. Soc.* **1994**, *116*, 5959-5960.

(53)   Asperger, S.; Cetina-Cizmek, B. *Inorg. Chem.* **1996**, *35*, 5232-5236.

Table 3.1. Summary of X-ray crystallographic Data

	$1\cdot CH_2Cl_2$	2	$3\cdot C_4H_{10}O$	5
Empirical Formula	$Fe_2C_{109}H_{92}N_2O_8Cl_2$	$Fe_2C_{108}H_{88}N_2O_8Cl_2$	$Fe_2C_{106}H_{112}N_2O_9$	$Fe_2C_{110}H_{94}N_2O_8$
Formula Weight	1740.50	1724.40	1729.64	1683.57
Space Group	$P\bar{1}$	Pbca	$P\bar{1}$	$P2_1/c$
a, Å	11.8024(11)	13.751(3)	14.516(3)	13.774(3)
b, Å	14.7291(13)	23.133(5)	17.236(4)	23.088(5)
c, Å	25.142(2)	27.455(6)	20.031(5)	14.488(3)
α, deg	94.819(2)		115.140(3)	
β, deg	97.452(2)		91.959(4)	107.498(4)
γ, deg	91.443(2)		93.572(4)	
V, Å^3	4315.5(7)	8734(3)	4517.8(18)	4394.4(15)
Z	2	4	2	2
ρ_{calc}, g/cm^3	1.339	1.311	1.271	1.272
T, °C	-100	-100	-100	-100
μ(Mo Kα), mm^{-1}	0.461	0.455	0.383	0.392
θ limits, deg	1.39 – 26.73	1.88 – 27.50	1.74 – 26.37	1.78 – 26.38
total no. of data	36786	72872	36881	28010
no. of unique data	18034	9955	18153	7686
no. of params	1134	554	1134	550
Goodness-of-fit on F^2	1.108	1.320	1.029	1.029
R1^a	0.0642	0.0738	0.0423	0.0634
wR^{2b}	0.1367	0.1684	0.1096	0.1191
max, min peaks, e/Å^3	0.474, -0.354	0.731, -0.493	0.688, -0.358	0.357, -0.313

^{a}R1 $= \Sigma||F_o|-F_c||/\Sigma|F_o|$. ^{b}wR$^2 = \{\Sigma[w(F_o^2-F_c^2)^2]/\Sigma[w(F_o^2)^2]\}^{1/2}$.

Table 3.1. Continued

	6·2.5CH$_2$Cl$_2$	7	8	9
Empirical Formula	Fe$_2$C$_{101}$H$_{92}$N$_2$O$_8$Cl$_5$	Fe$_2$C$_{98}$H$_{86}$N$_2$O$_8$	Fe$_2$C$_{98}$H$_{86}$N$_2$O$_8$	Fe$_2$C$_{90}$H$_{62}$N$_2$O$_8$F$_8$
Formula Weight	1750.72	1531.39	1531.39	1563.12
Space Group	P2$_1$/c	P$\bar{1}$	P2$_1$/c	P$\bar{1}$
a, Å	15.219(2)	12.311(3)	10.775(3)	12.2612(16)
b, Å	10.8186(16)	13.322(3)	24.890(8)	13.3582(17)
c, Å	29.434(4)	14.608(3)	15.118(5)	23.981(3)
α, deg		115.544(3)		84.355(2)
β, deg	117.387(6)	108.042(4)	106.178(6)	86.811(2)
γ, deg		98.087(4)		67.916(2)
V, Å^3	4303.1(10)	1947.5(8)	3894(2)	3621.2(8)
Z	2	1	2	2
ρ$_{calc}$, g/cm^3	1.351	1.306	1.306	1.434
T, °C	-100	-100	-100	-100
μ(Mo Kα), mm^{-1}	0.553	0.434	0.434	0.484
θ limits, deg	2.04 – 26.38	1.74 – 26.37	1.62 – 26.39	1.65 – 26.37
total no. of data	34613	16083	31640	29709
no. of unique data	8807	7841	7957	14571
no. of params	583	500	500	991
Goodness-of-fit on F^2	1.206	1.224	1.314	1.061
R1[a]	0.0894	0.0533	0.0734	0.0552
wR2[b]	0.1886	0.1317	0.1467	0.1237
max, min peaks, e/Å^3	0.952, -0.664	0.865, -0.225	1.058, -0.497	0.495, -0.324

[a]R1 $= \Sigma||F_o|-F_c||/\Sigma|F_o|$. [b]wR2 $= \{\Sigma[w(F_o^2-F_c^2)^2]/\Sigma[w(F_o^2)^2]\}^{1/2}$.

Table 3.2. Selected Bond Lengths (Å) and Angles (deg) for **1, 2, 3**, and **5**[a]

	1	2	3	5
Fe1⋯Fe2	4.2380(9)[b] 4.6052(9)[c]	4.3908(11)	2.7715(6)	4.0646(10)
Fe1–N1	2.124(2)[b] 2.150(2)[c]	2.146(2)	2.0830(16) 2.0901(16)[e]	2.175(2)
Fe1–O1	2.0270(19)[b] 1.977(2)[c]	2.001(2)	2.1349(13) 2.0238(13)[e]	1.978(2)
Fe1–O2	1.956(2)[b] 2.003(2)[c]	1.971(2)	2.0251(13) 2.1372(14)[e]	1.989(2)
Fe1–O3	2.014(2)[b] 2.118(2)[c]	2.068(2)	2.1322(13) 2.0176(13)[e]	2.0798(19)
Fe1–O4	2.463(2)[b,d] 2.281(2)[c]	2.308(2)	2.0319(13) 2.1310(14)[e]	2.2150(19)
O1–Fe1–N1	100.40(9)[b] 113.05(9)[c]	97.59(9)	95.58(6) 103.97(6)[e]	96.36(9)
O2–Fe1–	95.26(9)[b] 96.61(9)[c]	98.87(9)	101.82(6) 97.19(6)[e]	87.29(9)
O3–Fe1–N1	93.09(9)[b] 85.70(8)[c]	91.46(8)	98.14(6) 96.69(6)[e]	98.26(9)
O4–Fe1–N1	150.10(8)[b] 144.90(8)[c]	150.39(8)	99.31(6) 97.05(6)[e]	153.99(9)
O1–Fe1–O2	115.98(9)[b] 106.16(9)[c]	112.41(9)	87.59(5) 88.65(5)[e]	121.42(9)
O1–Fe1–O3	110.50(8)[b] 125.43(9)[c]	119.39(9)	166.24(5) 159.29(5)[e]	113.22(9)
O1–Fe1–O4	95.37(8)[b] 89.56(8)[c]	101.99(8)	91.39(5) 91.06(5)[e]	106.18(8)
O2–Fe1–O3	130.19(9)[b] 122.66(9)[c]	125.10(9)	90.61(5) 87.26(5)[e]	124.06(9)
O2–Fe1–O4	100.44(8)[b] 102.55(8)[c]	93.97(8)	158.85(5) 165.38(5)[e]	91.75(8)
O3–Fe1–O4	57.45(8)[b] 59.20(8)[c]	59.56(7)	85.39(5) 87.86(5)[e]	61.18(7)

[a]Numbers in parentheses are estimated standard deviations of the last significant figures. Atoms are labeled as indicated in Figures 3.1 – 3.4. [b]Molecule 1 in asymmetric unit. [c]Molecule 2 in the asymmetric unit. [d]Fe⋯O$_{non\text{-}coordinating}$. [e]Parameter for Fe2 with N2, O5 – O8.

Table 3.3. Selected Bond Distances (Å) and Angles (deg) for **6** – **9**[a]

	6	7	8	9
Fe1···Fe2	4.3366(12)	4.0861(10)	4.1542(14)	4.4830(10)[b]
				4.4434(10)[c]
Fe1–N1	2.143(3)	2.104(2)	2.130(3)	2.135(3)[b]
				2.136(3)[c]
Fe1–O1	1.959(3)	1.9569(17)	2.013(3)	1.943(2)[b]
				1.952(2)[c]
Fe1–O2	2.010(3)	1.9861(17)	1.972(2)	2.013(2)[b]
				2.002(2)[c]
Fe1–O3	2.023(3)	1.9711(18)	2.061(3)	2.118(2)[b]
				2.052(2)[c]
Fe1–O4	2.517(3)[d]	2.715(2)[d]	2.323(3)	2.225(2)[b]
				2.330(2)[c]
O1–Fe1–N1	104.61(13)	97.73(8)	94.20(11)	104.54(11)[b]
				98.49(11)[c]
O2–Fe1–N1	96.74(12)	99.99(8)	95.68(11)	99.25(10)[b]
				103.44(11)[c]
O3–Fe1–N1	92.79(12)	91.64(8)	93.37(11)	91.94(10)[b]
				92.61(9)[c]
O4–Fe1–N1	149.18(12)	144.49(7)	150.91(10)	151.20(9)[b]
				151.40(10)[c]
O1–Fe1–O2	114.46(13)	122.82(8)	120.61(11)	108.07(11)[b]
				110.24(11)[c]
O1–Fe1–O3	125.14(12)	121.68(8)	114.31(10)	133.70(10)[b]
				132.13(11)[c]
O1–Fe1–O4	98.37(11)	96.76(7)	88.49(10)	91.44(9)[b]
				96.41(10)[c]
O2–Fe1–O3	114.46(13)	111.64(8)	123.29(11)	111.53(10)[b]
				112.06(10)[c]
O2–Fe1–O4	93.25(12)	99.01(7)	107.80(10)	98.28(9)[b]
				94.02(9)[c]
O3–Fe1–O4	56.43(11)	53.36(7)	59.53(9)	60.29(8)[b]
				59.57(8)[c]

[a]Numbers in parentheses are estimated standard deviations of the last significant figures. Atoms are labeled as indicated in Figures 3.5 – 3.8. [b]Molecule 1 in asymmetric unit. [c]Molecule 2 in the asymmetric unit. [d]Fe···O$_{non-coordinating}$.

Table 3.4. Summary of the Conditions and Amount of Oxidation Product Isolated Following the Reaction of Compounds **1 – 5** with Dioxygen in CH_2Cl_2 at Room Temperature

	$[Fe_2]$ (mM)	Reaction Time (min)	% Oxidized Ligand Recovered[a]
1	4.0	40	82
2	1.8	30	40
3	2.4	30	0
4	4.3	30	66
5	1.8	30	0

[a]Based on $[Fe_2]$

Table 3.5 Summary of the Conditions and Amount of Oxidation Product Isolated Following the Reaction of Compounds **6 – 9** with Dioxygen in CH_2Cl_2 at Room Temperature.

	$[Fe_2]$ (mM)	Reaction Time (min)	% Oxidized Ligand Recovered[a]	
			2-acetylpyridine	2-MeCHOHpy
6	7.0	60	40	5
7	3.3	60	0	0
8	3.3	60	0	0
9	6.6	60	29	6

[a]Based on $[Fe_2]$

Table 3.6. A Comparison of Fe$\cdots$Fe and Fe–O Distances in Carboxylate-Bridged Diiron(II) Windmill Structures with Their Coordination Number.

	Coordination Number	Fe$\cdots$Fe	Fe–O$_{av}$	Fe–O$_L$
1 (Fe1)	4	4.2380(9)	1.999(2)	2.463(2)
1 (Fe2)	5	4.6052(9)	2.033(2)	2.281(2)
2	5	4.3908(11)	2.013(2)	2.308(2)
4	5	4.2886(12)	2.004(3)	2.373(3)
5	5	4.0656(10)	2.016(3)	2.214(2)
6	4	4.3361(12)	1.998(3)	2.517(3)
7	4	4.0861(10)	1.9714(17)	2.715(2)
8	5	4.1542(14)	2.068(3)	2.323(3)
9 (Fe1)	5	4.4830(10)	2.025(2)	2.225(2)
9 (Fe2)	5	4.4434(10)	2.002(2)	2.330(2)

Chart 3.1.

Ar^RCO_2H

R = CH₃, Tol

R = F, 4-FPh
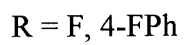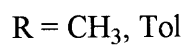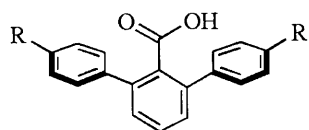
Chart 3.2.
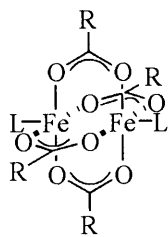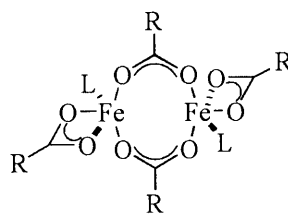
Paddlewheel   Windmill

Scheme 3.1.
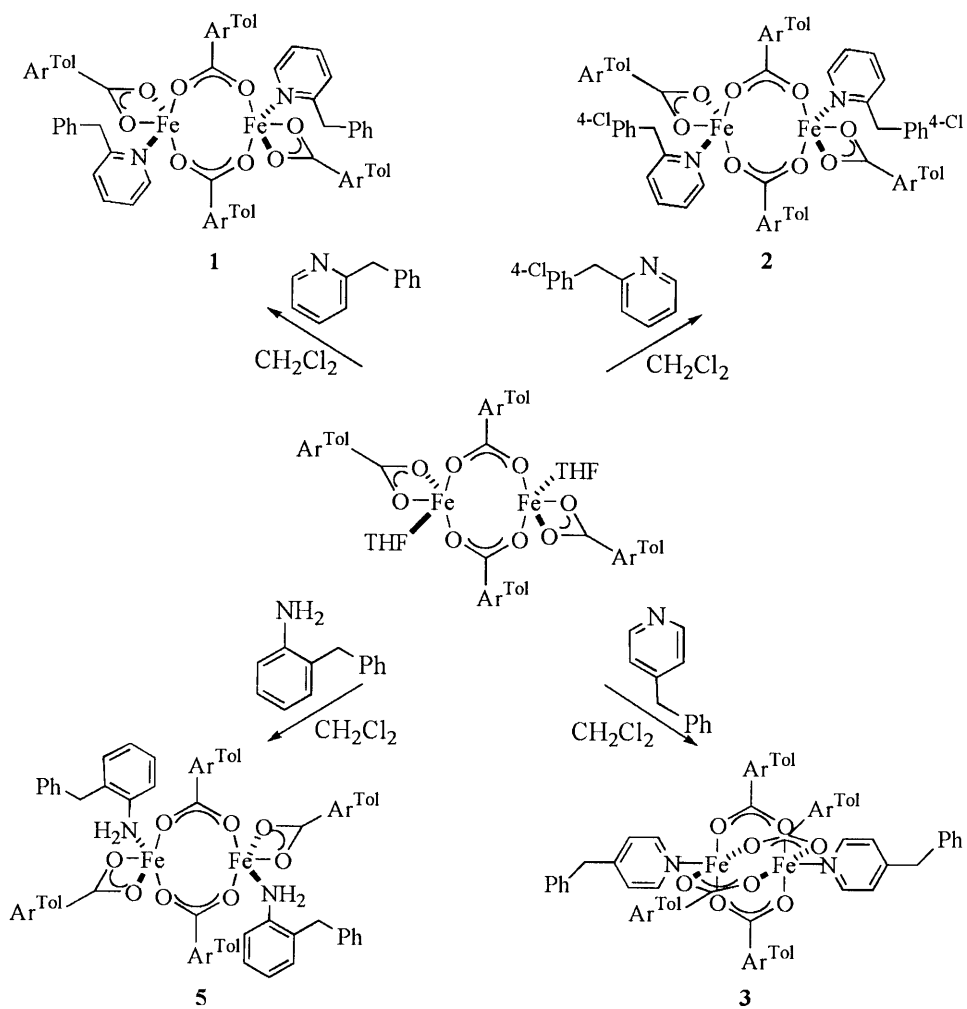
Scheme 3.2.
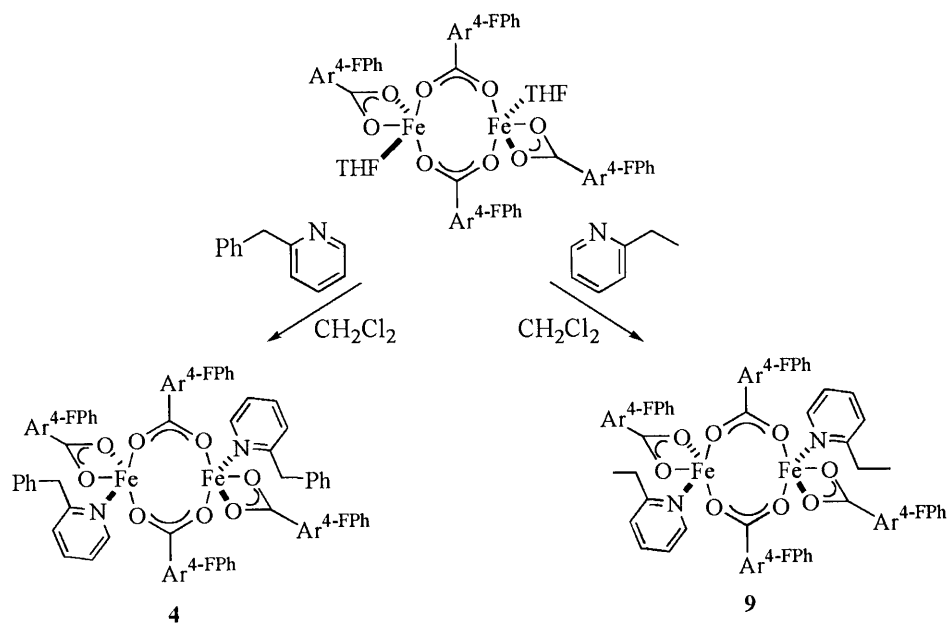
Scheme 3.3.
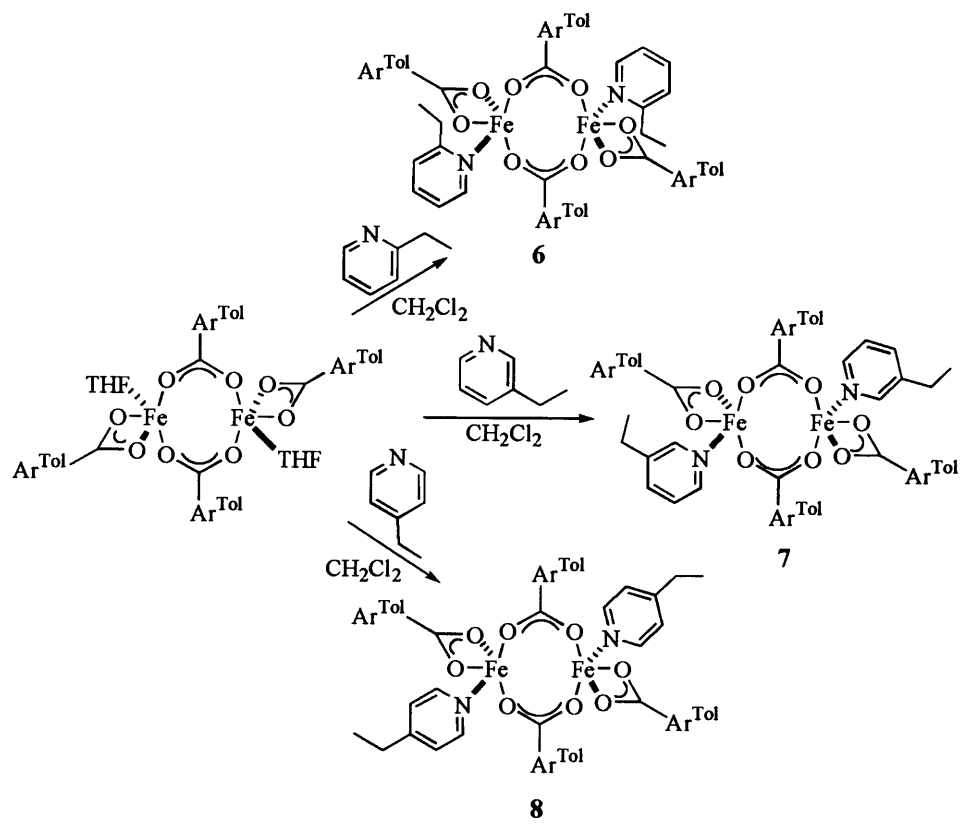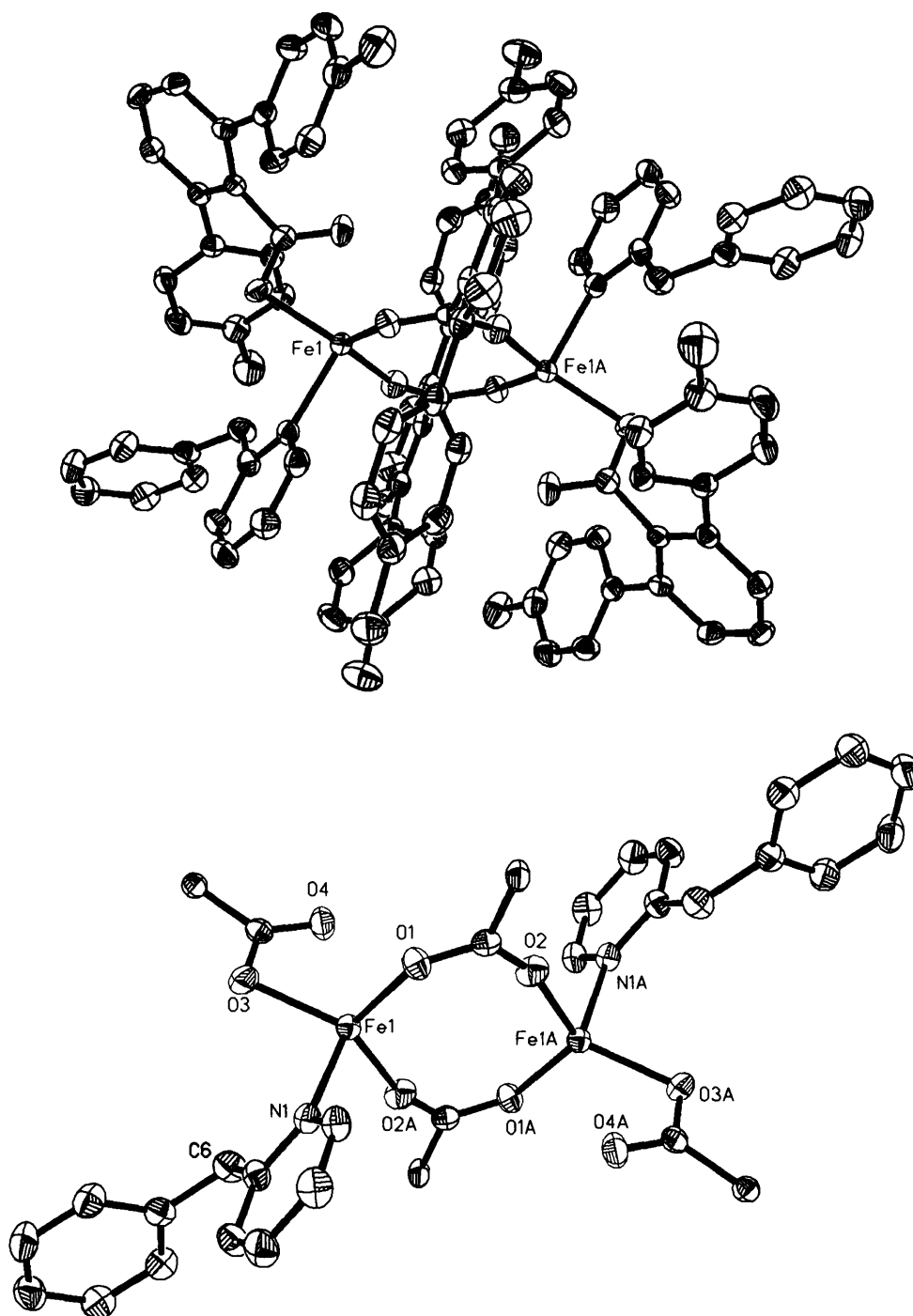
Figure 3.1. Top: ORTEP diagram of [Fe$_2$(μ-O$_2$CAr^{Tol})$_2$(O$_2$CAr^{Tol})$_2$(2-Bnpy)$_2$] (**1**) illustrating 50% probability thermal ellipsoids for all non-hydrogen atoms. Bottom: Drawing in which the aromatic rings of the $^-$O$_2$CAr^{Tol} ligands are omitted for clarity.
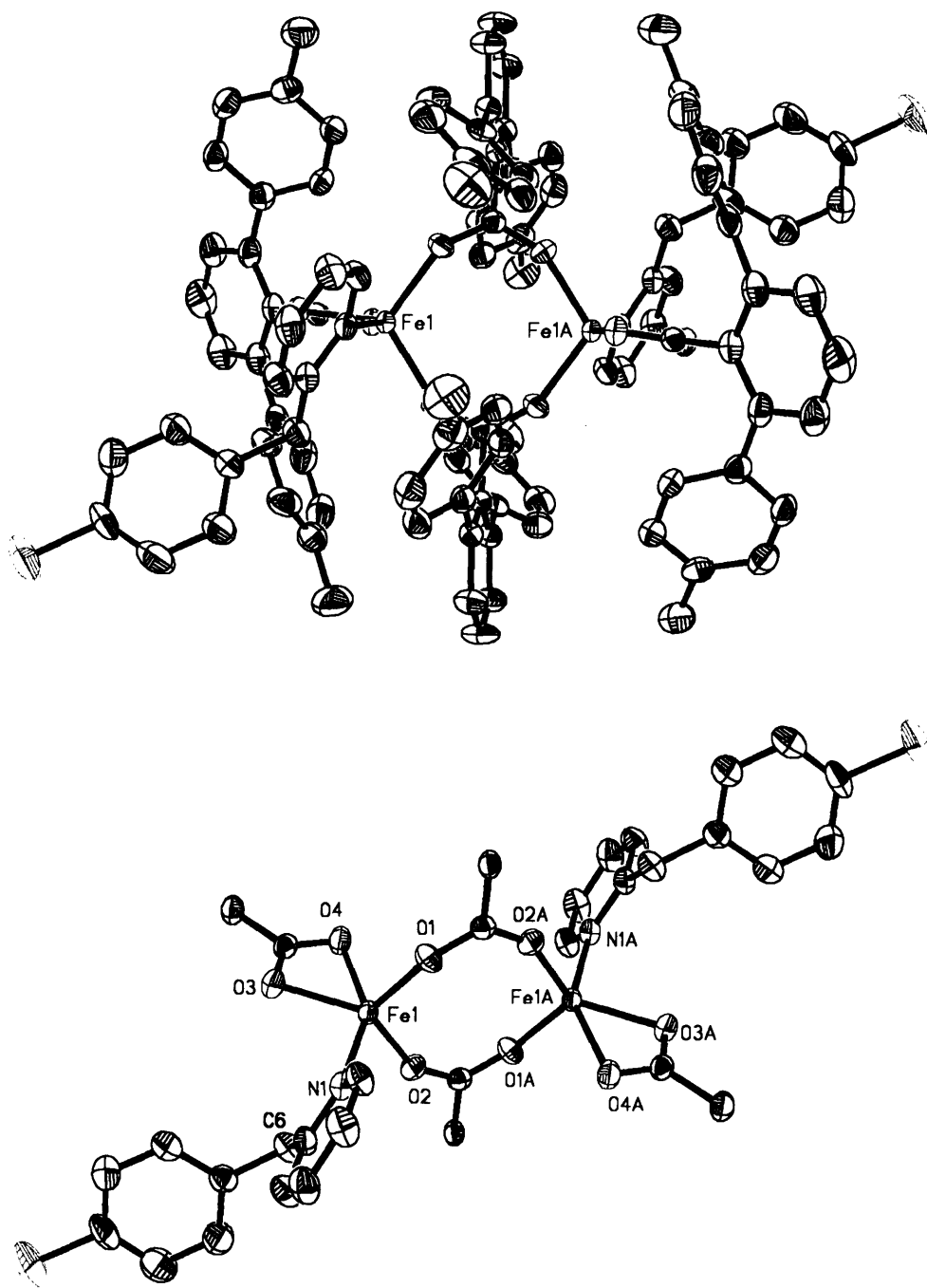
Figure 3.2. Top: ORTEP diagram of [Fe$_2$(μ-O$_2$CAr^{Tol})$_2$(O$_2$CAr^{Tol})$_2$(2-(4-ClBn)py)$_2$] (**2**) illustrating 50% probability thermal ellipsoids for all non-hydrogen atoms. Bottom: Drawing in which the aromatic rings of the $^-$O$_2$CAr^{Tol} ligands are omitted for clarity.
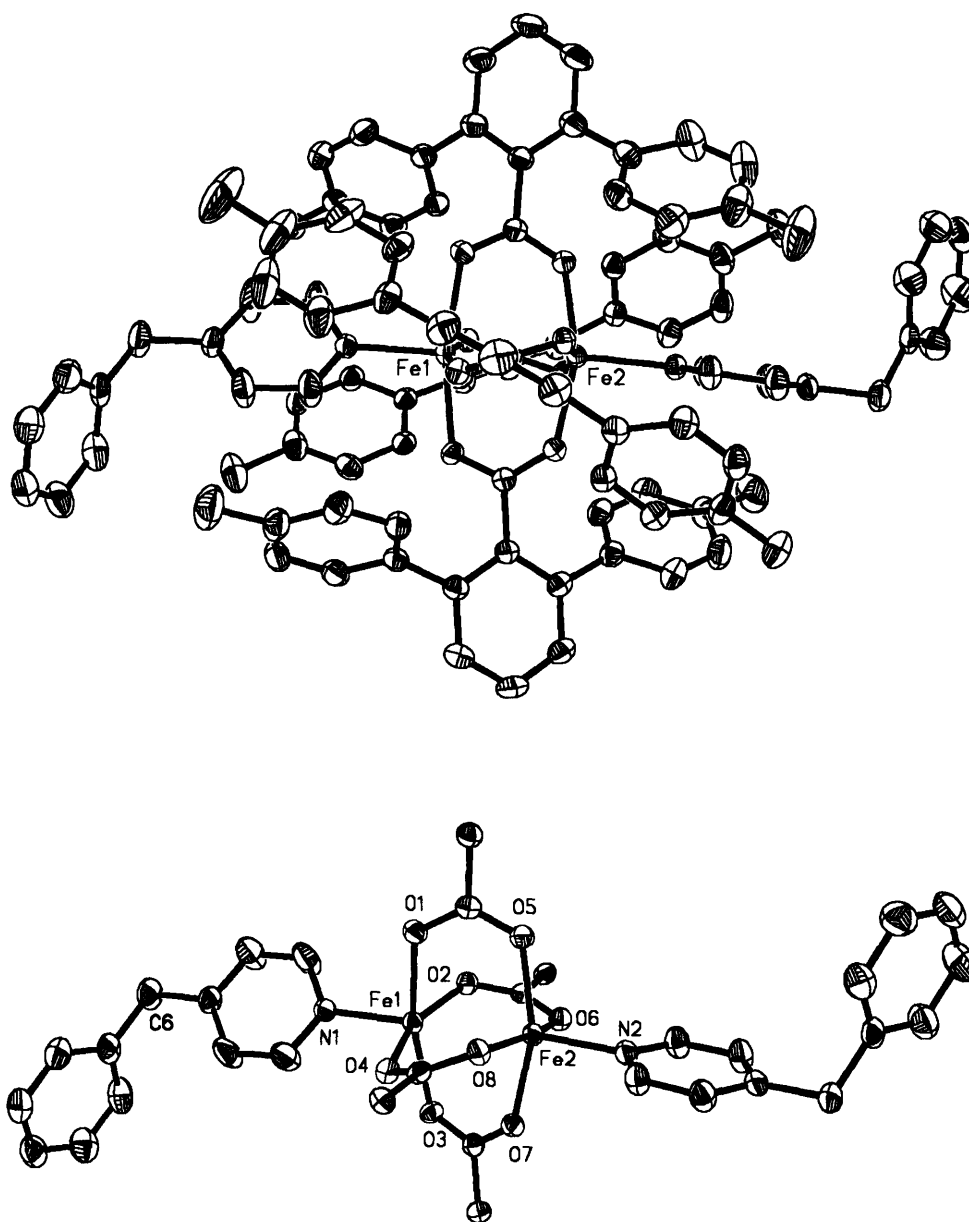
Figure 3.3. Top: ORTEP diagram of [Fe$_2$(μ-O$_2$CAr^{Tol})$_2$(O$_2$CAr^{Tol})$_2$(4-Bnpy)$_2$] (**3**) illustrating 50% probability thermal ellipsoids for all non-hydrogen atoms. Bottom: Drawing in which the aromatic rings of the $^-$O$_2$CAr^{Tol} ligands are omitted for clarity.
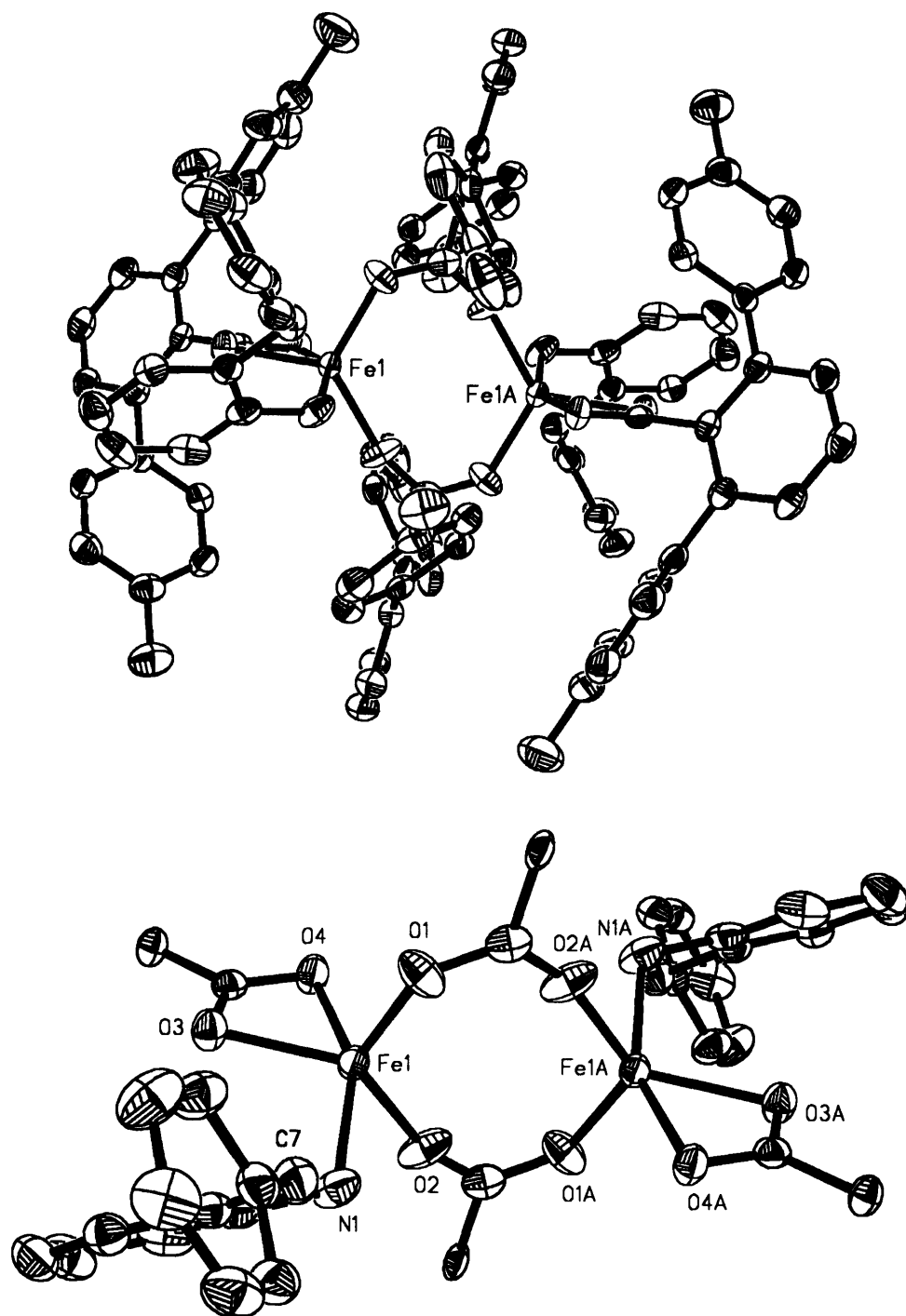
Figure 3.4. Top: ORTEP diagram of [Fe$_2$(μ-O$_2$CAr^{Tol})$_2$(O$_2$CAr^{Tol})$_2$(2-Bnan)$_2$] **(5)** illustrating 50% probability thermal ellipsoids for all non-hydrogen atoms. Bottom: Drawing in which the aromatic rings of the $^-$O$_2$CAr^{Tol} ligands are omitted for clarity.
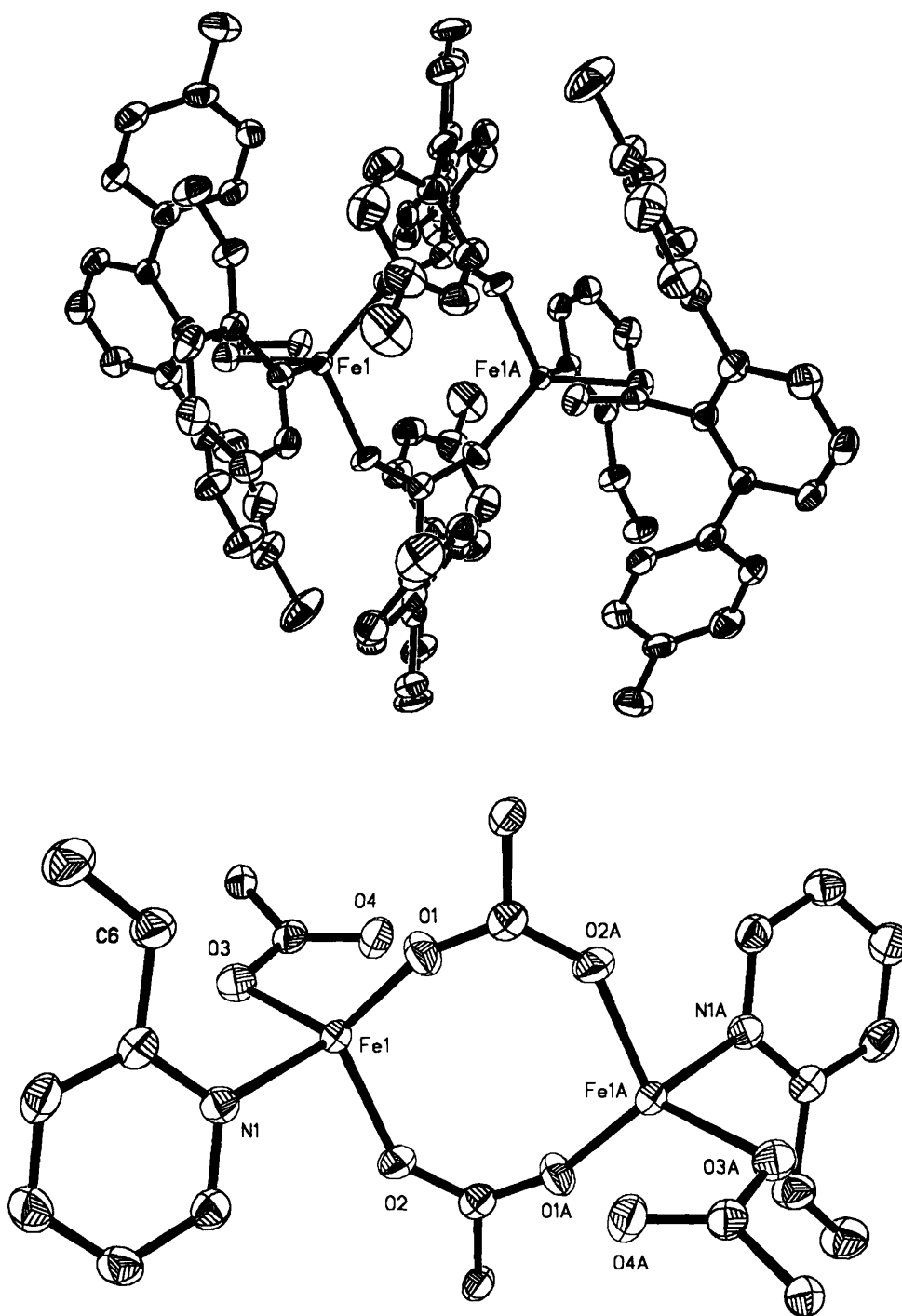
Figure 3.5. Top: ORTEP diagram of [Fe$_2$(μ-O$_2$CAr^{Tol})$_2$(O$_2$CAr^{Tol})$_2$(2-Etpy)$_2$] (**6**) illustrating 50% probability thermal ellipsoids for all non-hydrogen atoms. Bottom: Drawing in which the aromatic rings of the $^-$O$_2$CAr^{Tol} ligands are omitted for clarity.
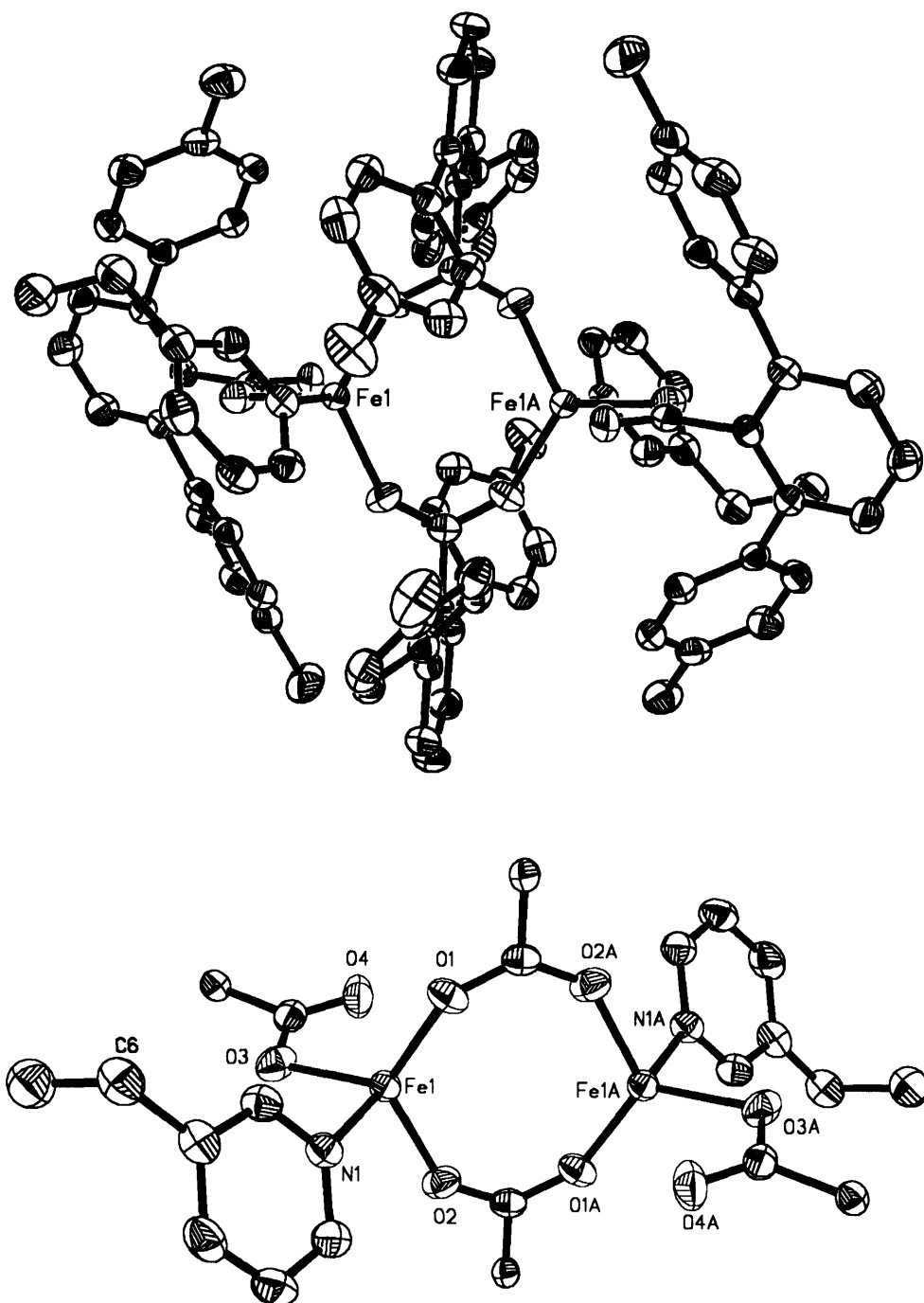
Figure 3.6. Top: ORTEP diagram of $[Fe_2(\mu\text{-}O_2CAr^{Tol})_2(O_2CAr^{Tol})_2(3\text{-}Etpy)_2]$ (**7**) illustrating 50% probability thermal ellipsoids for all non-hydrogen atoms. Bottom: Drawing in which the aromatic rings of the $^-O_2CAr^{Tol}$ ligands are omitted for clarity.
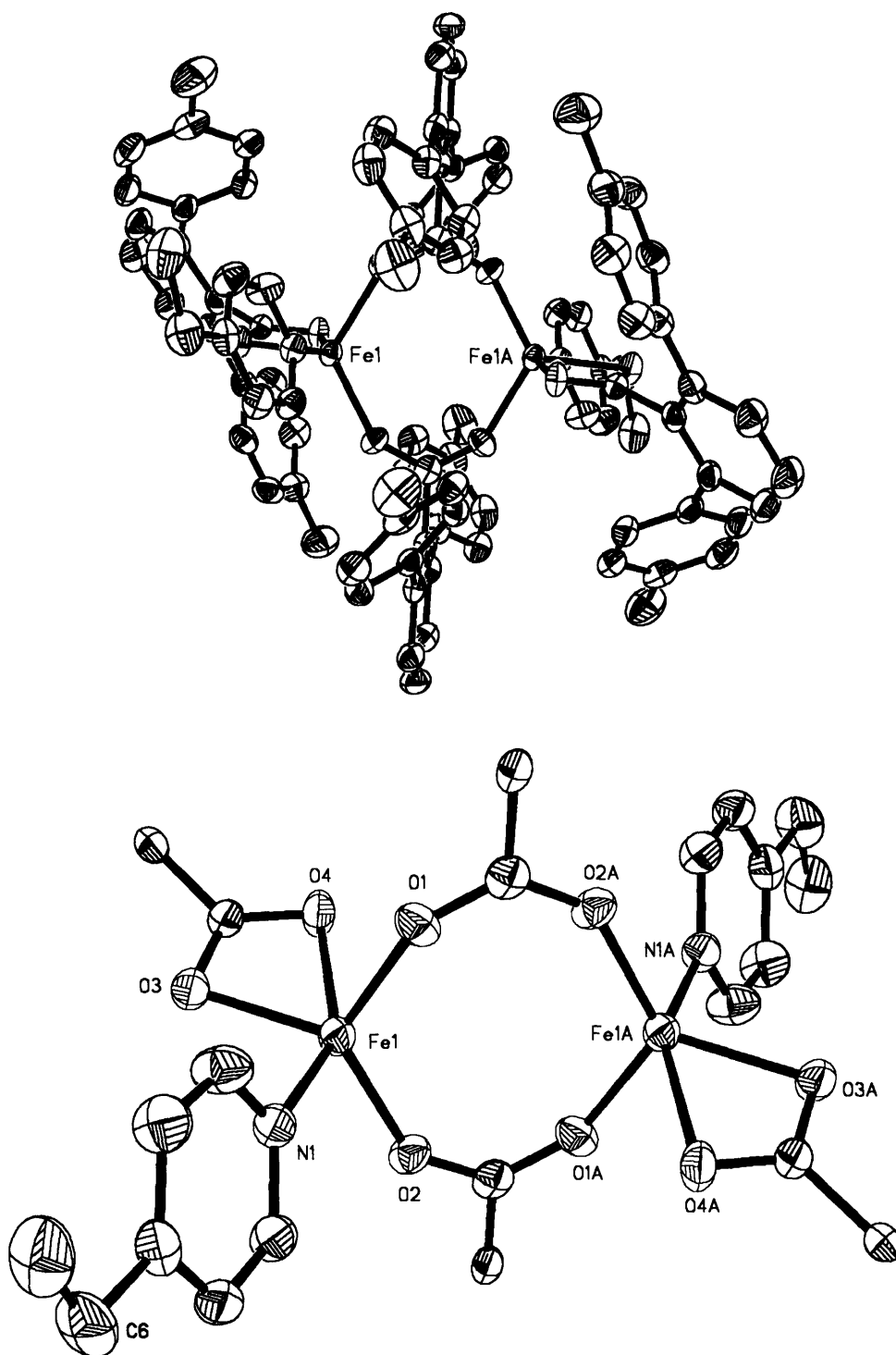
Figure 3.7. Top: ORTEP diagram of [Fe$_2$(μ-O$_2$CAr^{Tol})$_2$(O$_2$CAr^{Tol})$_2$(4-Etpy)$_2$] (**8**) illustrating 50% probability thermal ellipsoids for all non-hydrogen atoms. Bottom: Drawing in which the aromatic rings of the $^-$O$_2$CAr^{Tol} ligands are omitted for clarity.
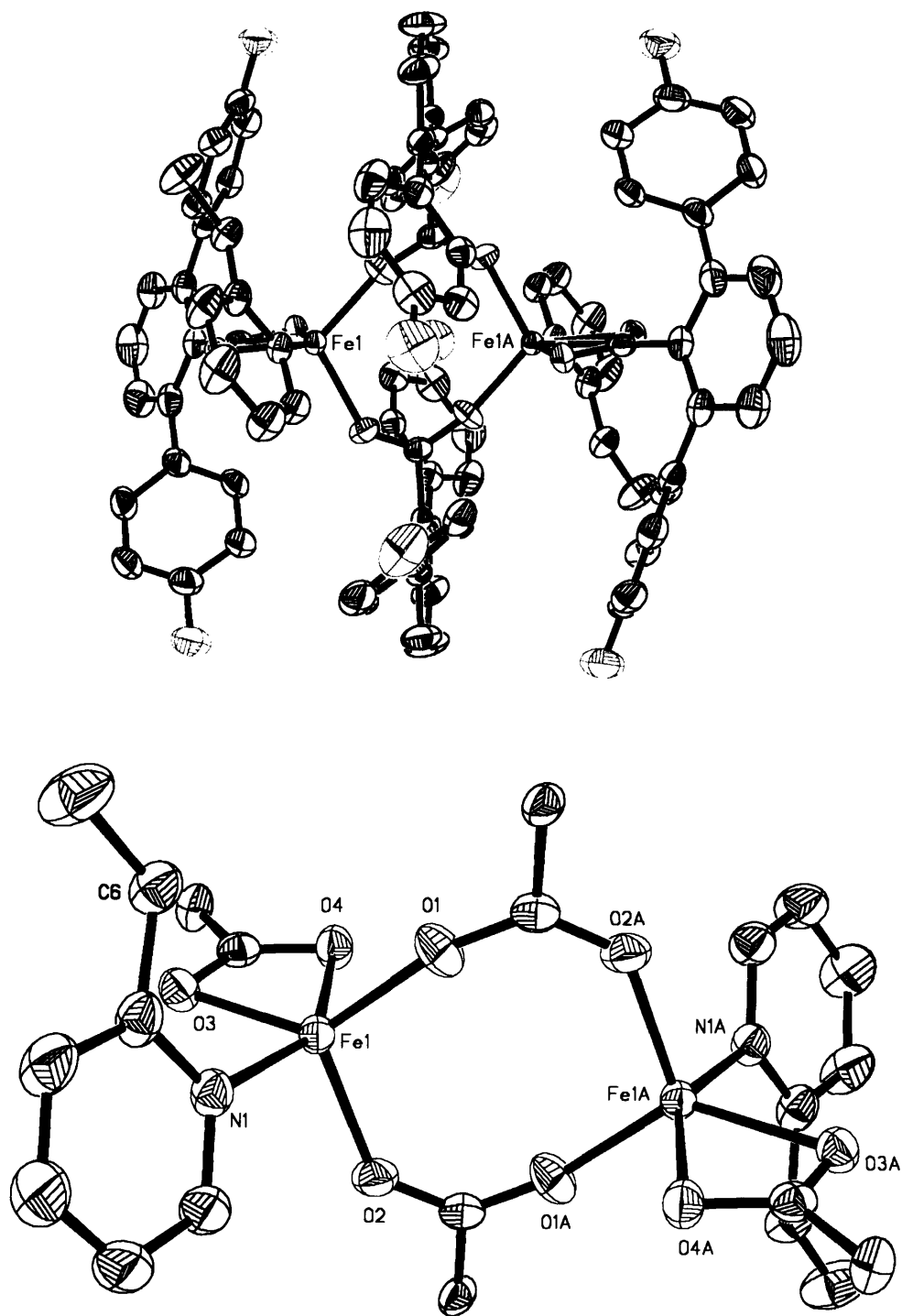
Figure 3.8. Top: ORTEP diagram of $[Fe_2(\mu\text{-}O_2CAr^{4\text{-}FPh})_2(O_2CAr^{4\text{-}FPh})_2(2\text{-}Etpy)_2]$ (**9**) illustrating 50% probability thermal ellipsoids for all non-hydrogen atoms. Bottom: Drawing in which the aromatic rings of the $^-O_2CAr^{4\text{-}FPh}$ ligands are omitted for clarity.
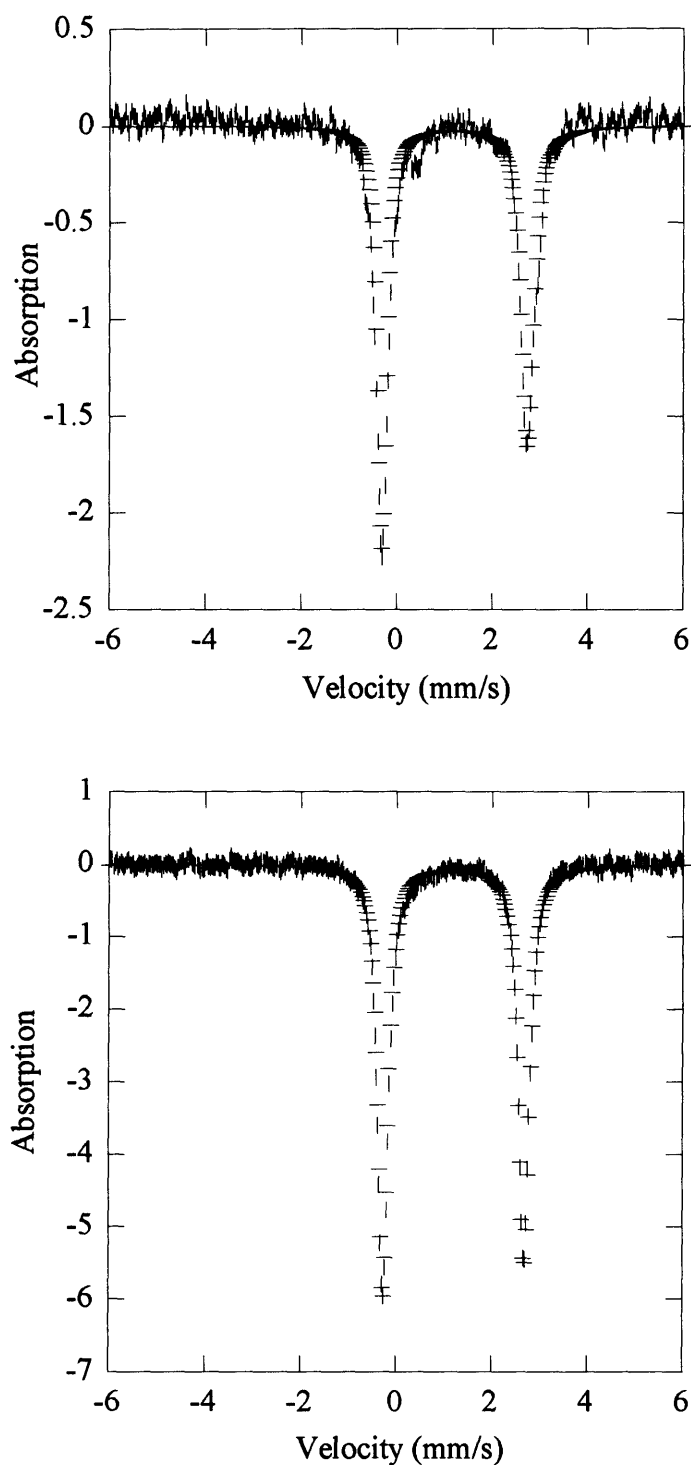
Figure 3.9. Mössbauer spectra (experimental data (|), calculated (–)) recorded at 4.2 K for solid samples of $[Fe_2(\mu\text{-}O_2CAr^{Tol})_2(O_2CAr^{Tol})_2(2\text{-Bnpy})_2]$ **(1)** (top) and $[Fe_2(\mu\text{-}O_2CAr^{Tol})_2(O_2CAr^{Tol})_2\text{-}(2\text{-Etpy})_2]$ **(6)** (bottom).

Chapter 4

A Thermally Sensitive Intermediate Generated in the Reaction of

$[Fe_2(\mu\text{-}O_2CAr^{Tol})_2(O_2CAr^{Tol})_2(2\text{-}Etpy)_2]$ with Dioxygen

Introduction

Dioxygen activation is carried out by certain non-heme diiron enzymes, including ribonucleotide reductase (RNR-R2),[1] soluble methane monooxygenase (sMMO),[2,3] fatty acid desaturase (Δ^9D),[4] at actives sites comprised of two iron atoms ligated by four carboxylate and two imidazole residues. To carry out the functions of these enzymes which include generation and storage of a tyrosyl radical in RNR-R2,[5] catalytic oxidation of methane to methanol under ambient conditions in sMMO,[6,7] and insertion of a *cis* double bond into the alkyl chain of an acyl carrier protein-linked fatty acid in Δ^9-desaturase,[8] high valent iron-dioxygen intermediates are generated. Both (μ-peroxo)diiron(III) and di(μ-oxo)diiron(IV) intermediates, H_{peroxo} and Q, have been spectroscopically characterized in the catalytic cycle of MMO,[9-11] an $Fe^{III}Fe^{IV}$ species, X, is used to generated the tyrosyl radical in RNR-R2,[12-17] and a (μ-peroxo)diiron(III) is believed to play a role in the catalytic cycle of Δ^9D.[18]

This diversity in enzyme function despite similar coordination environments inspires an interest in modeling these systems with small molecules. There have been several examples produced of (peroxo)diiron(III) clusters, however most comprised nitrogen-rich ligand environments.[19-24] Recent exploration of the oxidation chemistry of diiron(II) systems having terphenyl carboxylate ligands has provided more accurate representations of the active sites of MMOH and RNR-R2.[25-27] Several systems exhibit reactivity with dioxygen, which, at low temperature revealed the formation of intermediates containing iron(IV). Detailed UV-vis, EPR, and Mössbauer spectroscopic studies elucidated a mechanism in which an equimolar mixture of $Fe^{III}Fe^{IV}$ and $Fe^{II}Fe^{III}$ species formed in the reaction of $[Fe_2(\mu-O_2CAr^{Tol})_4(4-^tBupy)]$ system, where $Ar^{Tol}CO_2^-$ is 2,6-di(*p*-tolyl)benzoate and 4-^{t}Bupy is 4-*tert*-butylpyridine, with dioxygen.[28] In contrast for the $[Fe_2(\mu-O_2CAr^{Mes})_2(O_2CAr^{Mes})_2(MeCN)_2]$ system, where $Ar^{Mes}CO_2^-$ is

2,6-di(*p*-mesityl)benzoate, a symmetric (μ-peroxo)diiron(III) species was detected spectroscopically at low temperature.[29]

Using *m*-terphenyl-based carboxylate ligands the di(μ-carboxylato)diiron(II) cluster, $[Fe_2(\mu-O_2CAr^{Tol})_2(O_2CAr^{Tol})_2(2\text{-Etpy})_2]$ (**1a**) (Chart 4.1), geometrically analogous to the reduced active site of MMOH, was prepared and structurally characterized.[30] In this chapter the reaction of $[Fe_2(\mu-O_2CAr^{Tol})_2(O_2CAr^{Tol})_2(2\text{-Etpy})_2]$ (**1a**) with dioxygen was investigated at low temperature. An O_2-dependent intermediate, **1b**, was studied by UV-visible, resonance Raman (rR), electron paramagnetic resonance (EPR), and Mössbauer spectroscopy.

Experimental Section

General Considerations. All reagents were obtained from commercial suppliers and used as received, unless otherwise noted. Methylene chloride was saturated with nitrogen and purified by passage through activated Al_2O_3 columns under argon.[31] Dioxygen (99.994%, BOC Gases) was dried by passing the gas stream through a column of Drierite. ^{18}O-Enriched dioxygen (99%) was supplied by ICON, NY. The synthesis and characterization of $[Fe_2(\mu-O_2CAr^{Tol})_2(O_2CAr^{Tol})_2(2\text{-Etpy})]$ (**1a**) was reported previously.[30] Air-sensitive manipulations were carried out under nitrogen in an Mbraun drybox.

Oxygenation of 1a. In a typical reaction, **1a** was dissolved in CH_2Cl_2 and loaded into a vessel fitted with a rubber septum. The solution was cooled to -78 °C in a dry ice/acetone bath. Dioxygen was gently bubbled into the solution, resulting in a color change from pale yellow to dark brown, indicating the formation of **1b**.

UV-visible Spectroscopy. UV-vis spectra were recorded on a Hewlett-Packard 8453 diode array spectrophotometer. Low temperature UV-vis experiments were performed using a custom made quartz cuvette, 1-cm path length, fused into a vacuum-jacketed dewar. Solutions of

1a, ~0.5 mM in CH_2Cl_2 (6 mL) under N_2 in the low T UV-vis cell, were cooled to -78 °C. Dry O_2 was purged through the solution for 30 s, and the UV-vis spectra were measured at various time intervals.

Mössbauer Spectroscopy. Zero-field Mössbauer spectra were recorded on an MSI spectrometer (WEB Research Co.) with a ^{57}Co source in a Rh matrix maintained at room temperature in the MIT DCIF. Data were collected at 4.2 K, and the isomer shift (δ) values are reported with respect to natural iron foil that was used for velocity calibration at room temperature. A solid sample of **1b** was prepared by concentrating under 0.13 torr vacuum the solution generated by oxygenation of **1a** (199 mg, 0.130 mmol) in CH_2Cl_2 (10 mL) at 195 K. The dark brown material thus isolated was suspended in Apeizon N grease, coated on the lid of a nylon sample holder, and stored at 77 K. The spectra were fit to Lorentzian lines by using the WMOSS plot and fit program.[32]

EPR Spectroscopy. X-band EPR spectra were recorded on a Bruker EMX EPR spectrometer (9.37 GHz) running WinEPR software. The temperature (5 K) was maintained with an Oxford Instruments liquid helium EPR 900 cryostat and an ITC503 controller. Samples were prepared under dinitrogen by first making a 3.0 mM solution of **1a** in CH_2Cl_2. Aliquots of ~300 μL were transferred to ten EPR tubes in the drybox, which were septum-sealed. One of the samples was frozen at 77 K. The remaining ones were cooled to 195 K under N_2, treated with O_2 for 1 min, allowed to react at 195 K for a specified periods of time, 0.167, 0.5, 1, 1.5, 2, 3, 4, 5, and 6 h, and frozen at 77 K. EPR spectra were recorded at 5 K.

Resonance Raman Spectroscopy. Resonance Raman spectra of frozen CH_2Cl_2 solutions of **1b**, generated with either $^{16}O_2$ or $^{18}O_2$ at -78 °C, were obtained by using a Coherent Innova 90C Kr^+ ion laser exciting at 752.5 nm. Plasma lines for the laser were rejected with a

holographic band pass (Kaiser Optical) to obtain a clean background. Approximately 20 mW were focused to a ~100 μm spot. The resulting Raman light was filtered with a holographic notch filter (Kaiser Optical Systems) to attenuate the Rayleigh scattered light and focused into a 150 μm slit of a single stage spectrograph (Acton Spectro Pro SP300i). The spectrograph has a 300 mm focal length and is equipped with a 1200 grooves/nm grating giving a linear dispersion of 2.7 nm/mm. The spectral resolution is approximately 5.8 cm^{-1}. Spectra were recorded on a thermoelectrically-cooled back-illuminated CCD. Cooling the CCD detector to -70 ^{o}C significantly reduces the dark current (< 0.1 e/p/s).

A custom-made glass cryostat that incorporates a copper cold-finger enclosed in a glass shroud was used for all measurements.[33] In order to prepare the sample, the cryostat was evacuated, and the cold-finger was cooled with liquid-N_2 for 10 min. Subsequently, the shroud was removed, and the cold-finger was dipped into a solution of the sample, allowing it to freeze to the cold-finger. Immediately after replacing the shroud, the cryostat was replaced under vacuum and remained as such throughout the experiment. To prevent condensation on the windows of the cryostat during the measurements, a steady stream of dry compressed air was used to purge them where the laser penetrated.

Prior to each measurement, the Raman system was optimized using frozen CH_2Cl_2. The exposure time was adjusted to yield a signal with ~ 40,000 counts per accumulation, and the total number of exposures taken was adjusted for a 5-min acquisition time. Methylene chloride bands at 1156 cm^{-1}, 897 cm^{-1}, 704 cm^{-1}, and 286 cm^{-1} were used for a wavelength calibration. The sample concentrations were ~3 mM, and each measurement was made in triplicate on more than one freshly prepared sample to ensure the reproducibility of the results. Data were processed by

using WinSpec 3.2.1 (Princeton Instruments, Inc.), and the resultant ASCII files were further manipulated using Microsoft Excel.

Results

Reactions of [Fe$_2$(μ-O$_2$CAr^{Tol})$_2$(O$_2$CAr^{Tol})$_2$(2-Etpy)$_2$] (1a) with Dioxygen. (a) UV-Vis Spectroscopy. Oxygenation of a CH$_2$Cl$_2$ solution of **1a** at -78 °C results in the formation of a dark brown species **1b** with a broad visible absorption band centered at $\sim$725 nm (ε = 1400 M^{-1} cm^{-1}), which grows in over a period of hours as depicted in Figure 4.1. This metastable species reaches a maximum after 2.5 h and decays over 10 h to form a yellow solution. When the oxygenation reaction was carried out in toluene, THF, or chloroform (-40 °C), **1b** was not generated. The intermediate also did not form when 5 equiv of H$_2$O were added to the initial CH$_2$Cl$_2$ solution of **1a** and the oxygenation was repeated under the same conditions.

(b) Resonance Raman Spectroscopy. Raman spectra of **1b** were obtained in frozen CH$_2$Cl$_2$ solutions at 77 K. Upon excitation at 752.5 nm, two Raman active signals at 850 and 510 cm^{-1} were observed. These features are absent both in Raman spectra of **1a** and the decomposition product of **1b**. Although these peaks are in the range associated with the O–O and Fe–O vibrations observed for (μ-peroxo)diiron(III) species, no shift in peak position was observed for samples prepared by reacting **1a** with ^{18}O-labelled dioxygen (**1b***). A comparison of the Raman spectra for **1b** and **1b*** is shown in Figure 4.2.

(c) EPR Spectroscopy. The X-band EPR spectrum of **1b**, pictured in Figure 4.3, exhibits three distinct signals at g = 10, g = 4.3, and g = 2. Results from time-dependent oxygenation experiments show that both the g = 10 and g = 2 features are present within 10 min of **1a** exposure to dioxygen. The g = 10 signal steadily increases for first 3 h, after which point it levels off. The absorbance at g = 2 reaches a maximum after 2 h and decays into the baseline within 5 h.

The smaller g = 4.3 signal is present after 10 min, but increases only slightly throughout the 6 h timeframe of the experiment. The g = 10 signal corresponds to an S = 9/2 ground state originating from a ferromagnetically coupled high spin $Fe^{II}Fe^{III}$.[34] The g = 4.3 is probably due to a small amount of a high-spin ferric impurity. An antiferromagnetically coupled $Fe^{III}Fe^{IV}$ species gives rise to the g = 2 signal with an S = ½ ground state.[35]

(d) Mössbauer Spectroscopy. The intermediate **1b**, only forms when CH_2Cl_2 is used as the solvent for the low temperature oxidation of **1a**. Mössbauer spectra can not be recorded in CH_2Cl_2 because chlorine atoms absorb the gamma radiation. Therefore a method was devised to record the spectrum of **1b** in the absence of the solvent. Generation of **1b** was followed by removal of CH_2Cl_2 in vacuo while the temperature of the reaction flask was carefully monitored to ensure ⁻78 °C was maintained. The brown residue that resulted was then transferred to the sample holder, and a typical solid Mössbauer sample was measured.

Two distinct quadrupole doublets with 1:1 intensity ratio are observed in the solid state Mössbauer spectrum of **1b** at 4.2 K (Figure 4.4). The data portray an equal mixture of ferrous and ferric species. There is a high-spin iron(II) site with δ = 1.19(2) mm s⁻¹, ΔE_Q = 2.90(2) mm s⁻¹, and Γ = 0.29(2) mm s⁻¹ and a high-spin iron(III) site with δ = 0.47(2) mm s⁻¹, ΔE_Q = 1.04(2) mm s⁻¹, and Γ = 0.60(2) mm s⁻¹.

Discussion

Oxygenation of **1a** in CH_2Cl_2 at –78 °C generates the thermally sensitive intermediate **1b**. The electronic structure of **1b** has been probed by various spectroscopic techniques. Initial investigation to determine the nature of **1b** revealed an electronic absorption spectrum resembling those of (µ-peroxo)diiron(III) intermediates in natural systems.[18,36-38] The λ_{max} value

and extinction coefficient of **1b** (725 nm and 1400 M^{-1} cm^{-1}) are nearly identical to those observed for H_{peroxo} (725 nm and 1800 M^{-1} cm^{-1}).

Resonance Raman experiments were conducted to provide further information about the electronic structure of **1b**. Characteristic resonances observed in the Raman spectra of (μ-peroxo)diiron(III) moieties originate from O–O (800 – 900 cm^{-1})and Fe–O (450 – 550 cm^{-1}) stretching vibrations, respectively.[27] The resonance Raman spectrum of $^{16}O_2$-generated **1b** contains bands (851 and 510 cm^{-1}) that fall within these ranges. A shift of these values upon introduction of ^{18}O-labelled dioxygen to **1a** would indicate that these vibrations were due to an oxygen-containing intermediate. However, the Raman active peaks observed in the spectrum of **1b*** were identical to those of **1b**, suggesting an iron-dioxygen adduct is not responsible for these vibrations.

EPR spectroscopy revealed that **1b** is comprised of paramagnetic diiron(II,III) and diiron(III,IV) species. As the reaction of **1a** with dioxygen progresses, the ratio of $Fe^{II}Fe^{III}$ to $Fe^{III}Fe^{IV}$ changes. The high-valent $Fe^{III}Fe^{IV}$ reaches a maximum after only 2 h and has fully disappeared after 5 h. Whereas the $Fe^{II}Fe^{III}$ species continues to increase over time, being the only paramagnetic species in solution after 6 h. Mössbauer data, which provides information on the nature of the iron in the sample, confirmed that the mixed valent $Fe^{II}Fe^{III}$ is the only iron containing species remaining 9 h after exposure of **1a** to dioxygen.

This kind of reactivity, unusual for doubly carboxylate-bridged diiron(II) compounds, was previously observed when paddlewheel diiron(II) compounds were allowed to react with dioxygen at low temperatures. A proposed mechanism describing the formation of $Fe^{II}Fe^{III}$ and $Fe^{III}Fe^{IV}$ mixed valent species is depicted in Scheme 4.1.[28] Following identification of **1b** as this type of paramagnetic mixture, the UV-vis and resonance Raman spectroscopic data obtained for

1b were reexamined in the context of the previously reported systems. The transition at 725 nm in the electronic absorption spectrum of **1b** is the result of an intervalence charge transfer (IVCT) band of an $Fe^{II}Fe^{III}$ cation, and the Raman active peaks observed in the spectrum of **1b** result from excitation of the IVCT band from the valence-delocalized $Fe^{II}Fe^{III}$ cores. These transitions were observed previously, but the vibrations were not assigned.[28]

Unlike the previously reported systems in which the starting diferrous materials had the paddlewheel geometry, **1a** adopts a windmill structure. This may account for the differences observed in reactivity of **1a** with O_2 from aforementioned compounds. One such distinction is the time needed to buildup the UV-vis active species. Upon addition of dioxygen to the $\{Fe_2(\mu\text{-}O_2CAr^{Tol})_4\}$ complexes, the $Fe^{II}Fe^{III}$ was formed almost instantly as noted by the immediate appearance of the IVCT band.[28,39] When **1a** reacts with O_2, >20 min pass before **1b** is detected in any appreciable amount and 2 h before the maximum amount forms. The other disparity between doubly- and tetra-bridged diferrous systems is physical properties of the $Fe^{II}Fe^{III}$ cation manifested in the IVCT band. The latter have absorptions that are blue-shifted (645 – 670 nm) with respect to **1b** (725 nm) with larger extinction coefficients (1700 vs 1400 M^{-1} cm^{-1}).

Conclusion

The electronic absorption spectrum of the intermediate generated upon addition of dioxygen to a CH_2Cl_2 solution of **1a** at low temperatures resembles the H_{peroxo} intermediate in the catalytic cycle of MMOH. Through a series of spectroscopic techniques including resonance Raman, EPR, and Mössbauer, **1b** was determined to be comprised of mixed-valent $Fe^{II}Fe^{III}$ and $Fe^{III}Fe^{IV}$ species likely resulting from the bimolecular reaction of high-valent oxygen intermediates with unreacted diferrous complex. The differences in the physical properties of this

system and those previously reported could possibly stem from the differing geometries of the starting diiron(II) complexes which influences the subsequent dioxygen reactivity.

References

(1)   Logan, D. T.; Su, X.-D.; Åberg, A.; Regnström, K.; Hajdu, J.; Eklund, H.; Nordlund, P. *Structure* **1996**, *4*, 1053-1064.

(2)   Elango, N.; Radhakrishnan, R.; Froland, W. A.; Wallar, B. J.; Earhart, C. A.; Lipscomb, J. D.; Ohlendorf, D. H. *Protein Sci.* **1997**, *6*, 556-568.

(3)   Whittington, D. A.; Lippard, S. J. *J. Am. Chem. Soc.* **2001**, *123*, 827-838.

(4)   Lindqvist, Y.; Huang, W.; Schneider, G.; Shanklin, J. *EMBO J.* **1996**, *15*, 4081-4092.

(5)   Stubbe, J. *Curr. Opin. Chem. Biol.* **2003**, *7*, 183-188.

(6)   Merkx, M.; Kopp, D. A.; Sazinsky, M. H.; Blazyk, J. L.; Müller, J.; Lippard, S. J. *Angew. Chem., Int. Ed. Engl.* **2001**, *40*, 2782-2807.

(7)   Baik, M.-H.; Newcomb, M.; Friesner, R. A.; Lippard, S. J. *Chem. Rev.* **2003**, *103*, 2385-2419.

(8)   Yang, Y.-S.; Broadwater, J. A.; Pulver, S. C.; Fox, B. G.; Soloman, E. I. *J. Am. Chem. Soc.* **1999**, *121*, 2770-2783.

(9)   Lee, S.-K.; Fox, B. G.; Froland, W. A.; Lipscomb, J. D.; Münck, E. *J. Am. Chem. Soc.* **1993**, *115*, 6450-6451.

(10)   Liu, K. E.; Valentine, A. M.; Wang, D.; Huynh, B. H.; Edmonson, D. E.; Salifoglou, A.; Lippard, S. J. *J. Am. Chem. Soc.* **1995**, *117*, 10174-10185.

(11)   Shu, L.; Nesheim, J. C.; Kauffmann, K.; Münck, E.; Lipscomb, J. D.; Que, L., Jr. *Science* **1997**, *275*, 515-518.

(12)   Ravi, N.; Bollinger, J. M., Jr.; Huynh, B. H.; Edmondson, D. E.; Stubbe, J. *J. Am. Chem. Soc.* **1994**, *116*, 8007-8014.

(13) Bollinger, J. M., Jr.; Tong, W. H.; Ravi, N.; Huynh, B. H.; Edmondson, D. E.; Stubbe, J. *J. Am. Chem. Soc.* **1994**, *116*, 8015–8023.

(14) Sturgeon, B. E.; Burdi, D.; Chen, S.; Huynh, B. H.; Edmondson, D. E.; Stubbe, J.; Hoffman, B. M. *J. Am. Chem. Soc.* **1996**, *118*, 7551-7557.

(15) Burdi, D.; Sturgeon, B. E.; Tong, W. H.; Stubbe, J.; Hoffman, B. M. *J. Am. Chem. Soc.* **1996**, *118*, 281-282.

(16) Willems, J.-P.; Lee, H.-I.; Burdi, D.; Doan, P. E.; Stubbe, J.; Hoffman, B. M. *J. Am. Chem. Soc.* **1997**, *119*, 9816-9824.

(17) Burdi, D.; Willems, J.-P.; Riggs-Gelasco, P.; Antholine, W. E.; Stubbe, J.; Hoffman, B. M. *J. Am. Chem. Soc.* **1998**, *120*, 12910-12919.

(18) Broadwater, J. A.; Ai, J.; Loehr, T. M.; Sanders-Loehr, J.; Fox, B. G. *Biochemistry* **1998**, *37*, 14664-14671.

(19) Kim, K.; Lippard, S. J. *J. Am. Chem. Soc.* **1996**, *118*, 4914-4915.

(20) Dong, Y.; Yan, S.; Young, V. G., Jr.; Que, L., Jr. *Angew. Chem., Int. Ed. Engl.* **1996**, *35*, 618-620.

(21) Ookubo, T.; Sugimoto, H.; Nagayama, T.; Masuda, H.; Sato, T.; Tanaka, K.; Maeda, Y.; Okawa, H.; Hayashi, Y.; Uehara, A.; Suzuki, M. *J. Am. Chem. Soc.* **1996**, *118*, 701-702.

(22) Dong, Y.; Zang, Y.; Shu, L.; Wilkinson, E. C.; Que, L., Jr. *J. Am. Chem. Soc.* **1997**, *119*, 12683-12684.

(23) LeCloux, D. D.; Barrios, A. M.; Mizoguchi, T. J.; Lippard, S. J. *J. Am. Chem. Soc.* **1998**, *120*, 9001-9014.

(24) Kryatov, S. V.; Rybak-Akimova, E. V. *Chem. Rev.* **2005**, *105*, 2175-2226.

(25) Lee, D.; Lippard, S. J. *Inorg. Chem.* **2002**, *41*, 2704-2719.

(26)   Tolman, W. B.; Que, L., Jr. *J. Chem. Soc., Dalton Trans.* **2002**, 653-660.

(27)   Tshuva, E. Y.; Lippard, S. J. *Chem. Rev.* **2004**, *104*, 987-1012.

(28)   Lee, D.; Pierce, B.; Krebs, C.; Hendrich, M. P.; Huynh, B. H.; Lippard, S. J. *J. Am. Chem. Soc.* **2002**, *124*, 3993-4007.

(29)   Hagadorn, J. R.; Que, L., Jr.; Tolman, W. B. *J. Am. Chem. Soc.* **1998**, *120*, 13531-13532.

(30)   Carson, E. C. In *Doctoral Dissertation in Inorganic Chemistry*; Massachusetts Institute of Technology: Cambridge, MA, 2005; Chapter 3.

(31)   Pangborn, A. B.; Giardello, M. A.; Grubbs, R. H.; Rosen, R. K.; Timmers, F. J. *Organometallics* **1996**, *15*, 1518-1520.

(32)   Kent, T. A. *WMOSS v2.5: Mössbauer Spectral Analysis Software*; WEB Research Co.: Minneapolis, 1998.

(33)   Feig, A. L.; Bautista, M. T.; Lippard, S. J. *Inorg. Chem.* **1996**, *35*, 6892-6898.

(34)   Lee, D.; DuBois, J. L.; Pierce, B.; Hedman, B.; Hodgson, K. O.; Hendrich, M. P.; Lippard, S. J. *Inorg. Chem.* **2002**, *41*, 3172-3182.

(35)   Lee, D.; DuBois, J. L.; Petasis, D.; Hendrich, M. P.; Krebs, C.; Huynh, B. H.; Lippard, S. J. *J. Am. Chem. Soc.* **1999**, *121*, 9893–9894.

(36)   Valentine, A. M.; Stahl, S. S.; Lippard, S. J. *J. Am. Chem. Soc.* **1999**, *121*, 3876-3887.

(37)   Lee, S.-K.; Lipscomb, J. D. *Biochemistry* **1999**, *38*, 4423-4432.

(38)   Bollinger, J. M., Jr.; Krebs, C.; Vicol, A.; Chen, S.; Ley, B. A.; Edmondson, D. E.; Huynh, B. H. *J. Am. Chem. Soc.* **1998**, *120*, 1094-1095.

(39)   Yoon, S.; Lippard, S. J. *Inorg. Chem.* **2003**, *42*, 8606-8608.

Chart 4.1.

1a

145
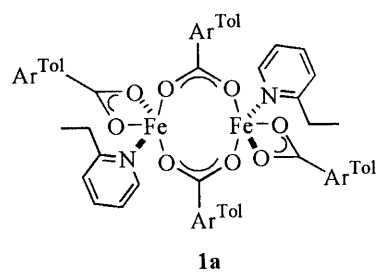
Scheme 4.1.
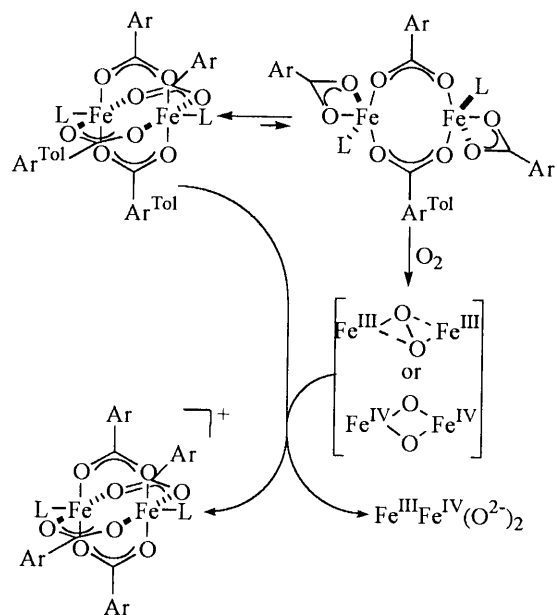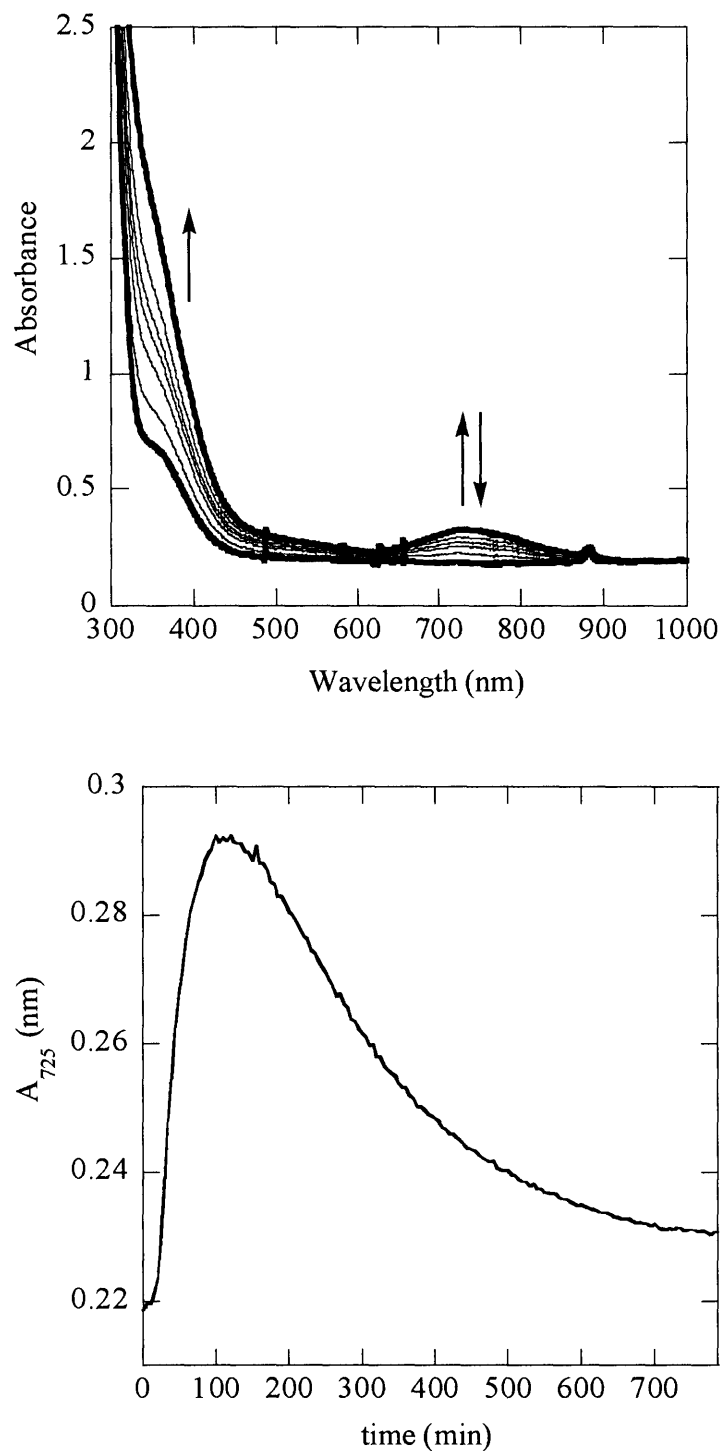
Figure 4.1. UV-vis spectra of **1b** generated over a period of 2.5 h from the reaction of $[Fe_2(\mu\text{-}O_2CAr^{Tol})_2(O_2CAr^{Tol})_2(2\text{-}Etpy)_2]$ (**1a**), 0.3 mM in CH_2Cl_2, with excess O_2 at -78 °C (top) and the absorbance at 725 nm monitored upon addition of O_2 over time (bottom).
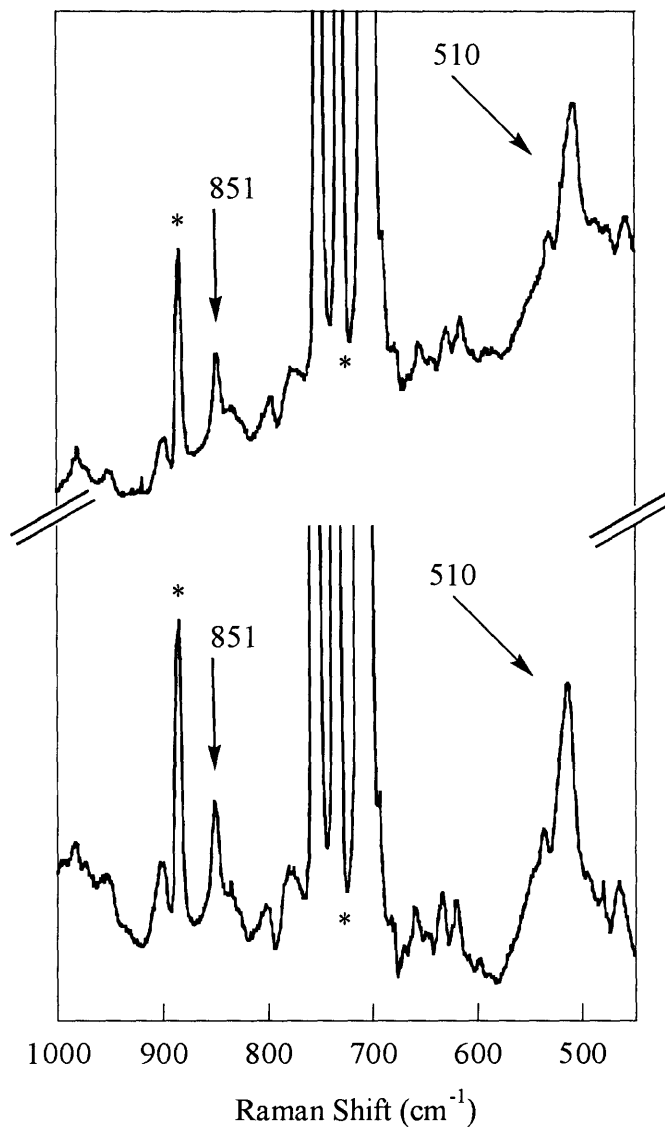
Figure 4.2. Resonance Raman spectra of a frozen CH_2Cl_2 solution of **1b** recorded at 77 K derived from the oxygenation at 196 K of $[Fe_2(\mu\text{-}O_2CAr^{Tol})_2(O_2CAr^{Tol})_2(2\text{-Etpy})_2]$ (**1a**) with $^{16}O_2$ (top) and $^{18}O_2$ (bottom). The asterisks indicate solvent bands.
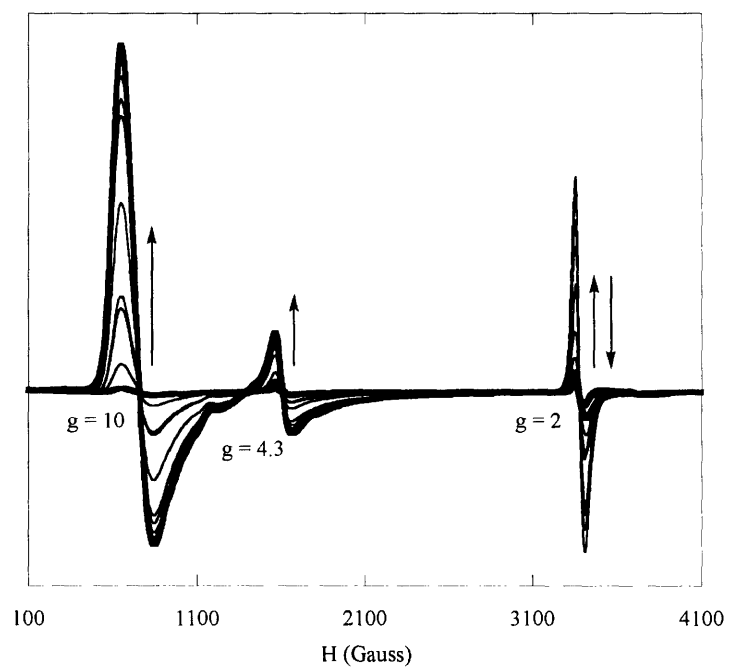
Figure 4.3. X-band EPR spectra of frozen CH₂Cl₂ solution samples of **1b** recorded at 5 K. The spectra represent 0.167, 0.5, 1, 1.5, 2, 3, 4, 5, and 6 h reactions of **1a** at −78 °C with dioxygen.
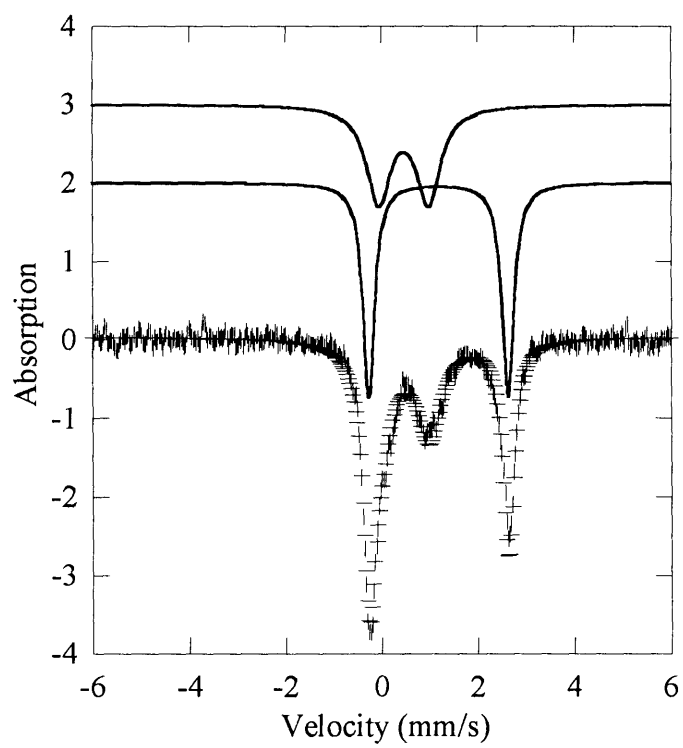
Figure 4.4. Mössbauer spectrum (experimental data (|), calculated fit (–)) recorded at 4.2 K for a solid sample of **1b**. The upper curves show two subsets for calculated spectra.

Chapter 5

Synthesis and Reactivity Studies of Carboxylate-Bridged Diiron(II) Compounds

with Pendant Sulfur-Containing Substrates

Introduction

Dioxygen activation and O-atom transfer reactions promoted by iron-containing metalloenzymes are of considerable interest both for ecological and industrial applications.[1,2] Soluble methane monooxygenase (sMMO) is one such enzyme system that is used by methanotropic bacteria to catalyze the selective conversion of methane to methanol.[3] A carboxylate-bridged non-heme diiron active site, housed in the hydroxylase component (MMOH) of sMMO, is responsible for the binding and reductive activation of dioxygen.[4-7] In addition the diiron core can activate dioxygen towards other substrates such as hydrocarbons, methane derivatives including methanethiol, olefins, amines, and sulfides.[3,8]

Functional models of these enzymes help to provide insight into the mechanism of the oxidation chemistry occurring at the diiron site. The synthesis of dimetallic cores in carboxylate-rich environments is necessary to provide an accurate representation of the MMOH active site. Self-assembly of discrete dinuclear centers with carboxylate ligands is challenged by their tendency to form oligomers.[9-14] Terphenyl-based based carboxylate ligands facilitate the assembly of discrete dinuclear complexes and mimic to some degree the hydrophobic pocket present at the protein active sites.[15-18]

In addition to four carboxylate ligands, two nitrogen donors are required to replicate the stoichiometry of the diiron core at the MMOH active site. One approach to emulate enzyme functionally is to tether a substrate to the N-donor ligand, increasing its chances of reacting with a dioxygen-activated dimetallic core. Introduction of dioxygen into the solutions of the diiron(II) complexes $[Fe_2(\mu\text{-}O_2CAr^{Tol})_2(O_2CAr^{Tol})_2(N,N\text{-}Bn_2en)_2]$,[19,20] $[Fe_2(\mu\text{-}O_2CAr^{Tol})_4(BA^{p\text{-}OMe})_2]$,[21] and $[Fe_2(\mu\text{-}O_2CAr^{Tol})_4(NH_2(CH_2)_2SBn)_2]$,[22] where $Ar^{Tol}CO_2^-$ is 2,6-di(p-tolyl)benzoate, N,N-Bn$_2$en is N,N-dibenzylethylenediamine, and $BA^{p\text{-}OMe}$ is p-methoxybenzylamine, led to the evolution of

benzaldehyde. This chemistry is formally the result of intramolecular benzylic hydroxylation followed by dealkylation. The strategy has been extended to include benzyl- or ethyl-derivatized pyridine ligands, which react to form the corresponding alcohol and/or ketone.[23]

In addition to C–H activation, the carboxylate-rich center in MMOH is capable of oxidizing alkyl sulfides and thiols.[3,8] We therefore extended our studies to examine carboxylate-bridged diiron(II) complexes with pyridine ligands incorporating of sulfide, sulfoxide, and thiol as tethered substrates. Upon exposure to dioxygen, these complexes react to form the corresponding sulfoxide and sulfone. The results of this study, a portion of which has been previously communicated,[24] are reported here.

Experimental Section

General Considerations. All reagents were obtained from commercial suppliers and used as received, unless otherwise noted. Dichloromethane and pentane were saturated with nitrogen and purified by passage through activated Al_2O_3 columns under argon.[25] Dioxygen (99.994%, BOC Gases) was dried by passing the gas stream through a column of Drierite. The synthesis and characterization of $[Fe_2(\mu\text{-}O_2CAr^{Tol})_2(O_2CAr^{Tol})_2(THF)_2]$ were reported previously.[18] 2-Phenylthiopyridine (2-PhSpy), 2-phenylpyridylsulfoxide (2-PhS(O)py), 2-methylthiopyridine (2-MeSpy), 2-methylpyridylsulfoxide (2-MeS(O)py), and 2-methylpyridylsulfone (2-MeS(O)$_2$py) were prepared by modified literature procedures, and their purity was ascertained by ^{1}H NMR spectroscopy.[26] Air-sensitive manipulations were carried out under nitrogen in an Mbraun drybox. All samples were pulverized and dried under vacuum at 60 °C to remove solvent prior to determining their elemental composition.

$[Fe_2(\mu\text{-}O_2CAr^{Tol})_3(O_2CAr^{Tol})(2\text{-PhSpy}]$ (1). To a stirred solution of $[Fe_2(\mu\text{-}O_2CAr^{Tol})_2$-$(O_2CAr^{Tol})_2(THF)_2]$ (161 mg, 0.110 mmol) in a CH_2Cl_2 (10 mL) solution, 2-PhSpy (39.6 mg,

0.211 mmol) was added and stirred for 20 min before the solvent was removed under reduced pressure. The residue was extracted into 3 mL of 1,2-dichlorethane and pentane vapor diffusion into the bright orange-yellow solution afforded yellow block crystals of **1** (123 mg, 76%) suitable for X-ray crystallography. FT-IR (KBr, cm^{-1}): 3019 (w), 2917 (w), 2862 (w), 1598 (s), 1559 (s), 1534 (m), 1513 (s), 1453 (s), 1405 (s), 1378 (s), 1304 (w), 1284 (w), 1231 (w), 1189 (w), 1149 (w), 1109, 1051 (w), 1019 (m), 972 (w), 942 (w), 910 (w), 860 (s), 843 (s), 817 (s), 809, 796 (s), 766 (s), 735 (s), 702 (s), 689 (s), 641 (w), 607 (w), 583 (s), 517 (s), 471 (w), 411 (w), 402 (w). Anal. Calcd. for $C_{95}H_{77}NFe_2O_8S\cdot C_2H_4Cl_2$: C, 72.66; H, 5.09; N, 0.87. Found: C, 73.11; H, 5.18; N, 0.91.

[Fe$_2$(μ-O$_2$CAr^{Tol})$_3$(O$_2$CAr^{Tol})(2-MeSpy)] (2). In a CH$_2$Cl$_2$ (4 mL) solution [Fe$_2$(μ-O$_2$CAr^{Tol})$_2$(O$_2$CAr^{Tol})$_2$(THF)$_2$] (114 mg, 0.782 mmol) was allowed to react with 2-MeSpy (21.6 mg, 0.173 mmol) for 15 min. Removal of the solvent under reduced pressure left a residue that was extracted into 2 mL of chlorobenzene. Diffusion of pentane vapor into the bright orange-yellow solution afforded yellow block crystals (0.106 mg, 94%) of **2** suitable for X-ray crystallography. FT-IR (KBr, cm^{-1}): 3050 (w), 3023 (w), 2918 (w), 2860 (w), 1601 (s), 1576 (m), 1559 (m), 1513 (s), 1453 (s), 1406 (s), 1382 (s), 1304 (w), 1283 (w), 1185 (w), 1149 (w), 1109 (w), 1071 (w), 1019 (m), 970 (w), 832 (w), 817 (s), 799 (s), 765 (s), 737 (m), 702 (s), 641 (m), 608 (w), 583 (m), 557 (w), 523 (m), 465 (m), 410 (w). Anal. Calcd. for $C_{90}H_{75}NO_8SFe_2\cdot 0.5C_2H_4Cl_2$: C, 73.27; H, 5.20; N, 0.94. Found: C, 73.29; H, 5.45; N, 1.12.

[Fe$_2$(μ-O$_2$CAr^{Tol})$_2$(O$_2$CAr^{Tol})$_2$(2-MeS(O)py)$_2$] (3). A bright red-orange solution was produced upon the addition of 2-MeS(O)py (28.2mg, 0.200 mmol) to [Fe$_2$(μ-O$_2$CAr^{Tol})$_2$-(O$_2$CAr^{Tol})$_2$(THF)$_2$] (98.9 mg, 0.0677 mmol) in 6 mL of CH$_2$Cl$_2$ and a red powder (91.8 mg, 85%) was isolated after diffusion of pentane into the reaction mixture. Red block crystals of **3**

suitable for X-ray diffraction studies were obtained by diffusing pentane vapor into a chlorobenzene solution of **3**. FT-IR (KBr, cm^{-1}): 3053 (w), 3022 (w), 2917 (w), 2862 (w), 1588 (s), 1562 (s), 1540 (s), 1514 (s), 1454 (s), 1410 (s), 1376 (s), 1304 (w), 1263 (w), 1186 (w), 1147 (w), 1109 (w), 1088 (w), 1020 (m), 1008 (s), 967, 818 (s), 800 (s), 785 (s), 765 (s), 737 (m), 711 (m), 703 (m), 637 (m), 608 (w), 584 (m), 542 (w), 520 (m), 450 (w), 411 (w). Anal. Calcd. for $C_{96}H_{82}N_2Fe_2O_{10}S_2$: C, 72.09; H, 5.17; N, 1.75. Found: C, 71.71; H, 4.85; N, 1.81.

[Fe(O$_2$CAr^{Tol})$_2$(2-HSpy)$_2$] (4a). A solution of [Fe$_2$(μ-O$_2$CAr^{Tol})$_2$(O$_2$CAr^{Tol})$_2$(THF)$_2$] (174 mg, 0.119 mmol) in CH$_2$Cl$_2$ (4 mL) was combined with 2-mercaptopyridine (2-HSpy) (62.9 mg, 0.566 mmol) and stirred for 15 min. Vapor diffusion of pentane into this orange solution afforded orange blocks of **4a** (199 mg, 95%) suitable for X-ray crystallography. FT-IR (KBr, cm^{-1}): 3195 (w), 3114 (w), 3053 (w), 2916 (w), 2862 (w), 1591 (s), 1539 (s), 1514 (s), 1446 (s), 1410 (s), 1375 (s), 1269 (w), 1130 (s), 1085 (w), 1020 (w), 995 (m), 916 (w), 847 (w), 818 (m), 801 (s), 786 (m), 755 (s), 726 (m), 707 (m), 619 (w), 584 (w), 539 (w), 521 (m), 486 (w), 442 (m). Anal. Calcd. for $C_{52}H_{44}N_2FeO_4S_2$: C, 70.90; H, 5.03; N, 3.18. Found: C, 71.81; H, 4.91; N, 3.32.

Physical Measurements. FT-IR spectra were recorded on a Thermo Nicolet Avatar 360 spectrometer with OMNIC software. ^{1}H NMR data were recorded on a Varian 300 spectrometer housed in the Massachusetts Institute of Technology Department of Chemistry Instrument Facility (MIT DCIF). Chemical shifts were referenced to the residual solvent peaks for proton experiments. All spectra were recorded at ambient probe temperature, 293 K.

X-ray Crystallographic Studies. Intensity data were collected on a Bruker (formerly Siemens) APEX CCD diffractometer with graphite-monochromated Mo Kα radiation (λ = 0.71073 Å), controlled by a Pentium-based PC running the SMART software package.[27] Single

crystals were mounted on the tips of glass fibers, coated with paratone-N oil, and cooled to −100 °C under a stream of N_2 maintained by a KRYO-FLEX low-temperature apparatus. Data collection and reduction protocols are described elsewhere.[28] The structures were solved by direct methods and refined on F^2 by using the SHELXTL-97 software[29] incorporated in the SHELXTL software package.[30] Empirical absorption corrections were applied with SADABS,[31] part of the SHELXTL program package, and the structures were checked for higher symmetry by using the PLATON software.[32] All non-hydrogen atoms were located and their positions refined with anisotropic thermal parameters by least-squares cycles and Fourier syntheses. In general hydrogen atoms were assigned to idealized positions and given thermal parameters equivalent to either 1.5 (methyl hydrogen atoms) or 1.2 (all other hydrogen atoms) times the thermal parameter of the carbon atom to which they were attached. The crystal of **1** contains half of a dichloroethane molecule for each dinuclear unit. In the structure of **2**, one of the $^-O_2CAr^{Tol}$ ligands was disordered and was modeled over two positions with 50% occupancy. A pentane and 1.5 dichloroethane molecules are present in the unit cell of **2**. The pentane molecule is severely disordered and each carbon atom was modeled over three positions using identical anisotropic displacement parameters. The half dichloroethane molecule lies on a center of symmetry and the chlorine atom is disordered and was refined with the atoms distributed equally over two positions. Compound **3** has a chlorobenzene molecule in the crystal lattice. Data collection and experimental details for **1** − **4** are summarized in Table 5.1. Selected bond lengths and angles for **1** − **4** are provided in Tables 5.2 − 5.4.

Oxidation Product Analyses. Oxidation reactions were performed by exposing CH_2Cl_2 solutions of the diiron(II) complex to dioxygen over a period of time at room temperature. During workup, Chelex was added to the reaction solutions to remove the iron salts. The

resulting slurry was stirred for 2 h, after which the Chelex was removed by filtration. The resin was washed with CH_2Cl_2 twice more and the filtrates were combined. The solvent was removed in vacuo to afford the N-donor species for analysis. The products were identified by NMR spectroscopy and GC-MS by comparing their NMR spectra and retention times and mass spectral patterns to those of authentic samples. The amount of oxidized ligand obtained for **1**, **2**, and **3** was quantitated by GC-MS using 1,2-dichlorobenzene as an internal standard. All samples were prepared in an anaerobic glove box prior to bubbling with dried dioxygen. Control experiments established that, in the absence of the diiron(II) complexes, neither dioxygen saturated CH_2Cl_2 nor the workup procedure induces ligand oxidation.

GC-MS Analyses. Analyses were carried out on a Hewlett-Packard HP-5890 gas chromatograph connected to a HP-5971 mass analyzer. An Alltech Econo-cap EC-1 capillary column of dimensions (30 m x 0.53 mm x 1.2 μm) was employed with the following program to effect all separations: initial temperature = 100 °C; initial time = 4 min; temperature ramp = 100 – 210 °C at 20 deg/min; and final time = 4.5 min. Quantitations were made by comparison of the total ion count of 2-PhSpy, 2-PhS(O)py, 2-MeSpy, 2-MeS(O)py and 2-MeS(O)$_2$py with that of 1,2-dichlorobenzene present as an internal standard. Calibration plots for the detector response were prepared for authentic samples of 2-PhSpy, 2-PhS(O)py, 2-MeSpy, 2-MeS(O)py, 2-MeS(O)$_2$py and 1,2-dichlorobenzene standard by using stock solutions of known concentrations.

Oxygenation of 4a. In a typical reaction compound **4a** was dissolved in CH_2Cl_2 and loaded into a vessel fitted with a rubber septum. The solution was cooled to –10 °C in an ice/acetone bath. Dioxygen was gently bubbled into the solution, resulting in a color change from pale orange to dark blue that signaled formation of **4b**.

UV-visible Spectroscopy. UV-vis spectra were recorded on a Hewlett-Packard 8453 diode array spectrophotometer. Low temperature UV-vis experiments were performed with a custom made quartz cuvette, 1 cm path length, fused into a vacuum jacketed dewar. A solution of **4a**, 1.1 mM in CH_2Cl_2 (6 mL), under N_2 was cooled to -10 °C. Dry O_2 was gently purged through the solution for 30 s, and the UV-vis spectra were recorded at various time intervals.

EPR Spectroscopy. EPR spectra were recorded on a Bruker Model 300 ESP X-band spectrometer operating at 9.42 GHz. Temperatures were maintained with an Oxford Instruments liquid helium EPR 900 cryostat. X-band EPR samples were prepared by making a 0.513 mM solution of **4a** in CH_2Cl_2. Aliquots of ~300 μL were transferred to the EPR tubes in the drybox; the tubes were septum-sealed. One of the samples was frozen at 77 K. Another was cooled to 4 °C under N_2, treated with O_2 for 45 s, and then frozen at 77 K.

Resonance Raman Spectroscopy. Solutions of **4a** in an NMR tube with a J-Young valve were oxygenated with either $^{16}O_2$ or $^{18}O_2$ at -78 °C and subsequently warmed to room temperature for the measurement. The sample was excited at 647.1nm using a Coherent Innova 90C Kr^+ ion laser. Plasma lines for the laser were rejected using a holographic band pass (Kaiser Optical) to obtain a clean background. Approximately 16 mW were focused to a ~100 μm spot. The resulting Raman light was filtered with a holographic notch filter (Kaiser Optical Systems) to attenuate the Rayleigh scattered light and focused into a 150 μm slit of a single stage spectrograph(An Acton Spectro Pro SP300i). The spectrograph has a 300 mm focal length and is equipped with a 1200 grooves/nm grating giving a linear dispersion of 2.7 nm/mm. The spectral resolution is approximately 5.8 cm^{-1}. Spectra were recorded on a thermoelectrically-cooled back-illuminated CCD. Cooling the CCD to -70 °C significantly reduces the dark current (< 0.1 e/p/s).

Prior to each measurement, the Raman system was initially optimized using frozen CH_2Cl_2. The exposure time was adjusted to yield a signal with ~ 40,000 counts per accumulation, and the total number of exposures taken was adjusted to yield a 5 min gathering. Methylene chloride bands at 1156 cm^{-1}, 897 cm^{-1}, 704 cm^{-1}, and 286 cm^{-1} were used as a wavelength calibration standard. The sample concentrations were between 2 – 4 mM, and each measurement was made on more than one freshly prepared sample and in triplicate to ensure the authenticity of the results. Data were processed by using WinSpec 3.2.1 (Princeton Instruments, Inc.), and the resultant ASCII files were further manipulated using Microsoft Excel.

Results

Synthesis and Structural Characterization of Diiron(II) Complexes with Pendant Sulfur-Containing Substrates [Fe$_2$(μ-O$_2$CAr^{Tol})$_3$(O$_2$CAr^{Tol})(2-PhSpy)] (1), [Fe$_2$(μ-O$_2$CAr^{Tol})$_3$-(O$_2$CAr^{Tol})(2-MeSpy)] (2), and [Fe$_2$(μ-O$_2$CAr^{Tol})$_2$(O$_2$CAr^{Tol})$_2$(2-MeS(O)py)$_2$] (3).

Compounds **1** and **2** differ only in the sulfide substituent. Combination of 2-PhSpy or 2-MeSpy with [Fe$_2$(μ-O$_2$CAr^{Tol})$_2$(O$_2$CAr^{Tol})$_2$(THF)$_2$] led to the isolation of [Fe$_2$(μ-O$_2$CAr^{Tol})$_3$-(O$_2$CAr^{Tol})(2-PhSpy)] (**1**) or [Fe$_2$(μ-O$_2$CAr^{Tol})$_3$(O$_2$CAr^{Tol})(2-MeSpy)] (**2**), respectively (Scheme 5.1). The structures of **1** and **2** are shown in Figures 6.1 and 6.2, and selected bond lengths and angles are provided in Table 5.2. Both **1** and **2** contain triply carboxylate-bridged diiron(II) centers with Fe$\cdots$Fe separations of 3.2712(8) and 3.2496(7) Å, respectively. The Fe$\cdots$S distance is longer in **1**, 3.0897(9) Å compared to 2.9091(10) Å in **2**. A fourth bidentate carboxylate ligand completes the metal coordination sphere of the iron atom not bound to a pyridine moiety.

Bright red crystals of **3** were obtained from the reaction of [Fe$_2$(μ-O$_2$CAr^{Tol})$_2$-(O$_2$CAr^{Tol})$_2$(THF)$_2$] with 2-MeS(O)py, Scheme 5.1. Figure 5.3 shows the structure of **3**, and selected bond lengths and angles are tabulated in Table 5.3. The compound is a doubly

carboxylate-bridged diiron(II) species with an Fe···Fe separation of 4.585(3) Å. The coordination sphere of each iron atom is completed by and additional bidentate carboxylate and an N-donor 2-MeS(O)py ligand that is ligated through both the N and O atoms, rendering each iron atom 6-coordinate. A five-membered ring is formed involving Fe1-N1-C1-S1-O1, with an Fe1–O1 distance of 2.247(6) Å. A comparison of the IR spectra of **2** and **3** (Figure 5.5) shows the vibrations of two compounds to be nearly identical, with the exception of the S=O stretch at 1008 cm^{-1} in **3**.[33]

Isolation of Mononuclear [Fe(O$_2$CAr^{Tol})$_2$(2-HSpy)$_2$] (4a). Combining one equiv of [Fe$_2$(μ-O$_2$CAr^{Tol})$_2$(O$_2$CAr^{Tol})$_2$(THF)$_2$] with 4 equiv of 2-HSpy, as indicated in Scheme 5.1, resulted in the formation of the mononuclear iron(II) complex, [Fe(O$_2$CAr^{Tol})$_2$(2-HSpy)$_2$] (**4a**). Its structure is shown in Figure 5.4 and selected bond lengths and angles are provided in Table 5.4. This pseudo-tetrahedral iron(II) complex is coordinated by two monodentate carboxylates and two thioamides bound to the metal center through the sulfur atoms. The largest of the metal centered bond angles is the O–Fe–O angle of 133.35(9)° and the smallest is the S–Fe–S bond of 92.04(2)°. The other four angles are closer to the ideal tetrahedral value of 109.5°, averaging 105.96(6)°. There is hydrogen bonding between the non-coordinated carboxylate oxygen atoms and the thioamide protons at distances of 2.767(14) Å for O1···N1 and 2.709(18) Å for O3···N2. The characteristic S–H stretching absorption in the range of ~2600 – 2550 cm^{-1} is absent from the solid state IR spectrum of **2**, depicted in Figure 5.6, but the N–H modes are observed at 3196 cm^{-1}.[33] This result is consistent with the X-ray structure.

Tethered Ligand Oxidation in 1 – 3. Oxidation of the substrates appended to the N-donor ligand was investigated by product analysis following introduction of O$_2$ into solutions of 1 – 3. A summary of the conditions and amount of oxidation product recovered is provided in

Table 5.5. A pale yellow CH_2Cl_2 solution of **1** reacts with dioxygen at room temperature and immediately turns golden brown. Workup of the mixture and analysis by GC-MS revealed 29% conversion to 2-pyridylphenylsulfoxide (2-PhS(O)py). The analogous oxidation of **2**, analyzed by GC-MS converts 58 % of the sulfide to the sulfoxide. The peaks were assigned by comparing the retention times of the M^+ = 187 and 203 signals for **1** with those of authentic samples of 2-phenylthiopyridine and 2-phenylpyridylsulfoxide and the M^+ = 125 and 141 signals for **2** with those of authentic samples of 2-methylthiopyridine and 2-methylpyridylsulfoxide . In both systems the unmodified sulfido ligand was quantitatively recovered. No other products such as the corresponding pyridylsulfones were evident in the GC traces.

The bright red CH_2Cl_2 solution of **3** becomes dark red-brown upon exposure to dioxygen. Analysis of the products using GC-MS revealed 40% conversion of the 2-MeS(O)py to the sulfone, based on **3**. This assignment was confirmed by comparison of the M^+ = 157 signal in the GC-MS with an authentic sample of 2-MeS(O)$_2$py. The remaining material recovered was identified as unaltered pyridylsulfoxide ligand.

Reactions of 4a with Dioxygen. When a CH_2Cl_2 or toluene solution of **4a** reacts with dioxygen at –10 °C, a deep blue intermediate (**4b**) develops over a period of 10 min. Absorptions in the UV-vis spectrum, presented in Figure 5.7, include maxima at 378 nm (ε = 3000 M^{-1} cm^{-1}), 627 nm (ε = 800 M^{-1} cm^{-1}), and >1100 nm ($\varepsilon \sim$ 500 M^{-1} cm^{-1}). Both the ferrous starting material, **4a**, and the blue intermediate, **4b**, are EPR silent.

Resonance Raman spectroscopy revealed that **4b** contains bound oxygen. Characteristic resonances observed in the Raman spectra of (μ-peroxo)diiron(III) moieties arise from O–O (800 – 900 cm^{-1}) and Fe–O (450 – 550 cm^{-1}) stretching vibrations.[34-36] Raman spectra were obtained for **6b** in CH_2Cl_2 at room temperature. Upon excitation at 647.1 nm, two Raman active bands

appear at 843 and 504 cm^{-1}. These features are absent both in Raman spectra of **4a** and the decomposition product of **4b**. When the blue intermediate is prepared by reacting **4a** with ^{18}O-labeled dioxygen (**4b***), the peak positions shift to 811 and 494 cm^{-1}. A comparison of the two spectra is shown in Figure 5.8.

Discussion

In addition to methane to methanol, MMOH can accept a variety of oxidizable substrates including methanethiol.[3] Therefore 2-mercaptopyridine was investigated as an ancillary ligand for the oxygen-rich core of the *m*-terphenyl carboxylate diiron(II) complexes. MMOH also catalyzes the conversion of sulfides to sulfoxides, amines to amine oxides, and olefins to epoxides.[3,8] The first of these transformations inspired the selection of 2-phenylthiopyridine and 2-methylthiopyridine as N-donor ligands. Although as yet unprecedented in the natural system, the oxidation of dimethylsulfoxide is thermodynamically more favorable than that of dimethylsulfide,[37] so 2-pyridylmethysulfoxide was installed in the {Fe$_2$(μ-O$_2$CAr^{Tol})$_2$-(O$_2$CAr^{Tol})$_2$} core.

Despite the differing substituents on the sulfur moiety, the iron atoms in **1** and **2** have nearly identical coordination environments. It was initially thought that steric bulk provided by the phenylthio moiety at the ortho position of the pyridine ring was responsible for only one pyridine ligand being accommodated at the diiron cores in **1**. Such also proved to be the case in **2**, however, where the heteroatom substituent is a less sterically demanding methyl group. The Fe–N bond lengths of 2.0869(15) and 2.077(3) Å for **1** and **2**, respectively, are ~0.06 Å shorter than those typically observed in diiron(II) windmill structures. In both structures the Fe–O bonds of the three bridging carboxylate ligands are on average 0.05 Å shorter for the iron atom to which the pyridine moiety is coordinated, 1.9903(15) vs 2.0453(16) Å in **1**, and 1.994(2) vs

2.044(2) Å in **2**. The Fe–O bonds of the terminal carboxylate ligand are the longest and asymmetric, being 2.0869(15) and 2.2013(16) Å in **1** and 2.059(2) Å and 2.256(2) Å in **2**. This result reflects the greater electron releasing character of a pyridine N-donor than a bidentate carboxylate, since the lower coordinate iron atom would be expected to have the shorter bond lengths, all other things being equal.

When 2-MeS(O)py rather than 2-MeSpy ligand was employed as the N-donor ligand, a more open doubly carboxylate-bridged structure is adopted for the resulting diiron(II) complex **5**. Two N-donors are now accommodated compared to only one in the triply-bridged complexes **1** and **2**. The four Fe–O bond distances increase by ~0.10 Å, from 1.959(6) to 2.268(5) Å. The Fe···Fe distance of 4.585(3) Å in **3** is >1 Å greater than those observed in the triply-bridged structures **1** and **2** of ~3.25 Å and quite long, reflecting the *syn,anti* binding mode of the bridging carboxylates.[38]

Instead of the carboxylate-bridged dimetallic unit anticipated upon displacement of the THF molecules in $[Fe_2(\mu\text{-}O_2CAr^{Tol})_2(O_2CAr^{Tol})_2(THF)_2]$ by 2-mercaptopyridine, a mononuclear species is isolated. The Cambridge Structural Database reports no other structures of four-coordinate iron containing only sulfur and oxygen ligands; **4a** appears to be the first. The hydrogen bonding between the carboxylate oxygen atoms and the thioamide protons is most likely stabilizing this unique mononuclear structure. The iron atom is coordinated by a thioamido ligand, the tautomer of 2-mercaptopyridine (Scheme 5.2), in which the nitrogen atom is protonated and a carbon-sulfur double bond is present. The C1–S1 and C6–S2 distances of 1.716(3) and 1.717(3) Å are characteristic of C=S double bonds,[39] and the bond lengths of the pyridine ring similarly reflect this assignment.

Oxidation of diphenyl sulfide is slightly more energetically favorable than oxidation of dimethyl sulfide ($\Delta H°$ –36 vs –33 kcal/mol),[40,41] which is inconsistent with greater conversion of 2-MeSpy (58 %) than 2-PhSpy (29%) to the sulfoxide in **2** and **1**, respectively. The higher activity of **2**, despite its carrying the less energetically favorable substrate, may be a result of increased access to the O_2-activated at the diiron center because of the smaller methyl substituent compared to the phenyl group of 2-PhSpy in **1**.

In a study involving Δ9-desaturase, which has a carboxylate-bridged diiron site similar to that in MMOH,[42-44] reaction of 10-thiasterarate-ACP with the reconstituted soluble stearoyl-ACP Δ9-desaturase complex produced the 10-sulfoxide as the sole product.[45] The comparable reaction with 9-thiasearoyl-ACP desaturase, however, gave the 9-sulfoxide as ~5% of the total products. It was concluded that the relative reactivity of the 9- and 10-thia-substituted acyl-ACPs is controlled by the proximity of two positions to the O_2-activated diiron center in the transition state. The reactivity of compound **2** suggests their view. Exposure of **2** to dioxygen leads only to the formation of the sulfoxide. No C–H bond activation of the methyl substituent was observed. Oxidation of an ethyl moiety tethered to pyridine in $[Fe_2(\mu\text{-}O_2CAr^{Tol})_2(O_2CAr^{Tol})_2(2\text{-Etpy})_2]$ affords only α-methyl-2-pyridinemethanol, a result that also may be a consequence of proximity to the O_2-activated diiron center.[23]

Although the two iron atoms in **3** are coordinatively saturated, the compound readily reacts at room temperature following exposure to dioxygen. The observed ligand oxidation may require carboxylate shifts or partial dissociation of the sulfoxide ligand.[18] The 40% conversion of the sulfoxide to the corresponding sulfone is, to the best of our knowledge, unprecedented in small molecule model compounds, but not surprising from a thermodynamic perspective.[34,46,47] The $\Delta H°$ for oxidation of dimethylsulfide to dimethylsulfoxide is –27 kcal/mol compared to –52

kcal/mol for oxidation of dimethylsulfoxide to dimethylsulfone.[37] Despite the fact that compound 3 is more sterically hindered than 2, once dioxygen can access the diiron center and become activated, the ligand oxidation reaction will be more favorable.

Clues to the identity of the blue intermediate observed upon oxygenation of 4a are provided by resonance Raman and EPR spectroscopic measurements. The electronic absorption spectrum of 4b is similar to those of paramagnetic $Fe^{II}Fe^{III}$ cations formed by other $\{Fe_2(\mu\text{-}O_2CAr^{Tol})_4\}$ systems, which display intervalence charge transfer transitions and have a characteristic g = 10 signal in their EPR spectra.[48] However, both the ferrous starting material, 4a, and the blue intermediate, 4b, are EPR silent. The UV-vis spectrum of the latter also resembles those of (μ-peroxo)diiron(III) units in both synthetic analog and biological systems.[34,46,49-52] Although 4a is a mononuclear compound, oxygenation of mononuclear iron(II) can result in diiron(II) complexes, possibly via an $\{Fe_2(O_2)\}$ intermediate.[53] Theoretically from a simple harmonic oscillator calculation the downshift upon $^{18}O_2$-labeling ($\Delta^{18}O$) should be –48 cm^{-1} for an O–O stretch and –23 cm^{-1} for the Fe–O stretch. For 4b the $\Delta^{18}O$ values are slightly less (–32 cm^{-1}, –10 cm^{-1}) for the O–O and Fe–O vibrations, respectively, suggesting coupling with other modes in the molecule or possibly an Fe–O–O–X unit.

Conclusion

Tethered thiol, sulfide, and sulfoxide moieties on pyridine ligands serve as excellent substrates for oxidation at O_2-activated, carboxylate-bridged diiron(II) centers. Intramolecular oxidation of the heteroatoms in these groups further demonstrate that proximity is important for oxidation. Only the group adjacent to the diiron center is oxidized, since no methyl group oxidation occurred for the case of 2-methylthiopyridine complex. These observations provide valuable information to guide future work on more advanced MMOH synthetic analogs.

References

(1)   Erwin, D. P.; Erickson, I. K.; Delwiche, M. E.; Colwell, F. S.; Strap, J. L.; Crawford, R. L. *Appl. Environ. Microbiol* **2005**, *71*, 2016-2024.

(2)   Vardar, G.; Wood, T. K. *Appl. Environ. Microbiol* **2004**, *70*, 3253-3161.

(3)   Colby, J.; Stirling, D. I.; Dalton, H. *Biochem. J.* **1977**, *165*, 395-402.

(4)   Feig, A. L.; Lippard, S. J. *Chem. Rev.* **1994**, *94*, 759-805.

(5)   Wallar, B. J.; Lipscomb, J. D. *Chem. Rev.* **1996**, *96*, 2625-2657.

(6)   Merkx, M.; Kopp, D. A.; Sazinsky, M. H.; Blazyk, J. L.; Müller, J.; Lippard, S. J. *Angew. Chem., Int. Ed. Engl.* **2001**, *40*, 2782-2807.

(7)   Baik, M.-H.; Newcomb, M.; Friesner, R. A.; Lippard, S. J. *Chem. Rev.* **2003**, *103*, 2385-2419.

(8)   Fuse, H.; Ohta, M.; Takimura, O.; Murakami, K.; Inoue, H.; Yamaoka, Y.; Oclarit, J. M.; Omori, T. *Biosci. Biotechnol. Biochem.* **1998**, *62*, 1925-1931.

(9)   Lippard, S. J. *Chemistry in Britain* **1986**, *22*, 221-228.

(10)   Lippard, S. J. *Angew. Chem., Int. Ed. Engl.* **1988**, *27*, 344-361.

(11)   Goldberg, D. P.; Telser, J.; Bastos, C. M.; Lippard, S. J. *Inorg. Chem.* **1995**, *34*, 3011-3024.

(12)   Herold, S.; Lippard, S. J. *J. Am. Chem. Soc.* **1997**, *119*, 145-156.

(13)   Mandal, S. K.; Young, V. G., Jr.; Que, L., Jr. *Inorg. Chem.* **2000**, *39*, 1831-1833.

(14)   Lee, D.; Sorace, L.; Caneschi, A.; Lippard, S. J. *Inorg. Chem.* **2001**, *40*, 6774-6781.

(15)   Lee, D.; Lippard, S. J. *J. Am. Chem. Soc.* **1998**, *120*, 12153-12154.

(16)   Hagadorn, J. R.; Que, L., Jr.; Tolman, W. B. *J. Am. Chem. Soc.* **1998**, *120*, 13531-13532.

(17)   Tolman, W. B.; Que, L., Jr. *J. Chem. Soc., Dalton Trans.* **2002**, 653-660.

(18)   Lee, D.; Lippard, S. J. *Inorg. Chem.* **2002**, *41*, 2704-2719.

(19)   Lee, D.; Lippard, S. J. *J. Am. Chem. Soc.* **2001**, *123*, 4611-4612.

(20)   Lee, D.; Lippard, S. J. *Inorg. Chem.* **2002**, *41*, 827-837.

(21)   Yoon, S.; Lippard, S. J. *Inorg. Chem.* **2003**, *42*, 8606-8608.

(22)   Carson, E. C. In *Doctoral Dissertation in Inorganic Chemistry*; Massachusetts Institute of Technology: Cambridge, MA, 2005; Chapter 2.

(23)   Carson, E. C. In *Doctoral Dissertation in Inorganic Chemistry*; Massachusetts Institute of Technology: Cambridge, MA, 2005; Chapter 3.

(24)   Carson, E. C.; Lippard, S. J. *J. Am. Chem. Soc.* **2004**, *126*, 3412-3413.

(25)   Pangborn, A. B.; Giardello, M. A.; Grubbs, R. H.; Rosen, R. K.; Timmers, F. J. *Organometallics* **1996**, *15*, 1518-1520.

(26)   Furukawa, N.; Ogawa, S.; Matsumura, K.; Fujihara, H. *J. Org. Chem.* **1991**, *56*, 6341-6348.

(27)   *SMART v5.626: Software for the CCD Detector System*; Bruker AXS: Madison, WI, 2000.

(28)   Kuzelka, J.; Mukhopadhyay, S.; Spingler, B.; Lippard, S. J. *Inorg. Chem.* **2003**, *42*, 6447-6457.

(29)   Sheldrick, G. M. *SHELXTL97-2: Program for Refinement of Crystal Structures;* University of Göttingen, Germany, 1997.

(30)   *SHELXTL v5.10: Program Library for Structure Solution and Molecular Graphics;* Bruker AXS: Madison, WI, 1998.

(31)   Sheldrick, G. M. *SADABS: Area-Detector Absorption Correction;* University of Göttingen, Germany, 1996.

(32)   Spek, A. L. *PLATON, A Multipurpose Crystallographic Tool*; Utrecht University: Utrecht, The Netherlands, 1998.

(33)   Silverstein, R. M.; Webster, F. X. *Spectrometric Identification of Organic Compounds*; Sixth ed.; John Wiley & Sons, Inc.: New York, 1998.

(34)   Tshuva, E. Y.; Lippard, S. J. *Chem. Rev.* **2004**, *104*, 987-1012.

(35)   Chavez, F. A.; Ho, R. Y. N.; Pink, M.; Young, V. G., Jr.; Kryatov, S. V.; Rybak-Akimova, E. V.; Andres, H.; Munck, E.; Que, L., Jr.; Tolman, W. B. *Angew. Chem., Int. Ed. Engl.* **2002**, *41*, 149-152.

(36)   Costas, M.; Cady, C. W.; Kryatov, S. V.; Ray, M.; Ryan, M. J.; Rybak-Akimova, E. V.; Que, L., Jr *Inorg. Chem.* **2003**, *42*, 7519-7530.

(37)   Harlan, E. W.; Berg, J. M.; Holm, R. H. *J. Am. Chem. Soc.* **1986**, *108*, 6992 - 7000.

(38)   Rardin, R. L.; Tolman, W. B.; Lippard, S. J. *New J. Chem.* **1991**, *15*, 417-430.

(39)   *CRC Handbook of Chemistry and Physics*; CRC Press, Inc.: Boca Raton, FL, 1979; Vol. 60.

(40)   Mackle, H.; O'Hare, P. A. G. *Tetrahedron* **1963**, *19*, 961-971.

(41)   Douglas, T. B. *J. Am. Chem. Soc.* **1946**, *68*, 1072-1076.

(42)   Logan, D. T.; Su, X.-D.; Åberg, A.; Regnström, K.; Hajdu, J.; Eklund, H.; Nordlund, P. *Structure* **1996**, *4*, 1053-1064.

(43)   Whittington, D. A.; Lippard, S. J. *J. Am. Chem. Soc.* **2001**, *123*, 827-838.

(44)   Rosenzweig, A. C.; Nordlund, P.; Takahara, P. M.; Frederick, C. A.; Lippard, S. J. *Chem. Biol.* **1995**, *2*, 409-418.

(45)   White, R. D.; Fox, B. G. *Biochemistry* **2003**, *42*, 7828-7835.

(46)   Kryatov, S. V.; Rybak-Akimova, E. V. *Chem. Rev.* **2005**, *105*, 2175-2226.

(47)   Punniyamurthy, T.; Velusamy, S.; Iqbal , J. *Chem. Rev.* **2005**, *105*, 2329 -2363.

(48)   Lee, D.; DuBois, J. L.; Pierce, B.; Hedman, B.; Hodgson, K. O.; Hendrich, M. P.; Lippard, S. J. *Inorg. Chem.* **2002**, *41*, 3172-3182.

(49)   Broadwater, J. A.; Ai, J.; Loehr, T. M.; Sanders-Loehr, J.; Fox, B. G. *Biochemistry* **1998**, *37*, 14664-14671.

(50)   Valentine, A. M.; Stahl, S. S.; Lippard, S. J. *J. Am. Chem. Soc.* **1999**, *121*, 3876-3887.

(51)   Lee, S.-K.; Lipscomb, J. D. *Biochemistry* **1999**, *38*, 4423-4432.

(52)   Bollinger, J. M., Jr.; Tong, W. H.; Ravi, N.; Huynh, B. H.; Edmondson, D. E.; Stubbe, J. *J. Am. Chem. Soc.* **1994**, *116*, 8015–8023.

(53)   Yoon, S.; Lippard, S. J. *J. Am. Chem. Soc.* **2004**, *126*, 2666-2667.

Table 5.1. Summary of X-ray crystallographic Data

	$1 \cdot 0.5C_2H_4Cl_2$	$2 \cdot 1.5C_2H_4Cl_2/C_5H_{12}$	$3 \cdot C_6H_5Cl$	4
Empirical Formula	$Fe_2C_{96}H_{79}NO_8SCl$	$Fe_2C_{98}H_{93}NO_8SCl_3$	$Fe_2C_{102}H_{87}N_2O_{10}S_2Cl$	$FeC_{52}H_{44}N_2O_4S_2$
Formula Weight	1553.81	1662.84	1712.01	880.86
Space Group	$P\bar{1}$	$P2_1/c$	$P\bar{1}$	$P2_1/c$
a, Å	12.595(4)	13.0032(6)	12.3498(13)	18.821(19)
b, Å	15.545(5)	26.3878(12)	13.2855(14)	12.262(12)
c, Å	21.915(6)	24.6935(12)	14.8497(16)	21.18(2)
α, deg	95.539(5)		107.010(2)	
β, deg	90.483(5)	95.8440(10)	103.262(2)	115.123(16)
γ, deg	113.723(4)		95.288(3)	
V, Å^3	3904.5(19)	8428.9(7)	2234.3(4)	4425(8)
Z	2	4	1	4
ρ_{calc}, g/cm^3	1.322	1.310	1.272	1.322
T, °C	-100	-100	-100	-100
μ(Mo Kα), mm^{-1}	0.493	0.523	0.462	0.483
θ limits, deg	1.44 – 26.73	1.66 – 27.10	1.63 – 25.00	1.95 – 27.16
total no. of data	32778	72962	16643	37528
no. of unique data	16281	18576	7823	9779
no. of params	990	1279	568	550
Goodness-of-fit on F^2	1.058	1.196	0.887	1.131
R1^a	0.0474	0.0786	0.1042	0.0566
wR^{2b}	0.1064	0.1679	0.1412	0.1240
max, min peaks, e/Å^3	0.447, -0.279	1.031, -0.610	0.519, -0.384	0.505, -0.278

^{a}R1 $= \Sigma||F_o|-F_c||/\Sigma|F_o|$. ^{b}wR$^2 = \{\Sigma[w(F_o^2-F_c^2)^2]/\Sigma[w(F_o^2)^2]\}^{1/2}$.

Table 5.2. Selected interatomic distances (Å) and angles (deg) for $[Fe_2(\mu\text{-}O_2CAr^{Tol})_3(O_2CAr^{Tol})$-$(2\text{-}PhSpy)]$ (**1**) and $[Fe_2(\mu\text{-}O_2CAr^{Tol})_3(O_2CAr^{Tol})(2\text{-}MeSpy)]$ (**2**)[a]

	1	2
Fe1⋯Fe2	3.2712(8)	3.2496(7)
Fe2⋯S1	3.0897(9)	2.9091(10)
Fe1–O1	2.0869(15)	2.256(2)
Fe1–O2	2.2013(16)	2.059(2)
Fe1–O3	2.0610(16)	2.055(2)
Fe1–O5	2.0266(15)	2.026(2)
Fe1–O7	2.0484(15)	2.046(14)
Fe2–N1	2.1024(18)	2.077(3)
Fe2–O4	1.9767(16)	1.977(2)
Fe2–O6	2.0155(15)	2.034(2)
Fe2–O8	1.9786(15)	1.982(12)
O1–Fe1–O2	61.19(6)	60.8(15)
O1–Fe1–O3	109.83(7)	87.4(16)
O1–Fe1–O5	109.45(6)	168.1(15)
O1–Fe1–O7	114.07(6)	91.7(16)
O2–Fe1–O3	88.64(6)	109.4(17)
O2–Fe1–O5	169.04(6)	108.4(16)
O2–Fe1–O7	92.77(6)	111.3(18)
O3–Fe1–O5	89.61(6)	92.2(16)
O3–Fe1–O7	130.35(6)	132.5(17)
O5–Fe1–O7	95.59(6)	97.3(16)
O4–Fe2–N1	106.40(7)	110(2)
O6–Fe2–N1	97.36(7)	95.8(18)
O8–Fe2–N1	99.52(7)	100(2)
O4–Fe2–O6	104.73(6)	102.1(17)
O4–Fe2–O8	138.73(7)	102.4(18)
O6–Fe2–O8	103.10(6)	102.4(18)

[a]Numbers in parentheses are estimated standard deviations of the last significant figure. Atoms are labeled as indicated Figures 5.1 and 5.2.

Table 5.3. Selected interatomic distances (Å) and angles (deg) for $[Fe_2(\mu\text{-}O_2CAr^{Tol})_2\text{-}(O_2CAr^{Tol})_2(2\text{-}MeS(O)py)_2]$ (**3**)^a

	Bond Length (Å)		Bond Angle (deg)
Fe1···Fe2	4.586(2)	O1–Fe1–N1	79.1(3)
Fe1–N1	2.156(6)	O2–Fe1–N1	96.7(2)
Fe1–O1	2.234(5)	O3–Fe1–N1	92.4(2)
Fe1–O2	1.961(5)	O4–Fe1–N1	83.62(18)
Fe1–O3	2.071(5)	O5–Fe1–N1	149.98(19)
Fe1–O4	2.160(5)	O1–Fe1–O2	82.09(19)
Fe1–O5	2.267(5)	O1–Fe1–O3	171.5(2)
		O1–Fe1–O4	83.7(2)
		O1–Fe1–O5	97.75(17)
		O2–Fe1–O3	98.6(2)
		O2–Fe1–O4	163.3(2)
		O2–Fe1–O5	112.7(2)
		O3–Fe1–O4	96.08(18)
		O3–Fe1–O5	89.31(17)
		O4–Fe1–O5	59.28(17)

^{a}Numbers in parentheses are estimated standard deviations of the last significant figure. Atoms are labeled as indicated Figure 5.3.

Table 5.4. Selected bond distances (Å) and angles (deg) for $[Fe_2(O_2CAr^{Tol})_2(2\text{-}HSpy)_2]$ **(4)**^{a}

	Bond Length (Å)		Bond Angle (deg)
Fe1–O1	2.052(2)	O1–Fe1–S1	102.69(8)
Fe1–O3	2.029(3)	O1–Fe1–S2	110.22(6)
Fe1–S1	2.398(2)	O3–Fe1–S1	112.35(5)
Fe1–S2	2.398(3)	O3–Fe1–S2	98.59(6)
N1–C1	1.348(3)	O1–Fe1–O3	133.35(9)
C1–C2	1.407(4)	S1–Fe1–S2	92.04(2)
C2–C3	1.367(4)	Fe1–S1–C6	108.93(9)
C3–C4	1.393(4)	Fe1–S2–C6	106.95(9)
C4–C5	1.355(4)		
C5–N1	1.353(4)		
S1–C1	1.716(3)		
N2–C6	1.346(3)		
C6–C7	1.412(4)		
C7–C8	1.363(4)		
C8–C9	1.394(4)		
C9–C10	1.364(4)		
C10–N2	1.346(3)		
S2–C6	1.717(3)		
N1···O4	2.747(3)		
N2···O2	2.706(3)		

^{a}Numbers in parentheses are estimated standard deviations of the last significant figure. Atoms are labeled as indicated Figure 5.4.

Table 5.5. Summary of the Conditions and Amount of Oxidation Product Isolated for the Reaction of Compounds **1 – 3** with Dioxygen in CH_2Cl_2

Compound	$[Fe_2]$ (mM)	Reaction Time (h)	% Oxidized Ligand Recovered[a]
1	8.6	1.5	29
2	8.2	1.5	58
3	5.1	16	40

[a]Based on $[Fe_2]$

Scheme 5.1.
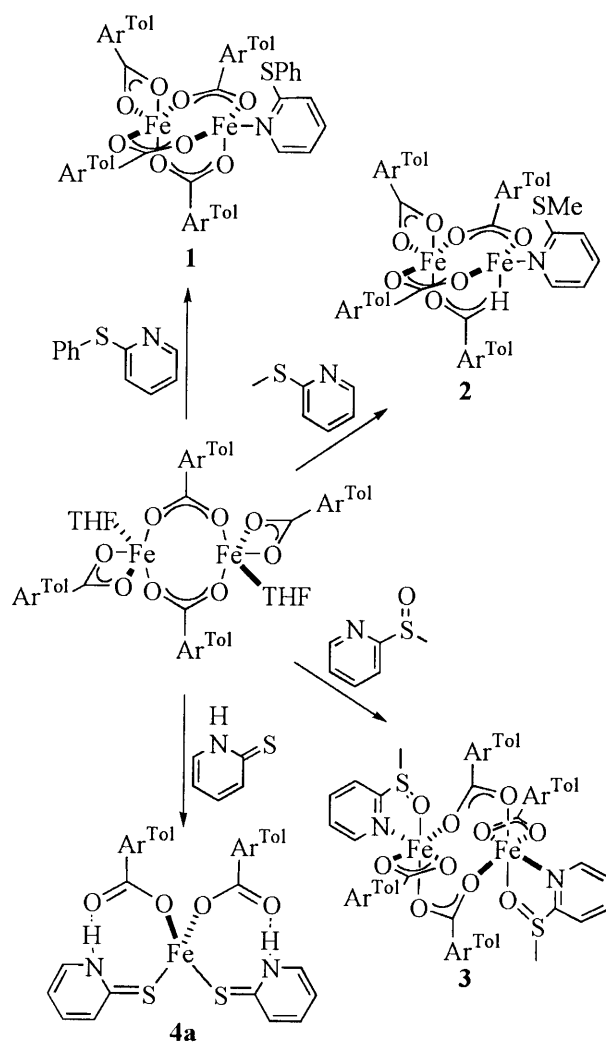
Scheme 5.2.
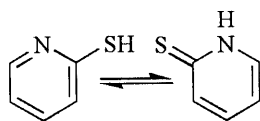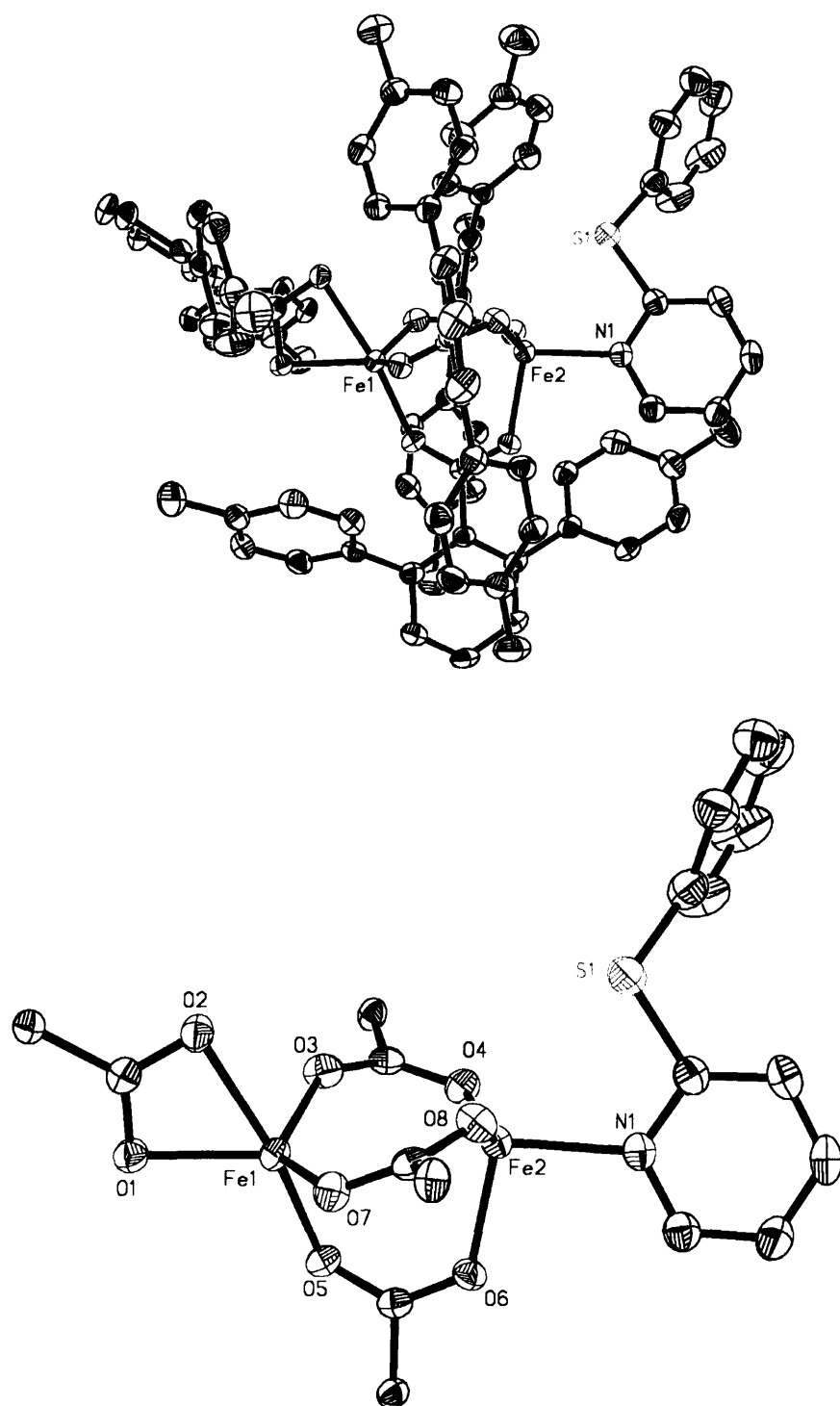
Figure 5.1. Top: ORTEP diagram of [Fe$_2$(μ-O$_2$CAr^{Tol})$_3$(O$_2$CAr^{Tol})(2-PhSpy)] (**1**) showing 50% probability thermal ellipsoids for all non-hydrogen atoms. Bottom: The aromatic rings of the $^-$O$_2$CAr^{Tol} are omitted for clarity.
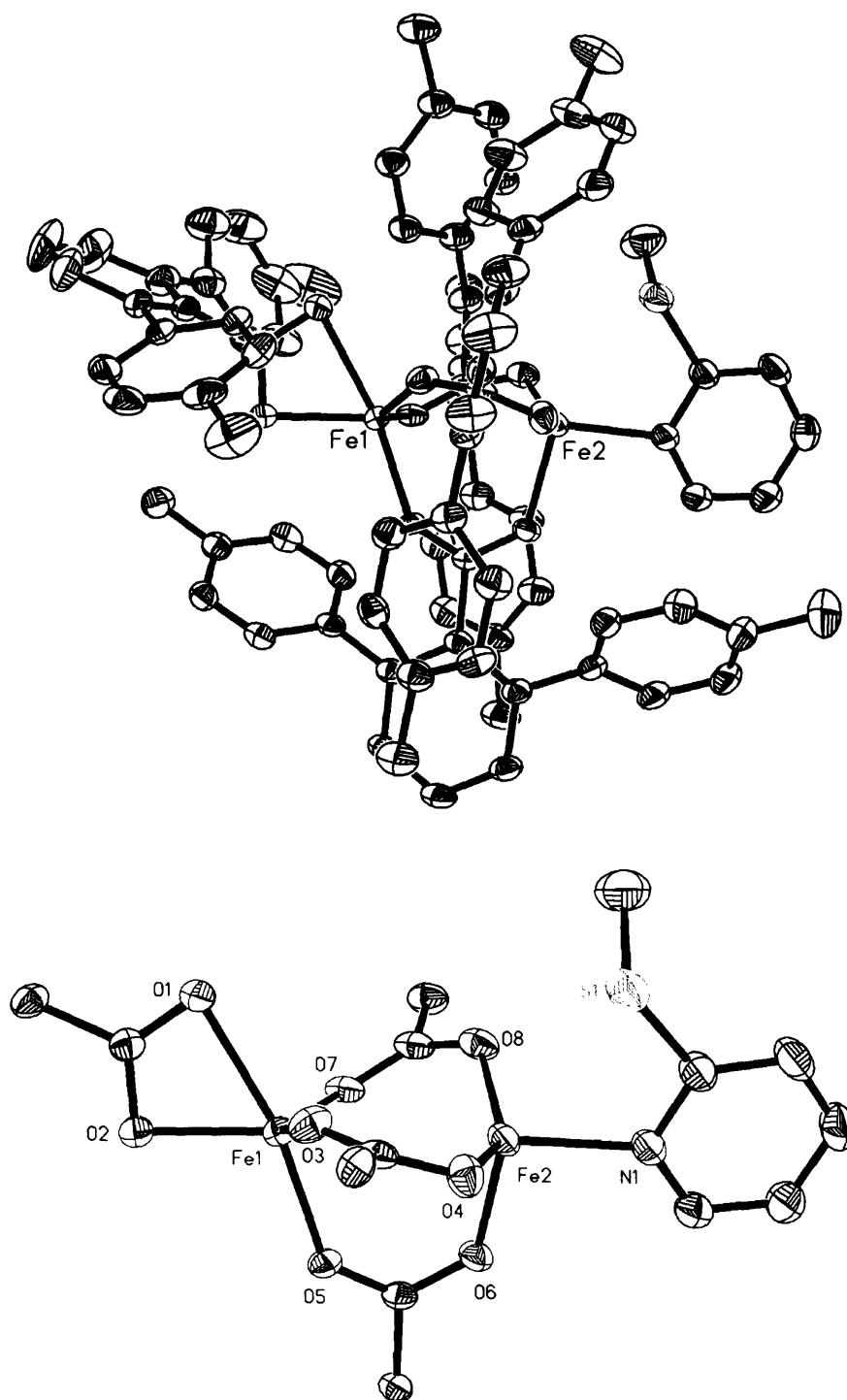
Figure 5.2. Top: ORTEP diagram of [Fe$_2$(μ-O$_2$CAr^{Tol})$_3$(O$_2$CAr^{Tol})(2-MeSpy)] (**2**) showing 50% probability thermal ellipsoids for all non-hydrogen atoms. Bottom: The aromatic rings of $^-$O$_2$CAr^{Tol} are omitted for clarity.
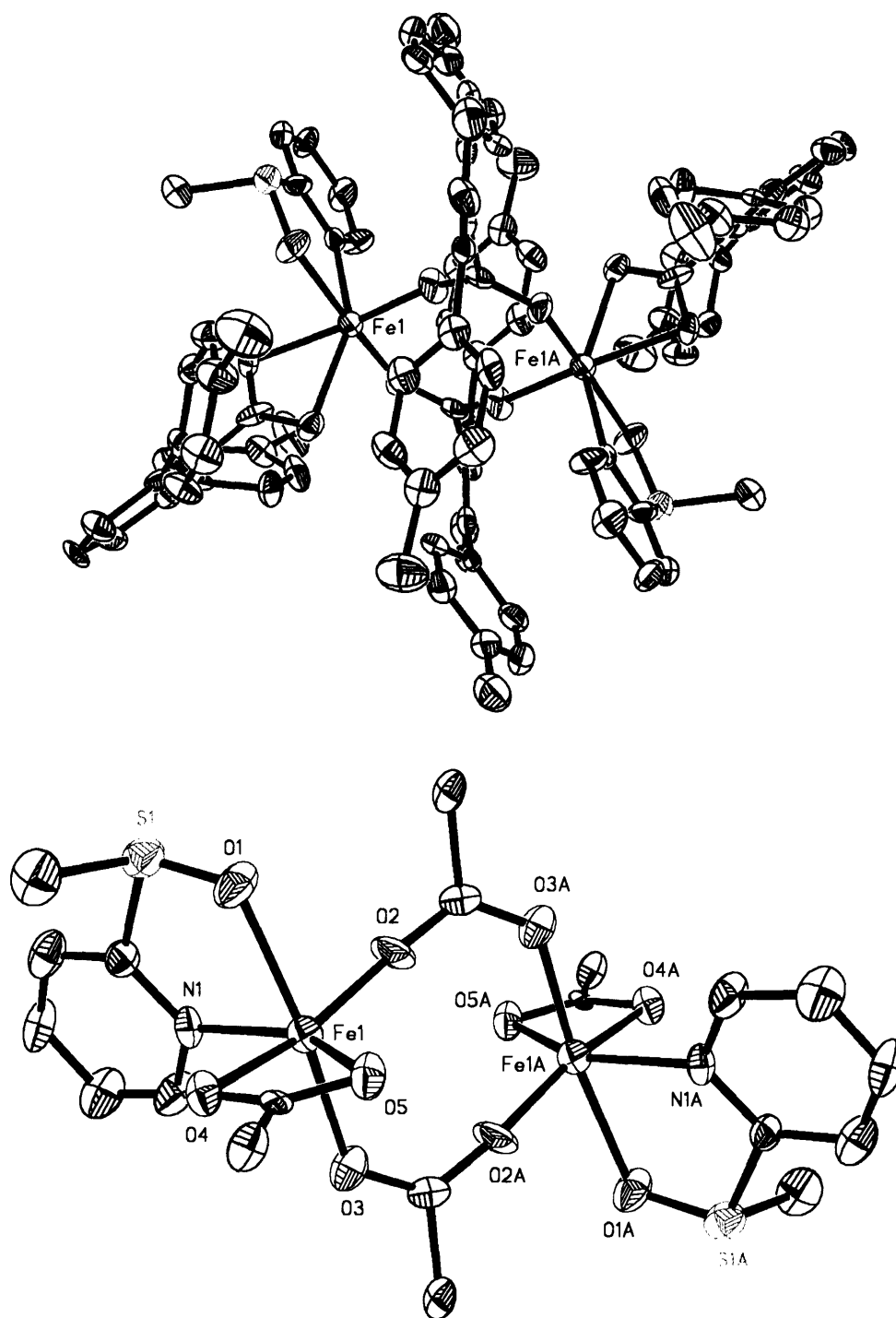
Figure 5.3. Top: ORTEP diagram of [Fe$_2$(μ-O$_2$CAr^{Tol})(O$_2$CAr^{Tol})$_2$(2-MeS(O)py)$_2$] (**3**) showing 50 % probability thermal ellipsoids for all non-hydrogen atoms. Bottom: The aromatic rings of $^-$O$_2$CAr^{Tol} are omitted for clarity.
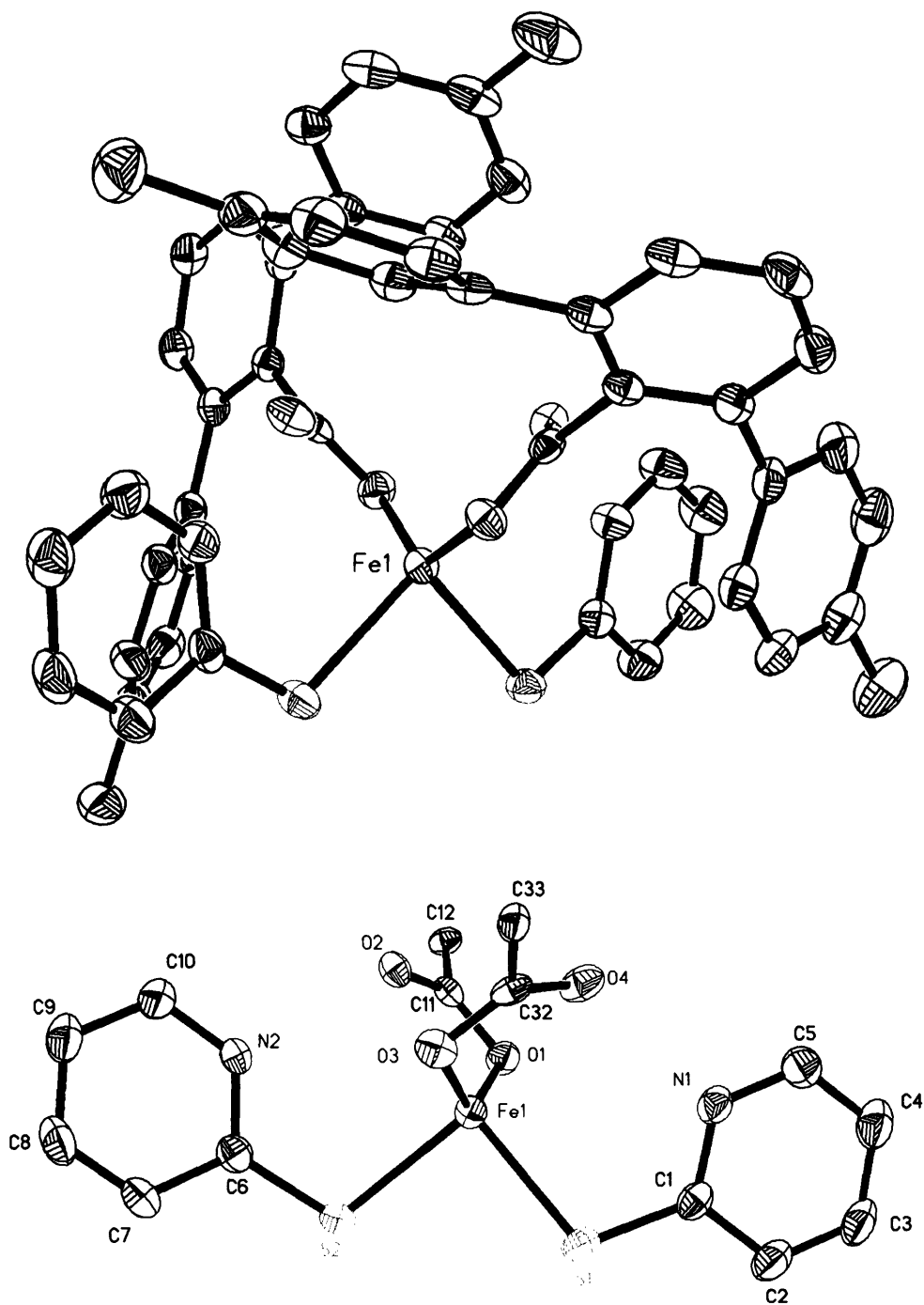
Figure 5.4. Top: ORTEP diagram of [Fe(O₂CAr^{Tol})₂(2-HSpy)₂] (**4**) showing 50 % probability thermal ellipsoids for all non-hydrogen atoms. Bottom: The aromatic rings of ⁻O₂CAr^{Tol} are omitted for clarity.
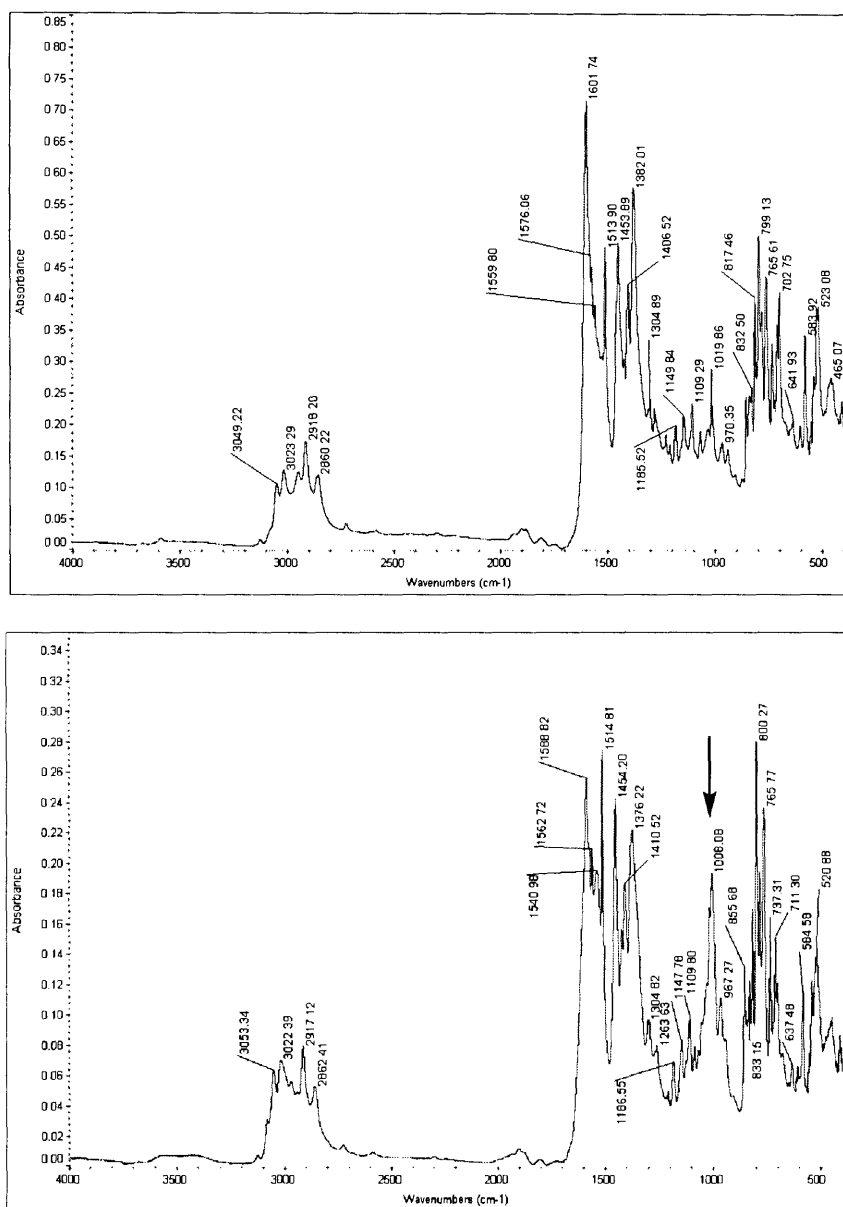
Figure 5.5. FT-IR spectra of KBr pellets of [Fe$_2$(μ-O$_2$CAr^{Tol})$_3$(O$_2$CAr^{Tol})(2-MeSpy) (**2**) (top spectrum) and [Fe$_2$(μ-O$_2$CAr^{Tol})$_2$(O$_2$CAr^{Tol})$_2$(2-MeS(O)py)$_2$] (**3**) (bottom spectrum). The arrow designates ν_{S-O}.
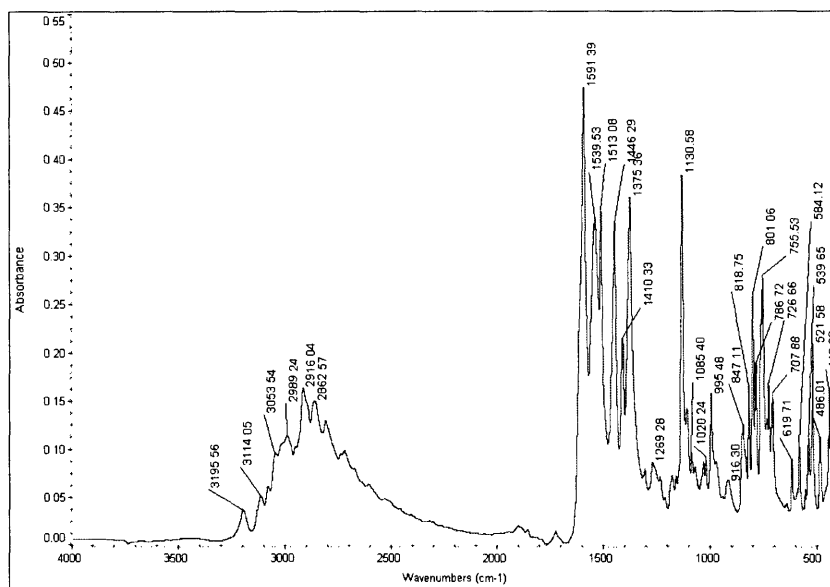
Figure 5.6. FT-IR spectrum of a KBr pellet of $[Fe(O_2CAr^{Tol})_2(2\text{-HSpy})_2]$ **(4a)**.
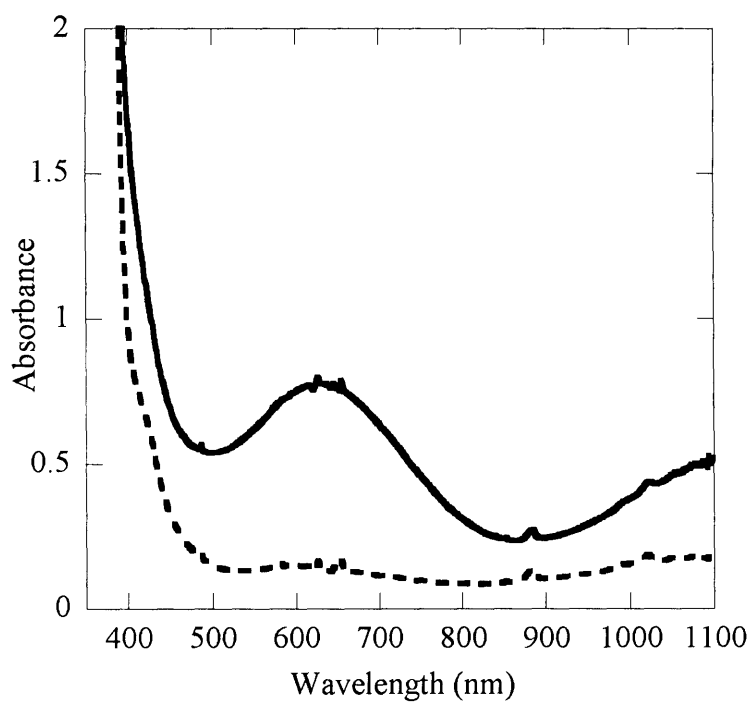
Figure 5.7. UV-vis spectra of [Fe(O$_2$CAr^{Tol})$_2$(2-HSpy)$_2$] **(1a)** (---) and the intermediate **1b** (—) in CH$_2$Cl$_2$ at –10 °C.
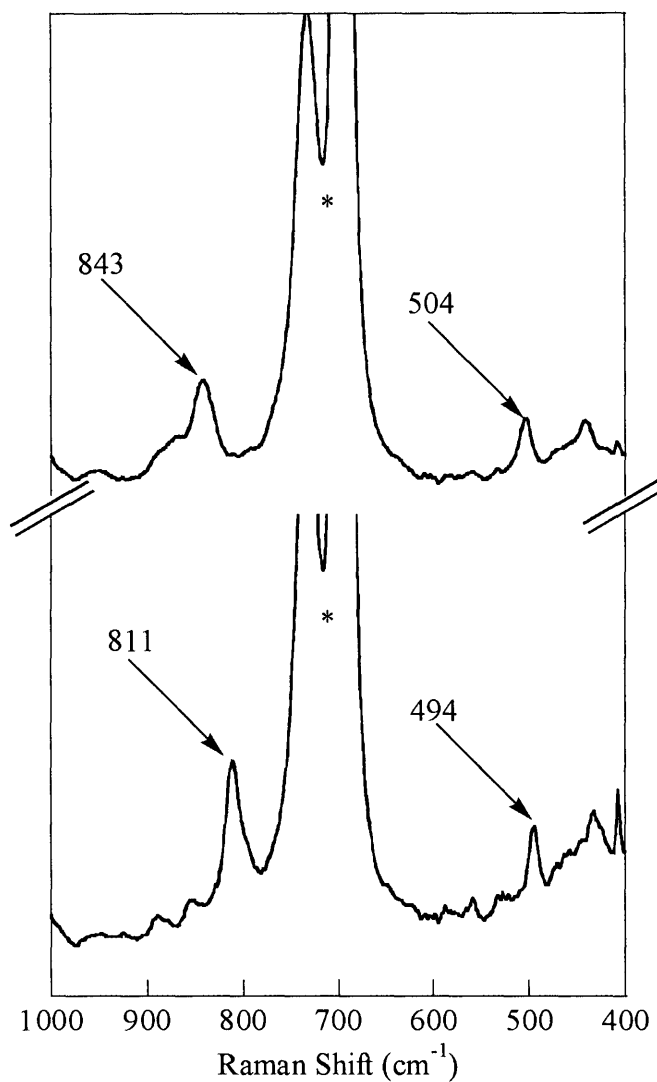
Figure 5.8. Resonance Raman spectra of a CH_2Cl_2 solution of **4b** derived from the oxygenation $[Fe(O_2CAr^{Tol})_2(2\text{-Hspy})_2]$ **(4a)** with $^{16}O_2$ (top spectrum) and $^{18}O_2$ (bottom spectrum). The asterisk indicates a solvent band.

Chapter 6

Effect of Substrate Position in Diphenylphosphinopyridine Ligands on Geometry and

Reactivity of Diiron(II) Carboxylate-Bridged Compounds

Introduction

Soluble methane monooxygenase (MMO) is an enzyme found in methanotropic bacteria that catalyzes the selective conversion of methane to methanol and can oxidize other substrates including methane derivatives, olefins, amines and sulfides.[1,2] The active site housed in the hydroxylase subunit (MMOH) is a non-heme diiron center surrounded by four carboxylate and two histidine residues[3,4] and is responsible for the binding and reductive activation of dioxygen in the enzymes.[5-9] In the reduced state (MMOH$_{red}$), the diiron(II) centers are bridged by two carboxylates and each contains two additional monodentate carboxylate ligands. One of the latter is involved in hydrogen bonding with a coordinated water molecule. In the oxidized, resting state of the enzyme (MMOH$_{ox}$), the diiron(III) center is bridged by two hydroxide ions and a single carboxylate group. The other three carboxylate residues are monodentate, one hydrogen bonded to a coordinated water molecule. Representations of MMOH$_{red}$ and MMOH$_{ox}$ are proffered in Chart 6.1.

The preparation and study of structural, spectroscopic, and functional models for the active sites in metalloproteins have provided insight into the mechanisms of their oxidation chemistry, enhancing and extending our understanding of the natural systems.[10] A variety of symmetric diiron complexes carrying N-donor and assorted O-donor have been reported as mimics for the diiron sites in the enzymes.[11-13] Complexes having two carboxylate ligands per iron atom are necessary to provide an accurate representation of the MMOH active site. Self-assembly of discrete dinuclear centers with such carboxylate ligands is challenged by their tendency to form oligomers.[14-19] In order to replicate more closely the coordination environment of the protein active site in small molecule compounds, a successful approach has been to apply

terphenyl-based carboxylates as ligands to assemble the desired dinuclear complexes and to mimic the protective pocket present at the protein active sites (Chart 6.2).[20-23]

Previous research focused on the design and synthesis of model complexes that activate dioxygen for the oxidation of external substrates.[5,13] In the diiron(II) complexes [Fe$_2$(μ-O$_2$CAr^{Tol})$_2$(O$_2$CAr^{Tol})$_2$(N,N-Bn$_2$en)$_2$],[24,25] where $^-$O$_2$CAr^{Tol} is 2,6-di(p-tolyl)benzoate and N,N-Bn$_2$en is N,N-dibenzylethylenediamine, [Fe$_2$(μ-O$_2$CAr^{Tol})$_4$(BA$^{p\text{-}OMe}$)$_2$],[26] where BA$^{p\text{-}OMe}$ is p-methoxybenzylamine, and [Fe$_2$(μ-O$_2$CAr^{Tol})$_4$(NH$_2$(CH$_2$)$_2$SBn)$_2$],[27] the potential substrate is incorporated as part of a terminal N-donor ligand. Upon reaction with dioxygen, intramolecular benzylic oxidation results in N-dealkylation to afford benzaldehyde.

This strategy has been extended to include tethered substrates disclosed in the form of benzyl-, ethyl-, or sulfido-derivatized pyridine ligands.[28-30] The substrates are brought into close proximity to the carboxylate-bridged diiron(II) center through coordination of the N-donor ligand. To expand further the range of substrates, diiron(II) compounds containing phosphino-derivatized pyridine ligands have been explored, as disclosed in this chapter. This work demonstrates that the position of substitution affects both the solid state geometry of the starting diiron(II) complex and the subsequent chemistry following exposure to dioxygen, and that the nature of the substrate affects the extent of oxidation. Also the effect of different carboxylates is manifest in the results of the oxygenation reactions, as measured by the final product isolated and structurally characterized in two cases. A portion of this work has been previously communicated.[28]

Experimental Section

General Considerations. All reagents were obtained from commercial suppliers and used as received unless otherwise noted. Diethyl ether (Et$_2$O), dichloromethane, acetonitrile,

toluene, and pentane were saturated with nitrogen and purified by passing through activated Al_2O_3 columns under argon.[31] Dioxygen (99.994%, BOC Gases) was dried by passing the gas stream through a column of Drierite. The synthesis and characterization of the compound $[Fe_2(\mu-O_2CAr^{Tol})_2(O_2CAr^{Tol})_2(THF)_2]$ was reported previously.[23] The ligand 3-Ph_2Ppy was synthesized according to a literature procedure,[32] and 4-Ph_2Ppy was prepared in a similar manner. 2-Pyridyldiphenylphosphine oxide (2-$Ph_2P(O)py$) was synthesized according to a published procedure,[33] and 3-$Ph_2P(O)py$ and 4-$Ph_2P(O)py$ were prepared analogously; the purity was ascertained by ^1H and ^{31}P NMR spectroscopy. Air-sensitive manipulations were carried out under nitrogen in an Mbraun dry box. All samples were pulverized and thoroughly dried to remove solvent prior to determining their elemental composition. Solvent molecules included in the elemental composition of **1** and **2** were detected in the ^1H NMR spectra of these compounds.

$[Fe_2(\mu-O_2CAr^{Tol})_3(O_2CAr^{Tol})(2-Ph_2Ppy)]$ (1). A CH_2Cl_2 (1 mL) solution of 2-Ph_2Ppy (43.6 mg, 0.166 mmol) was added dropwise into a CH_2Cl_2 (3 mL) solution of $[Fe_2(\mu-O_2CAr^{Tol})_2(O_2CAr^{Tol})_2(THF)_2]$ (218 mg, 0.149 mmol), which was stirred for 20 min. Vapor diffusion of diethyl ether into the orange-yellow solution generated orange crystals (210 mg, 89%) of **1** suitable for X-ray crystallography. FT-IR (KBr, cm^{-1}): 3044 (w), 3015 (w), 2918 (w), 2859 (w), 1598 (s), 1538, 1513 (s), 1452 (s), 1406 (s), 1379 (s), 1304 (w), 1182 (w), 1148 (w), 1110 (w), 1072 (w), 1018 (w), 973 (w), 910 (w), 860 (w), 842 (m), 819 (m), 796 (s), 767 (s), 752 (m), 736 (m), 714 (m), 698 (m), 641 (w), 609 (m), 583 (w), 557 (w), 530 (w), 509(w), 493 (w), 463 (w). Anal. Calcd. for $C_{101}H_{82}NFe_2O_8P \cdot 0.25CH_2Cl_2$: C, 75.93; H, 5.19; N, 0.87. Found: C, 76.07; H, 5.39; N, 0.83.

$[Fe_2(\mu-O_2CAr^{Tol})_2(O_2CAr^{Tol})_2(3-Ph_2Ppy)_2]$ (2). Ligand substitution of 3-Ph_2Ppy (71.9 mg, 0.273 mmol) for THF in $[Fe_2(\mu-O_2CAr^{Tol})_2(O_2CAr^{Tol})_2(THF)_2]$ (168 mg, 0.115 mmol)

afforded compound **2** in 87% yield. Canary yellow crystals of **2** suitable for X-ray diffraction studies were obtained from vapor diffusion of Et$_2$O into a chlorobenzene (1 mL) solution of **2**. FT-IR (KBr, cm^{-1}): 3026 (w), 2915 (w), 1601 (s), 1570 (s), 1515 (s), 1454 (s), 1407 (s), 1374 (s), 1326 (w), 1307 (w), 1193 (w), 1110 (w), 1045 (w), 853 (w), 818 (m), 798, 781 (m), 751 (s), 699 (s), 647 (w), 583 (w), 543 (m), 513 (m), 497 (w), 424 (w). Anal. Calcd. for C$_{118}$H$_{96}$N$_2$Fe$_2$O$_8$P$_2$·0.25CH$_2$Cl$_2$: C, 76.16; H, 5.22; N, 1.50; P, 3.32. Found: C, 76.19; H, 5.21; N, 1.37; P, 3.48.

[Fe$_2$(μ-O$_2$CAr^{Tol})$_4$(4-Ph$_2$Ppy)$_2$] (3). X-ray quality crystals of **3** were isolated in 85% yield by ligand substitution of 4-Ph$_2$Ppy (42.3 mg, 0.161 mmol) for THF in [Fe$_2$(μ-O$_2$CAr^{Tol})$_2$(O$_2$CAr^{Tol})$_2$(THF)$_2$] (112 mg, 0.0767 mmol) in a CH$_2$Cl$_2$ (5 mL) solution. FT-IR (KBr, cm^{-1}): 3047 (w), 3018 (w), 2916 (w), 1614 (s), 1595 (s), 1584 (m), 1551 (m), 1512 (s), 1479 (w), 1434 (s), 1402 (w), 1383 (s), 1303 (w), 1223 (w), 1179 (w), 1150 (w), 1105 (w), 1091 (w), 1067 (w), 1019 (m), 999 (w), 842 (m), 811 (s), 740 (m), 695 (s), 582 (m), 526(s), 495 (m), 453 (w). Anal. Calcd. for C$_{118}$H$_{96}$N$_2$Fe$_2$O$_8$P$_2$: C, 76.87; H, 5.25; N, 1.52. Found: C, 76.95; H, 5.30; N, 1.55.

[Fe$_2$(μ-O$_2$CAr^{4-FPh})$_3$(O$_2$CAr^{4-FPh})(2-Ph$_2$Ppy)] (4). To a CH$_2$Cl$_2$ (4 mL) solution of [Fe$_2$(μ-O$_2$CAr^{4-FPh})$_2$(O$_2$CAr^{4-FPh})$_2$(THF)$_2$] (150 mg, 0.100 mmol), 2-Ph$_2$Ppy (28.5 mg, 0.108 mmol) was added to form an orange solution that was stirred for 20 min. Diffusion of pentane into the reaction mixture yielded orange block crystals (151 mg, 93%) of **4**. FT-IR (KBr, cm^{-1}): 3062 (w), 2954 (w), 2863 (w), 1891 (w), 1604 (s), 1560 (m), 1510 (s), 1455 (s), 1406 (s), 1380 (s), 1299 (w), 1221 (s), 1158 (s), 1093 (m), 1049 (w), 1015 (m), 841 (m), 833 (m), 806 (s), 791 (m), 767 (m), 747 (w), 701 (m), 582 (w), 554 (s), 528 (s), 502 (w), 463 (w), 417 (w). Anal.

Calcd. for $C_{93}H_{58}NFe_2O_8F_8P$: C, 69.29; H, 3.63; N, 0.87; P, 1.92. Found: C, 68.92; H, 3.70; N, 1.11; P, 1.68.

[Fe$_6$(μ_4-O)$_2$(μ-OH)$_6$(μ-O$_2$CAr^{Tol})$_4$Cl$_4$(2-Ph$_2$P(O)py)$_2$] (5). An orange 6.0 mM CH$_2$Cl$_2$ solution of **1** (95.3 mg, 0.0603 mmol) was bubbled with O$_2$ for 10 min and stirred for 50 additional min under an atmosphere of dioxygen. The solvent was reduced in vacuo and the remaining residue was extracted into 1.5 mL of CH$_2$Cl$_2$. Vapor diffusion of pentane into the solution yielded orange crystalline clusters of **5**, one of which was used for X-ray diffraction studies. Although the structure of **5** could be determined, bulk samples could not be obtained.

[Fe$_2$(μ-OH)$_2$(μ-O$_2$CAr$^{4\text{-}FPh}$)(O$_2$CAr$^{4\text{-}FPh}$)$_3$(OH$_2$)(2-Ph$_2$P(O)py)] (6). A bright yellow 5.80 mM toluene solution of **4** (mg, mmol) was bubbled with dry dioxygen for 10 min and allowed to stir for 50 additional min under an atmosphere of O$_2$. The solvent was then removed under vacuum leaving a residue that was extracted into 1.5 mL of CH$_2$Cl$_2$. Bright yellow block crystals of **6** (49.3 mg, 25%) suitable for X-ray diffraction studies were isolated by diffusing pentane into the solution. FT-IR (KBr, cm^{-1}): 3572 (m), 3432 (br), 3057 (w), 1735 (w), 1604 (s), 1511 (s), 1455(s), 1407 (m), 1345 (s), 1222 (s), 1159 (s), 1136 (m), 1095 (w), 1009 (w), 839 (s), 808 (s), 791 (s), 771 (m), 736 (w), 698 (s), 555 (s), 536 (s), 460 (w), 414 (w). Anal. Calcd. for $C_{93}H_{62}NFe_2O_{12}F_8P$: C, 66.48; H, 3.72; N, 0.83; P, 1.84. Found: C, 66.23; H, 3.69; N, 0.76; P, 1.58.

X-ray Crystallography Studies. Intensity data were collected on a Bruker (formerly Siemens) APEX CCD diffractometer with graphite-monochromated Mo Kα radiation (λ = 0.71073 Å), controlled by a Pentium-based PC running the SMART software package.[34] Single crystals were mounted on the tips of glass fibers, coated with paratone-N oil, and cooled to –100 °C under a stream of N$_2$ maintained by a KRYO-FLEX low-temperature apparatus. Data

collection and reduction protocols are described elsewhere.[35] The structures were solved by direct methods and refined on F^2 by using the SHELXTL-97 software[36] incorporated in the SHELXTL software package.[37] Empirical absorption corrections were applied by using the SADABS program,[38] and the structures were checked for higher symmetry by using the PLATON software.[39] All non-hydrogen atoms were located and their positions refined with anisotropic thermal parameters by least-squares cycles and Fourier syntheses. Hydrogen atoms were mostly assigned to idealized positions and given thermal parameters equivalent to either 1.5 (methyl hydrogen atoms) or 1.2 (all other hydrogen atoms) times the thermal parameter of the carbon atom to which they were attached. Hydrogen atoms of the bridging hydroxides and water molecule for **6** were located on difference electron density maps. A terminal carbon atom of one of the lattice solvent Et_2O molecules in the structure of **2** is located on a center of symmetry, and the rest of the molecule is disordered over two positions. The CH_2Cl_2 molecule in the structure of **3** is located on a special position of twofold symmetry and has disordered chlorine atoms, each of which was modeled and refined with 50% occupancy factors. The structure of **4** has one dichloroethane molecule in the lattice in which one of the chlorine atoms is disordered over two positions and was refined with a 70/30 occupancy. Four carbon atoms in one of the *p*-fluorophenyl rings were disordered over two positions and were refined at 50% occupancy. The structure of **5** has four CH_2Cl_2 molecules in the lattice. The structure of **6** has three CH_2Cl_2 molecules in the lattice. Data collection and experimental details are summarized in Table 6.1. Selected bond lengths and angles for **1 – 6** are provided in Tables 6.2, 6.3, 6.6, and 6.7.

Physical Measurements. FT-IR spectra were recorded on a Thermo Nicolet Avatar 360 spectrometer with OMNIC software. ^{31}P NMR spectra were recorded on a Varian 500 spectrometer housed in the Massachusetts Institute of Technology Department of Chemistry

Instrument Facility (MIT DCIF). Chemical shifts were referenced to an external standard, H_3PO_4. All spectra were obtained at ambient probe temperature, 293 K.

^{57}Fe Mössbauer Spectroscopy. Mössbauer spectra were recorded on an MSI spectrometer (WEB Research Co.) with a ^{57}Co source in a Rh matrix maintained at room temperature in the MIT DCIF. Solid samples of 4 and 6 were prepared by suspending ~0.024 mmol of the yellow powdered material in Apeizon N grease and coating the mixture on the lid of a nylon sample holder. Data were collected at 4.2 K, and the isomer shift (δ) values are reported with respect to natural iron foil that was used for velocity calibration at room temperature. The spectra were fit to Lorentzian lines by using the WMOSS plot and fit program.[40]

Oxidation Product Analyses. Oxidation reactions were performed by exposing a CH_2Cl_2 solution of the diiron(II) complex to dioxygen over a period of time, and in the case of 1 and 2, also in the presence of additional 2-Ph$_2$Ppy. To isolate the N-donor species for analysis, Chelex was added to the reaction solutions to remove the iron. The resulting slurry was stirred for 2 h, after which the Chelex was removed by filtration. The resin was washed with CH_2Cl_2 twice more prior to combining the filtrates. The solvent was removed in vacuo to afford the N-donor species for analysis. The products were identified by NMR spectroscopy, comparing their spectra to those of authentic samples. The amount of oxidized ligand obtained was quantified by ^{31}P NMR spectroscopy using triphenylphosphine oxide as an internal standard. All samples were prepared in an anaerobic glove box prior to the introduction of dried dioxygen by bubbling. Control experiments established that, in the absence of the diiron(II) complexes, neither dioxygen-saturated CH_2Cl_2 nor the workup process induces significant ligand oxidation.

Results

Synthesis and Structural Characterization of Diiron(II) Complexes

[Fe$_2$(μ-O$_2$CAr^{Tol})$_3$(O$_2$CAr^{Tol})(2-Ph$_2$Ppy)] (1), [Fe$_2$(μ-O$_2$CAr^{Tol})$_2$(O$_2$CAr^{Tol})$_2$(3-Ph$_2$Ppy)$_2$] (2),

[Fe$_2$(μ-O$_2$CAr^{Tol})$_4$(4-Ph$_2$Ppy)$_2$] (3), and [Fe$_2$(μ-O$_2$CAr^{4-FPh})$_3$(O$_2$CAr^{4-FPh})(2-Ph$_2$Ppy)] (4). The

triply-bridged diiron(II) complex **1** is generated by treating [Fe$_2$(μ-O$_2$CAr^{Tol})$_2$-

(O$_2$CAr^{Tol})$_2$(THF)$_2$] with 1 equiv of 2-Ph$_2$Ppy (Scheme 6.1). The isolated complex features both

5- and 4-coordinate iron(II) centers within the dimetallic unit. The fourth carboxylate is ligated

in a bidentate fashion to the 5-coordinate iron atom, the coordination sphere of which is

completed by the pyridine ligand. Failure to prepare a diiron core containing two N-donor

ligands occurred even when the THF precursor complex was treated with 8 equiv of 2-Ph$_2$Ppy.

The doubly- and quadruply-carboxylate-bridged compounds [Fe$_2$(μ-O$_2$CAr^{Tol})$_2$(O$_2$CAr^{Tol})$_2$-

(3-Ph$_2$Ppy)$_2$] (**2**) and [Fe$_2$(μ-O$_2$CAr^{Tol})$_4$(4-Ph$_2$Ppy)$_2$] (**3**) are prepared by combining 2 equiv of

3-Ph$_2$Ppy or 4-Ph$_2$Ppy with [Fe$_2$(μ-O$_2$CAr^{Tol})$_2$(O$_2$CAr^{Tol})$_2$(THF)$_2$] (Scheme 6.1). The structures

of **1 – 3** are displayed in Figures 6.1, 6.2, and 6.3 and selected bond lengths and angles are listed

in Tables 6.2 and 6.3. Structural characterization of **1, 2,** and **3** by X-ray crystallography revealed

an Fe⋯Fe distance of 3.3099(6) Å for **1**, which lies between the values of 4.0372(15) Å and

2.8127(10) Å observed for **2** and **3**, respectively. The windmill complex **2** has the largest

separation between the iron atoms. The iron centers, related by a crystallographic inversion

center, are four-coordinate, each bound by three carboxylate ligands, two bridging and one

monodentate, and one N-donor ligand. The pyridine ligands are situated anti to one another

across the Fe–Fe vector. In the paddlewheel configuration of **3**, four oxygen atoms from the

bridging carboxylates form the base of a square pyramid with a 4-Ph$_2$Ppy capping the

coordination sphere of each iron center. The distance of the phosphorus atom from the closest

iron atom increases in the order of substitution, ortho < meta < para, the corresponding values

being 2.8321(7) Å in **1**, 5.811(3) Å in **2** and 6.7205(15) Å in **3**.

Compound **4** is synthesized by displacement of THF from [Fe$_2$(μ-O$_2$CAr$^{4\text{-FPh}}$)$_2$-

(O$_2$CAr$^{4\text{-FPh}}$)$_2$(THF)$_2$] with 2-Ph$_2$Ppy, Scheme 6.2. The solid state structure of **4** determined by

X-ray diffraction reveals a triply-bridged diiron(II) center with an Fe⋯Fe distance of 3.4517(9)

Å. Figure 6.4 shows the structure, and Table 6.2 lists selected bond lengths and angles. A fourth

chelating carboxylate is bound to one of iron atoms to complete its coordination sphere. On the

other metal center the 2-Ph$_2$Ppy coordinates through the pyridine nitrogen atom, and the Fe⋯P

distance is 2.958(2) Å. The structural parameters are nearly identical to those already reported

for **1**. The IR spectra of **4**, displayed in Figure 6.5, exhibits features associated with aromatic and

carboxylate groups. In addition the C–F stretches originating from the ⁻O$_2$CAr$^{4\text{-FPh}}$ ligands are

visible at 1221 cm^{-1}.[41]

Mössbauer Spectroscopic Properties of 4. The Mössbauer spectrum, measured at 4.2

K, of a solid sample of **4** is pictured in Figure 6.6. Although the two iron(II) sites differ in

coordination environment, there is no evidence for two overlapping signals. The single sharp

quadrupole doublet (Γ = 0.37 – 0.39 mm s^{-1}) reveals that the iron centers are indistinguishable by

Mössbauer spectroscopy. The quadrupole splitting (ΔE_Q = 2.66(2) mm s^{-1}) and isomer shift (δ =

1.22(2) mm s^{-1}) parameters are consistent with those of high-spin iron(II) complexes having

oxygen-rich coordination environments, indicating that **3** has a high spin S = 2 ground state.[42,43]

Ligand Oxidation Upon Reaction of 1 – 4 with Dioxygen. Oxidation of the substrates

appended to the N-donor ligand was investigated by product analysis following introduction of

dioxygen into solutions of **1 – 4**. A pale yellow CH$_2$Cl$_2$ solution of **1** reacts with dioxygen and

immediately turns golden orange. Quantitative formation of 2-Ph$_2$P(O)py occurs within 30 min

after exposure of **1** to dioxygen, and the reaction is 95% complete in 25 min. A 10-fold dilution of the metal complex concentration results in 100% conversion occurring in 5 min and 88% in 2.5 min. Control experiments established that, in the absence of **1**, neither O_2-saturated CH_2Cl_2 nor the workup process induced ligand oxidation over the same time interval (~ 1 h). ^{31}P NMR spectroscopy with Ph_3PO as an internal standard was used to analyze the products of the reaction and monitor the recovery of all species. A summary of the reaction conditions used and the products recovered is provided in Table 6.4.

Catalytic formation of 2-$Ph_2P(O)$py ensues when a CH_2Cl_2 solution of **1** is supplied with additional equivalents of 2-Ph_2Ppy (Table 6.5). Results from several experiments show that 4 equiv are converted in an hour and slightly more than 13 equiv over a period of 12 h at a metal complex concentration of 1.5 mM. A 5-fold dilution of the concentration of **1** leads to 17 equiv being oxidized in 17 h. When a non-coordinating phosphine, such as triphenylphosphine, is added to the reaction mixture, the extent of oxidation is >20-fold less than that from the coordinating phosphine ligand under the same conditions. Catalytic oxidation is not observed to the same degree in MeCN or C_6H_6. In both cases 2 equiv of 2-Ph_2Ppy are converted to the phosphine oxide overnight.

Shifting the substitution position of the diphenylphosphino moiety on the pyridine ligand affects the oxygenation efficiency of the resultant diiron(II) complexes. After exposure of a CH_2Cl_2 solution of **2** to dioxygen at room temperature, ^{31}P NMR spectroscopy reveals the formation of 3-$Ph_2P(O)$py in an average yield of 70% based on **2**. The reaction of **3** with dioxygen yields even less oxidized ligand, with only 50% 4-$Ph_2P(O)$py isolated. In both cases the unmodified phosphinopyridine ligand was quantitatively recovered. A 10-fold dilution of the diiron(II) starting material did not change the final percentages of phosphine oxide recovered.

Upon exposure of **4** to O_2, 100% of the 2-Ph_2Ppy is converted to 2-$Ph_2P(O)py$ in 30 min with quantitative recovery of the pyridine ligand. When a CH_2Cl_2 solution of **4** is provided with more of the pyridine ligand, catalytic phosphine oxidation similarly transpires. A 14 h reaction results in the conversion of 3 out of almost 9 equiv of 2-Ph_2Ppy to the phosphine oxide. This result is comparable to the 13 out of 50 equiv of 2-Ph_2Ppy oxidized under the same conditions by the corresponding $^-O_2CAr^{Tol}$ complex, **1**.

Isolation and Structural Characterization of Iron(III) Complexes [Fe$_6$(μ_4-O)$_2$-(μ-OH)$_6$(μ-O$_2$CAr^{Tol})$_4$Cl$_4$(2-Ph$_2$P(O)py)$_2$] (5) and [Fe$_2$(μ-OH)$_2$(μ-O$_2$CAr^{4-FPh})(O$_2$CAr^{4-FPh})$_3$-(OH$_2$)(2-Ph$_2$P(O)py)] (6). The hexairon(III) species **5** was isolated as one of the final products from the reaction of **1** with dioxygen (Scheme 6.3). The structure is best described by the diagrams in Figure 6.7, and a list of selected interatomic distances and angles is included in Table 6.6. The structure of **5** consists two (μ_3-oxo)triiron(III) units that are related by an inversion center and linked through two O^{2-}, two OH^-, and two $^-O_2CAr^{Tol}$ bridging groups. Four octahedral and two distorted trigonal bipyramidal iron(III) sites result. A noteworthy feature in the structure of **5** is that two octahedral and two trigonal bipyramidal iron centers are coordinated by chloride ions. Their origin is thought to be a result of solvent oxidation because no comparable material could be obtained when toluene was used as a solvent for this reaction. The two outside iron centers are bound to 2-$Ph_2P(O)py$, the oxidized N-donor ligand, through the oxygen atom of the phosphine oxide.

Pentane diffusion into the yellow-orange CH_2Cl_2 or toluene solution generated upon oxygenation of **4** afforded [Fe$_2$(μ-OH)$_2$(μ-O$_2$CAr^{4-FPh})(O$_2$CAr^{4-FPh})$_3$(OH$_2$)(2-Ph$_2$P(O)py)] (6) (Scheme 6.4) in 25% yield. The structure of **6** is depicted in Figure 6.8, and selected interatomic distances and angles are listed in Table 6.7. Two distorted octahedral iron(III) atoms are bridged

by two hydroxides and one carboxylate ligand. The largest deviations from ideal $90°$ interbond angles are $11.60(2)°$ and $12.15(2)°$ for Fe1 and Fe2, respectively, and occur at the O–Fe–O angle of the bent four-membered $Fe_2(\mu\text{-OH})_2$ ring. The Fe1–O2–Fe2 unit has Fe1–O2 and Fe2–O2 distances of $1.954(4)$ and $1.981(4)$ Å, respectively, and a $98.10(19)°$ bridging angle. The Fe–O bond lengths in the Fe1–O3–Fe2 unit are slightly longer at $1.981(4)$ and $1.977(4)$ Å for Fe1–O3 and Fe2–O3, respectively, but the bridging angle is smaller, $97.35(18)°$. The longest Fe–O distances are those to the oxygen atoms of the bridging carboxylate ligand, $2.003(3)$ and $2.017(3)$ Å. The Fe···Fe separation of $2.972(1)$ Å is similar to those reported for the $\{Fe_2(\mu\text{-OH})_2\text{-}(\mu\text{-O}_2CR)\}^{3+}$ core in the resting state of $MMOH_{ox}$[3,44] and two other synthetic analogues.[23,24,45]

In addition to the bridging ligands, one iron atom (Fe1) is coordinated by a monodentate carboxylate oxygen. The other two coordination sites are occupied by O- and N-atoms from the oxidized N-donor ligand, $2\text{-Ph}_2P(O)py$, generating a five-membered Fe1-N1-C1-P1-O1 ring. The other iron center (Fe2) has two monodentate carboxylate ligands and a coordinated water molecule to complete its coordination sphere. Notwithstanding the bridging hydroxide groups, the three monodentate carboxylate ligands provide the shortest Fe–O distances, $1.947(3)$, $1.974(3)$, and $1.976(3)$ Å. The Fe–O bond to the terminally bound water molecule is longer than to the O-atom of $2\text{-Ph}_2P(O)py$, $2.099(4)$ vs $2.023(3)$ Å. The Fe–N distance of $2.210(4)$ Å is ~0.1 Å longer than that in the diferrous starting material, **4**.

The three terminal carboxylate ligands are involved in hydrogen bonding interactions with the bridging hydroxides, O2···O10, $2.712(5)$ Å and O3···O8, $2.801(6)$ Å, and the coordinated water molecule, O4···O12, $2.537(5)$ Å. The IR spectrum of **6**, depicted in Figure 6.5, shows the hydrogen-bonded and non-hydrogen-bonded hydroxide stretches as a broad band centered around 3400 cm^{-1} and a sharper peak at 3572 cm^{-1}, respectively.[41]

Mössbauer Spectroscopic Properties of 6. The Mössbauer spectrum, recorded 4.2 K, of a solid sample of **6** is presented in Figure 6.6. A single sharp quadrupole doublet is observed (δ = 0.50(2) mm s^{-1}, ΔE_Q = 0.83(2) mm s^{-1}). The isomer shift (δ) falls in the range typical of the high-spin Fe(III) complexes.[46,47] Although the two iron(III) sites differ, having O_6 and NO_5 donor-atom sets, there is no evidence for two overlapping doublets. The line widths (Γ = 0.31 – 0.32 mm s^{-1}) are close to natural line widths indicating that the two ferric atoms are indistinguishable by Mössbauer spectroscopy.

Bond Valence Sum Analysis of 5 and 6. The bond valence sum (BVS) is an empirical quantity that has been used to determine the oxidation state of metal ions in coordination complexes based on crystallographically determined metal-ligand bond distances.[48] Bond valences, s_{ij} between cation i and anion j, are calculated according to eq 1, where r is the observed bond distance and r_0 and B are empirically determined parameters. The summation of the bond valences for a particular metal cation yields the oxidation state, V_i. Bond valence sum analysis of both **5** and **6** supports the assignment of the six metal centers in **5** and the two in **6** as iron(III). The calculation of the individual bond valences as well as their summation is available in Table 6.8.

$$V_i = \sum_j s_{ij} = \sum_j \exp\left(\frac{(r_o - r)}{B}\right) \tag{1}$$

Discussion

Small molecule model compounds are synthesized to study their properties and reactivity in order to expand our understanding of the biological systems. The oxidation of triphenylphosphine is thermodynamically more facile, $\Delta H°$ being –67 kcal/mol vs –27 kcal/mol for dimethyl sulfide,.[49] Since oxidation of sulfido moieties has already been observed in

carboxylate-rich diiron(II) complexes,[30] the phosphine substrate was employed. Although not a known substrate of the native enzyme, this potentially more reactive species was provided as a 2-diphenylphosphinopyridine ancillary ligand in the carboxylate-rich diiron(II) centers to gain further insight into the chemistry. The relationship between the distance of the substrate with respect to the active site and the reactivity of the complex was investigated by using *o*-, *m*-, and *p*-diphenylphosphinopyridine as the ancillary nitrogen ligands in terphenyl-based carboxylate diiron complexes.

Despite the similar composition of **1** – **3**, the three different structures are obtained. The steric bulk provided by the diphenylphosphino moiety at the ortho position of the pyridine ring was responsible for only one 2-Ph$_2$Ppy being accommodated at the diiron core in **1**. The meta substitution of the diphenylphosphino group allows for the ligation of two 3-Ph$_2$Ppy around the metal centers while still maintaining a doubly carboxylate-bridged metal center in **2**. When the steric bulk of the diphenylphosphino moiety is positioned on the para position of the pyridine ring, four carboxylates are contained around the metal centers leading to the paddlewheel isomer in **3**. The Fe–O bonds in **1** of the three bridging carboxylate ligands are on average 0.05 Å shorter for the iron atom to which the pyridine moiety is coordinated, 2.0191(12) vs 2.0485(13) Å. The terminal bidentate carboxylate Fe–O bond lengths are the longest and asymmetric being 2.2162(13) and 2.0826(13) Å. This result reflects the greater electron releasing character of a pyridine N-donor than a bidentate carboxylate, since the lower coordinate iron atom would be expected to have the shorter bond lengths, all other things being equal. Three Fe–O bond distances of **2** with an average of 1.9818(19) Å are shorter than those in **1** or **3**. The other Fe–O interaction, the non-bonding O-atom of the monodentate carboxylate ligand, is 2.417(2) Å from the metal center. The tetrabridged center of **3** results in two shorter Fe–O bonds and two ~0.1 Å

longer, the averages being 2.016(2) and 2.127(2) Å. The Fe–N distance in **3** is shorter than in **1** and **2**, 2.094(3) vs 2.1314(16) and 2.135(2) Å, respectively.

The iron atoms of **4** have an identical coordination environment to those of **1**. The different carboxylate substitution does not alter the geometry of the resultant diiron(II) complex, **4**. Overall the most ligands surrounding the iron atoms have slightly shorter bond lengths in **4** compared to **1**, but the metal-metal separation is 0.15 Å further in **4** than **1**. As was observed for **1**, the Fe–O bonds in **4** of the three bridging carboxylate ligands are shorter for the iron atom to which the pyridine moiety is coordinated, 2.002(3) vs 2.024(3) Å. The terminal bidentate carboxylate Fe–O bond lengths are the longest, 2.297(3) and 2.068(3) Å.

A single sharp quadrupole doublet occurs in the Mössbauer spectrum of **4**, the quadrupole splitting (ΔE_Q = 2.66(2) mm s^{-1}) and isomer shift (δ = 1.22(2) mm s^{-1}) values of which are consistent with those of high spin diiron(II) complexes in oxygen-rich coordination environments.[43] The isomer shift is among the lowest reported for five coordinate, and slightly higher than those observed for four-coordinate, iron(II) sites (1.0 – 1.1 mm s^{-1}).[50] The quadrupole splitting and isomer shift parameters obtained for **4** are slightly lower than those of MMOH$_{red}$, 3.01 and 1.3 mm s^{-1}, respectively.[51] This disparity is ascribed to fewer nitrogen ligands for **4** compared to the MMOH$_{red}$ active site.

There are two significant differences among compounds **1 – 3** that may affect their oxygenation chemistry, the position of the substrate on the coordinated pyridine and the geometry of the diiron(II) complex. The pyridine substitution site determines the distance of the substrate from the diiron core; the carboxylate geometry modulates the steric bulk around the iron centers. The triply carboxylate-bridged complex **1** shows full conversion to the phosphine oxide, less oxidation occurs for the windmill complex **2**, and the least obtains for paddlewheel

complex **3**. The quantity of ligand oxidized for **1**, **2**, and **3** also decreases as the $-PPh_2$ moiety moves from ortho to meta to para.

The catalytic ligand oxidation exhibited by **1** is difficult to rationalize. Previously we reported the catalytic oxidation of PPh_3 in the presence of dioxygen by the diiron(II) complex $[Fe_2(\mu\text{-}O_2CAr^{Tol})_2(Me_3TACN)_2(MeCN)](OTf)_2$, where $Me_3TACN = 1,4,7\text{-trimethyl-}1,4,7\text{-triaza-}$ cyclononane.[52] Further studies revealed that the corresponding diiron(III) complex, $[Fe_2(\mu\text{-}O)\text{-}(\mu\text{-}O_2CAr^{Tol})_2(Me_3TACN)_2](OTf)_2$, the only detectable iron-containing species during the reaction, could itself promote the catalysis.[53] Furthermore, it was determined that the phosphine oxidation is coupled to catalytic oxidation of THF solvent, affording a C–C bond cleavage product, which occurs until the phosphine is consumed. For **1**, however, substituting the added 2-Ph_2Ppy with PPh_3 dramatically decreases the reactivity, >20-fold, strongly indicating that the metal center not only the initiates the catalysis but that substrate binding and intramolecular oxygenation most likely occur. The reactivity of $[Fe_2(\mu\text{-}O_2CAr^{Tol})_3(O_2CAr^{Tol})(2\text{-}Ph_2Ppy)_2]$ also differs from the previous catalytic system because the catalytic reaction also occurs in MeCN and C_6H_6 albeit with lower conversion which we attribute to the limited solubility of the starting diiron(II) complex.

A small difference in the remote carboxylate substituents, $^-O_2CAr^{Tol}$ (**1**) vs $^-O_2CAr^{4\text{-}FPh}$ (**4**), leads to pronounced differences in dioxygen reactivity. Previous work revealed that carboxylate ligands with *p*-tolyl substituents form more reactive diiron(II) centers than the *p*-fluorophenyl analogs for both 2-benzyl- and 2-ethylpyridine derivatives.[29] This situation also obtains for the present 2-diphenylphosphinopyridine complexes, because **1** catalytically oxidizes five times the amount of phosphine as **4**. The steric properties of these two terphenyl carboxylate groups are similar, so the decrease in catalytic activity between the $^-O_2CAr^{Tol}$ and $^-O_2CAr^{4\text{-}FPh}$

systems is attributed to electronic factors. The pK_a values of HO_2CAr^{4-FPh} and HO_2CAr^{Tol} are

6.14 and 6.50, respectively,[54] but there are four such ligands, which may be sufficient to alter the

properties of the O_2-generated, catalytically active species and decrease the turnover number.

The effect of different carboxylates is also manifest in the results of oxygenation

reactions of **1** and **4**, as measured by the final product isolated. Whereas oxidation of **4** leads to

the formation of a discrete dinuclear $\{Fe_2(\mu\text{-}OH)_2(\mu\text{-}O_2CR)\}^{3+}$ core, a hexanuclear complex, **5**, is

recovered from the reaction of **1** with O_2. Most notably, the structure of **5** contains coordinated

chloride ions. Decomposition of the solvent, CH_2Cl_2, could generate Cl^-, which may promote the

formation of the hexanuclear compound **5**. An analogous hexanuclear complex with coordinated

chloride ligands is isolated following oxygenation of $[Fe_2(\mu\text{-}O_2CAr^{Tol})_4(4\text{-}CNpy)_2]$, where 4-

CNpy is 4-cyanopyridine.[50] Oxidation of CH_2Cl_2 does occur in MMOH,[1] the product formed

being unstable and decomposing to formaldehyde and HCl, so the present results may relate to

the enzyme system. Solvent oxidation by **1** would provide the chloride ions observed in the final

species isolated, **5**. Our observations of increased C–H activation with more electron releasing

ligands at the diiron(II) center suggests that the MMOH active site may be similarly activated.

The synthesis of complexes with a $\{Fe_2(\mu\text{-}OH)_2(\mu\text{-}O_2CR)\}^{3+}$ core has been challenging

because of the tendency of iron(III) salts to form oligo- or polynuclear clusters. The first such

compound to be isolated, $[Fe_2(\mu\text{-}OH)_2(\mu\text{-}O_2CAr^{Tol})(O_2CAr^{Tol})_3(N\text{-}Bnen)(N,N\text{-}Bn_2en)]$ (**7**), was

generated by oxygenation of $[Fe_2(\mu\text{-}O_2CAr^{Tol})_2(O_2CAr^{Tol})_2(N,N\text{-}Bn_2en)_2]$.[24,25] This approach

mimics the chemistry occurring at the enzyme active sites. A second route to the $\{Fe_2(\mu\text{-}OH)_2\text{-}$

$(\mu\text{-}O_2CR)\}^{3+}$ core was discovered during oxygenation of mononuclear $[Fe(O_2CAr^{Tol})_2(Hdmpz)_2]$,

where Hdmpz is dimethylpyrazole, which afforded $[Fe_2(\mu\text{-}OH)_2(\mu\text{-}O_2CAr^{Tol})(O_2CAr^{Tol})(OH_2)\text{-}$

$(Hdmpz)_2]$ (**8**).[45] Representations of **7** and **8** are provided in Chart 6.3. In the present work,

exposure of **4** to dioxygen led to **6**, which has the $\{Fe_2(\mu\text{-OH})_2\text{-}(\mu\text{-O}_2CR)\}^{3+}$ core and is only the third structural mimic of the $MMOH_{ox}$ core structure. There was no evidence for solvent oxidation in this reaction. The Fe···Fe and $Fe\text{-}O_{hydroxide}$ distances of 2.972(1) and 1.954(4) – 1.981(4) Å, respectively, in **6** are similar to those in $MMOH_{ox}$, for which the Fe···Fe distance is 2.99 Å and the $Fe\text{-}O_{hydroxide}$ distances are 1.7 – 2.2 Å.[44] In the protein two histidine and three carboxylate terminal ligands, a bridging carboxylate, and solvent-derived molecules complete the NO_5 donor-atom sets at each metal. A slightly different ligand combination is adopted by **6**, which has an NO_5 set for one iron atom and an O_6 set for the other. One of the O-donors is a terminally bound water molecule, exactly like that observed in all structurally characterized forms of MMOH to date.[3,44] Hydrogen bonding interactions between axial carboxylate ligands and bridging hydroxide ligands in **6** also are observed in $MMOH_{ox}$.[3,44]

The single sharp quadrupole doublet exhibited in the Mössbauer spectrum of **6** differs from the results obtained for $MMOH_{ox}$ from both *M. capsulatus* (Bath) and *M. trichosporium* OB3b, both of which have Mössbauer spectra indicating the presence of two slightly inequivalent high-spin iron(III) sites.[55,56] The isomer shift ($\delta = 0.50(2)$ mm s^{-1}) of **6** falls in the range associated with high-spin Fe(III) complexes,[46,47] and is analogous to those reported for $MMOH_{ox}$. As indicated in Table 6.9, the quadrupole splitting parameter ($\Delta E_Q = 0.83(2$ mm s^{-1}) in **6** lies in between that of the structurally related compounds **7** and **8**.[24,45] Their Mössbauer parameters, along with those of **6**, are compared to those of $MMOH_{ox}$ in Table 6.9. The ΔE_Q values obtained for these three compounds are significantly different, despite similar octahedral coordination geometries at the iron(II) sites. Most reported hydroxo-bridged diiron(III) complexes have quadrupole splitting values ~0.5 mm s^{-1}.[46] Notably, **6** and **8** have a more O-rich coordination environments than **7**, with a H_2O (O-donor) ligand instead of an N-donor ligand on

the second iron atom. The $\{Fe_2(\mu\text{-}OH)_2(\mu\text{-}O_2CR)\}^{3+}$ core in $MMOH_{ox}$, which also has one

terminally bound water molecule,[3,44] displays the similar ΔE_Q values, 0.79(3), 1.12(3) mm s^{-1} and

0.87, 1.16 mm s^{-1} for *M. capsulatus* (Bath) and *M. trichosporium* OB3b, respectively.[55,56] An

O-rich metal coordination environment may be the source of the similar ΔE_Q (~1 mm s^{-1}) values

in **6**, **8**, and the diiron sites of $MMOH_{ox}$.

Conclusion

Small changes in the geometry or composition of the ancillary ligands of carboxylate-rich

diiron(II) compounds have a profound effect on their oxygenation chemistry. The movement of

the diphenyphosphino substituent from ortho to meta or para position on the pyridine donor

ligand causes decreased substrate oxidation. The reactivity of these compounds is not only

affected by the N-donor ligand, but also by the remote substituents on the carboxylate ligands.

The more electron-releasing carboxylate groups showed increased C–H activation, in agreement

with results for related systems having tethered benzyl- and ethylpyridine ligands.[29] When the

less electron-releasing carboxylate group was used, subsequent solvent oxidation did not occur;

instead, the $\{Fe_2(\mu\text{-}OH)_2(\mu\text{-}O_2CR)\}^{3+}$core of $MMOH_{ox}$ was recovered having structural and

Mössbauer spectroscopic properties analogous to those observed in the enzyme. These

observations provide valuable information to guide future work on more advanced MMOH

synthetic analogs.

References

(1)   Colby, J.; Stirling, D. I.; Dalton, H. *Biochem. J.* **1977**, *165*, 395-402.

(2)   Fuse, H.; Ohta, M.; Takimura, O.; Murakami, K.; Inoue, H.; Yamaoka, Y.; Oclarit, J. M.; Omori, T. *Biosci. Biotechnol. Biochem.* **1998**, *62*, 1925-1931.

(3)   Whittington, D. A.; Lippard, S. J. *J. Am. Chem. Soc.* **2001**, *123*, 827-838.

(4)   Rosenzweig, A. C.; Frederick, C. A.; Lippard, S. J.; Nordlund, P. *Nature* **1993**, *366*, 537-543.

(5)   Feig, A. L.; Lippard, S. J. *Chem. Rev.* **1994**, *94*, 759-805.

(6)   Wallar, B. J.; Lipscomb, J. D. *Chem. Rev.* **1996**, *96*, 2625-2657.

(7)   Merkx, M.; Kopp, D. A.; Sazinsky, M. H.; Blazyk, J. L.; Müller, J.; Lippard, S. J. *Angew. Chem., Int. Ed. Engl.* **2001**, *40*, 2782-2807.

(8)   Baik, M.-H.; Newcomb, M.; Friesner, R. A.; Lippard, S. J. *Chem. Rev.* **2003**, *103*, 2385-2419.

(9)   Sazinsky, M. H.; Bard, J.; Donato, A. D.; Lippard, S. J. *J. Biol. Chem.* **2004**, *279*, 30600-30610.

(10)   Kryatov, S. V.; Rybak-Akimova, E. V. *Chem. Rev.* **2005**, *105*, 2175-2226.

(11)   Que, L., Jr.; Dong, Y. *Acc. Chem. Res.* **1996**, *29*, 190-196.

(12)   Que, L., Jr. *J. Chem. Soc., Dalton Trans.* **1997**, 3933-3940.

(13)   Du Bois, J.; Mizoguchi, T. J.; Lippard, S. J. *Coord. Chem. Rev.* **2000**, *200–202*, 443–485.

(14)   Lippard, S. J. *Chemistry in Britain* **1986**, *22*, 221-228.

(15)   Lippard, S. J. *Angew. Chem., Int. Ed. Engl.* **1988**, *27*, 344-361.

(16)   Goldberg, D. P.; Telser, J.; Bastos, C. M.; Lippard, S. J. *Inorg. Chem.* **1995**, *34*, 3011-3024.

(17)   Herold, S.; Lippard, S. J. *J. Am. Chem. Soc.* **1997**, *119*, 145-156.

(18)   Mandal, S. K.; Young, V. G., Jr.; Que, L., Jr. *Inorg. Chem.* **2000**, *39*, 1831-1833.

(19)   Lee, D.; Sorace, L.; Caneschi, A.; Lippard, S. J. *Inorg. Chem.* **2001**, *40*, 6774-6781.

(20)   Lee, D.; Lippard, S. J. *J. Am. Chem. Soc.* **1998**, *120*, 12153-12154.

(21)   Hagadorn, J. R.; Que, L., Jr.; Tolman, W. B. *J. Am. Chem. Soc.* **1998**, *120*, 13531-13532.

(22)   Tolman, W. B.; Que, L., Jr. *J. Chem. Soc., Dalton Trans.* **2002**, 653-660.

(23)   Lee, D.; Lippard, S. J. *Inorg. Chem.* **2002**, *41*, 2704-2719.

(24)   Lee, D.; Lippard, S. J. *J. Am. Chem. Soc.* **2001**, *123*, 4611-4612.

(25)   Lee, D.; Lippard, S. J. *Inorg. Chem.* **2002**, *41*, 827-837.

(26)   Yoon, S.; Lippard, S. J. *Inorg. Chem.* **2003**, *42*, 8606-8608.

(27)   Carson, E. C. In *Doctoral Dissertation in Inorganic Chemistry*; Massachusetts Institute of Technology: Cambridge, MA, 2005; Chapter 2.

(28)   Carson, E. C.; Lippard, S. J. *J. Am. Chem. Soc.* **2004**, *126*, 3412-3413.

(29)   Carson, E. C. In *Doctoral Dissertation in Inorganic Chemistry*; Massachusetts Institute of Technology: Cambridge, MA, 2005; Chapter 3.

(30)   Carson, E. C. In *Doctoral Dissertation in Inorganic Chemistry*; Massachusetts Institute of Technology: Cambridge, MA, 2005; Chapter 5.

(31)   Pangborn, A. B.; Giardello, M. A.; Grubbs, R. H.; Rosen, R. K.; Timmers, F. J. *Organometallics* **1996**, *15*, 1518-1520.

(32)   Lazarowych, N. J.; Morris, R. H.; Ressner, J. M. *Inorg. Chem* **1986**, *25*, 3926-3932.

(33)   Newkome, G. R.; Hager, D. C. *J. Org. Chem.* **1978**, *43*, 947-949.

(34)   *SMART v5.626: Software for the CCD Detector System*; Bruker AXS: Madison, WI, 2000.

(35)   Kuzelka, J.; Mukhopadhyay, S.; Spingler, B.; Lippard, S. J. *Inorg. Chem.* **2003**, *42*, 6447-6457.

(36)   Sheldrick, G. M. *SHELXTL97-2: Program for Refinement of Crystal Structures;* University of Göttingen, Germany, 1997.

(37)   *SHELXTL v5.10: Program Library for Structure Solution and Molecular Graphics;* Bruker AXS: Madison, WI, 1998.

(38)   Sheldrick, G. M. *SADABS: Area-Detector Absorption Correction;* University of Göttingen, Germany, 1996.

(39)   Spek, A. L. *PLATON, A Multipurpose Crystallographic Tool;* Utrecht University: Utrecht, The Netherlands, 1998.

(40)   Kent, T. A. *WMOSS v2.5: Mössbauer Spectral Analysis Software;* WEB Research Co.: Minneapolis, 1998.

(41)   Silverstein, R. M.; Webster, F. X. *Spectrometric Identification of Organic Compounds;* Sixth ed.; John Wiley & Sons, Inc.: New York, 1998.

(42)   Münck, E. In *Physical Methods in Bioinorganic Chemistry: Spectroscopy and Magnetism;* Que, L., Jr., Ed.; University Science Books: Sausalito, CA, 2000; pp 287-319.

(43)   Tshuva, E. Y.; Lippard, S. J. *Chem. Rev.* **2004**, *104*, 987-1012.

(44)   Elango, N.; Radhakrishnan, R.; Froland, W. A.; Wallar, B. J.; Earhart, C. A.; Lipscomb, J. D.; Ohlendorf, D. H. *Protein Sci.* **1997**, *6*, 556-568.

(45)   Yoon, S.; Lippard, S. J. *J. Am. Chem. Soc.* **2004**, *126*, 2666-2667.

(46)   Kurtz, D. M., Jr. *Chem. Rev.* **1990**, *90*, 585-606.

(47)   Liu, T.; Lovell, T.; Han, W.-G.; Noodleman, L. *Inorg. Chem.* **2003**, *42*, 5244-5251.

(48)   Brown, I. D.; Altermatt, D. *Acta Cryst.* **1985**, *B41*, 244-247.

(49)   Harlan, E. W.; Berg, J. M.; Holm, R. H. *J. Am. Chem. Soc.* **1986**, *108*, 6992 - 7000.

(50)   Yoon, S.; Lippard, S. J. *J. Am. Chem. Soc.* **2005**, *127*, 8386-8397.

(51)   DeWitt, J. G.; Bentsen, J. G.; Rosenzweig, A. C.; Hedman, B.; Green, J.; Pilkington, S.
J.; Papaefthymiou, G. C.; Dalton, H.; Hodgson, K. O.; Lippard, S. J. *J. Am. Chem. Soc.*
1991, *113*, 9219-9235.

(52)   Tshuva, E. Y.; Lee, D.; Bu, W.; Lippard, S. J. *J. Am. Chem. Soc.* **2002**, *124*, 2416-2417.

(53)   Moreira, R. F.; Tshuva, E. Y.; Lippard, S. J. *Inorg. Chem.* **2004**, *43*, 4427-4434.

(54)   Chen, C.-T.; Siegel, J. S. *J. Am. Chem. Soc.* **1994**, *116*, 5959-5960.

(55)   Liu, K. E.; Valentine, A. M.; Wang, D.; Huynh, B. H.; Edmonson, D. E.; Salifoglou, A.;
Lippard, S. J. *J. Am. Chem. Soc.* **1995**, *117*, 10174-10185.

(56)   Fox, B. G.; Hendrich, M. P.; Surerus, K. K.; Andersson, K. K.; Froland, W. A.;
Lipscomb, J. D.; Munck, E. *J. Am. Chem. Soc.* **1993**, *115*, 3688-3701.

Table 6.1. Summary of X-ray Crystallographic Data

	1	2·3C$_4$H$_{10}$O	3·CH$_2$Cl$_2$
Empirical Formula	Fe$_2$C$_{101}$H$_{82}$NO$_8$P	Fe$_2$C$_{130}$H$_{126}$N$_2$O$_{11}$P$_2$	Fe$_2$C$_{119}$H$_{98}$N$_2$O$_8$P$_2$Cl$_2$
Formula Weight	1580.35	2065.97	1928.53
Space Group	P$\bar{1}$	P$\bar{1}$	C2/c
a, Å	12.810(2)	13.1023(15)	22.322(5)
b, Å	15.785(3)	16.1989(18)	17.485(4)
c, Å	21.780(4)	16.5295(18)	25.357(5)
α, deg	96.150(5)	108.520(2)	
β, deg	90.847(6)	101.298(2)	105.275(4)
γ, deg	112.399(3)	113.080(2)	
V, Å^3	4041.0(12)	2846.4(5)	9547(4)
Z	2	1	4
ρ_{calc}, g/cm^3	1.299	1.205	1.342
T, °C	-100	-100	-100
μ(Mo Kα), mm^{-1}	0.440	0.343	0.456
θ limits, deg	1.75 – 26.53	1.71 – 26.37	1.83 – 26.38
total no. of data	32562	23474	38803
no. of unique data	16191	11461	9764
no. of params	1026	682	622
Goodness-of-fit on F^2	1.044	1.044	1.195
R1[a]	0.0427	0.0591	0.0722
wR^{2}[b]	0.1145	0.1579	0.1628
max, min peaks, e/Å^3	0.467, -0.261	0.976, -0.468	1.1421, -0.927

[a] R1 $= \Sigma ||F_o|-F_c||/\Sigma|F_o|$. [b] wR$^2 = \{\Sigma[w(F_o^2-F_c^2)^2]/\Sigma[w(F_o^2)^2]\}^{1/2}$.

Table 6.1. Continued

	4·$C_2H_4Cl_2$	5·4CH_2Cl_2	6·3CH_2Cl_2
Empirical Formula	$Fe_2C_{95}H_{62}NO_8F_8PCl_2$	$Fe_6C_{122}H_{110}N_2O_{18}P_2Cl_{12}$	$Fe_2C_{96}H_{68}NO_{12}F_8PCl_6$
Formula Weight	1711.03	2714.56	1934.88
Space Group	$P\bar{1}$	$P\bar{1}$	$P\bar{1}$
a, Å	13.6676(14)	14.508(2)	12.9063(17)
b, Å	14.0155(14)	15.852(2)	14.1811(18)
c, Å	21.278(2)	15.904(3)	24.990(3)
α, deg	80.799(2)	78.407(3)	78.235(3)
β, deg	89.079(2)	77.951(3)	86.110(2)
γ, deg	86.533(2)	63.832(3)	86.837(3)
V, Å^3	4016.0(7)	4042(9)	4463.4(10)
Z	2	1	2
ρ_{calc}, g/cm^3	1.415	1.415	1.440
T, °C	-100	-100	-100
μ(Mo Kα), mm^{-1}	0.526	1.004	0.602
θ limits, deg	1.47 – 26.73	1.64 – 25.00	1.67 – 27.10
total no. of data	33796	23654	39033
no. of unique data	16744	11127	19334
no. of params	1099	730	1151
Goodness-of-fit on F^2	1.030	0.997	0.997
R1[a]	0.0709	0.1032	0.0855
wR2[b]	0.1767	0.1826	0.1521
max, min peaks, e/Å^3	1.124, -1.036	1.028, -0.551	0.779, -0.721

[a]R1 = $\Sigma||F_o|-F_c||/\Sigma|F_o|$. [b]wR2 = $\{\Sigma[w(F_o^2-F_c^2)^2]/\Sigma[w(F_o^2)^2]\}^{1/2}$.

Table 6.2. Selected Interatomic Distances (Å) and Angles (deg) for $[Fe_2(\mu\text{-}O_2CAr^{Tol})_3\text{-}(O_2CAr^{Tol})(2\text{-}Ph_2Ppy)]$ (**1**) and $[Fe_2(\mu\text{-}O_2CAr^{4\text{-}FPh})_3(O_2CAr^{4\text{-}FPh})(2\text{-}Ph_2Ppy)]$ (**4**)[a]

	1	4
Fe1···Fe2	3.3094(6)	3.4534(8)
Fe2···P1	2.8322(7)	2.9551(13)
Fe1–O1	2.2162(13)	2.297(3)
Fe1–O2	2.0826(13)	2.068(3)
Fe1–O3	2.0512(13)	2.000(3)
Fe1–O5	2.0342(12)	2.054(3)
Fe1–O7	2.0602(12)	2.017(3)
Fe2–N1	2.1314(16)	2.127(3)
Fe2–O4	1.9892(12)	2.022(3)
Fe2–O6	2.0570(12)	1.985(2)
Fe2–O8	1.9981(13)	1.998(3)
O1–Fe1–O2	61.35(5)	60.07(9)
O1–Fe1–O3	91.81(5)	86.96(10)
O1–Fe1–O5	167.13(5)	166.37(10)
O1–Fe1–O7	87.81(5)	91.98(10)
O2–Fe1–O3	111.56(5)	104.65(11)
O2–Fe1–O5	107.01(5)	106.30(10)
O2–Fe1–O7	110.11(6)	118.47(11)
O3–Fe1–O5	98.07(5)	97.32(11)
O3–Fe1–O7	131.95(5)	129.17(12)
O5–Fe1–O7	91.65(5)	95.25(11)
O4–Fe2–N1	103.14(6)	88.53(12)
O6–Fe2–N1	91.33(5)	122.81(12)
O8–Fe2–N1	111.28(6)	120.56(12)
O4–Fe2–O6	100.35(5)	103.10(11)
O4–Fe2–O8	139.10(5)	122.18(11)
O6–Fe2–O8	100.29(5)	99.91(11)

[a]Numbers in parentheses are estimated standard deviations of the last significant figure. Atoms are labeled as indicated Figures 6.1 and 6.4.

Table 6.3. Selected interatomic distances (Å) and angles (deg) for $[Fe_2(\mu\text{-}O_2CAr^{Tol})_2\text{-}(O_2CAr^{Tol})_2(3\text{-}Ph_2Ppy)_2]$ (**2**) and $[Fe_2(\mu\text{-}_2CAr^{Tol})_4(4\text{-}Ph_2Ppy)_2]$ (**3**)[a]

	2	**3**
Fe1⋯Fe1A	4.0355(8)	2.8128(10)
Fe1–N1	2.135(2)	2.094(3)
Fe1–O1	1.9364(19)	2.121(2)
Fe1–O2	1.9983(19)	2.019(2)
Fe1–O3	2.417(2)	2.133(2)
Fe1–O4	2.0107(19)	2.014(2)
O1–Fe1–N1	102.11(8)	97.46(10)
O2–Fe1–N1	95.93(8)	109.86(10)
O3–Fe1–N1	146.37(8)	93.32(10)
O4–Fe1–N1	88.02(8)	96.51(10)
O1–Fe1–O2	123.61(9)	88.81(9)
O1–Fe1–O3	94.77(8)	169.16(9)
O1–Fe1–O4	122.15(9)	92.87(9)
O2–Fe1–O3	98.59(7)	86.68(9)
O2–Fe1–O4	111.33(8)	153.14(9)
O3–Fe1–O4	58.45(7)	87.09(9)

[a]Numbers in parentheses are estimated standard deviations of the last significant figure. Atoms are labeled as indicated Figures 6.2 and 6.3.

Table 6.4. Summary of Reaction Conditions and Amount of Ligand Oxidation for the Reaction of $[Fe_2(\mu\text{-}O_2CAr^{Tol})_3(O_2CAr^{Tol})(2\text{-}Ph_2Ppy)]$ (1) with Dioxygen

[1] (mM)	Solvent	Reaction Time (min)	Equiv Oxidized[a]
2.91	CH_2Cl_2	25	0.95
1.70	CH_2Cl_2	30	1.0
0.324	CH_2Cl_2	2.5	0.88
0.314	CH_2Cl_2	10	1.0
0.337	CH_2Cl_2	25	1.0
1.68	C_6H_6	60	0.48
0.95	MeCN	870	0.56

[a]Based on **1**

Table 6.5. Summary of Conditions and Amount of Oxidation Product Isolated for the Reaction of $[Fe_2(\mu\text{-}O_2CAr^{Tol})_3(O_2CAr^{Tol})(2\text{-}Ph_2Ppy)]$ (1) with Additional Equiv of Phosphine and Dioxygen

[1] (mM)	Solvent	Phosphine	Equiv PR_3	Reaction Time (h)	Equiv PR_3 Oxidized
2.5	CH_2Cl_2	2-Ph_2Ppy	8.4	1	3.98^a
1.4	CH_2Cl_2	2-Ph_2Ppy	47	13	13.4^a
0.31	CH_2Cl_2	2-Ph_2Ppy	51	17	17.0^a
0.42	CH_2Cl_2	PPh_3	5.6	13	1.7^a
2.83	C_6H_6	2-Ph_2Ppy	15.2	24	1.95^a
0.32	MeCN	2-Ph_2Ppy	5.1	17	1.43^a

^{a}Including 1 equiv of 2-Ph_2Ppy from **1**

Table 6.6. Selected Interatomic Distances (Å) and Angles (deg) for $[Fe_6(\mu_4\text{-}O)_2(\mu\text{-}OH)_6\text{-}(\mu\text{-}O_2CAr^{Tol})_4Cl_4(2\text{-}Ph_2P(O)py)_2]$ (**5**)[a]

Fe1–O1	2.010(7)	Fe2–O3	1.993(6)	Fe3–O2	1.890(7)
Fe1–O2	2.036(6)	Fe2–O3A	1.990(6)	Fe3–O3	2.260(6)
Fe1–O3	1.911(6)	Fe2–O6	2.036(6)	Fe3–O7A	1.922(6)
Fe1–O4	2.049(6)	Fe2–O7	2.022(6)	Fe3–O9	1.898(6)
Fe1–O5	2.044(6)	Fe2–O8	2.007(6)	Fe3–Cl2	2.215(3)
Fe1–Cl1	2.290(3)	Fe2–O9	2.007(6)	Fe3···Fe2	3.143(2)
Fe1–Fe3	3.157(2)	Fe2···Fe2A	3.029(3)	Fe3A···Fe2	3.158(2)
O1–Fe1–Cl1	95.8(2)	O3–Fe2–O3A	81.0(3)	Cl2–Fe3–O2	104.9(2)
O2–Fe1–Cl1	176.8(2)	O3–Fe2–O6	98.5(3)	Cl2–Fe3–O3	177.57(19)
O3–Fe1–Cl1	97.0(2)	O3–Fe2–O7	101.6(3)	Cl2–Fe3–O7A	101.9(2)
O4–Fe1–Cl1	91.7(2)	O3–Fe2–O8	164.8(3)	Cl2–Fe3–O9	105.9(2)
O5–Fe1–Cl1	89.4(2)	O3–Fe2–O9	80.5(3)	O2–Fe3–O3	74.9(2)
O1–Fe1–O2	87.1(3)	O6–Fe2–O3A	164.3(3)	O2–Fe3–O7A	117.2(3)
O1–Fe1–O3	167.1(3)	O6–Fe2–O7	84.2(3)	O2–Fe3–O9	115.5(3)
O1–Fe1–O4	84.9(3)	O6–Fe2–O8	87.6(3)	O3–Fe3–O7A	76.2(2)
O1–Fe1–O5	84.3(3)	O6–Fe2–O9	93.9(3)	O3–Fe3–O9	76.3(2)
O2–Fe1–O3	80.0(3)	O7–Fe2–O3A	80.6(3)	O9–Fe3–O7A	109.7(3)
O2–Fe1–O4	89.8(3)	O7–Fe2–O8	92.7(3)		
O2–Fe1–O5	89.7(3)	O7–Fe2–O9	177.3(3)		
O3–Fe1–O4	95.2(3)	O8–Fe2–O3A	96.893)		
O3–Fe1–O5	95.2(3)	O8–Fe2–O9	85.3(3)		
O4–Fe1–O5	169.3(3)	O9–Fe2–O3A	101.5(3)		

[a]Numbers in parentheses are estimated standard deviations of the last significant figure. Atoms are labeled as indicated Figure 6.7.

Table 6.7. Selected bond lengths and angles for $[Fe_2(\mu\text{-OH})_2(\mu\text{-O}_2CAr^{4FPh})(O_2CAr^{4\text{-}FPh})_3\text{-}(2\text{-}Ph_2P(O)py)(OH_2)]$ **(6)**[a]

	Bond length (Å)		Bond Angle (deg)
Fe1···Fe2	2.9725(11)	Fe1–O2–Fe2	98.10(19)
		Fe2–O3–Fe1	97.35(18)
Fe1–N1	2.210(4)	O1–Fe1–N1	80.49(15)
Fe1–O1	2.023(3)	O2–Fe1–N1	84.76(17)
Fe1–O2	1.954(4)	O3–Fe1–N1	92.34(17)
Fe1–O3	1.981(4)	O5–Fe1–N1	172.91(15)
Fe1–O5	2.003(3)	O7–Fe1–N1	92.17(15)
Fe1–O7	1.947(3)	O1–Fe1–O2	97.51(16)
Fe2–O2	1.981(4)	O1–Fe1–O3	172.11(17)
Fe2–O3	1.977(4)	O1–Fe1–O5	93.26(14)
Fe2–O4	2.097(4)	O1–Fe1–O7	89.81(14)
Fe2–O6	2.017(3)	O2–Fe1–O3	78.40(17)
Fe2–O9	1.974(3)	O2–Fe1–O5	92.81(17)
Fe2–O11	1.976(3)	O2–Fe1–O7	171.47(17)
		O3–Fe1–O5	93.68(16)
O2···O10	2.708(6)	O3–Fe1–O7	93.80(16)
O3···O8	2.803(6)	O5–Fe1–O7	91.14(14)
O4···O12	2.537(6)	O2–Fe2–O3	77.85(17)
		O2–Fe2–O4	89.52(19)
		O2–Fe2–O6	91.58(16)
		O2–Fe2–O9	91.96(16)
		O2–Fe2–O11	174.61(17)
		O3–Fe2–O4	88.81(17)
		O3–Fe2–O6	93.02(15)
		O3–Fe2–O9	168.94(16)
		O3–Fe2–O11	97.06(15)
		O4–Fe2–O6	178.02(16)
		O4–Fe2–O9	86.77(17)
		O4–Fe2–O11	88.61(17)
		O6–Fe2–O9	91.55(14)
		O6–Fe2–O11	90.43(14)
		O9–Fe2–O11	92.97(14)

[a]Numbers in parentheses are estimated standard deviations of the last significant figure. Atoms are labeled as indicated Figure 6.8.

Table 6.8. Bond Valence Sum Analysis of Iron-Ligand Bonds in **5** and **6**.

Bond	Bond Length (Å)	Bond Valence	Bond Valence Sum
[Fe$_6$(μ_4-O)$_2$(μ-OH)$_6$(μ-O$_2$CAr^{Tol})$_4$Cl$_4$(2-Ph$_2$P(O)py)$_2$] (**5**)			
Fe1–O1	2.010(7)	0.507	
Fe1–O2	2.036(6)	0.473	
Fe1–O3	1.911(6)	0.663	3.306
Fe1–O4	2.049(6)	0.457	
Fe1–O5	2.044(6)	0.463	
Fe1–Cl1	2.290(3)	0.743	
Fe2–O3	1.993(6)	0.531	
Fe2–O3A	1.990(6)	0.536	
Fe2–O6	2.036(6)	0.473	3.054
Fe2–O7	2.022(6)	0.491	
Fe2–O8	2.007(6)	0.512	
Fe2–O9	2.007(6)	0.512	
Fe3–O2	1.890(7)	0.702	
Fe3–O3	2.260(6)	0.258	
Fe3–O7A	1.922(6)	0.644	3.20
Fe3–O9	1.898(6)	0.687	
Fe3–Cl2	2.215(3)	0.910	
[Fe$_2$(μ-OH)$_2$(μ-O$_2$CAr$^{4\text{-}FPh}$)(O$_2$CAr$^{4\text{-}FPh}$)$_3$(OH$_2$)(2-Ph$_2$P(O)py)] (**6**)			
Fe1–N1	2.210(4)	0.383	
Fe1–O1	2.023(3)	0.490	
Fe1–O2	1.954(4)	0.590	3.131
Fe1–O3	1.981(4)	0.549	
Fe1–O5	2.003(3)	0.517	
Fe1–O7	1.947(3)	0.602	
Fe2–O2	1.981(4)	0.549	
Fe2–O3	1.977(4)	0.555	
Fe2–O4	2.097(4)	0.401	3.118
Fe2–O6	2.017(3)	0.498	
Fe2–O9	1.974(3)	0.559	
Fe2–O11	1.976(3)	0.556	

Table 6.9. Mössbauer parameters for **6**, **7**, **8**, and $MMOH_{ox}$.

	Coordinate Atoms		δ (mm s^{-1})	ΔE_Q (mm s^{-1})	ref
	Fe1	Fe2			
6	NO_5	O_6	0.50(2)	0.83(2)	*a*
7	N_2O_4	NO_5	0.48(2)	0.61(2)	24
8	NO_5	O_6	0.45(2)	1.21(2)	45
$MMOH_{ox}$	NO_5	NO_5	0.51(2), 0.50(2)^b	0.79(3), 1.12(3)^b	55
			0.50, 0.51^c	0.87, 1.16^c	56

*a*This work.

Chart 6.1.

MMOH$_{red}$ MMOH$_{ox}$

Chart 6.2.

Ar^{Tol}CO$_2$H   Ar^{4-FPh}CO$_2$H

Chart 6.3.

6   **7**   **8**
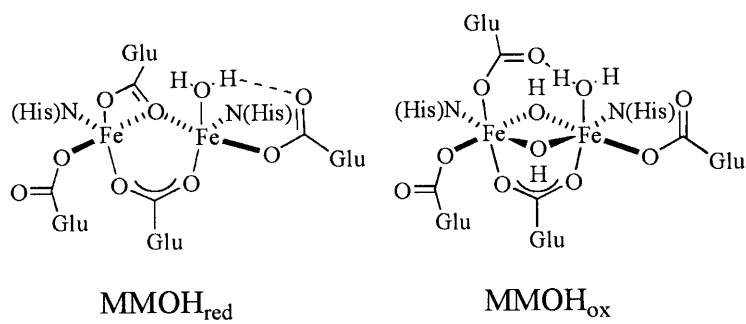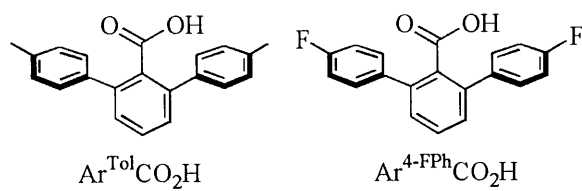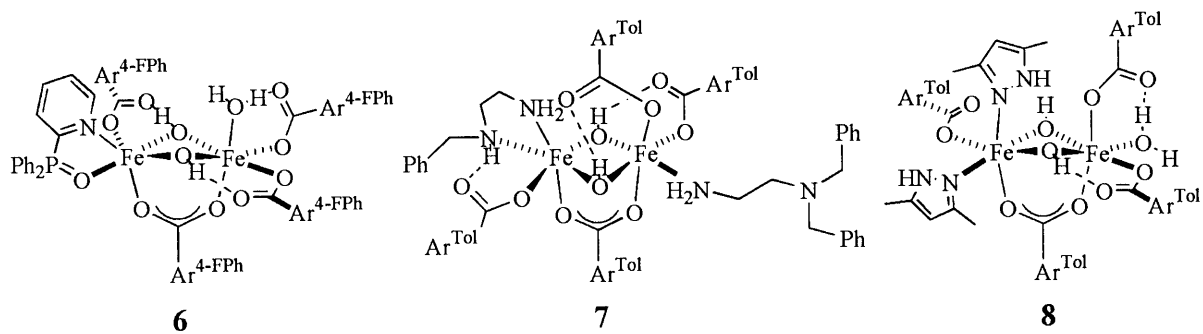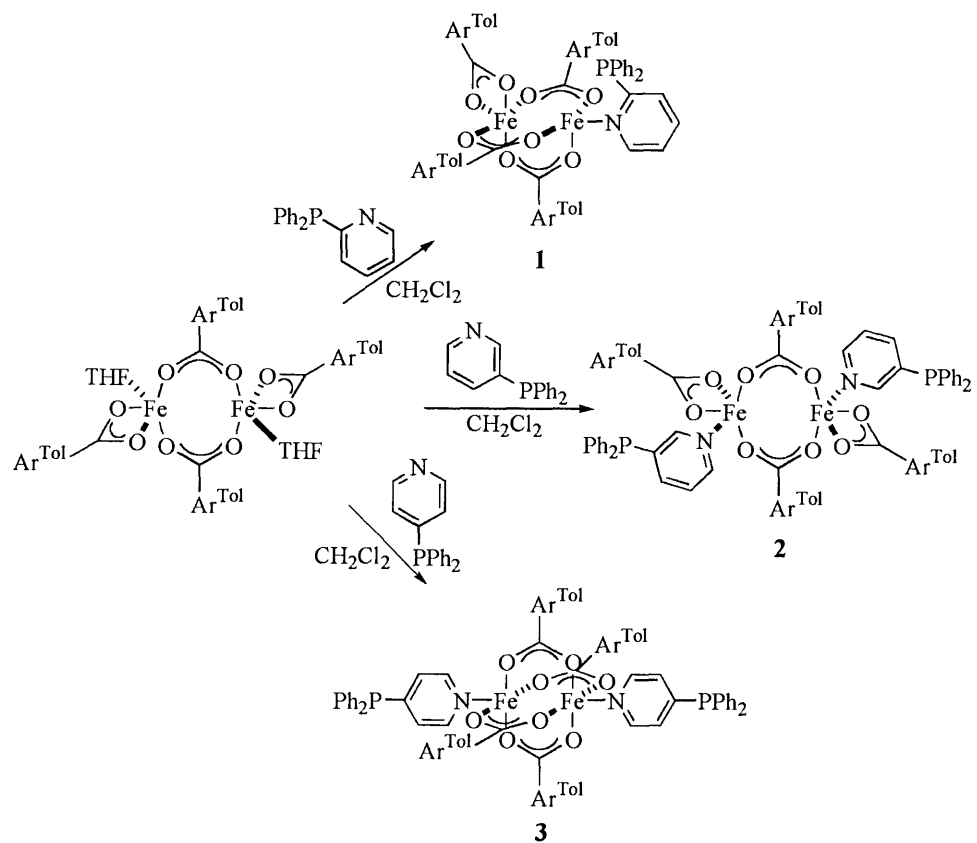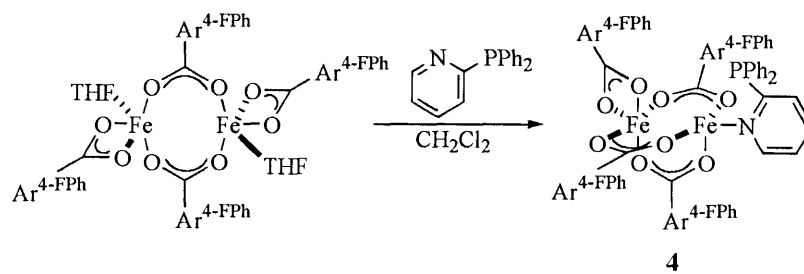
Scheme 6.1.

Scheme 6.2.

Scheme 6.3
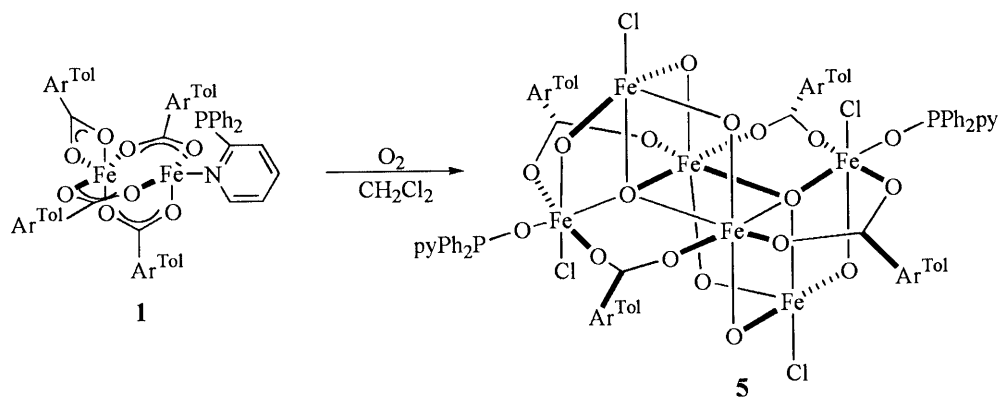
Scheme 6.4.
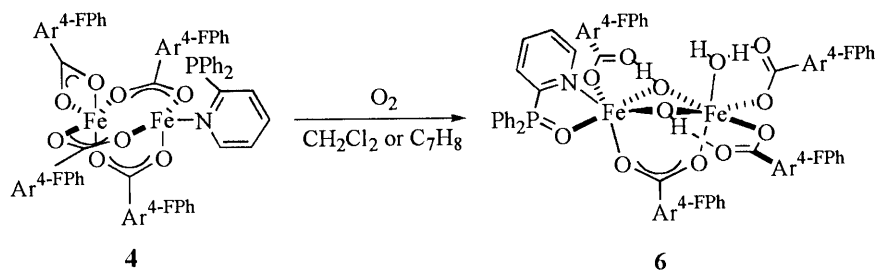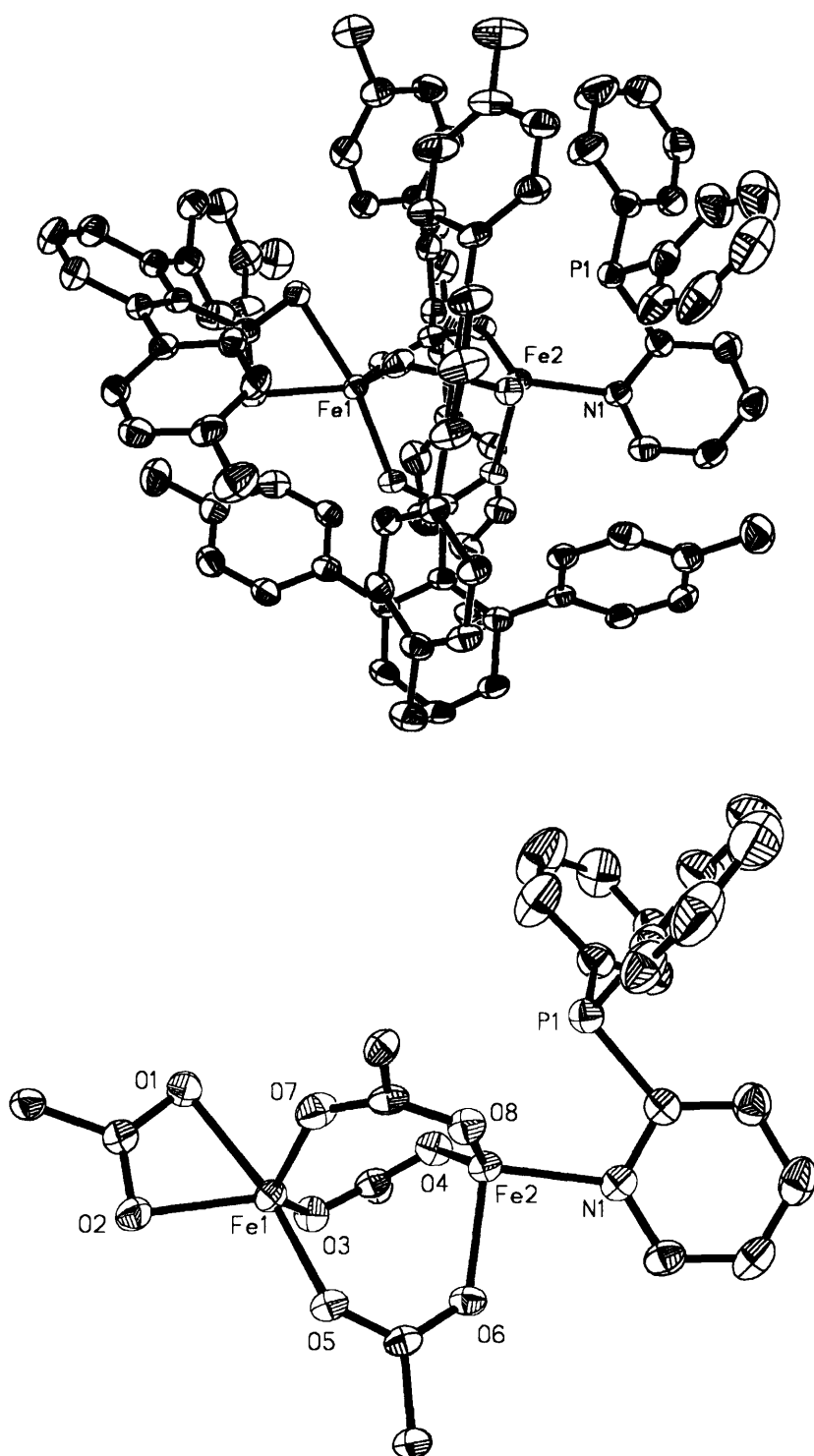
Figure 6.1. Top: ORTEP drawing of $[Fe_2(\mu\text{-}O_2CAr^{Tol})_3(O_2CAr^{Tol})(2\text{-}Ph_2Ppy)]$ (**1**) illustrating 50% probability thermal ellipsoids for all non-hydrogen atoms. Bottom: Drawings in which the aromatic rings of the $^-O_2CAr^{Tol}$ ligands are omitted for clarity.
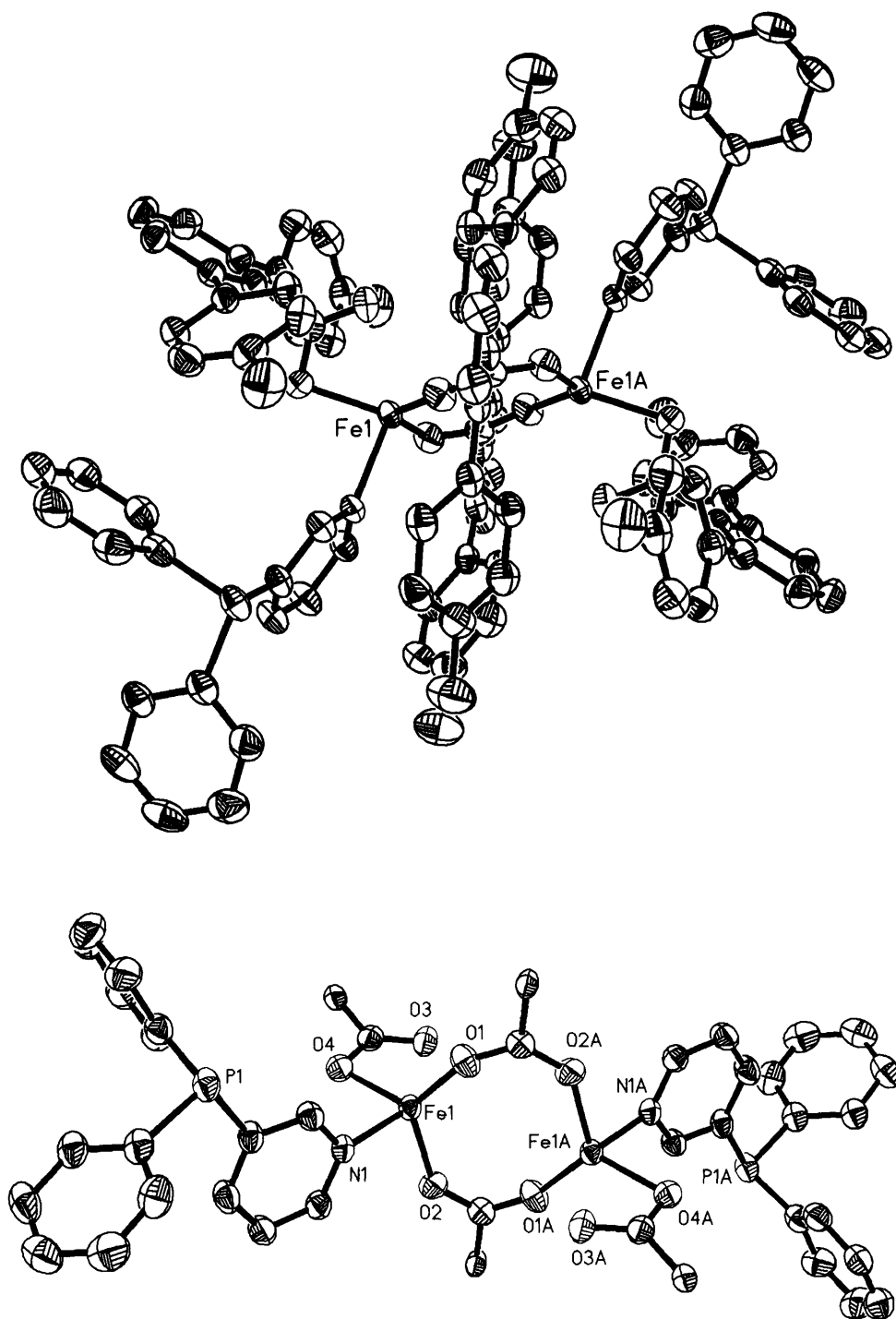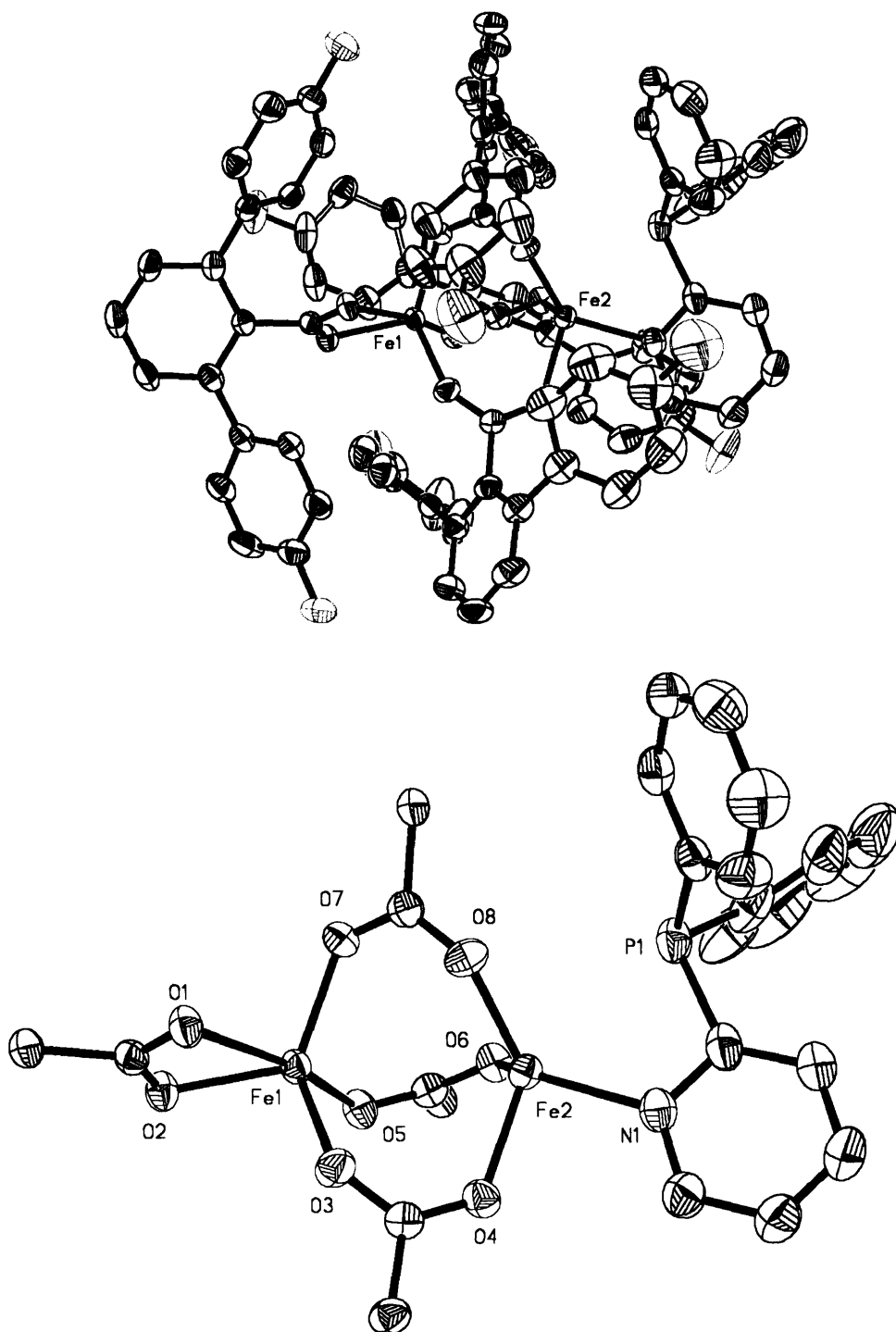
Figure 6.2. Top: ORTEP drawings of [Fe$_2$(μ-O$_2$CAr^{Tol})$_2$(O$_2$CAr^{Tol})$_2$(3-Ph$_2$Ppy)$_2$] (**2**) showing 50% probability thermal ellipsoids for all non-hydrogen atoms. Bottom: Drawings in which the aromatic rings of the $^-$O$_2$CAr^{Tol} ligands are omitted for clarity.
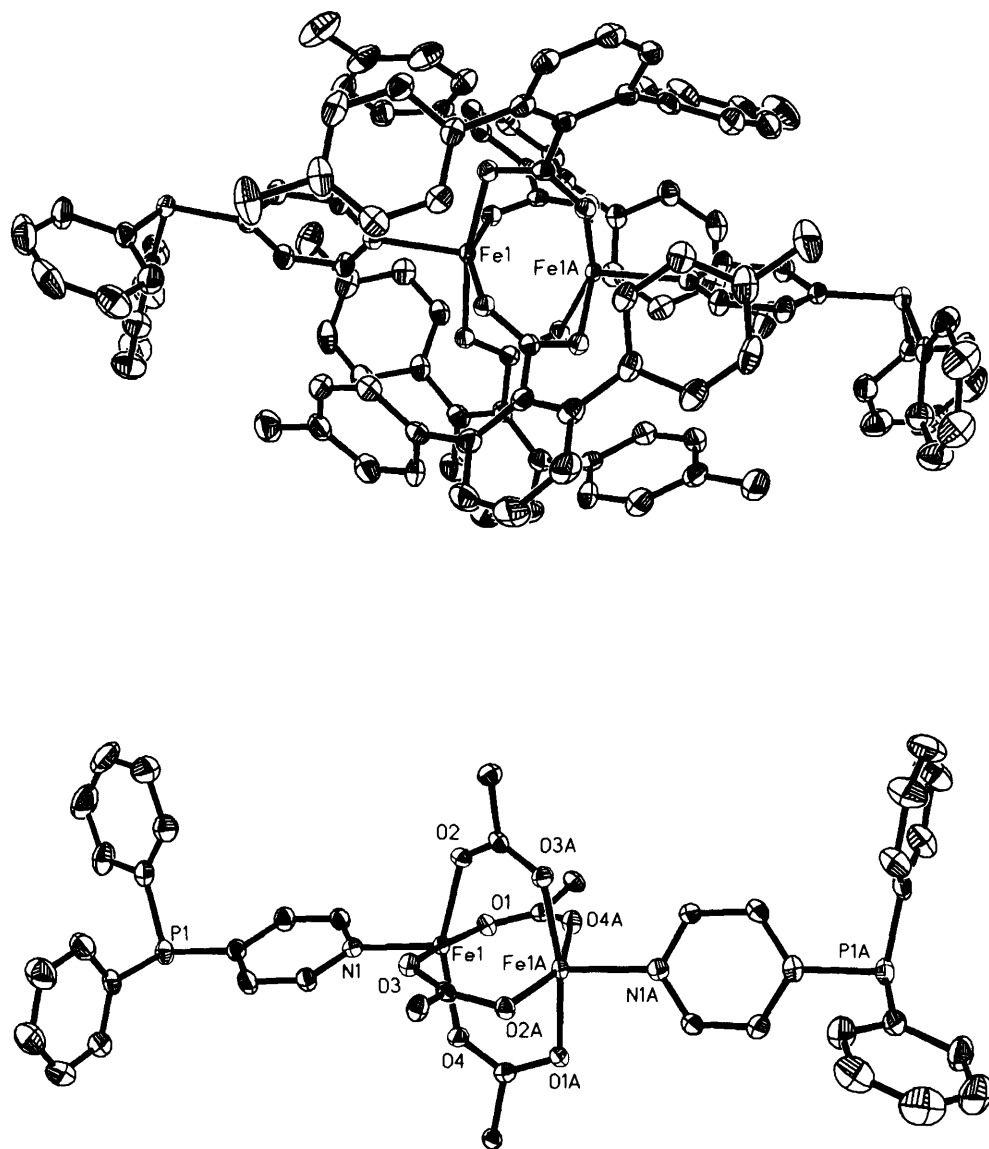
**Figure 6.3.** Top: ORTEP drawings of [Fe$_2$(μ-O$_2$CAr^{Tol})$_4$(4-Ph$_2$Ppy)$_2$] (**3**) displaying 50% probability thermal ellipsoids for all non-hydrogen atoms. Bottom: Drawings in which the aromatic rings of the $^-$O$_2$CAr^{Tol} ligands are omitted for clarity.

Figure 6.4. Top: ORTEP drawing of [Fe$_2$(μ-O$_2$CAr$^{4\text{-FPh}}$)$_3$(O$_2$CAr$^{4\text{-FPh}}$)(2-Ph$_2$Ppy)] (**4**) illustrating 50% probability thermal ellipsoids for all non-hydrogen atoms. Bottom: Drawings in which the aromatic rings of the $^-$O$_2$CAr$^{4\text{-FPh}}$ ligands are omitted for clarity.
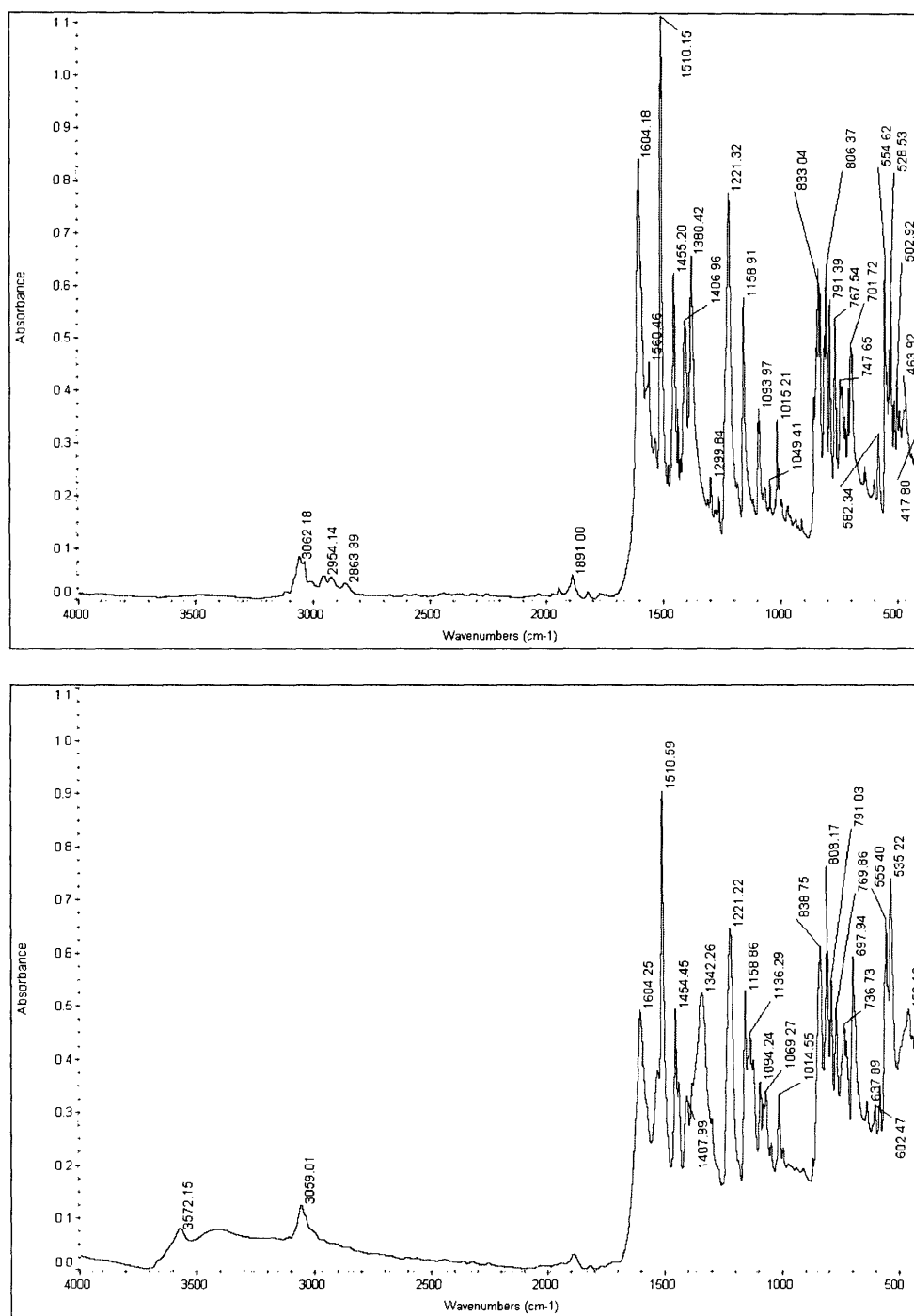
Figure 6.5. FT-IR spectra of KBr pellets of $[Fe_2(\mu\text{-}O_2CAr^{4\text{-}FPh})_3(O_2CAr^{4\text{-}FPh})(2\text{-}Ph_2Ppy)]$ **(4)** (top) and $[Fe_2(\mu\text{-}OH)_2(\mu\text{-}O_2CAr^{4\text{-}FPh})(O_2CAr^{4\text{-}FPh})_3(OH_2)(2\text{-}Ph_2P(O)py)]$ **(6)** (bottom).
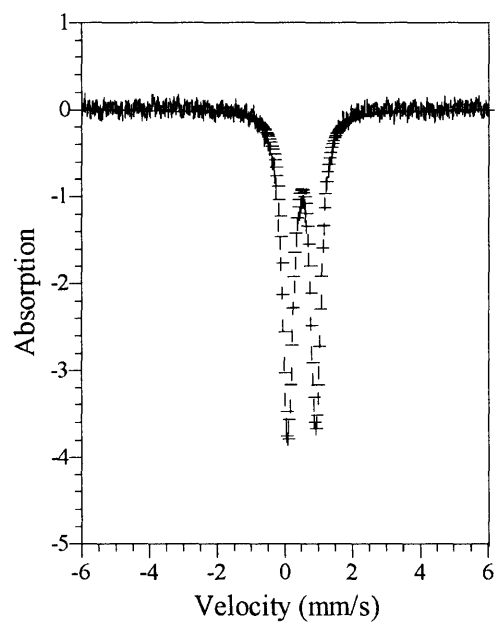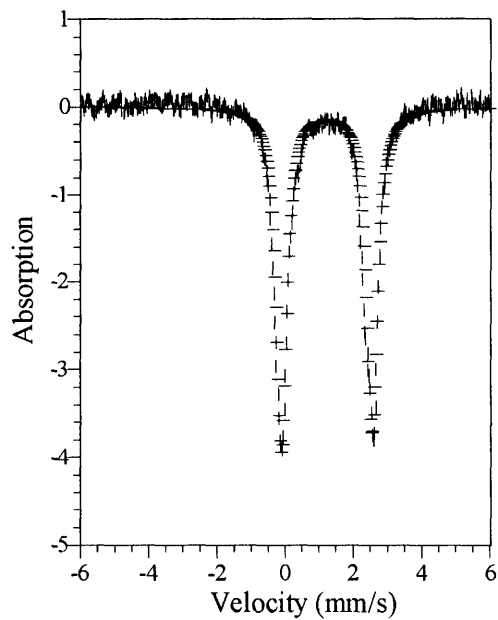
Figure 6.6. Mössbauer spectra (experimental data (|), calculated fit (–)) recorded at 4.2 K for solid samples of $[Fe_2(\mu\text{-}O_2CAr^{4\text{-}FPh})_3(O_2CAr^{4\text{-}FPh})(2\text{-}Ph_2Ppy)]$ **(4)** (top) and $[Fe_2(\mu\text{-}OH)_2\text{-}(\mu\text{-}O_2CAr^{4\text{-}FPh})(O_2CAr^{4\text{-}FPh})_3(2\text{-}Ph_2P(O)py)(OH_2)]$ **(6)** (bottom).
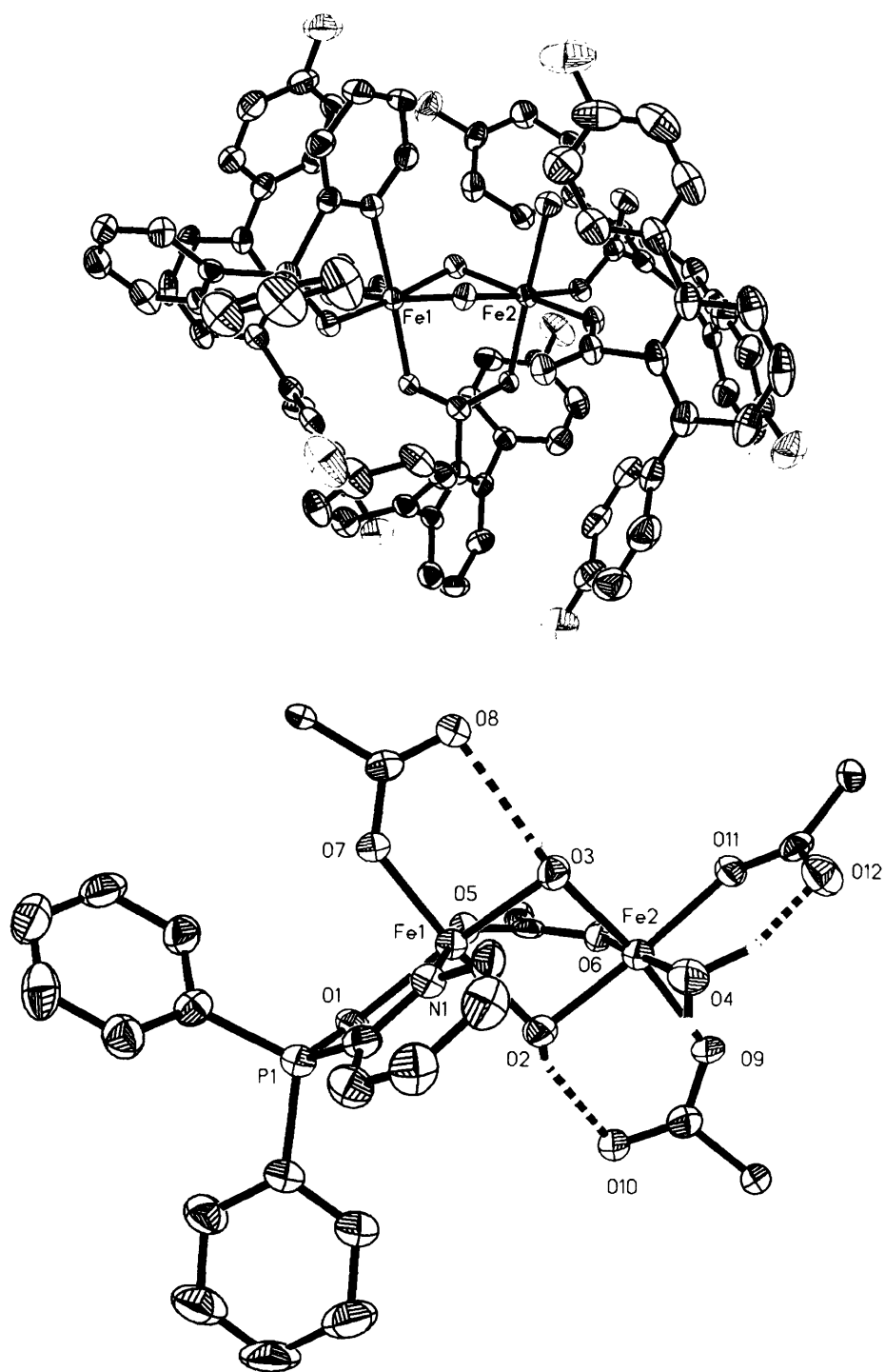
Figure 6.8. Top: ORTEP drawing of [Fe$_2$(μ-OH)$_2$(μ-O$_2$CAr$^{4\text{-FPh}}$)(O$_2$CAr$^{4\text{-FPh}}$)$_3$(OH$_2$)-(2-Ph$_2$P(O)py)] (**6**) illustrating 50% probability thermal ellipsoids for all non-hydrogen atoms. Bottom: Drawings in which the aromatic rings of the $^-$O$_2$CAr$^{4\text{-FPh}}$ ligands are omitted for clarity.

Figure 6.7. Top: ORTEP drawing of [Fe$_6$(μ_4-O)$_2$(μ-OH)$_6$(μ-O$_2$CAr^{Tol})$_4$Cl$_4$(2-Ph$_2$P(O)py)$_2$] (**5**) illustrating 50% probability thermal ellipsoids for all non-hydrogen atoms. Bottom: Drawings in which the aromatic rings of the $^-$O$_2$CAr^{Tol} ligands are omitted for clarity.
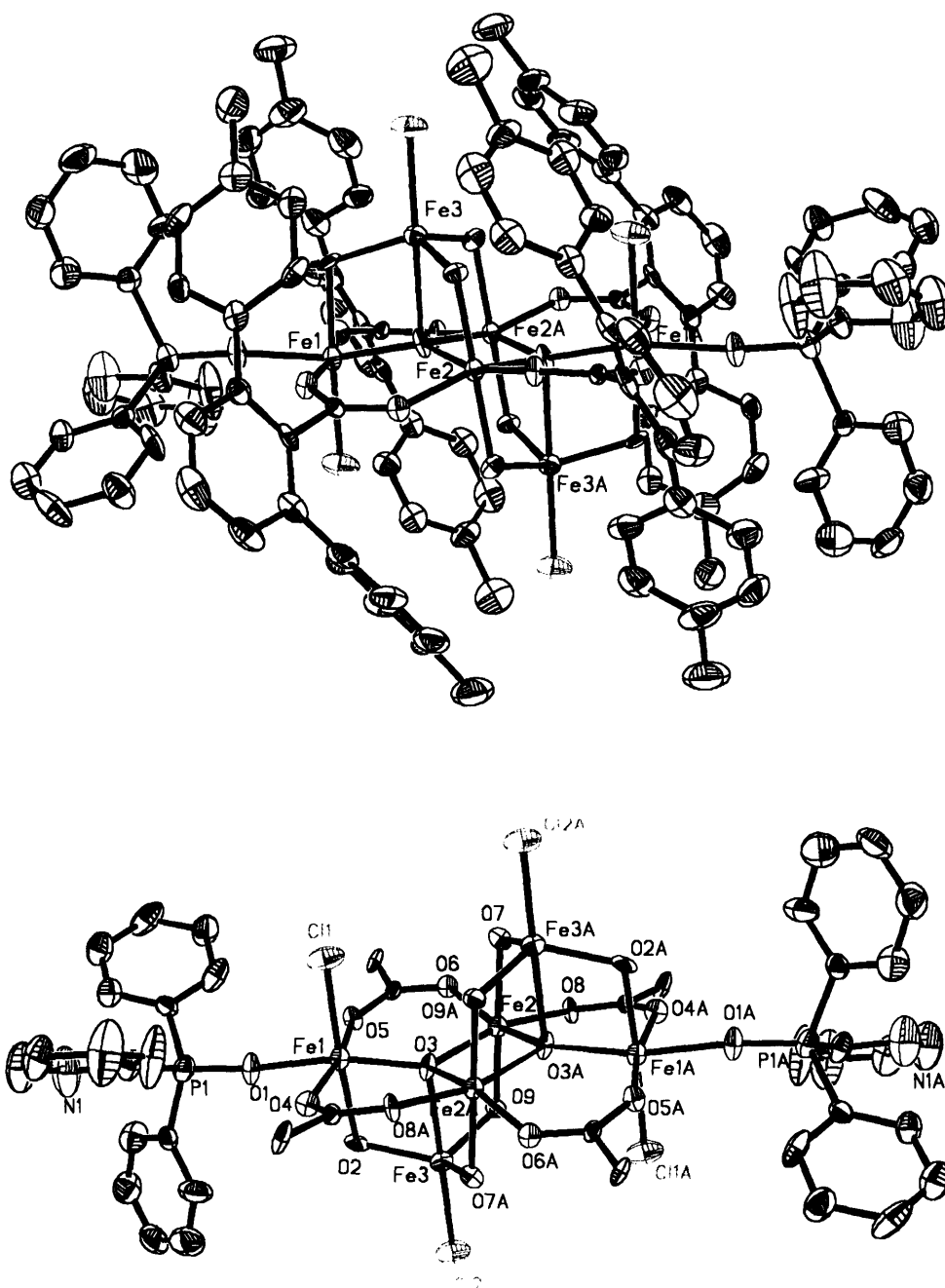
Biographical Note

The author was born Emily Houghton Carrig on June 2, 1978 in Richmond, VA. She received her B.Sc. in Chemistry from the University of Virginia in 2000. As a graduate student she completed her doctoral work in the laboratory of Professor Stephen J. Lippard at the Massachusetts Institute of Technology. She married Brec Carson in August 2001. Following graduation she will pursue postdoctoral research with Professor Brookhart at the University of North Carolina.

Emily Carrig Carson

Education

Massachusetts Institute of Technology, Cambridge, MA.
Ph.D. in Inorganic Chemistry, 2005.
Thesis advisor: Professor Stephen J. Lippard

University of Virginia, Charlottesville, VA.
B.Sc. with high distinction, Chemistry, 2000.
Advisor: Professor W. Dean Harman

Publications

Carson, E. C.; Lippard, S. J. Dioxygen-Initiated Oxidation of Heteroatomic Substrates Incorporated into Ancillary Pyridine Ligands of Carboxylate-Rich Diiron(II) Complexes. Submitted for publication to *Inorg. Chem.*

Carson, E. C.; Lippard, S. J. C–H Activation of Benzyl- and Ethyl- Substituted Pyridine Ligands in the Reactions of Carboxylate-Bridged Diiron(II) Complexes with Dioxygen. Submitted for publication to *Inorg. Chem.*

Carson, E. C.; Lippard, S. J. Synthesis and Oxidation of Carboxylate-Bridged Diiron(II) Complexes with Substrates Tethered to Primary Alkyl Amine Ligands. Submitted for publication to *J. Inorg. Biochem.*

Carson, E. C.; Lippard, S. J. Oxidation of Sulfide, Phosphine, and Benzyl Substrates Tethered to N-Donor Ligands in Carboxylate-Bridged Diiron(II) Complexes. *J. Am. Chem. Soc.* **2004**, *126*, 3412-3413.

Meiere, S. H.; Brooks, B. C.; Gunnoe, T. B.; Carrig, E. H.; Sabat, M.; Harman, W. D. Dihapto Coordination of Aromatic Molecules by the Asymmetric π-Bases {TpRe(CO)(L)} (Tp = hydridotris(pyrazolyl)borate; L = ^{t}BuNC, PMe$_3$, pyridine, 1-methylimidazole, or NH$_3$). *Organometallics* **2001**, *20*, 3661-3671.

Brooks, B. C.; Meiere, S. H.; Friedman, L. A.; Carrig, E. H.; Gunnoe, T. B.; Harman, W. D. Interfacial and Intrafacial Linkage Isomerizations of Rhenium Complexes with Aromatic Molecules. *J. Am. Chem. Soc.* **2001**, *123*, 3541-3550.

Presentations

E. C. Carson, S. J. Lippard. Oxidation of Substrates Tethered to Pyridine Ligands as Non-Heme Diiron Enzyme Models. Boston Regional Inorganic Chemistry Colloquium (Medford, MA: February 2005)

E. C. Carson, S. J. Lippard. Effect of Substituted Carboxylate and Pyridine Ligands on Structure and Reactivity of Diiron(II) Complexes. 9th Annual Bruker/MIT Crystallographic Symposium (Cambridge, MA: January 2005).

E. C. Carson, S. J. Lippard. Carboxylate-Bridged Diiron(II) Complexes with Substrates Tethered to N-donor Ligands as Functional Models for the Dioxygen Activating Core of Soluble Methane Monooxygenase. 226th National ACS Meeting (New York, NY: 2003)